

University of New Hampshire

## University of New Hampshire Scholars' Repository

---

Doctoral Dissertations

Student Scholarship

---

Spring 2000

### **Swellable polymer substrates for use in magnetochemical and optical chemical sensing**

Stephen Arnold Doherty  
*University of New Hampshire, Durham*

Follow this and additional works at: <https://scholars.unh.edu/dissertation>

---

#### **Recommended Citation**

Doherty, Stephen Arnold, "Swellable polymer substrates for use in magnetochemical and optical chemical sensing" (2000). *Doctoral Dissertations*. 2119.  
<https://scholars.unh.edu/dissertation/2119>

This Dissertation is brought to you for free and open access by the Student Scholarship at University of New Hampshire Scholars' Repository. It has been accepted for inclusion in Doctoral Dissertations by an authorized administrator of University of New Hampshire Scholars' Repository. For more information, please contact [Scholarly.Communication@unh.edu](mailto:Scholarly.Communication@unh.edu).

## **INFORMATION TO USERS**

**This manuscript has been reproduced from the microfilm master. UMI films the text directly from the original or copy submitted. Thus, some thesis and dissertation copies are in typewriter face, while others may be from any type of computer printer.**

**The quality of this reproduction is dependent upon the quality of the copy submitted. Broken or indistinct print, colored or poor quality illustrations and photographs, print bleedthrough, substandard margins, and improper alignment can adversely affect reproduction.**

**In the unlikely event that the author did not send UMI a complete manuscript and there are missing pages, these will be noted. Also, if unauthorized copyright material had to be removed, a note will indicate the deletion.**

**Oversize materials (e.g., maps, drawings, charts) are reproduced by sectioning the original, beginning at the upper left-hand corner and continuing from left to right in equal sections with small overlaps.**

**Photographs included in the original manuscript have been reproduced xerographically in this copy. Higher quality 6" x 9" black and white photographic prints are available for any photographs or illustrations appearing in this copy for an additional charge. Contact UMI directly to order.**

**Bell & Howell Information and Learning  
300 North Zeeb Road, Ann Arbor, MI 48106-1346 USA  
800-521-0600**

**UMI<sup>®</sup>**



**Swellable Polymer Substrates  
for use in Magnetochemical and  
Optical Chemical Sensing**

**By**

**Stephen A. Doherty  
B.A., Colby College, 1994**

**DISSERTATION**

**Submitted to the University of New Hampshire  
in Partial Fulfillment of  
the Requirements for the Degree of**

**Doctor of Philosophy**

**in**

**Chemistry**

**May 2000**

UMI Number: 9969204

UMI<sup>®</sup>

---

UMI Microform 9969204


Copyright 2000 by Bell & Howell Information and Learning Company.


All rights reserved. This microform edition is protected against  
unauthorized copying under Title 17, United States Code.

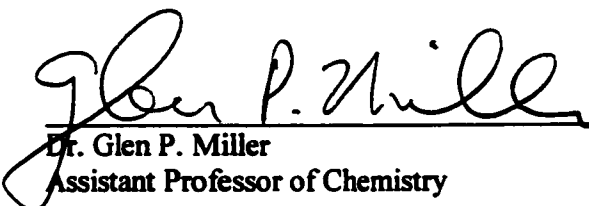
---

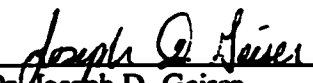
Bell & Howell Information and Learning Company  
300 North Zeeb Road  
P.O. Box 1346  
Ann Arbor, MI 48106-1346

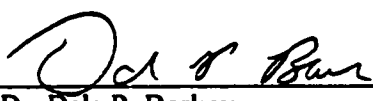
This dissertation has been examined and approved.

  
\_\_\_\_\_  
Dissertation Director/Dr. W. Rudolf Seitz  
Professor of Chemistry

  
\_\_\_\_\_  
Dr. Sterling A. Tomellini  
Associate Professor of Chemistry

  
\_\_\_\_\_  
Dr. Glen P. Miller  
Assistant Professor of Chemistry

  
\_\_\_\_\_  
Dr. Joseph D. Geiser  
Assistant Professor of Chemistry

  
\_\_\_\_\_  
Dr. Dale P. Barkey  
Associate Professor of Chemical Engineering

4/14/00

\_\_\_\_\_  
Date

## DEDICATION

**This dissertation is dedicated to my parents and brother. Their love and support made this possible and I cannot thank them enough. Thanks for always being there.**

**and**

**In memory of Elsie D. Arnold.  
They finally stopped being mean to me and let leave.**

## ACKNOWLEDGEMENTS

The first person I must thank is my advisor W. Rudolf Seitz, for your support and guidance during my time here. You gave me a nudge to get me going, but let me do it myself.

Next, my extreme thanks to Emily Webster for your love, support and putting up with me when I went a little nuts.

My thanks to my committee and the faculty of the chemistry department for encouraging me in my classes, help in this research and always having an open door.

Also my thanks to the chemistry department at Colby College for their guidance, especially Tom, Brad and Whitney, without whose encouragement I wouldn't be here now.

To Al Lake, who first made me appreciate chemistry all those years ago.

Thanks to Jerry Elkind and Texas Instruments for the SPR device and help in using it.

A special thanks to Bev and Dan Hanson and Deb and Jim Grochmal for keeping me fed and sane over the last few years.

To the staff of the chemistry department for making life that much easier, thanks Cindi, Peggy, Susan, Nancy, Bill, Bob and Shirley.

To my family, and friends from other places, who didn't quite understand why I was so crazy all the time, but put up with me anyway.

Finally, my thanks to my colleagues and friends at UNH who helped me through, even if it was just listening to me complain.



## TABLE OF CONTENTS

<b>DEDICATION</b>	<b>iii</b>
<b>ACKNOWLEDGMENTS</b>	<b>iv</b>
<b>LIST OF TABLES</b>	<b>viii</b>
<b>LIST OF FIGURES</b>	<b>x</b>
<b>ABSTRACT</b>	<b>xviii</b>
<b>CHAPTER</b>	<b>Page</b>
<b>I. INTRODUCTION</b>	<b>1</b>
I.1. Background of Chemical Sensors	1
I.2. Classes of Chemical Sensors	3
I.3. Chemical Sensors Based on Polymer Swelling	6
<b>II. THEORY</b>	<b>12</b>
II.1. Polymers	12
II.2. Dispersion Polymerization	18
II.3. Seeded Emulsion Polymerization	23
II.4. Hydrogels	24
II.5. Theory of Fiber Optics	26
II.6. Optical Measurements by Light Scattering	30
II.7. Polymer Swelling	32
II.8. Porosity	36
II.9. Surface Plasmon Resonance	37
II.10. Magnetic Sensing	43
II.11. Research Objectives	50
<b>III. EXPERIMENTAL</b>	<b>53</b>
III.1. Reagents	53
III.2. Apparatus	55
III.3. Procedures	56
III.4. Characterization	65
III.5. Experimental Design	73

IV.	<b>PREPARATION AND CHARACTERIZATION OF pH SENSITIVE HYDROGEL MEMBRANES AND ADHESION OF HYDROGEL MEMBRANES TO A SURFACE</b>	<b>78</b>
IV.1.	Introduction	78
IV.2.	Results and Discussion of Factorial Experiment Examining Cross-linker and DMAEMA Level on Size Ratio	83
IV.3.	Results and Discussion of Systematic Studies of Cross-linker and DMAEMA Concentration on Size Ratio	94
IV.4.	Effect of Comonomer Identity on Size Ratio	103
IV.5.	Hydration of Membranes	115
IV.6.	Results and Discussion of Factorial Experiment Examining Adhesion of Hydrogel Membranes	120
IV.7.	Conclusions	132
V.	<b>PREPARATION AND CHARACTERIZATION OF POLYMER MICROSPHERES BY DISPERSION POLYMERIZATION FOR CHEMICAL SENSING</b>	<b>134</b>
V.1.	Introduction	134
V.2.	Results and Discussion of Factorial Experiment	137
V.3.	Results and Discussion of Systematic Studies on Particle Size	145
V.4.	Swellable Membrane	156
V.5.	Conclusions	160
VI.	<b>REMOTELY INTERROGATABLE MAGNETOSTATIC-COUPLED AND MAGNETOELASTIC SENSORS FOR ENVIRONMENTAL MONITORING</b>	<b>161</b>
VI.1.	Introduction	161
VI.2.	Magnetostatic-coupled Sensors	162
VI.3.	Magnetoelastic Sensors	171
VI.4.	Conclusions	197
VII.	<b>POLYMERIZATION MONITORING TECHNIQUES</b>	<b>199</b>
VII.1.	Introduction	199
VII.2.	Polymerization Monitoring	200
VII.3.	Conclusions	220

VIII.	<b>FUNCTIONALIZED MICROSPHERES IN HYDROGEL MEMBRANES FOR OPTICAL SENSING</b>	222
VIII.1.	Introduction	222
VIII.2.	pH Monitoring by Surface Plasmon Resonance	224
VIII.3.	Alternative Hydrogel Membranes for Immobilizing Microspheres for Optical Sensing	238
VIII.4.	Reproducibility and Stability of poly(VBC) Microspheres Prepared by Seeded Emulsion Polymerization Immobilized in a HEMA Membrane	254
VIII.5.	Conclusions	269
IX.	<b>CONCLUSIONS</b>	271
	<b>APPENDIX A</b>	275
	<b>APPENDIX B</b>	277
	<b>APPENDIX C</b>	283
	<b>REFERENCES</b>	286

## LIST OF TABLES

	Page
Table II.1. Comparison of heterogeneous polymerization systems.	17
Table III.1. Factorial experiment design for cross-linker swelling ratio.	74
Table III.2. Factorial experiment design for comonomer swelling ratio.	75
Table III.3. Factorial experiment design for hydrogel adhesion.	76
Table III.4. Factorial experiment design for microsphere particle size.	77
Table IV.1. Results of Analysis of Variance for size ratio examining effect of cross-linker level and concentration of DMAEMA.	85
Table IV.2. Effect of cross-linking level and cross-linker type on size ratio.	95
Table IV.3. CHN analysis results and expected values for HEMA membrane with varying DMAEMA concentrations and cross-linkers.	98
Table IV.4. Mechanical properties of membranes with varying DMAEMA concentration.	100
Table IV.5. Results of DMAEMA comonomer preliminary study.	105
Table IV.6. Results of Analysis of Variance for size ratio examining effect of comonomer hydrophilicity and concentration of DMAEMA.	108
Table IV.7. CHN analysis results and expected values for various comonomer membrane formulations.	114
Table IV.8. Results of Analysis of Variance for time until adhesion failure of hydrogel membranes.	124

Table V.1.	Results of Analysis of Variance for microsphere particle size.	139
Table V.2.	Average particle size and R.S.D. % of particles with varying water concentrations in dispersion media.	146
Table V.3.	Average particle size and R.S.D. % of particles with varying monomer concentrations.	149
Table V.4.	Average particle size and R.S.D. % of particles with varying stabilizer concentrations and molecular weight.	153
Table VI.1.	Viscosity effect on resonant frequency of magnetoelastic strip	174
Table VI.2.	Effect of salt concentration on solution viscosity, density and resonant frequency of magnetoelastic strip.	182
Table VI.3.	Solution viscosity and resonant frequency in pH buffer solutions with different buffer capacities.	184
Table VI.4.	Atomic composition of magnetoelastic strip.	185
Table VI.5.	Resonant frequency of polymer coated magnetoelastic strips in pH 4 and pH 10 buffer solutions.	194
Table VIII.1.	Theoretical refractive index of PVA membrane with VBC/TCPA microspheres in pH 4 and pH 10 buffer solutions.	229
Table VIII.2.	Theoretical and experimental refractive index of PVA membrane with VBC/TCPA microspheres in pH 4 and pH 10 buffer solutions.	232
Table VIII.3.	Refractive indices and hydration levels of hydrogel membranes.	241
Table VIII.4.	Response times and hydration levels of hydrogel membranes.	251

## LIST OF FIGURES

	Page
Figure I.1. Diagram of remote distributive fiber optic chemical sensor.	10
Figure II.1. Polymerization Process of Free Radical Polymerization for for a Generic Polymer System: (I) Initiator, (M) Monomer.	13
Figure II.2. Schematic of particle growth by dispersion polymerization.	22
Figure II.3. Schematic of optical fiber showing light transmittance by total internal reflection. Total internal reflection will occur when the incident angle of light, $\theta$ , is greater than the critical angle, $\alpha$ . $R_1$ is incident at an angle greater than $\alpha$ and will be internally reflected. $R_2$ is incident at less than $\alpha$ and will refract into the cladding and not be propagated.	28
Figure II.4. Refractive Index Profiles of Step-Index and Graded-Index Optical Fiber.	29
Figure II.5. Schematic showing ionic polymer swelling. (A) illustrates unswollen polymer, (B) illustrates swollen polymer. Circles represent mobile charge in solution. Squares represent charges fixed on the polymer backbone.	35
Figure II.6. Kretschmann prism arrangement for coupling light into surface plasmons.	38
Figure II.7. Schematic of Texas Instruments Spreeta SPR Device.	41
Figure II.8. Sample SPR Curves at two refractive indices.	42
Figure II.9. Schematic of Magnetostatic-Coupled Chemical Sensor A swellable polymer layer separates two magnetic films. 'M' denotes the magnetization vector.	45
Figure II.10. Schematic of Magnetostatic-Coupled Chemical Sensor.	45
Figure II.11. Example of response of magnetoelastic ribbon in air.	46
Figure II.12. Schematic drawing of magnetoelastic resonance meter.	47
Figure III.1. Synthesis of TCPA.	59

Figure III.2.	FTIR showing conversion of 1. TCP into 2. TCPA.	60
Figure III.3.	Polymerization reaction of VBC and TCPA to form VBC/TCPA microparticles.	62
Figure III.4.	Derivatization reaction for VBC/TCPA microparticles with diethylamine.	66
Figure III.5.	FTIR of VBC/TCPA microparticles 1. before and 2. after derivatization.	67
Figure III.6.	FTIR of VBC microparticles 1. before and 2. after derivatization.	68
Figure III.7.	Diagram of sample cell and holder for FTIR monitoring of thermal polymerization.	71
Figure IV.1.	Structure of monomers, cross-linkers and initiators used in pH sensitive membrane preparation.	80
Figure IV.2.	Schematic showing ionic swelling of hydrogel. (A) Shows unswollen state, (B) shows swollen state with protonated amines and counter ions.	82
Figure IV.3.	The mean size ratio, membrane diameter in acid (pH 4) divided by membrane diameter in base (pH 10). The error bars represent one standard deviation (n=3).	84
Figure IV.4.	The average effect on the size ratio of changing amounts of the main factors. Points are the average values of all membranes from formulations containing either high or low levels of a particular factor.	87
Figure IV.5.	The effect of DMAEMA *% cross-linker interaction on the size ratio.	90
Figure IV.6.	The effect of % cross-linker*cross-linker type on the size ratio.	91
Figure IV.7.A.	The effect of DMAEMA *% cross-linker*cross-linker type on the size ratio for 50 % DMAEMA membranes.	93
Figure IV.7.B.	The effect of DMAEMA *% cross-linker*cross-linker type on the size ratio for 25 % DMAEMA membranes.	93

Figure IV.8.	Effect of varying DMAEMA concentration and cross-linker type on size ratio.	99
Figure IV.9.	The size ratio of 25 % DMAEMA-co-HEMA membrane as a function of buffer pH. All buffers 0.1 M and I.S. 0.1 M.	102
Figure IV.10.	The mean size ratio and standard deviations for formulations of comonomer factorial experiment(n=3).	107
Figure IV.11.	The average effect on the size ratio of changing amounts of the main factors.	110
Figure IV.12.	The effect of % DMAEMA*Comonomer Type on the size ratio.	111
Figure IV.13.	Effect of varying DMAEMA concentration and comonomer type on size ratio.	113
Figure IV.14.	The effect of cross-linking level and type on hydration of poly-(HEMA) membrane.	116
Figure IV.15.	The hydration level of HEMA membrane as a function of DMAEMA concentration. Membrane cross-linked with 1.5 % TEGDM. Buffers 0.1 M and I.S. 0.1 M.	117
Figure IV.16.	The hydration level of 25 % DMAEMA-co-HEMA membrane as a function of buffer pH. All buffers 0.1 M and I.S. 0.1 M. Membrane cross-linked with 1.5 % EGDM.	118
Figure IV.17.	Surface derivatization for hydrogel adhesion with Trimethoxysilyl propyl methacrylate.	121
Figure IV.18.	The mean time until failure(n=2) and standard deviations for formulations used in hydrogel adhesion experiment.	123
Figure IV.19.	The average effect on time until adhesion failure of changing amounts of main factors.	125
Figure IV.20.	Schematic diagram showing direction of swelling forces as polymer swells in acidic solution.	127
Figure IV.21.	The effect of DMAEMA Concentration*pH interaction on time until adhesion failure.	129



Figure IV.22. The effect of DMAEMA Concentration*solution interaction on time until adhesion failure.	130
Figure IV.23.A. The effect of Solution*DMAEMA Concentration*pH interaction on the time until adhesion failure for ethanol solution.	131
Figure IV.23.B. The effect of Solution*DMAEMA Concentration*pH interaction on the time until adhesion failure for ethanol solution.	131
Figure V.1. Structures of monomers, cross-linker, stabilizer and initiator for preparing microparticles.	136
Figure V.2. The mean particle size and standard deviations for formulations used in particle size factorial(n=3).	138
Figure V.3. The average effect on particle size of changing amounts of the main factors.	140
Figure V.4. The effect of % Water*% Stabilizer on the particle size.	143
Figure V.5. The effect of % Water*% Monomer on the particle size.	144
Figure V.6. Scanning Electron Micrographs of VBC/TCPA particles in media with various water concentrations.	147
Figure V.7. Effect of monomer concentration on particle size.	150
Figure V.8. Scanning Electron Micrographs of VBC/TCPA particles at various monomer concentrations.	151
Figure V.9. Effect of stabilizer concentration and molecular weight on particle size.	154
Figure V.10. Schematic diagram showing polymer microspheres embedded in hydrogel membrane, causing membrane to swell. The bead is adhered at the top and bottom to a surface. At low pH the beads swell into each other, forcing them to elongate and swell perpendicular to the adhered surface.	157
Figure V.11. Effect of VBC/TCPA bead concentration on size ratio of HEMA membrane.	158
Figure VI.1. 10 Hz voltage spike wavetrain for magnetic sensor. 1) pH 7.5 2) pH 4, and 3) pH 10.	163

Figure VI.2.	Schematic diagram of split square sensor. Gap between squares is 2 mm, within squares gap is 0.05 mm.	166
Figure VI.3.	Voltage-spike wavetrain of split square design magnetostatic coupled sensor. Voltage amplitude as a function of time and solution pH.	166
Figure VI.4.	Coercivity versus time and pH for powder sensor prepared in 25 % DMAEMA membrane.	169
Figure VI.5.	Resonant frequency shift as a function of polystyrene concentration and molecular weight.	175
Figure VI.6.	Resonant frequency shift as a function of the square root of the viscosity and density product.	176
Figure VI.7.	Resonant frequency shift as a function of the square root of the solution viscosity.	176
Figure VI.8.A.	Resonant frequency as a function of volume ethanol added, small strip.	178
Figure VI.8.A.	Resonant frequency as a function of volume ethanol added, large strip.	178
Figure VI.9.	Frequency shift as function of salt concentration.	181
Figure VI.10.	Resonant frequency as a function of buffer capacity and pH.	183
Figure VI.11.	Resonant frequency as a function of time immersed in aqueous solution.	188
Figure VI.12.	Response curve of magnetoelastic strip before and after coating with spin-on-glass protective layer.	189
Figure VI.13.	Response of magnetoelastic strip coated with 3 % DMAEMA hydrogel in pH 4 and pH 10 buffer solutions.	193
Figure VI.14.	Response of magnetoelastic strip coated with 1 % VBC/TCPA microspheres embedded in HEMA membrane in pH 4 and pH 10 buffer solutions.	195
Figure VII.1.	Cross-linking reaction of poly vinyl alcohol with glutaraldehyde	201

Figure VII.2.	Solution viscosity of poly-vinyl alcohol as cross-linking reaction proceeds with time.	202
Figure VII.3.	Resonant frequency of poly-vinyl alcohol coated magnetoelastic strip as cross-linking reaction proceeds with time.	203
Figure VII.4.	Resonant frequency as a function of time for thermally initiated polymerization of VBC.	206
Figure VII.5.	Solution viscosity as a function of time for thermally initiated polymerization of VBC.	207
Figure VII.6.	Resonant frequency as a function of time for photo initiated polymerization of VBC.	210
Figure VII.7.	Solution viscosity as a function of time for photo initiated polymerization of VBC.	211
Figure VII.8.	Resonant frequency as a function of time for thermal initiated polymerization of HEMA-co-DMAEMA.	214
Figure VII.9.	Solution viscosity as a function of time for thermal initiated polymerization of HEMA-co-DMAEMA.	215
Figure VII.10.	Ratio of C=C band to C=O band decreasing as a function of time for thermal initiated polymerization of HEMA-co-DMAEMA.	216
Figure VII.11.	Solution viscosity as a function of time for photo initiated polymerization of HEMA-co-DMAEMA.	218
Figure VII.12.	Ratio of C=C band to C=O band decreasing as a function of time for photo initiated polymerization of HEMA-co-DMAEMA.	219
Figure VIII.1.	Scanning electron micrograph of VBC/TCPA microspheres used in SPR and hydrogel studies.	226
Figure VIII.2.	SPR response for 0.2 % VBC/TCPA beads in PVA membrane. Sensor was cycled between pH 4 and pH 10 buffer solutions with buffer capacity of 0.1 M and ionic strength of 0.1 M.	228
Figure VIII.3.	SPR response for pH 4 and pH 10 buffer solutions. Buffer capacity of each solution was 0.1 M and ionic strength was of 0.1 M.	230

Figure VIII.4. SPR response for 20 % VBC/TCPA beads in PVA membrane. Sensor was cycled between pH 4 and pH 10 buffer solutions.	233
Figure VIII.5. SPR response for 40 % VBC/TCPA beads in PVA membrane. Sensor was cycled between pH 4 and pH 10 buffer solutions.	234
Figure VIII.6. Predicted refractive index for VBC/TCPA microspheres in a PVA membrane as a function of microsphere concentration.	235
Figure VIII.7. Schematic diagram of hydrogel membrane containing swellable microspheres.	237
Figure VIII.8. Turbidity spectra of VBC/TCPA microspheres embedded in 76 $\mu$ m HPMA membrane. Microsphere concentration was 2 % (wt./wt.).	242
Figure VIII.9. Turbidity spectra of VBC/TCPA microspheres embedded in 76 $\mu$ m HEMA membrane. Microsphere concentration was 2 % (wt./wt.).	243
Figure VIII.10. Turbidity spectra of VBC/TCPA microspheres embedded in 76 $\mu$ m HPA membrane. Microsphere concentration was 2 % (wt./wt.).	244
Figure VIII.11. Turbidity spectra of VBC/TCPA microspheres embedded in 76 $\mu$ m HEA membrane. Microsphere concentration was 2 % (wt./wt.).	245
Figure VIII.12. Response time of a 76 $\mu$ m HPMA membrane embedded with VBC/TCPA microspheres. Microsphere concentration was 2 % (wt./wt.). Buffers prepared with 0.1 M buffer capacity and 0.1 M ionic strength.	248
Figure VIII.13. Response time of a 76 $\mu$ m HEMA membrane embedded with VBC/TCPA microspheres. Microsphere concentration was 2 % (wt./wt.). Buffers prepared with 0.1 M buffer capacity and 0.1 M ionic strength.	249
Figure VIII.14. Response time of a 76 $\mu$ m HPA membrane embedded with VBC/TCPA microspheres. Microsphere concentration was 2 % (wt./wt.). Buffers prepared with 0.1 M buffer capacity and 0.1 M ionic strength.	250
Figure VIII.15. Scanning electron micrographs of a) poly-(VBC) seed particles, prepared by dispersion polymerization, and b) poly-(VBC) seeded particles prepared by seeded emulsion polymerization.	253

Figure VIII.16. Response reproducibility within and between membranes in pH 4 and pH 10 buffer solutions. The membranes are 1.5 % by weight seeded microspheres in HEMA.	257
Figure VIII.17. Reproducibility of absorbance difference within and between membranes.	258
Figure VIII.18. Reproducibility of sensor response as membrane is cycled between pH 4 and pH 10. The concentration of seeded microspheres was 1.5 % in HEMA.	259
Figure VIII.19. Reproducibility of response as membrane is cycled between pH 4 and pH 10. Membrane remained in sample cuvette during cycling. The concentration of seeded microspheres was 1.5 % by weight in HEMA.	260
Figure VIII.20. Reproducibility of response as membrane is cycled between pH 4 and pH 10. Membrane was removed from sample cuvette during cycling. The concentration of seeded microspheres was 1.5 % by weight in HEMA.	260
Figure VIII.21. Response of membrane stored in buffer solutions at 80 °C. The concentration of seeded microspheres was 1.5 % in HEMA.	264
Figure VIII.22. Response of membrane cycled from pH 4 to pH 10 before and after storage for 42 days in 80 °C oven. Microsphere concentration was 1.5 % in HEMA membrane.	265
Figure VIII.23. Response of membrane stored in buffer solutions in light. The concentration of seeded microspheres was 1.5 % in HEMA.	266
Figure VIII.24. Response of membrane cycled from pH 4 to pH 10 before and after 42 days of storage in light. Microsphere concentration was 1.5 % in HEMA membrane.	267

## ABSTRACT

### SWELLBLE POLYMER SUBSTRATES FOR USE IN MAGNETOCHEMICAL AND OPTICAL CHEMICAL SENSING

By

Stephen A. Doherty  
University of New Hampshire, May 2000

Lightly cross-linked, animated polymers that swell and shrink with changing pH were prepared and evaluated. At low pHs amine sites protonate causing charge to accumulate along the polymer backbone. The polymer then swells to maximize the charge separation. The swelling of the polymer causes a change in a magnetic or optical property that can be measured and related to pH.

Animated hydrogel membranes were prepared by copolymerizing dimethyl amino ethyl methacrylate(DMAEMA) with various comonomer hydrogels. Experiments were conducted to examine the effect of formulation on the ability of the hydrogel membrane to swell. Factors examined included cross-linker type, cross-linker concentration, DMAEMA concentration and comonomer hydrophilicity.

Polymer microspheres were prepared using dispersion polymerization and seeded emulsion polymerization techniques. Poly-(vinyl benzyl chloride-co-2,4,5-trichloro phenyl acrylate)(VBC/TCPA) microspheres were prepared by dispersion polymerization. A factorial design experiment was carried out to examine the effect of monomer concentration, stabilizer concentration and water concentration on the size of VBC/TCPA particles stabilized with poly-acrylic acid. Microspheres were prepared using

poly(vinylpyrrolidone) as the steric stabilizer. These particles were 0.6  $\mu\text{m}$  in diameter and were used in optical sensing experiments. Seeded emulsion polymerization was used to produce porous particles of poly(VBC) with diameters of 1.3  $\mu\text{m}$ .

The pH sensitive hydrogel membranes were incorporated into two types of magnetochemical sensors; the magnetostatic coupled sensor and the magnetoelastic sensor. Both sensor designs responded to solution pH due to swelling or shrinking of the hydrogel. In addition, the magnetoelastic strip was evaluated for measuring viscosity and for monitoring polymerization processes.

VBC/TCPA microspheres were used in several optical sensing methods. Poly(vinyl alcohol) membranes with VBC/TCPA microspheres were used to examine the feasibility of monitoring solution pH by surface plasmon resonance. A number of hydrogels of varying hydrophilicities with VBC/TCPA microspheres were examined by UV/Vis spectrophotometry, to examine the effect of membrane hydrophilicity on response for potential use in a remote fiber optic chemical sensor. The reproducibility of poly(VBC) microspheres in a HEMA membrane was examined. No change in response was observed after 100 swelling and shrinking cycles. Exposure to 80  $^{\circ}\text{C}$  temperature or light for 40 days had only a small change on the magnitude of response.

# CHAPTER I

## Introduction

### I.1 Background of Chemical Sensors

The field of chemical sensors has experienced tremendous growth over the last several years. During the last four years, there has been nearly a 50% increase in the number of sensor papers published per year.<sup>1</sup> Every category of sensors has seen an increase in publications as sensors become more diverse and specialized to serve a broader range of applications.

The growth of the field can be attributed to the desire to move away from conventional laboratory instrumentation to smaller more convenient methods of analysis. Conventional instrumentation usually involves the transport of a sample to a laboratory, followed by sample treatment and manipulations, and finally analysis. Each step increases the time and cost of analysis, as well as introducing potential sources of error. A chemical sensor can often be used to make *in situ* measurements remote from the laboratory, providing savings in time, labor, and often cost. Additionally, the potential for contamination or degradation of the sample during collection, transport or analysis is reduced. A further benefit of sensors is their ability to be placed in hazardous or inhospitable environments and make continuous measurements over a period of time to provide information of the temporal distribution of the analyte of interest. This feature can also be utilized to provide spatial information, as sensors only need to be placed and then monitored remotely. The site does not have to be visited repeatedly to collect



samples. Sensors can be used in a wide variety of environments from soil extracts<sup>2</sup> to *in vivo* measurements that would be impossible to conduct using conventional instruments.<sup>3</sup>

A chemical sensor is a device that provides information on the quantity of a chemical species.<sup>4</sup> Ideally the sensor should provide this information continuously, in real time and reversibly. Additionally the sensor should be robust for a long operational lifetime. The sensor is comprised of a chemically sensitive component coupled with a transducer. Transducers generally convert some input signal such as current, light intensity or potential into an electrical signal, the magnitude of which is proportional to the concentration of the analyte being sampled. The sensing component can take many forms, but all provide for interaction with the analyte in some selective fashion. Most sensing mechanisms make use of size or shape as a method of selectivity; molecules of a certain shape or size that fit the recognition site of the sensing component are measured. This mechanism is most readily visible in the use of enzymes or the antibody-antigen reaction. The antibody-antigen interaction has been exploited for an optical cell detector.<sup>5</sup> Enzymes have been used to construct sensors for the measurement of glucose and lactate.<sup>6,7</sup> Molecularly imprinted polymers have been gaining in popularity as recognition elements for a sensing component.<sup>8</sup>

## **I.2 Classes of Chemical Sensors**

The field of chemical sensors can be divided into several classes based on their mode of measurement: thermal, mass, optical and electrochemical, in order of increasing numbers of publications.<sup>1</sup>

### **I.2.1 Electrochemical sensors**

Electrochemical sensors are the oldest and most mature class of sensors. This class of sensor can be broken down further to amperometric, conductimetric and potentiometric sensors, based on the phenomenon that is exploited. The maturity of this field is reflected in the number of commercial sensors available. The most prevalent commercial sensor is the pH electrode. Electrochemical sensors are also commercially available for a variety of analytes such as calcium, chloride and nitrate ions. A variety of sensing strategies have been utilized to increase sensitivity or selectivity, including antibodies, ionophores, and enzymes. The potential for mass production using microfabrication techniques has caused a renewed interest in this area of sensor development. The simplicity of the sensor design compared to other types makes it especially well suited for microfabrication.<sup>9,10</sup> Biosensing for clinical analysis is especially suited for the use of inexpensive disposable sensors, which could give more rapid analysis. Microfabricated potentiometric sensor arrays have been constructed to conduct *in vivo* myocardial pH and potassium ion measurements.<sup>3,11</sup>

### **I.2.2 Mass sensors**

Mass sensors are a popular class of sensors that simply measure the mass applied to a sensor surface.<sup>1</sup> The popularity of this type of sensor may be traced to the low cost and ready availability of piezoelectric sensors. While all mass sensors are based on

piezoelectric effects, they can be divided into piezoelectric and SAW(Surface Acoustic Wave) Devices. The Curie brothers first observed the piezoelectric phenomenon in 1880.<sup>12</sup> They noted that when compressed, quartz crystals produce an electric potential, whereas the application of an electric potential causes deformation of the crystals. The deformation of the crystal produces an acoustic wave, which will propagate through the medium. Changes in the medium will alter the propagation of the wave, for example the addition of mass to the surface. The change in frequency of the propagated wave is the most common and accurate parameter used for output.<sup>12</sup> The method is capable of detecting very small mass changes; however, it is susceptible to interference from moisture and temperature. Selectivity is achieved through the addition of a chemically sensitive layer.<sup>13</sup> Sensors for Staphylococcal Enterptoxin B, a component of biological weapons, and for immunoglobulin M have been developed using antibody-antigen binding for selectivity.<sup>14,15</sup> The detection of organic vapors has been conducted using sensors coated with gas chromatographic stationary phases for selectivity.<sup>16</sup>

### **I.2.3 Optical sensors**

These types of sensors make use of the interaction of a material with electromagnetic radiation. A sample is irradiated with monochromatic radiation and the attenuation of the light due to adsorption or intensity of emission due to luminescence is used to determine the extent of interaction. Optical sensors are very similar to traditional spectroscopic techniques, but do not require the transport of the sample to the spectrophotometer. This arrangement necessitates that light be transmitted from the source to the sample and then back to the detector without allowing extraneous interaction with the environment. This is usually accomplished with optical fibers.

Developments in the fiber optics communication industry have been adapted for chemical sensing at different wavelengths and longer distances with decreased attenuation. This is one of the major advantages of fiber optic chemical sensors (FOCS), as well as the ability to spatially separate the sensor and source/detection equipment.

Selectivity is introduced by complexing agents or indicators, which interact with the analyte of interest at the end of the fiber. Optical chemical sensors have been constructed for a wide range of applications. In 1980 Peterson provided the first detailed description of a pH fiber optic chemical sensor.<sup>17</sup> Seitz described the first chemiluminescence based FOCS in 1978<sup>18</sup> and a fluorescence based sensor in 1982.<sup>19</sup> Sensors for potassium have been reported,<sup>20</sup> as have sensors for penicillin.<sup>21</sup>

Surface Plasmon Resonance (SPR) is a technique becoming more prevalent as a type of optical sensor. This technique measures changes in the refractive index at the surface of the sensor.<sup>12</sup> The SPR phenomenon has been exploited for cell detection<sup>5</sup> and sensing of the herbicide simazine.<sup>22</sup> The introduction of a single chip compact SPR device by Texas Instruments has brought this technique to actual sensor use.<sup>23</sup>

#### **1.2.4 Thermal sensors**

Thermal sensors function by measuring the heat produced or consumed during a chemical reaction.<sup>12</sup> This class of sensor is a distinct minority in the field of chemical sensors, representing 3% of the total number of sensor papers over the last 4 years. However this is a 435% increase, making thermal sensors the fastest growing type of sensor in terms of papers published.<sup>1</sup> Sensors based on thermal measurements for glucose and urea have been reported.<sup>24,25</sup>

### **I. 3 Chemical Sensors Based on Polymer Swelling**

Chemical sensors based on polymer swelling are a relatively new phenomenon. While polymers have been used in a variety of sensing designs and techniques they have not been used extensively as the sensing element. They primarily have been used as: a substrate to support a chemically sensitive material, such as an enzyme; a containment material to entrap a chromophore or ionophore; or to provide size exclusion to enhance selectivity at a secondary detection layer. In these instances, polymer swelling is usually to be avoided, since it would interfere with the measurement. Sensors based on polymer swelling have been constructed, such as a humidity detector.<sup>26</sup> The impact of polymer swelling has been observed in SAW devices where the unintended effect of polymer swelling was found to be greater than the measured effect of mass loading.<sup>27</sup>

Our research group has been working to exploit polymer swelling as a sensing technique. The primary focus of this work has been to utilize polymer swelling to cause a change in optical properties.<sup>28,32</sup> Initial designs utilized a swelling polymer bead coupled with a movable diaphragm to change the amount of light reflected into an optical fiber. Following trials with commercial beads that were highly crosslinked, polymer beads were prepared with lower levels of crosslinking and improved selectivity. Conway examined the preparation of polymer beads by suspension polymerization.<sup>29</sup> The monomer chosen was vinylbenzyl chloride (VBC), which was polymerized with the block copolymer Kraton G1652 and a porogenic solvent. The VBC monomer was chosen because of the wide variety of derivatizations that are possible, most notably for this work VBC was derivatized to introduce functionalities sensitive to pH.<sup>33</sup> The inclusion of Kraton had been studied previously and was found to improve the

mechanical properties of the polymer, to enable them to undergo multiple swelling and shrinking cycles.<sup>34,35</sup> Kraton is a tri-block copolymer of styrene-ethylene/butylene-styrene. It acts to improve mechanical properties by terminating microcracks before they can propagate throughout the polymer. Toluene or another porogenic solvent is added to induce the formation of micropores. These pores allow for more rapid infusion of the analyte solution into the polymer. These beads proved unable to generate the force needed to effectively move the diaphragm. However it was observed that these beads became clearer as they swelled, which led to a reflectance-based sensor.

This phenomenon was used to construct a single fiber-optic pH sensor.<sup>36</sup> A drop of amine derivatized polystyrene was placed at the tip of a single optical fiber. In an acidic environment the amine becomes protonated, and the bead swells. The polymer becomes clearer and the amount of light reflected back is decreased.

The use of swellable polymers for reflectance-based sensing was studied extensively by Rooney.<sup>30</sup> This work focused on two different strategies for sensing. The first involved the use of bulk membranes that were pH sensitive. The second made use of pH sensitive polymer microparticles that were embedded in a non-swellable pH insensitive hydrogel. It was determined that the change in reflection observed in the bulk pH sensitive membranes was the result of water entering the polymer as it swelled in an acidic medium. The membranes prepared contained pores that were filled with water. These pores scattered light due to the differences in the refractive indices of the polymer membrane and the water in the pores. Because the difference in the two indices is greater in the unswollen state, light is reflected, and the membrane appears opaque. When the membrane swells, there is an influx of water into the polymer; this results in a lowering

of the effective refractive index of the polymer. The difference between the refractive index of the polymer and the water filled pores is now less, therefore less light is scattered and the membrane appears clearer. A limitation in this design was that as the polymer swelled it would often swell to the point it would delaminate from the substrate to which it was attached. In an attempt to alleviate this problem, the use of polymer microparticles imbedded in a hydrogel was examined. One advantage of this design is that only the microparticles swell, while the larger hydrogel does not. The hydrogel could thereby be attached to a surface and would not be affected by the swelling of the particles. Microparticles were prepared by dispersion polymerization of VBC and modified with an amine to induce pH sensitivity. In this design, the light is scattered by the particles rather than the pores. The refractive index difference between the hydrogel and the microparticle determines the amount of scattering. As the microparticle swells in an acidic medium, the water content of the particle increases, decreasing the refractive index of the particle. The membrane appears clearer as the difference between the refractive indices of the particle and the membrane is smaller and less light is scattered.

The preparation of swellable microparticles has been investigated. The incorporation of the comonomer, 2,4,5-trichlorophenol acrylate(TCPA) into dispersion polymerized VBC was studied.<sup>37</sup> After derivatization to an amide, TCPA monomer units are hydrophilic. This allow the polymer to swell in water so that the interior is more accessible to analyte and the response time is decreased

Factors affecting the formation of particles were explored by Miele.<sup>31</sup> The effects of solvent composition, monomer concentration, initiator concentration, stabilizer molecular weight and concentration, and temperature on particle size were examined.

This allowed for the preparation of particles of a desired size. Previously particles were around 0.6  $\mu\text{m}$  in size. Larger particles were desired to allow for the use of a longer wavelength NIR source in the remote distributive sensor prepared by Civiello.<sup>32</sup> The use of a longer wavelength NIR is desired as it is attenuated less in optical fibers.

Preparation of particles by seeded emulsion polymerization was also explored and particles with 1-1.5  $\mu\text{m}$  diameters were prepared. Poly(VBC) particles prepared by seeded emulsion polymerization were found to have faster response times and larger signal changes than poly(VBC-co-TCPA) beads prepared by dispersion polymerization.

To date, the polymers prepared were to be utilized in the remote fiber-optic chemical sensor(FOCS) constructed by Civiello,<sup>32</sup> shown in Figure I.1. A NIR laser diode is pulsed along a fiber optic cable at a frequency of 33 kHz. A 2x2 coupler then splits this into 2 fibers of different lengths, 300 and 500 meters. This allows the signals from each fiber to be resolved temporally from each other. The polymers would be attached to the distal end of the fiber that would be placed in the medium to be examined. The light would reflect at the polymer-fiber interface, back along the fiber to a photodiode detector. The intensity of the reflected signal would be dependent upon the concentration of the analyte of interest. The instrument is controlled and the output displayed using the LabVIEW data acquisition program.



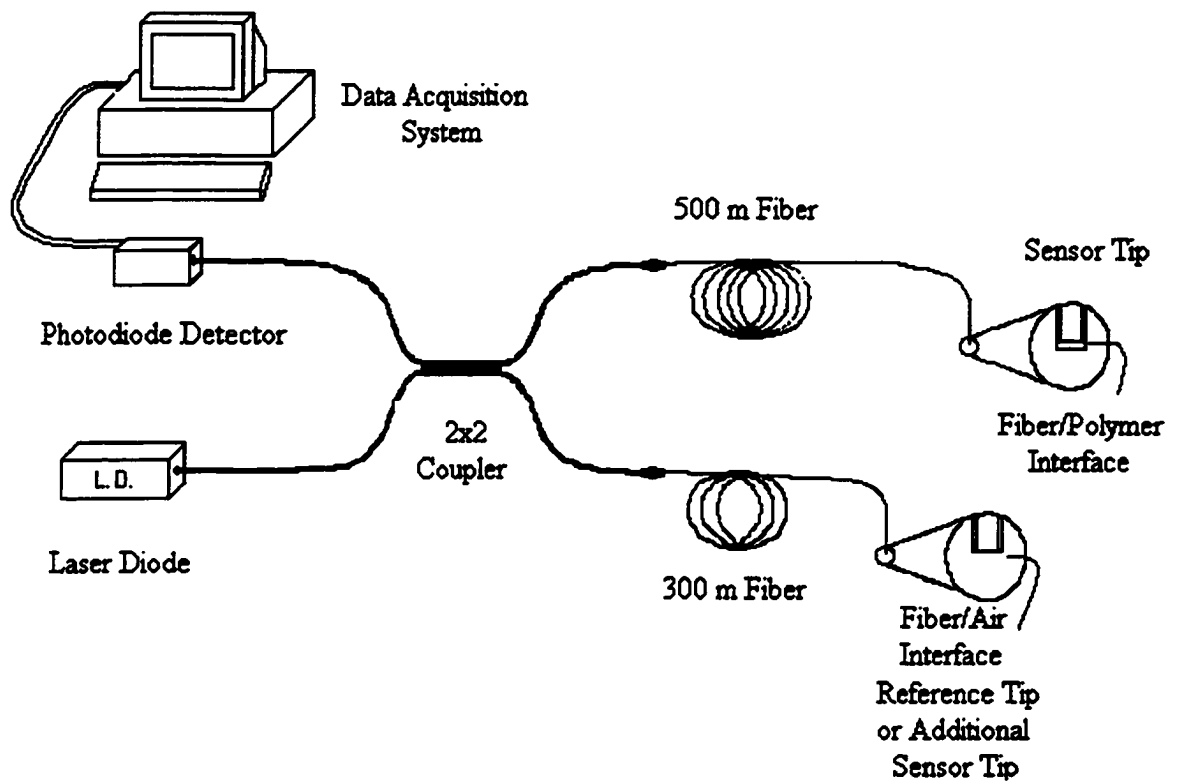


**Figure I.1. Diagram of remote distributive fiber optic chemical sensor**

**This reflectance based system offers several advantages over other sensing designs such as chemiluminescence and fluorescence based systems. Sensing strategies using these techniques suffer from the problem of leaching or photodegradation of the indicators. Also the reflectance system is not wavelength specific, allowing for the use of longer wavelengths and less expensive LED's as the light source. The long wavelengths of the NIR are scattered less by the fiber and can be transmitted longer distances with lower attenuation than the shorter wavelengths.**

# CHAPTER II

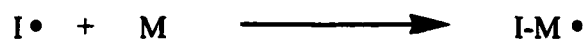
## Theory

### II.1 Polymers

The word 'polymer' was derived from the Greek words 'poly' meaning 'many' and 'meros' meaning 'parts'.<sup>38</sup> This alludes to polymers consisting of many small repeating parts known as monomers. Polymers may be natural or artificial. Examples of natural polymers include cellulose and proteins. Natural polymers were used by early humans to make elastic articles, waterproof fabrics and as caulking materials.<sup>38</sup> Artificial polymers, those not produced directly by nature, will be discussed in this dissertation.

Polymers can be divided into two basic categories based on their structure. The first category is that in which the structure of the monomer components and the polymer is not the same. This is known as a condensation polymer. As the polymer forms, atoms are displaced from the monomer units; often water is lost. Poly(styrene) is an example of a condensation polymer. Condensation polymers will not be discussed, since none were used in this work. The second category of polymers is chain polymers. In this case, the polymer and the monomer unit consist of the same atoms. An example of a chain polymer is poly(styrene). Typically chain polymers consist of only carbon atoms in the main chain, while condensation polymers may contain other atoms.<sup>39</sup> All polymers used in this work are chain polymers. The free radical polymerization process can be divided into three distinct phases: initiation, propagation and termination, see Figure II.1.

### 1. Initiation



### 2. Propagation



### 3. Termination

#### a. Combination



#### b. Disproportionation

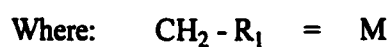


**Figure II.1.** Polymerization Process of Free Radical Polymerization for for a Generic Polymer System: (I) Initiator, (M) Monomer

## **II.1.1 Polymerization Process**

### **II.1.1.1 Initiation**

The first phase in the polymerization process is initiation of the reaction by the production of a free radical, see Figure II.1. This step may be carried out by redox mechanisms, such as the decomposition of peroxide. This is often used in the case of heterogeneous polymerizations. More often the radical is produced through homolytic bond cleavage using light or heat. These types of initiators were used in this work. Benzoyl peroxide (BP) and 2,2-azobis(isobutyronitrile) (AIBN) were used as thermal initiators and 2,2-dimethoxy-2-phenyl-acetophenone (DMPAP) as a photoinitiator. Upon heating, BP degrades to form two benzyl radicals and carbon dioxide, while AIBN forms two cyanopropyl radicals and nitrogen gas. The DMPAP forms substituted benzyl radicals when exposed to light. AIBN is often used in place of BP because of its ability to initiate at lower temperatures. Photoinitiated polymerization is often favored over thermally initiated polymerization since the intensity of the light source can be varied to control the rate of radical generation.

The second step in the initiation phase is the reaction of the radical with the monomer. In the polymerizations studied in this work, the radical reacts with the vinyl group of the vinylbenzyl chloride (VBC) or on hydroxyethyl methacrylate. The radical replaces the carbon double bond with a single bond, forming a new bond and a new radical on the monomer. This new radical can then go on to react with another monomer unit; this process will continue with the chain propagating with the addition of each monomer unit.

### **II.1.1.2 Propagation**

The second phase of polymerization is the propagation step, see Figure II.1. It is in this phase that the polymer forms long chains. The polymer chain consists of the initiator unit on one end and a radical monomer unit on the other. The radical reacts with additional monomer units, adding that new monomer unit to the chain and moving the radical to the new unit at the end of the chain. Propagation will continue until termination occurs.

### **II.1.1.3 Termination**

As shown in Figure II.1, there are two mechanisms by which the reaction can be terminated: combination and disproportionation. In a reaction terminated by combination the radical ends of two polymer chains come together to form a carbon-carbon bond. The final polymer chain contains an initiator fragment at each end. In a disproportionation terminated reaction, there is a proton transfer between the polymer chain ends. Instead of producing one long polymer chain as in combination, two chains are formed. At one end of each chain is an initiator fragment. The other end has a monomer fragment that is saturated on one chain and unsaturated on the other chain.

## **II.1.2 Polymerization Systems**

The method by which the polymers are prepared can also be used as a basis for classification. Polymerization systems can be divided into two basic categories: homogeneous and heterogeneous.

### **II.1.2.1 Homogeneous Polymerization**

The primary example of this category is bulk polymerization. In this method, a solution predominantly consisting of monomer and initiator is polymerized into a solid

block of polymer. The container in which the polymerization is carried out determines the shape of the formed polymer. This method is used when casting polymers and in injection molding. The advantage of this type of polymerization is the ease with which it can be carried out and the simplicity of the required equipment. The major disadvantage is poor heat transfer, which causes the temperature of the reaction to increase rapidly. One method of dealing with this problem is to carry out a solution polymerization. The monomer and initiator are dissolved in a solvent, and polymerization is carried out in the solvent. The solvent allows for the more efficient transfer of heat out of the system. However, care must be taken to ensure that the solvent will not react during the polymerization. This method is preferable when the formed polymer is to be used in solution. The hydrogel membranes described in this dissertation were prepared using the bulk technique.

### **II.1.2.2 Heterogeneous Polymerization**

Homogeneous polymerization is used to produce large masses of polymer, while heterogeneous polymerization is used to produce smaller beads of polymer. Examples of this type of polymerization include suspension, emulsion and dispersion polymerization. This is known as a heterogeneous technique since two distinct phases are present. In emulsion polymerization, the initial reaction mixture consists of two phases. Dispersion polymerization starts with a homogeneous solution that becomes heterogeneous as the reaction proceeds and the polymer precipitates out.<sup>40</sup> In these types of polymerization, the monomer is suspended in a solvent along with the initiator and a stabilizer. Instead of forming a mass of polymer suspended in the solvent as in bulk techniques, the stabilizer stabilizes the surface of the growing polymer in these systems and allows for the

formation of spherical polymer beads. The absence of a stabilizer would result in uncontrolled polymerization and produce coagulated masses of polymer.

The various heterogeneous techniques have been studied extensively to produce polymer microspheres for a wide range of potential industrial applications.<sup>41</sup> These polymers have been used in surface coatings and the paint industry and as chromatographic packing materials. Additional uses for microspheres include: use as a substrate for immunoassay, drug delivery and as a mask for photopatterning.<sup>42-44</sup> The method used for preparation of the microspheres is greatly influenced by the desired size of the particles. Table II.1 shows the size of particles produced by common polymerization techniques.

Table II.1 Comparison of Heterogeneous Polymerization Systems

<b>Process</b>	<b>Continuous Phase</b>	<b>Particle Size</b>
Emulsion	Water	0.1 – 0.3 $\mu\text{m}$
Dispersion	Organic	0.1 – 5.0 $\mu\text{m}$
Suspension	Water	10 – 500 $\mu\text{m}$



## **II.2 Dispersion Polymerization**

### **II.2.1 Background**

Dispersion polymerization is a method to produce particles in the 0.1 – 5.0  $\mu\text{m}$  size range. As shown in Table II.1, particles produced by this method are of a size between that produced by emulsion polymerization, at the lower size range, and suspension polymerization, at the higher size range. The particles are prepared in a method that is a modified precipitation polymerization.<sup>41</sup> The modification is the inclusion of a stabilizer that stabilizes the growing particles. Without the stabilizer, the particles grow to an uncontrolled size. The method was first described by Osmond et. al. and has been extensively reviewed by Barrett.<sup>40</sup>

In a dispersion polymerization the monomer, initiator and steric stabilizer are dissolved in a solvent to yield a homogeneous mixture. As the polymerization proceeds, the polymer precipitates out of solution and the mixture becomes heterogeneous. If left unstirred for a period of time, the particles will eventually settle out, although with agitation they will resuspend.

### **II.2.2 Components of Dispersion Polymerization**

A basic dispersion polymerization includes monomer, initiator, stabilizer and solvent. Comonomers, cosolvents and costabilizers may be included in the reaction mixture depending upon the desired product.

Each factor described below as well as temperature affects the final particle size. The general trends of changing one variable is fairly straight forward to hypothesize. However, due to the interaction of the different factors it can be difficult to easily predict how changing conditions will affect the final particle size.

### **II.2.2.1 Monomer**

The primary requirement for the monomer of a dispersion polymerization is that it be soluble in the solvent. A comonomer may be included to change the properties of the final particle. For example a more hydrophilic comonomer may be added to introduce greater hydrophilicity into the particle. The majority of work reported in the literature involves the use of styrene and methyl methacrylate, although a number of other monomers have been studied, particularly in the industrial setting.<sup>40</sup>

### **II.2.2.2 Solvent**

The solvent is perhaps better called a solvent/non-solvent. This is because the solvent should be a good solvent for the monomer, but a poor solvent for the polymer, so it will precipitate out of solution. The solvent must also dissolve the stabilizer and the initiator. All material initially added to the reaction vessel must be soluble in the solvent. While early work used predominately hydrocarbons and petroleum distillates as solvents, much of the more recent work has been done with alcohols. A cosolvent may be included to 'fine tune' the solvency of the system. This may be done to ensure that some initial component will dissolve in the solvent, or to influence the size at which the particles will precipitate out of solution.

### **II.2.2.3 Initiator**

The only requirement for the initiator is that it be soluble in the solvent. Initiators are most often thermal, with the majority being either the azo type such as AIBN, or a peroxide.

#### **II.2.2.4 Stabilizer**

An important requirement of the stabilizer, as with most components, is that it dissolves in the solvent. The purpose of the stabilizer is to stabilize the surface of the particle as it grows, thereby preventing the particle from coagulating. To be effective as a stabilizer, the material must be amphipathic, that is, contain two different segments. One segment must have a strong affinity for the polymer so that it will anchor itself in the polymer. The second segment should have a strong affinity for the solvent. These stabilizers can generally be divided into 3 classes: homopolymers, block and graft copolymers and macromonomers.<sup>41</sup> Homopolymers produce a graft copolymer, by a chain transfer with the growing oligomer. Block and graft copolymers already contain distinct chemical segments and macromonomers are able to copolymerize with the monomer to form a graft copolymer. The stabilizer type most often used is the homopolymer.

A costabilizer may also be included. These are typically low molecular weight ionic surfactants.<sup>41</sup> Used alone, they will not produce stable particles. In some cases they are necessary to produce monodisperse particles. The usefulness of these compounds is a matter of debate, with many workers finding they have no effect. Since no costabilizers were used in this work they will not be discussed further.

#### **II.2.3 Formation and Growth of Particles**

The process of dispersion polymerization can generally be described as follows. The initial reaction mixture is a homogeneous mixture of monomer, solvent, stabilizer and initiator. At this stage the mixture is clear. As the mixture is heated with stirring, it begins to turn slightly opaque as the polymer begins to form.<sup>40</sup> After several minutes the

solution turns completely opaque white as the polymer precipitates out of solution. The reaction is then allowed to proceed for several hours to ensure a high conversion.

This process can be broken down into several intermediate steps described below and shown in Figure II.2. The polymerization starts with a homogeneous mixture of monomer, solvent, stabilizer and initiator. The mixture is heated, activating the initiator that begins to form free radicals. Free radicals begin reacting with the monomer and grow into oligomers. Propagation of the reaction continues with the addition of more monomer units until a critical chain length is reached and the oligomers precipitate out of the solvent as nuclei. Initially the nuclei are not colloidally stable. The nuclei condense into a spherical form to limit the exposed surface area. Stabilizer is then adsorbed into the polymer and resulting in a stabilized nuclei. Prior to the adsorption of the stabilizer, nuclei may collide with other nuclei forming a larger particle through a process known as homocoagulation. Following the appearance of the stable nuclei, the particle can grow by one of several methods. Growing oligomers can be captured by the particle or be stabilized to form a new particle. The monomer can also diffuse into the particle and propagate within the particle. The particle may also grow by heterocoagulation. This process is similar to homocoagulation, except instead of two nuclei colliding, a nucleus collides with a stabilized particle. Particles must be of a certain size in order for this process to occur, since the stabilizer units must be separated by a sufficient amount to allow the nuclei to reach the surface of the particle. As the particle grows the surface area increases and the distance between nearby stabilizer units is increased. The nucleation stage of the polymerization continues until the oligomers are captured by a particle before reaching the critical chain length to precipitate out of solution. The

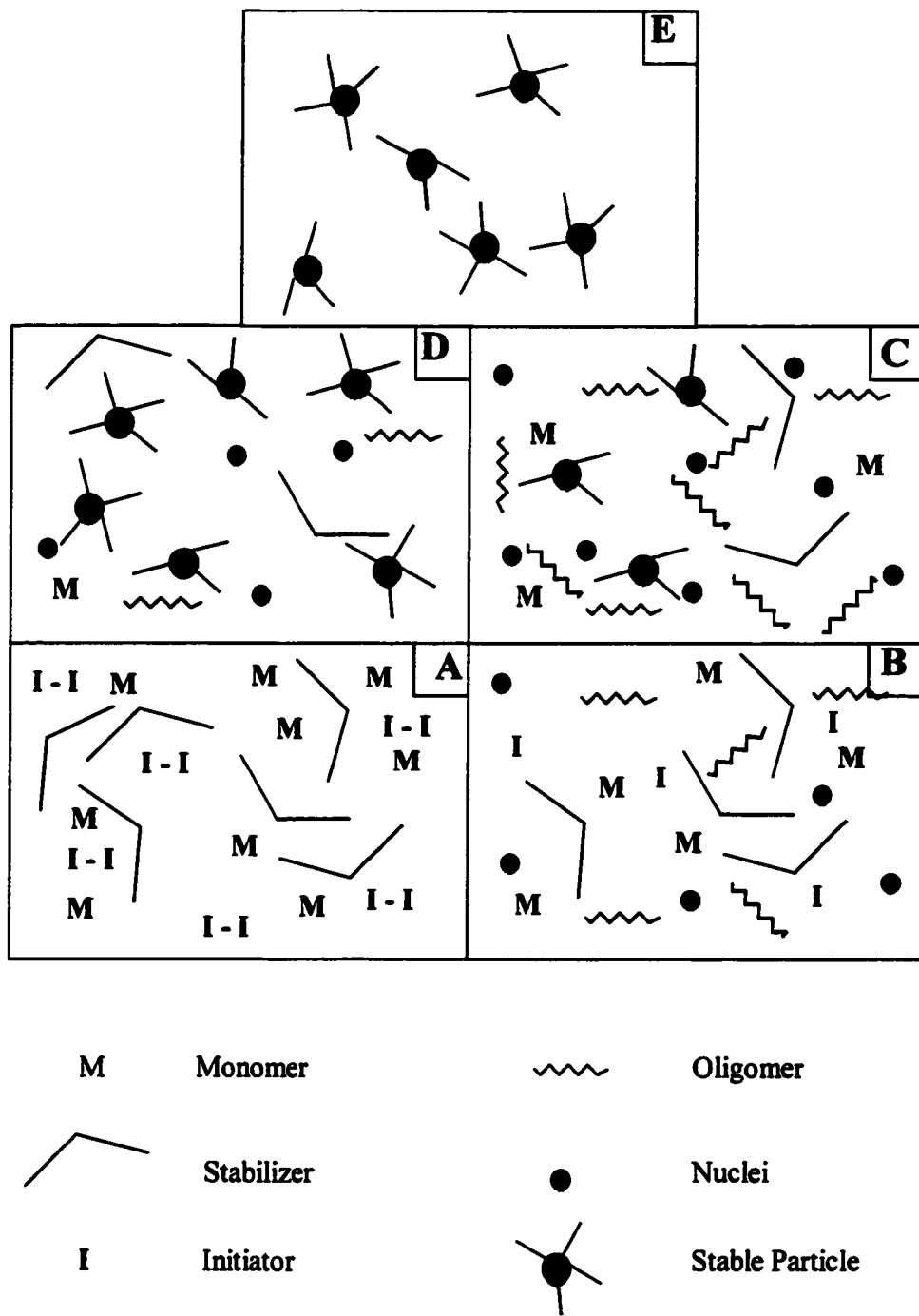


Figure II.2. Schematic of particle growth by dispersion polymerization.<sup>41</sup>

polymerization process for particle growth terminates when the reaction is cooled or the monomer supply is consumed.

### **II.3 Seeded Emulsion Polymerization**

This technique, which has also been known as the Norwegian method,<sup>45</sup> is used to produce particles with sizes between dispersion and suspension polymerization. The polymerization takes place in an aqueous dispersion. The method of seeded polymerization uses a “seed” template that dictates the shape of the final polymer particle. In order to prepare monosized particles, it is necessary to begin with monodisperse seed particles. Seed particles are swollen with monomer prior to polymerization. The process can be repeated several times in order to obtain particles with the desired size. Uglestad has reported volume increases of 1000 times.<sup>45</sup>

The technique used involves two steps. Monodisperse particles are prepared for use as the seed particles. Typical initial seed sizes are around 0.5  $\mu\text{m}$ .<sup>46</sup> The first step involves swelling the seed particles, which facilitates the transfer of monomer into the particle. This step is referred to as “activating” the seed. The swelling agent is a low molecular weight compound that is water insoluble. Swelling must be uniform in all seed particles to ensure that monodispersity is maintained.<sup>47</sup> The second step involves the addition of monomer, crosslinker, initiator and solvent. This mixture is added as small emulsions in water to aid in the transfer of the mixture into the swollen seed particle. Polymerization is initiated after allowing time, approximately 12 - 24 hours, for the monomer mixture to diffuse into the particle. Diffusion of the monomer mixture into the seeds is enhanced by phase separation, resulting from the aqueous dispersion medium. All of the desired components are in the swollen seed particle when polymerization is

initiated. A surfactant is used to stabilize the particles as they grow and to prevent the formation of new particles.

Porous particles in this size range are useful for a number of applications such as ion exchangers, chromatographic supports, catalytic supports, and size exclusion chromatography.<sup>47</sup> Multiple swelling steps have been used to create porous particles of larger size for use in chromatographic columns.<sup>48</sup> Uglestad has used the method to produce macroporous poly(styrene -divinylbenzene) beads with diameters of 5, 10 and 20  $\mu\text{m}$ .<sup>49</sup> The Frechet group has used the method to prepare beads in a similar size range using styrene and methyl methacrylate.<sup>50</sup> Monodisperse particles in the 4.1 - 7.5  $\mu\text{m}$  range have been reported using a single step swelling and polymerization process.<sup>51</sup>

## **II.4 Hydrogels**

Hydrogels are polymer membranes with high degrees of hydrophilicity. When equilibrated in water these polymers take up large volumes of water, but retain their original shape. Naturally occurring hydrogels are found in the cartilage and muscles of living creatures. A number of synthetic hydrogels also exist, the predominant example being hydroxy(ethyl) methacrylate(HEMA). Hydrogels are often used for biological applications, since many are biocompatible. The use of hydrogels for biocompatibility can be traced to Wichterle who described the use of poly(HEMA) membranes.<sup>52</sup> Various devices such as drug delivery systems, catheters, and electrodes incorporate hydrogels to make the device better suited for use in biological systems. The material is also used in the fabrication of soft tissue replacement and as soft contact lenses.<sup>53</sup>

The water content of hydrogels can vary from around 30 % to over 90 % by weight.<sup>53</sup> In a hydrogel, water acts as a plasticizer, transport medium, and provides a

connection between the membrane and biological systems.<sup>54</sup> The amount of water uptake and the mechanical properties of the hydrogel are highly influenced by the amount of cross-linking present. The greater the crosslinking, the lower the water content and the increased rigidity of the membrane. The other factor affecting the water content of the hydrogel is the monomer components making up the hydrogel. The hydroxyalkyl methacrylates and acrylates are among the largest group of hydrogels. The acrylate is more hydrophilic than the corresponding methacrylate, due to the increased hydrophobicity imparted by the methyl substituent group. The hydrophilicity of a membrane can be adjusted to some degree by forming copolymers using monomers with different degrees of hydrophilicity. Davies describes a 25 % decrease in the water content of a HEMA membrane, when the formulation includes 30 % styrene.<sup>54</sup> Hydrogels can be prepared by a heterogeneous or homogeneous process. Homogeneous polymerization is the most prevalent, with membranes being prepared using bulk polymerization. The use of heterogeneous polymerizations to produce beads of hydrogels has also been reported.<sup>55,56</sup>

The use of hydrogels in chemical sensors has usually been limited to that of a coating or an immobilization substrate.<sup>3</sup> The use of hydrogel as the actual sensing layer has been reported as well.<sup>57,58</sup> Hydrogels with an amine group are sensitive to pH and have been coupled to a variety of sensing strategies.<sup>57-60</sup> The primary advantage of hydrogels for sensing is that the high water content of the membrane allows for more rapid diffusion of aqueous analyte, compared to more hydrophobic membranes. Another advantage of using a functional hydrogel component is the elimination of a secondary



derivatization step to introduce that functionality. Molecular imprinting has also been used to introduce functionality for sensing.<sup>58</sup>

An additional characteristic that makes hydrogels well suited for chemical sensing is the ability to couple the hydrogel to substrates, particularly glass, through silane chemistry. Hydrogels also exhibit tolerance to a wide range of pHs when a pH functional constituent is not present. Hydrogels such as HEMA and HEA show no response to different pH solutions. When used with embedded polymer beads for sensing as part of a FOCS, the high water content of the hydrogels enables a larger signal to be observed, since the difference in refractive indices between the suspended beads and the hydrogel is large.

## **II.5 Theory of Fiber Optics**

Fiber optics are cables that transport light much the way electric cables transport electricity. Originally developed for the communications industry, they have proven themselves to be extremely useful in the construction of chemical sensors and instrumentation.<sup>61</sup> Light sent into one end of the fiber will be transported to the other end. The fibers are small and flexible, allowing light to be sent in any direction, around corners or into very small spaces. One of the primary advantages of fiber optics is that they are not affected by electrical interference, which can disrupt or distort electrical signals. Optical fibers have three basic components: core, cladding and buffer, see Figure II.3. In most cases, the core is composed of glass, plastic or a glass-plastic composite. The refractive index of the fibers can be tuned by the use of dopants such as  $B_2O_3$  and  $GeO_3$ . Surrounding the core is the cladding, with a refractive index of  $n_2$ , which is lower than the core refractive index of  $n_1$ . The primary role of the cladding is to cause internal

reflection at the interface with the core as light propagates through the fiber without loss. The cladding also serves to protect the fiber from shocks and strengthens the fiber. Enclosing both the core and the cladding is the buffer, which adds additional mechanical strength.

Optical fibers can be classified using two classification systems.<sup>62</sup> The first is based on the refractive index profile of the fiber, see Figure II.4. Step-index fibers, have an abrupt change in the refractive indices between the core and the cladding. The second type of fiber is graded-index, where there is a gradual change in refractive indices between the core and the cladding. The second classification system is based on the number of modes a fiber can transmit. Single mode fiber can transmit only one mode, while multi-mode fiber is capable of transmitting multiple modes.

The amount of light entering the fiber is governed by the numerical aperture, NA. This describes the cone of light that is accepted into the fiber. The NA is related to the refractive indices of the core and the cladding,  $n_1$  and  $n_2$  respectively, by equation 1.

$$NA = \sqrt{n_1^2 - n_2^2} \quad (1)$$

In order for light to be transmitted through the fiber, it must undergo total internal reflection. This occurs when light is reflected at an interface of a material having a lower refractive index, provided that the incident light strikes the interface at an angle greater

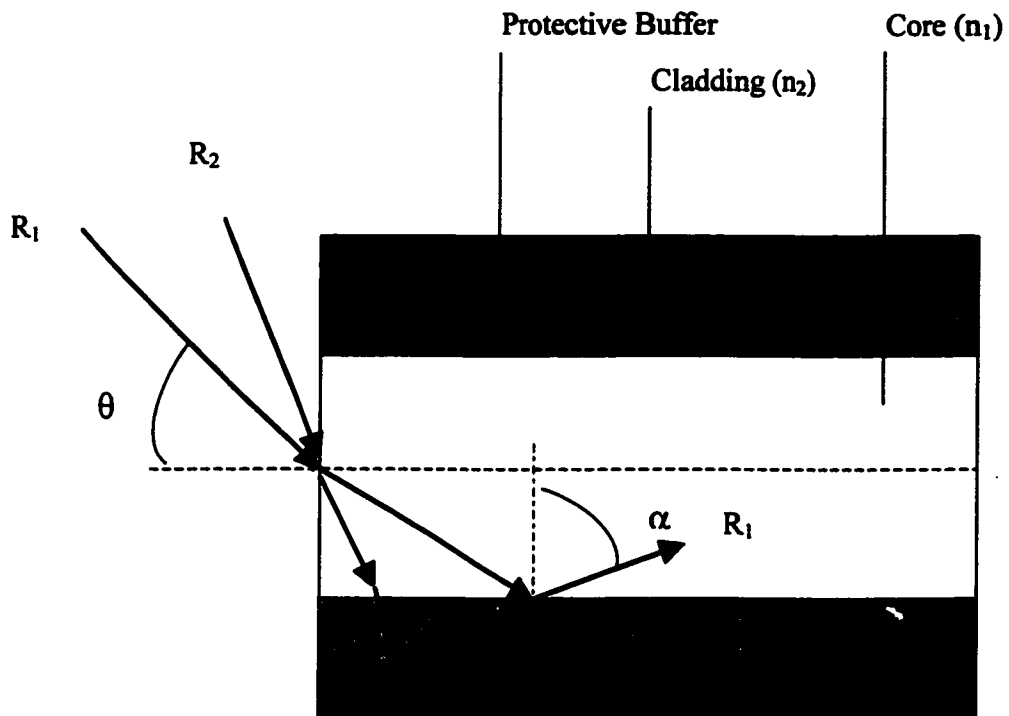
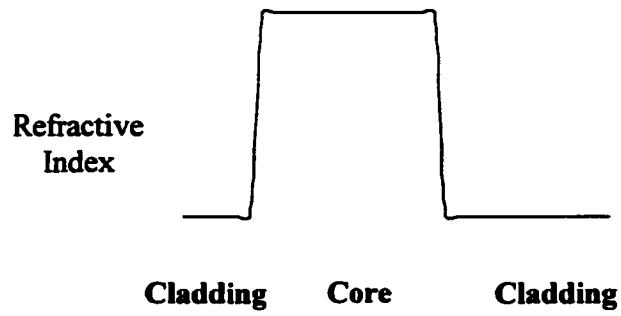
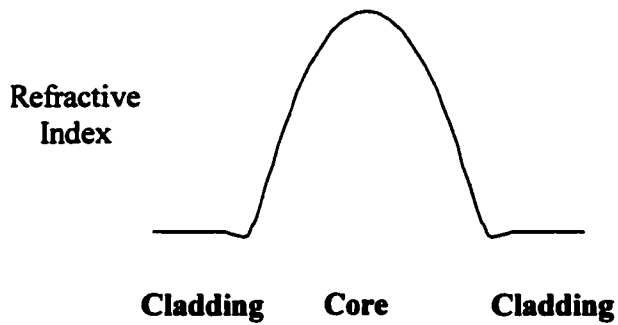


Figure II.3. Schematic of optical fiber showing light transmittance by total internal reflection. Total internal reflection will occur when the incident angle of light,  $\theta$ , is greater than the critical angle,  $\alpha$ . R<sub>1</sub> is incident at an angle greater than  $\alpha$  and will be internally reflected. R<sub>2</sub> is incident at less than  $\alpha$  and will refract into the cladding and not be propagated.



**A. Step-Index Fiber**



**B. Graded-Index Fiber**

**Figure II.4. Refractive Index Profiles of Step-Index and Graded-Index Optical Fiber**

then the critical angle, see Figure II.3. The critical angle is related to the NA of the fiber and the refractive index of the medium where the measurement is made, typically air,  $n_0$ , by equation 2.

$$NA = \sin(\theta_C) n_0 \quad (2)$$

## II.6 Optical Measurements by Light Scattering

A hydrogel membrane embedded with polymer microspheres becomes less opaque when the microspheres are swollen. This phenomenon can be exploited for chemical sensing. The turbidity of a material is a measure of how much light is scattered by that material. In the context of this dissertation, that material is the hydrogel with embedded particles. Turbidity is analogous to absorbance, except that transmitted intensity is decreased by particles scattering light, rather than absorbing the light. The turbidity of a solution is related to the measured light intensity passing through a membrane, as shown in equations 3 and 4:<sup>63</sup>

$$I = I_0 e^{-\tau b} \quad (3)$$

where,

**I** = intensity of light transmitted

**I<sub>0</sub>** = intensity of light

**τ** = turbidity

**b** = pathlength

Rearranged to solve for turbidity:

$$\tau = \left( \frac{2.303}{b} \right) \log \left( \frac{I_0}{I} \right) \quad (4)$$

The scattering and reflection observed are caused by changes in the refractive index of the microsphere as it swells and shrinks. The refractive index of the microspheres changes while the refractive index of the hydrogel remains constant. When swollen, the microspheres have a higher water content that lowers the effective refractive index of the particle. The amount of light reflected at the interface of materials with two different indices is defined by Fresnel equation for normal incidence:<sup>64</sup>

$$R(\lambda) = \left( \frac{n_2 - n_1}{n_1 + n_2} \right)^2 \quad (5)$$

The larger the difference between the indices, the larger the observed reflection.

The observed reflection is also dependent on the size of the particles. The larger the microsphere, the larger the amount of scattering. This is the result of particles occupying more of the area exposed to the transmitted light as it travels through the membrane. In the system observed in this work, the refractive index effects are the dominant cause of change in reflection.

## II.7 Polymer Swelling

The phenomenon exploited for use in the sensors described is polymer swelling. Cross-linked polymers will swell when placed in a compatible solvent. Polymer swelling can be classified as ionic or non-ionic. Ionic swelling results from charge accumulation on the polymer, while non-ionic swelling is caused by absorption of solution by the polymer.

### II.7.1 Non-Ionic Polymer Swelling

Non-ionic polymer swelling is more general and not utilized as the basis for sensing in this dissertation. When placed in a compatible solvent a polymer will absorb some of the solvent and the polymer will swell. If a linear polymer is placed in a compatible solution, it will dissolve forming a polymer solution. Polymers that have been crosslinked will not dissolve in solution. The crosslinks will allow swelling to occur to the point at which the swelling force is counteracted by the restraining force of the crosslinks. In his classic text on polymers, Flory derives equation 6 to describe this process:<sup>65</sup>

$$q_m^{5/3} = \frac{(\bar{v}M_c) \left(1 - \frac{2M_c}{M}\right) \left(\frac{1}{2} - X_1\right)}{V_1} \quad (6)$$

where,

$q_m$  = equilibrium swelling ratio,  $V/V_0$  volume swollen to volume unswollen

$\bar{v}$  = specific volume of the polymer (l/g)

$M_c$  = molecular weight per crosslink unit (g/mole)

$M$  = molecular weight of the polymer network (g/mole)

$X_1$  = interaction parameter – characterizes interaction free energy divided by  $kT$  for the solvent with polymer, represents the affinity of polymer for solvent  
 $V_1$  = molar volume of solvent (l/mole)

The equation depicts the inverse relationship between crosslinking level and swelling. As the degree of crosslinking is increased, the molecular weight per crosslink will be decreased, as will the swelling ratio. As the polymer's affinity for a solvent is increased, the swelling ratio will also increase. The second term in the equation,  $(1-2M_c/M)$ , is a correction term, that accounts for the effect of chain ends on the polymer network.

### **II.7.2 Ionic Polymer Swelling**

The phenomenon of ionic polymer swelling is utilized for the purpose of chemical sensing in this dissertation. Ionic swelling is the result of charge build up on the polymer. The accumulation of charge on the polymer results in electrostatic repulsion to separate the charges, causing the polymer to swell. Swelling allows the polymer to increase the distance between the charges and minimize the charge interaction. This can be used for chemical sensing when a charge builds up with changing analyte concentration. For the work described in this dissertation, changes in swelling are due to protonation as a result of changing solution pH. The ability to accumulate charge was accomplished using dimethyl amino ethylmethacrylate or by derivatizing poly(vinylbenzyl chloride) with diethanolamine. In both situations this introduces an amine functionality, which will become protonated when placed in an acidic environment. Equation 7 was developed by Flory to describe ionic polymer swelling:<sup>65</sup>



$$q_m^{5/3} \cong \frac{\left[ \left( \frac{i}{2V_u \sqrt{S}} \right)^2 + \frac{\left( \frac{1}{2} - X_1 \right)}{V_1} \right]}{\frac{v_e}{V_o}} \quad (7)$$

where,

- $q_m$  = equilibrium swelling ratio
- $i$  = number of electronic charges per polymer unit
- $V_u$  = molecular volume of polymer repeating unit (l/mole)
- $S$  = molar ionic strength (mole/l)
- $X_1$  = interaction parameter
- $V_1$  = molar volume of solvent (l/mole)
- $v_e$  = effective number of chains in the network
- $V_o$  = unswollen network volume (l/mole)

The equation shows that the greater the number of charged sites, the greater the degree of swelling. More potential sites allow for a greater charge accumulation.

Related to this is the ionic strength of the solution. The affinity of the polymer for the solvent is seen again. The divisor term is another correction factor, designed to compensate for the effect of polymer chain ends.

There are two descriptions for ionic polymer swelling. The first is the electrostatic, or repulsion, argument. The polymer swelling is explained as a response to maximize the distance between the like charges that have accumulated on the polymer. Higher ionic strength solutions will tend to mask the charges, which will result in a lower degree of swelling. The second is that the swelling is caused by osmotic pressure. As the polymer accumulates charge, the charge density of the polymer increases. If the charge

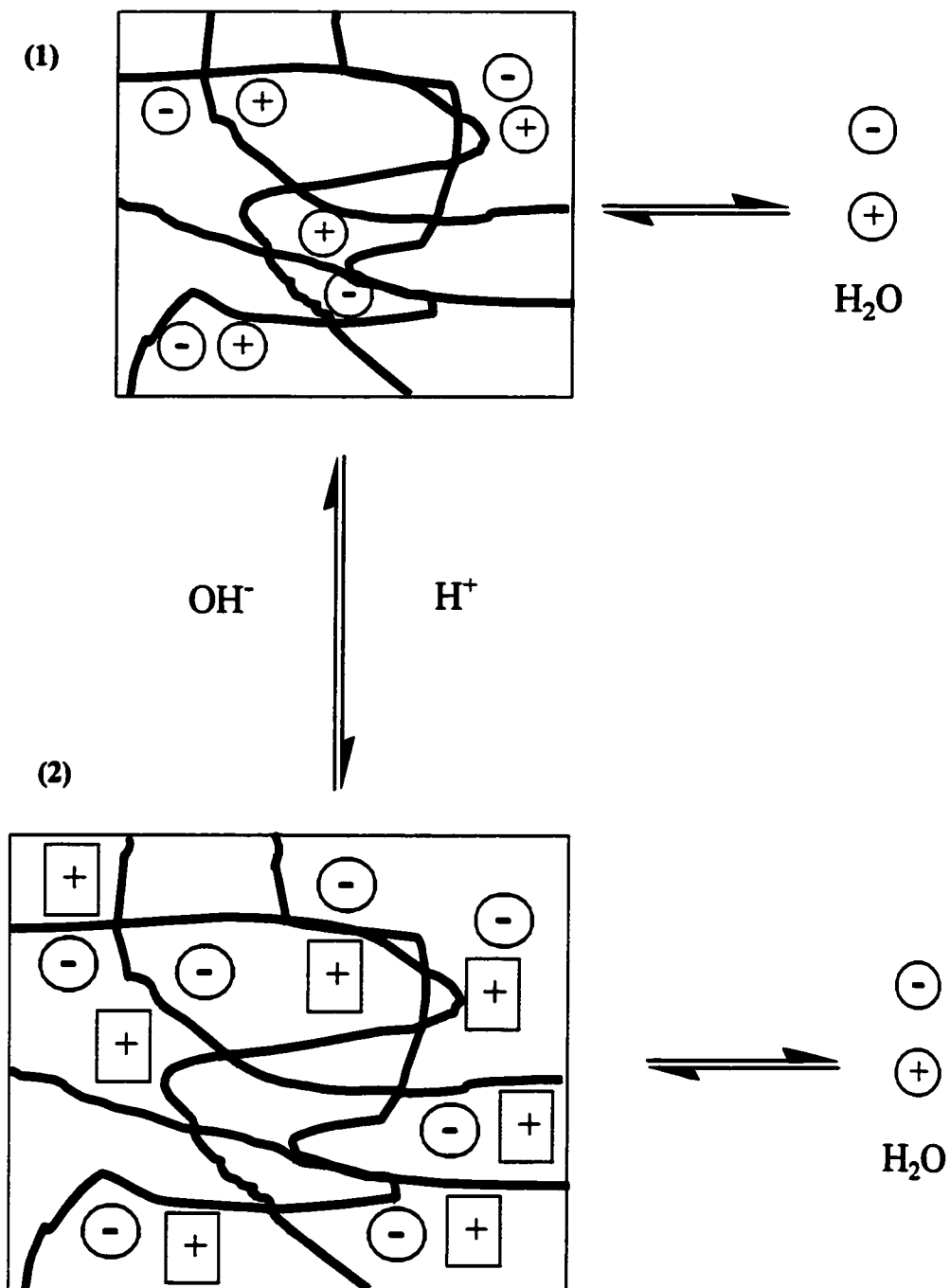


**Figure II.5.** Schematic showing ionic polymer swelling. (1) illustrates unswollen polymer, (2) illustrates swollen polymer. Circles represent mobile charge in solution. Squares represent charges fixed on the polymer backbone.

density is greater than that of the surrounding solution, the solution will enter the polymer to restore equilibrium. The influx of solution will cause the particle to swell. If the charge density of the polymer were lowered below that of the solution, then the solution would move out of the polymer and it would shrink

The phenomenon of ionic polymer swelling is shown in Figure II.5. In (1) the polymer is in its unswollen state. In (2) the polymer is swollen after protonation of the amine sites.

## **II.8 Porosity**

A major problem the research group has had in using poly(VBC) for sensing has been response time. One of the major factors affecting this is the porosity of the polymer. A polymer with a high degree of porosity allows the analyte solution to diffuse more easily into the polymer, leading to a shorter response time. Porosity can be introduced into the polymer by including a porogenic solvent, or diluent, into the polymer formulation. This solvent occupies space during the polymerization, but is not polymerized itself. Following the polymerization, the diluent is removed and the space it occupied becomes pore space. Formation of pore space is dependent upon a sufficient level of crosslinking to prevent the pores from collapsing. Pores produced in this manner are true pores and are known as macroreticular pores.<sup>66</sup> Pores that exist only when the diluent is present are known as microreticular pores.

The pores are formed through the use of diluents, which are either 'good' or 'poor' solvents for the forming polymer. 'Poor' solvents were found by Millar to be unable to solvate the polymer.<sup>67</sup> These solvents had structures that were different from that of the polymer. As the polymer formed, the 'poor' solvent would phase separate

from the polymer. This caused the polymer to be formed with macropores and highly tangled polymer chains. A 'good' solvent will solvate the growing polymer chains, keeping them extended and untangled, forming a polymer with micropores.<sup>68</sup>

Another method to introduce porosity was used in the dispersion polymerization of poly(VBC-co-TCPA) beads. Rather than using a solvent to introduce porosity a TCPA component was included in the polymerization. When derivatized, the phenol ring system is displaced by the amine. The amine is much smaller than the phenol ring and the excess space becomes pore space. In this method, a physical process is used to form the pore after the polymerization is complete, rather than occupying space as the polymerization proceeds. Making the polymer backbone more hydrophilic also creates porosity. A more hydrophilic backbone will enhance water diffusion into the polymer, which will occupy volume in the polymer and create pore space.

The high water content of hydrogels makes the problem of porosity non-critical in their use described here. An aqueous analyte will be carried into the membrane by the water as it diffuses through the membrane.

## **II.9 Surface Plasmon Resonance**

The phenomenon of surface plasmon resonance (SPR) has been known since the early 1900's, but it is only since the 1960's that the usefulness of SPR has been begun to be exploited.<sup>64</sup> Surface plasmons (SP) are fluctuations of surface charge density that propagate along the surface of a metal.<sup>69</sup> These fluctuations are encountered at the surface of a metal and at dielectric interfaces. Typically SP are generated in a metal film which is surrounded by two dielectrics. One dielectric is the waveguide material and the

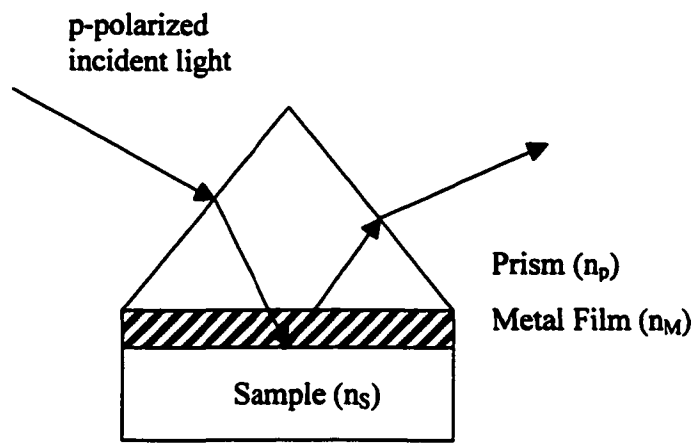


Figure II.6. Kretschmann prism arrangement for coupling light into surface plasmons.<sup>70</sup>

other is the sample of interest. The generation of surface plasmons with light is usually accomplished using the Kretschmann arrangement, see Figure II.6. In this arrangement, light travels through a prism, acting as a waveguide, and strikes the metal layer at an angle. Light incident to the metal at the appropriate angle will result in the generation of a SP. At all other angles the light will be reflected. In order to induce a SP, the light must be *p*-polarized, because this light has the electric field vector oscillating normal to the plane of the metal film. The generated SP decays exponentially as it travels away from the surface, making the system a surface limited measurement. This eliminates bulk solution effects on the measurement. However, refractive index changes at the surface can be readily observed.

The refractive index of the sample can be related to the angle of incidence by considering the equations for the wavevectors.<sup>70</sup>

$$k_l = \frac{2\pi}{\lambda} n_p \sin(\theta) \quad (8)$$

where:

$k_l$  = wavevector of light  
 $n_p$  = refractive index of prism  
 $\lambda$  = wavelength of light  
 $\theta$  = angle of incidence of light

$$k_{sp} = \frac{2\pi}{\lambda} \sqrt{\frac{n_M^2 n_S^2}{n_M^2 + n_S^2}} \quad (9)$$

where:

$k_{sp}$  = wavevector of SP  
 $n_M$  = refractive index of metal  
 $n_S$  = refractive index of sample

Surface plasmon resonance will be produced when the two wavevectors match. This occurs when  $k_i = k_{sp}$ . Solving for  $n_s$ , the following expression is obtained:

$$n_s = \frac{n_p^2 (\sin(\theta))^2}{n_M^2 - n_p^2 (\sin(\theta))^2} \quad (10)$$

This shows that the refractive index of the sample is related to the refractive index of the metal layer, the refractive index of the prism and the angle of incidence. Therefore the measured refractive index of the sample is related to the angle of incidence of the light.

SPR can be adapted to a variety of sensing applications. Refractive index detection in HPLC using an SPR system in place of a refractive index detector has been demonstrated.<sup>71</sup> The majority of uses for SPR have been in the field of biosensors. The use of SPR for biosensing has been the focus of several reviews and book chapters.<sup>70,72</sup> Screening assays for morphine and syphilis have been demonstrated using SPR devices.<sup>73,74</sup> Multisensing of four immunoreactions simultaneously in real time has been shown to be a rapid way of monitoring immunoreactions.<sup>75</sup> Fiber optic SPR devices have also been developed which allow for remote monitoring applications.<sup>76</sup> The use of gold as a metal layer makes SPR especially suited for biosensing. The gold layer can be readily coated with recognition sites using attachment through thiols. Antibody/antigen receptors are especially suited for this and a method for attaching recognition sites using a gold-binding polypeptide has been described.<sup>77</sup> A number of companies including Pharmacia Biosensor and Texas Instruments have developed commercial instrumentation for SPR sensing.

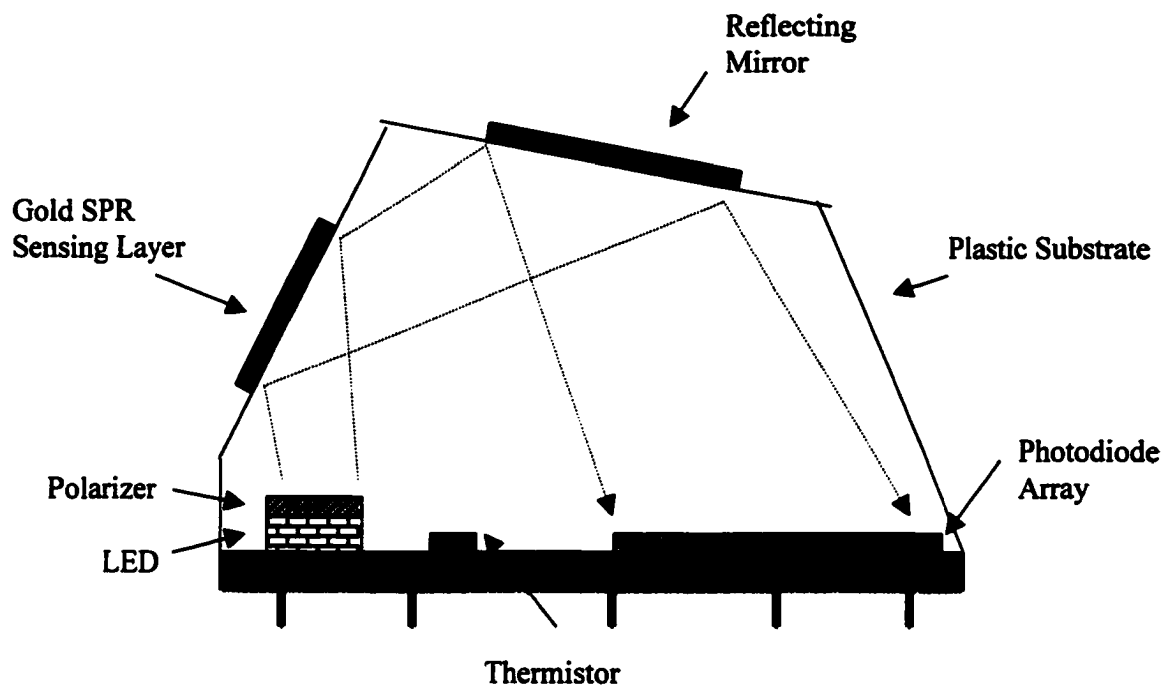


Figure II.7. Schematic of Texas Instruments Spreeta SPR Device.<sup>78</sup>



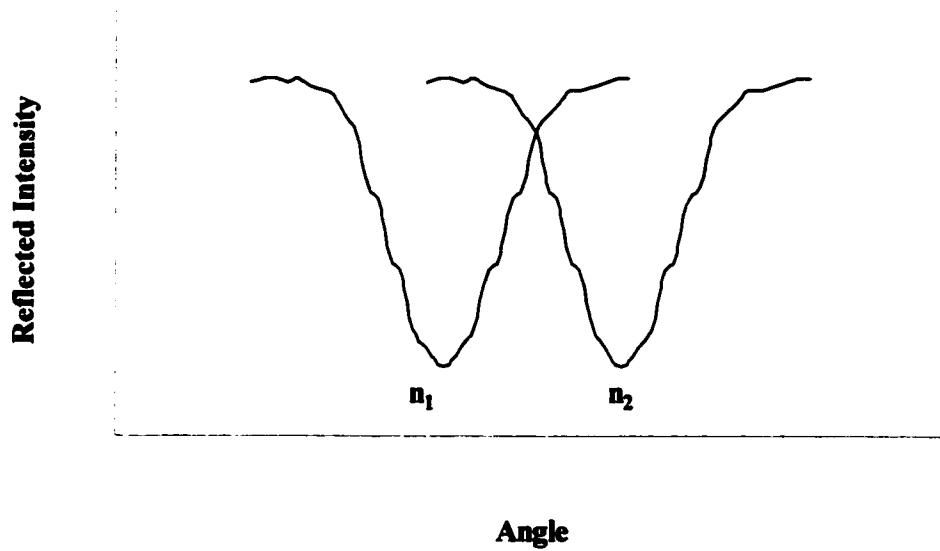


Figure II.8. Sample SPR Curves at two refractive indices ( $n_1 < n_2$ )

The work described in this dissertation made use of the Texas Instrument Spreeta SPR system. This device consists of an integrated system that includes all components mounted onto a base, see Figure II.7. The light source is a near-infrared LED, which passes through a polarizer and onto the sensing area. The orientation of the sensing area is such that a range of incident angles illuminates the area. Reflected light is directed onto a photodiode array by a gold reflecting mirror. Each pixel of the detector corresponds to a particular incident angle. The angle at which SPR was initiated will correspond with a minimum of light intensity, this can then be related back to the refractive index of the sample. This is shown in an idealized fashion in Figure II.8. The angle of minimum reflection is observed, as is the shift in angle that accompanies a refractive index change.

## **II.10 Magnetic Sensing**

A new type of chemical sensor was evaluated in this dissertation. The sensor has the advantage that no physical connection between the sensor and the detection electronics is required and no line of site as with laser telemetry is required. In addition, the sensor does not need to be connected to any external power source. This allows the sensor to be placed in enclosed or opaque containers, which are completely isolated from the outside environment. This type of sensor has been identified as a magnetochemical sensor. The measurement of a chemical parameter is conducted using magnetic fields to interrogate the sensor.

Detection of the magnetochemical sensors was carried out using two different sensing strategies. The first was a measurement of the degree of magnetic coupling between two layers of magnetic thin films separated by a non-magnetic sensing layer.

The second was the measurement of the resonance frequency of a magnetoelastic ribbon. Detection in both strategies involved the application of an alternating magnetic field, however the parameters examined were quite different.

### II.10.1 Magnetostatic-Coupling Sensing

The magnetostatic design makes use of switching the magnetization vector of magnetic layers which are separated by a non-magnetic sensing layer, a swellable polymer, see Figure II.9. When the sensor is placed in a sinusoidal magnetic field the magnetization vector will change orientation to follow the applied magnetic field. This will generate a voltage in the detection coils in accordance with Faradays Law:

$$V = -\frac{d\Phi}{dt} \quad (11)$$

Where:

V = induced voltage  
dΦ = total magnetic flux  
dt = time

The magnetic flux(Φ) is defined as the magnetic flux density(B) times the area of the detection coil(A).<sup>79</sup>

$$\Phi = BA \quad (12)$$

The flux density is a combination of the flux of the applied magnetic field and the flux caused by the magnetization of the material. For interrogation, the sensor is placed between two sets of detection coils. The first set imparts the sinusoidal magnetic wave

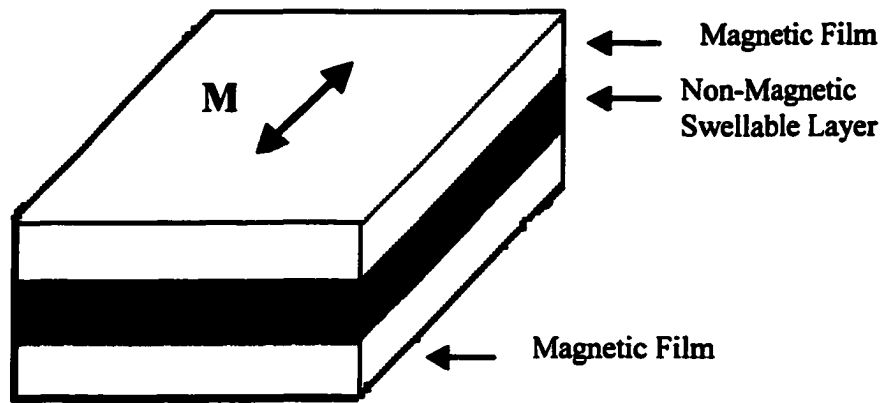


Figure II.9. Schematic of Magnetostatic-Coupled Chemical Sensor  
 A swellable polymer layer separates two magnetic films.  
 'M' denotes the magnetization vector.

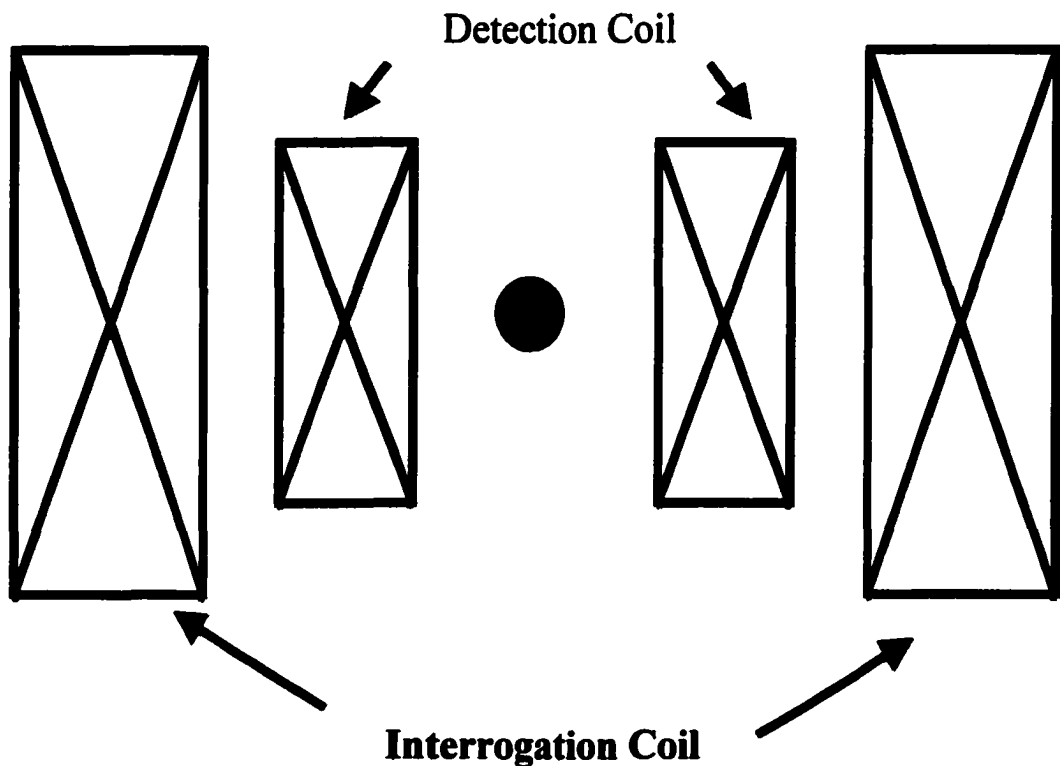


Figure II.10. Schematic of Magnetostatic-Coupled Chemical Sensor  
 The sensor shown above is positioned in the center of the coils.

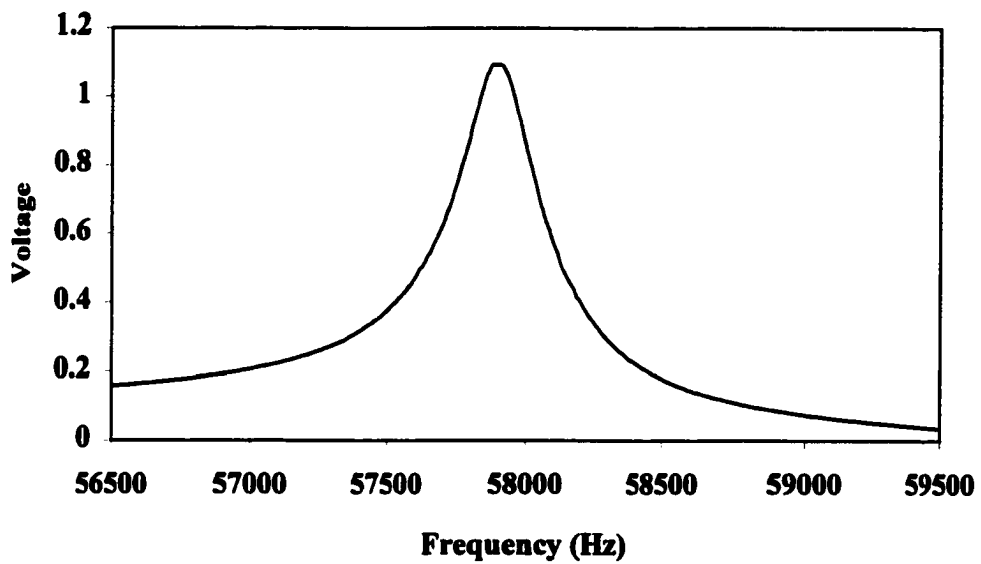


Figure II.11. Example of response of magnetoelastic ribbon in air. The frequency is that of the applied magnetic field.

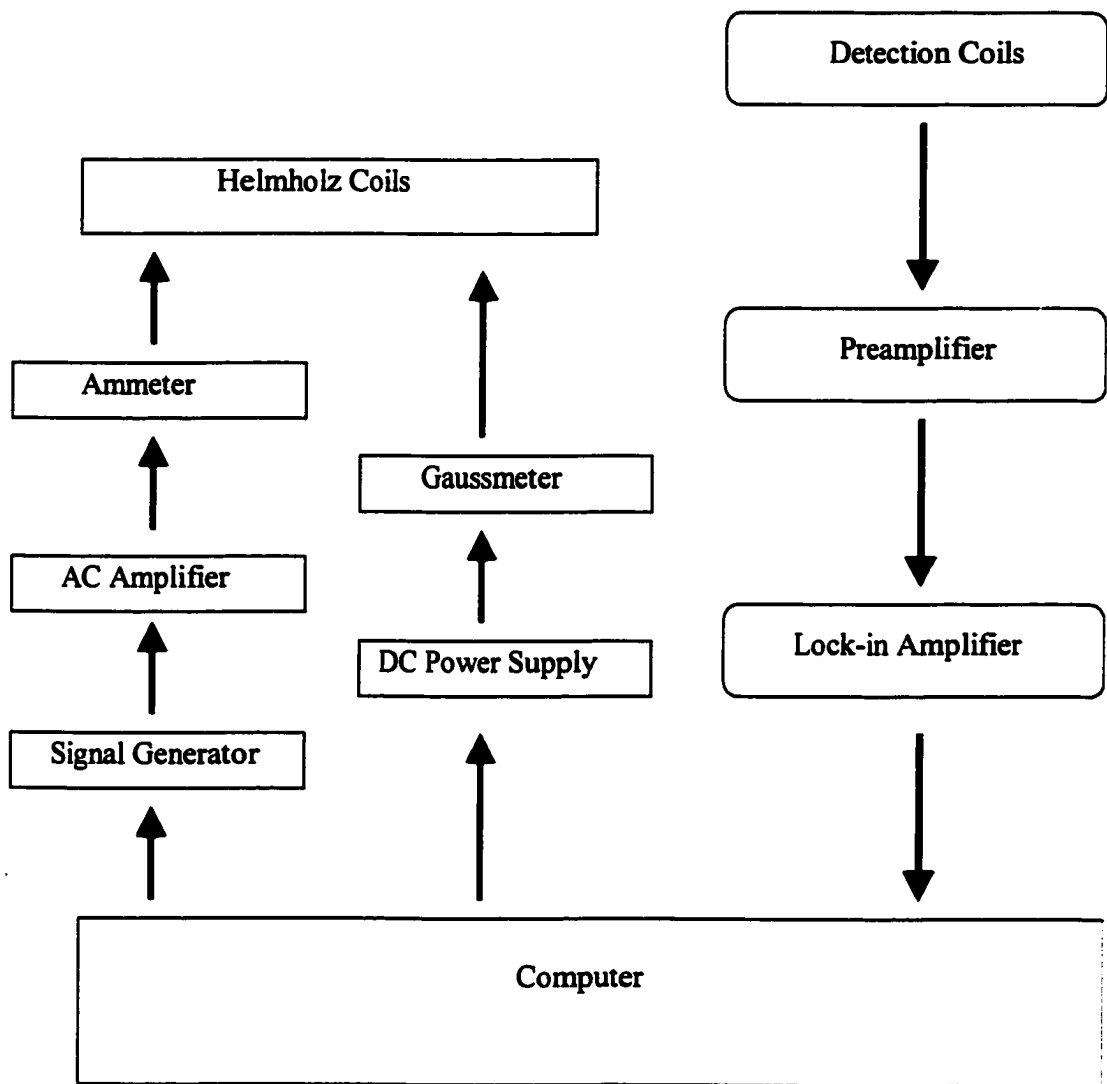


Figure II.12. Schematic drawing of magnetoelastic resonance meter.<sup>87</sup>

and the second set measures the induced voltage. This is shown schematically in Figure II.10.

In the ferromagnetic materials used in this work, the flux caused by the material is several thousand times larger than the flux caused by the applied magnetic field. When two magnetic film layers are used, the magnetization vectors will become coupled. The greater the degree of coupling, the easier it is for the orientation of the vectors to be changed. Greater coupling will yield a lower magnetic flux and therefore a lower induced voltage.<sup>80</sup> As the polymer swells and shrinks in response to the analyte of interest, the magnitude of the voltage will also change. The response will be a voltage spike with a magnitude that is a function of analyte concentration. The major disadvantage of this sensor design is that the magnetic material has a preferred axis of magnetization orientation, making the device anisotropic. The measured response is dependent upon the sensor orientation in the interrogation coils.

### **II.10.2 Magnetostrictive Sensing**

The magnetostrictive sensor is isotropic, i.e. the response is independent of sensor orientation in the detection coils. A magnetostrictive or magnetoelastic material is one which a mechanical vibration can be induced by exposure to an oscillating magnetic field. The material used in this dissertation was a metallic glass ribbon called Metglass<sup>TM</sup>.<sup>81</sup> Magnetostrictive devices are analogous to piezoelectric devices, with the difference being in the method the acoustic or elastic wave is initiated and measured. A piezoelectric device uses an electrical connection to create and measure the waves. A magnetostrictive device uses an ac magnetic field in place of the electrical signal. The technology exploited here is identical to that used for anti-shoplifting labels.<sup>82</sup> When

exposed to an ac magnetic field, the strip will vibrate in a longitudinal direction. A dc magnetic field is used to maximize and stabilize the signal. The field can be generated by the detection instrumentation or by a magnetic ribbon placed adjacent to the sensor strip. At the resonance frequency of the material there will be a maximum conversion of magnetic energy into vibrational energy. A sample output is shown in Figure II.11 and a schematic of the detection instrument is shown in Figure II.12.

Magnetostrictive devices, like their piezoelectric counterparts, are very sensitive to changes in mass and viscosity.<sup>83,84</sup> Selectivity for particular analytes can be introduced by the application of a selective material. A surface acoustic wave sensor for organic vapors in breath has been described.<sup>85</sup> The detection of immunoglobulin by a piezoelectric crystal has also been developed.<sup>86</sup> The use of magnetostrictive materials as sensors for viscosity monitoring has been reported.<sup>87-89</sup>

The fundamental resonance frequency of an unmodified strip can be described by the equation:<sup>87</sup>

$$f_0 = \sqrt{\frac{E}{\rho(1-\sigma^2)}} \frac{1}{L} \quad (13)$$

Where:

- E = Young's modulus of elasticity
- $\sigma$  = Poisson ratio
- $\rho$  = density of sample
- L = length of strip

Both mass added and solution viscosity can be related to the measured resonance frequency by the following equations.



For mass:<sup>87</sup>

$$\Delta f = -f_0 \frac{\Delta m}{M} \quad (14)$$

Where:

$\Delta f$  = frequency shift

$f_0$  = resonance frequency at zero viscosity(air)

$\Delta m$  = mass change

$M$  = mass of sensor

For viscosity:<sup>88</sup>

$$\Delta f = -\frac{\sqrt{\pi f_0}}{2\pi\rho d} (\eta \rho_l)^{1/2} \quad (15)$$

Where:

$\Delta f$  = frequency shift

$f_0$  = resonance frequency at zero viscosity(air)

$d$  = sensor strip thickness

$\rho$  = density of sensor strip

$\rho_l$  = density of liquid

$\eta$  = liquid viscosity

Both the addition of mass and an increase in solution viscosity will cause a decrease in the observed resonance frequency. By measuring the frequency shift, the added mass or the viscosity of the solution can be determined.

## II.11 Research Objectives

The goal of this research was to demonstrate the feasibility of a magnetochemical sensor and to examine the factors affecting the response time, magnitude and durability of the sensor. Alternative uses for the sensor in addition to chemical sensing were studied, such as using the magnetoelastic strips for viscosity measurements and

polymerization monitoring. The primary focus was on the use of swellable hydrogels for the substrate. A hydrogel used for the sensing layer should exhibit a large size ratio and be hydrophilic enough to allow for a rapid response time and be mechanically viable. Various sensor designs were examined in an attempt to determine the most viable arrangement. Adhesion of the hydrogel to the magnetic layer is also an important factor. The research also expanded to study the feasibility of using these hydrogels as an immobilizing membrane for the polymer microspheres used by the research group for optical sensing. The potential to use the developed microspheres for optical sensing as a sensing layer in the magnetochemical sensor was also investigated. This research for the magnetochemical sensor was interconnected with the work carried out for the optical sensor developed by the research group. An additional optical sensor based on SPR was also briefly investigated.

The use of a sensor in terms of selectivity and reproducibility was not examined, since the research was focused on development of a preliminary sensor design. The numerous sensor designs and sensing strategies used over the course of sensor development did not allow these parameters to be fully investigated.

Chapter III describes the experimental methods used to prepare the polymers. The instruments and procedures used to characterize and evaluate the polymers are also presented. The designs of factorial experiments are described.

Chapter IV describes the study of factors affecting the formation of functionalized hydrogel membranes. Factors affecting the size ratio and mechanical characteristics of the hydrogels were examined. Also studied were the factors affecting hydrogel adhesion to a glass surface using a silane.

Chapter V describes the factors affecting the formation of polymer microspheres by dispersion polymerization. The factors were examined to study their impact on the size and size distribution of particles produced.

Chapter VI describes the use of magnetochemical sensors. Various sensor designs were examined to study the robustness of the sensor. Factors affecting the use of a magnetoelastic strip sensor response were investigated.

Chapter VII demonstrates the ability to use a magnetoelastic strip to monitor polymerizations. The results are compared to traditional monitoring techniques, such as viscosity and spectroscopy.

Chapter VIII describes the use of polymer microspheres prepared by dispersion polymerization embedded in a hydrogel used as an optical sensor based on SPR. The response of dispersion microspheres in several hydrogels was examined to study the response time and response magnitude. The stability of microspheres prepared by seeded emulsion polymerization immobilized in a hydrogel was examined.

Chapter IX presents the conclusions from this research.

# CHAPTER III

## Experimental

### III.1 Reagents

#### Aldrich Chemical Company, Inc., Milwaukee, WI 53233

Acryloyl chloride F.W. 90.51, b.p. 72-76 °C,  
2,4,5-Trichlorophenol, F.W. 197.45, m.p. 67-69 °C  
Divinylbenzene (DVB), 55%, mixture of isomers, F.W. 130.19, b.p. 195 °C  
2,2'-Azobisisobutyronitrile (AIBN), 98%, F.W. 164.21, m.p. 103-105 °C  
2,2-Dimethoxy-2-phenyl-acetophenone (DMPAP), 99%, F.W. 256.30,  
m.p. 67-70 °C  
2-Hydroxyethyl methacrylate (HEMA), 97%, F.W. 130.14, b.p. 67 °C/3.5 mm  
2-Dimethylamino(ethyl) methacrylate (DMAEMA), 98%, F.W. 157.22,  
b.p. 182-192 °C  
Ethylene glycol dimethacrylate (EGDMA), 98%, F.W. 198.22,  
b.p. 98-100 °C/5 mm  
Diethanolamine, 99%, F.W. 61.08, b.p. 170 °C  
Dodecyl Sulfate, Sodium Salt, F.W. 288.38, m.p. 204-207 °C  
2-Hydroxyethyl acrylate (HEA), 96%, F.W. 116.12, b.p. 90-92 °C/12 mm  
Hydroxypropyl methacrylate (HPMA), 97%, F.W. 144.17, b.p. 57 °C/0.5 mm  
Hydroxypropyl acrylate (HPA), 95%, F.W. 130.14, b.p. 67 °C/5 mm  
Butyl methacrylate (BMA), 99%, F.W. 1142.2, b.p. 160-163 °C  
Methyl methacrylate (MMA), 99%, F.W. 100.12, b.p. 100 °C  
Poly(vinyl alcohol) (PVA), 100% hydrolyzed, average MW 14,000  
Poly(vinyl alcohol) (PVA), 87-88% hydrolyzed, average MW 85,000-146,000  
Poly(acrylic Acid) , (PAA) Av. MW 240,000, 25% solution in water  
Poly(acrylic Acid) , (PAA) Av. MW 40,000  
Poly(acrylic Acid) , (PAA) Av. MW 750,000  
Dichloromethane, 99%, F.W. 84.93, b.p. 40 °C  
Poly Ethylene glycol dimethacrylate (TEGDM), 98%, MW 330,  
b.p. >200 °C/2 mm  
Potassium Carbonate, 99%, F.W. 138.21, m.p. 891 °C  
Potassium Chloride 99%, F.W. 74.56, m.p. 770 °C  
Sodium Carbonate 99%, F.W. 105.99, m.p. 851 °C  
Sodium Hydrogen Phosphate 99.995%, F.W. 141.96,  
Sodium Sulfate 99.99%, F.W. 142.04, m.p. 884 °C  
Tetrahydrofuran (THF), F.W. 72.11, b.p. 65-67 °C  
Toluene, 99%, F.W. 92.14, b.p. 110.6 °C  
Vinyltrimethoxysilane 98%, F.W. 148.24, m.p. 129 °C

**Dow Chemical Company, Midland, MI 48674**

Vinylbenzyl chloride(VBC), Mixture of 3- and 4-isomers, F.W. 152.62,  
b.p. 229 °C

**EM Science, Gibbstown, NJ**

Sodium Sulfate  
Hydrochloric Acid, glacial

**Fisher Scientific, Fairlawn, NJ**

Acetone, F.W. 58.08, b.p 56 °C  
Gluteraldehyde, 50 % aqueous solution, F.W. 100.12  
Sodium Acetate, F.W. 82.03, m.p. 324 °C  
Sodium Chloride (NaCl), F.W. 58.44, m.p. 801 °C  
Calcium Chloride, F.W. 110.99

**Pharmco, Brookfield, CT**

Ethyl Alcohol, dehydrated, 200 proof

**Polyscience, Warrington, PA**

2,4,5-Trichlorophenol, F.W. 197.45, m.p. 67-69 °C  
Poly(Acrylic Acid), (PAA) Av. MW 450,000  
Poly(acrylic Acid) , (PAA) Av. MW 5,000, 50% solution in water  
Poly(acrylic Acid) , (PAA) Av. MW 50,000, 25% solution in water

**Schweizerhall, Inc., S. Plainfield, N.J. 07080**

Triethylamine, 99%, F.W. 101.19, b.p. 88.8 °C

**Sigma Chemical Company, St. Louis, MO 63718**

Polyvinylpyrrolidone (PVP), Av. Mol. Wt. 40,000

**VWR Scientific, San Francisco, CA**

Acetic Acid  
Ammonium Hydroxide

**Allied Signal, Santa Clara, CA**

Accuglass Spin-On-Glass 311

**Gelest, Tullytown, PA 19007**

Vinyl methoxy silane- homopolymer

Buffer solutions were prepared with concentrations of 0.1 M and ionic strengths  
of 0.1 M adjusted with NaCl, unless noted. Doubly deionized distilled water prepared

with a Corning Mega-Pure Distillation Apparatus was used in the preparation of all aqueous solutions.

## **III.2 Apparatus**

### **III.2.1 Instrumentation**

Scanning electron micrographs were obtained using an Amray 3300FE Scanning Electron Microscope. The nitrogen content of functionalized polymers was obtained with a Perkin-Elmer Model 2400 CHN analyzer. Polymers were characterized by FTIR on a Nicolet 520 spectrometer. An Orion 901 digital analyzer with an Orion 91/55 combination pH electrode was used to measure pH when buffer solutions were prepared. Microspheres were concentrated using a Fisher laboratory centrifuge (3400-rpm). Microspheres were resuspended using a Bronson Model 1210 sonicator. Photopolymerization was carried out under a 400 Watt UV lamp. Surface Plasmon Resonance (SPR) measurements were obtained using a Spreetra Evaluation Model Liquid Sensor donated by Texas Instruments. Turbidity was measured on a Cary 5 UV/Vis/NIR spectrophotometer, using 1 cm cuvettes. Magnetic resonance measurements were taken using a “home-built” magnetic resonance meter. Viscosity was measured with a Brookfield Model LV-DV-1 viscometer with the UL adapter. The refractive index measurements were made on a Baush and Lomb Abbe refractometer. X-ray photoelectron spectroscopy was conducted with a Kratos Axis HS XPS. Spin coating was done using a Specialty Coating Systems Spin Coater Model P6204-A.

### **III.2.2 Software**

Statistical analysis for factorial experiments were conducted using Minitab Student Edition, Release 9.

### **III.3 Procedures**

#### **III.3.1 Preparation of Functionalized Monomer Solution**

The functionalized membranes were prepared from a monomer mixture. The mixture was prepared by combining the non-functionalized monomer (e.g. HEMA) and appropriate amounts of the 2-Dimethylamino(ethyl) methacrylate (DMAEMA) (mol/mol), initiator, 2%(wt/wt monomer), and crosslinker (mol/mol monomer). Water was often added in a 1:1 mole ratio with the monomers to induce a higher percent hydration in the final membrane. The mixture was sonicated for several minutes to dissolve the solid initiator and ensure that the solution was well mixed. It was then stored in refrigerator.

#### **III.3.2 Preparation of Hydrogel Membranes**

##### **III.3.2.1 Preparation of Functionalized Membranes**

Membranes were prepared by applying an aliquot of the functionalized monomer mixture into a well that was fashioned out of a Teflon tape spacer on a microscope slide completely coated with Teflon tape. This was covered with another slide completely coated with the Teflon tape and the slides held together using spring clips. Monomer mixtures with the photoinitiator DMPAP were placed under a 400 Watt Mercury lamp for 5-10 minutes. Mixtures containing the thermal initiator AIBN were placed in an 80 °C

oven for at least 2 hours. After polymerization the membranes were removed from the slides and soaked in distilled water for 3 days prior to use.

### **III.3.2.2 Preparation of HEMA Membranes with Microparticles**

The preparation of these membranes is similar to that of the functionalized membranes. An aliquot of the monomer mixture: HEMA, bead suspension, crosslinker, initiator and water, is applied to the well fashioned out of a Teflon spacer on a microscope slide completely coated with Teflon tape. This was then covered with another Teflon coated slide and placed under a 400 Watt Mercury lamp for 5-10 minutes. The membrane was soaked in distilled water for several days prior to use.

### **III.3.2.3 Preparation of Poly(Vinyl alcohol) Membranes**

A 5% (wt/wt) solution of PVA (MW 14,000) was prepared by stirring 5 grams of PVA with 95 grams of water until dissolved. A 10% glutaraldehyde solution was prepared by diluting a 25% stock solution with water. To prepare the membrane, 1 ml of 5% PVA solution and 100  $\mu$ l of 10% glutaraldehyde were combined with the microparticle suspension. The mixture was sonicated and vortex mixed until completely homogenous. To initiate polymerization, 100  $\mu$ l of 4M HCl was added and mixed by stirring. The solution was applied to the well as previously described. The polymerization was allowed to proceed for 15 minutes, then the membrane was carefully removed and placed in distilled water.

### **III.3.3 Silanization of Glass Surfaces**

Glass slides were silanized to covalently couple polymer membranes to the glass surface. The slides were heated under reflux in 2 M HCl for 4 hours, then washed exhaustively with distilled water and allowed to dry overnight. The slides were then



placed in a 0.5% (v/v) solution of 3-(trimethoxysilyl) propyl methacrylate in water or ethanol adjusted to pH 3 with acetic acid. The slides were left in the solution with occasional agitation for one hour. The slides were then cured in an 85 °C oven for thirty minutes. The silanized slide was used in place of the Teflon coated cover slide when forming the hydrogel membrane.

An alternative method used for surface silanization was to use a vinyl-trimethoxysilane. A procedure similar to that described above was used. The glass substrate was treated for 4 hours in 2 M HCl under reflux, then rinsed with distilled water and dried overnight. A solution of 1:3 silane in toluene was prepared and the slides immersed for 3 hours. The slides were then cured in an 80 °C oven for thirty minutes. The silanized slide was used as above.

### **III.3.4 Preparation of 2,4,5-Trichlorophenylacrylate**

The 2,4,5-trichlorophenylacrylate (TCPA) monomer was prepared by the following procedure.<sup>90</sup> A one-liter 3-neck flask with a magnetic stirrer was used as a reaction vessel. To this 150-ml of 3.33 M solution of 2,4,5-trichlorophenol(TCP) in dichloromethane was added. The flask was chilled in an ice bath with stirring. Solutions of 3.33 M acryloyl chloride and triethylamine in dichloromethane were placed in two 250-ml dropping funnels. The two solutions were added dropwise to the TCP with continuous stirring. Drop rates were set such that a minimum of 30 minutes was required for the two solutions to be exhausted. The reaction was stirred for an additional 3 hours in the ice bath, followed by 6 hours at room temperature. Figure III.1 shows the reaction for producing TCPA and Figure III.2 shows the FTIR spectra confirming the conversion

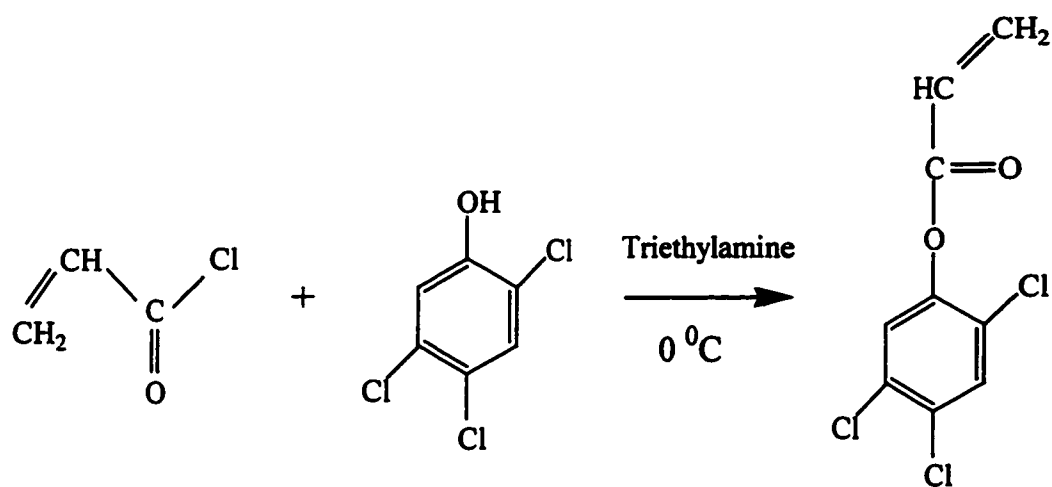


Figure III.1. Synthesis of TCPA

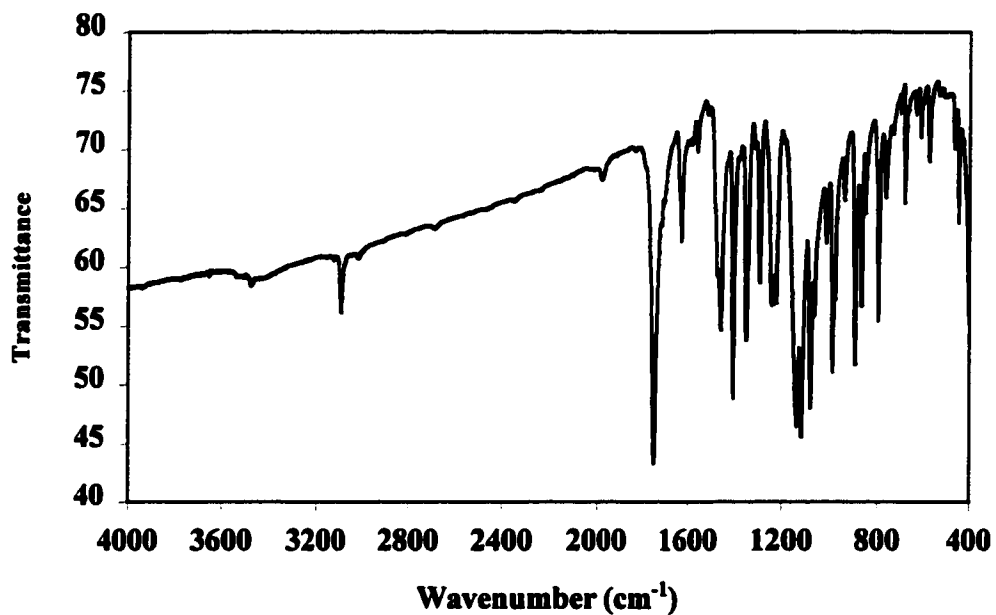
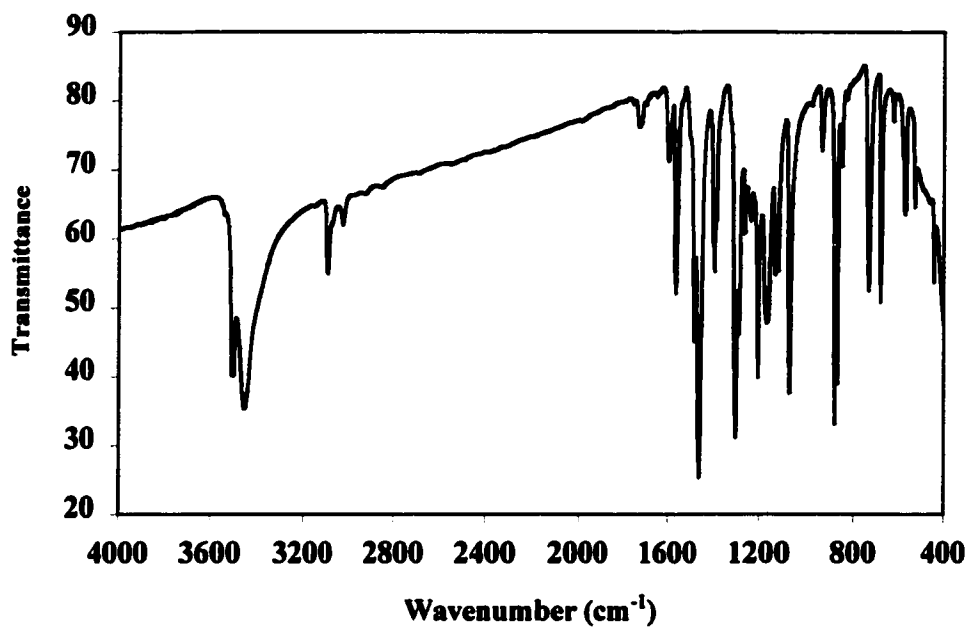
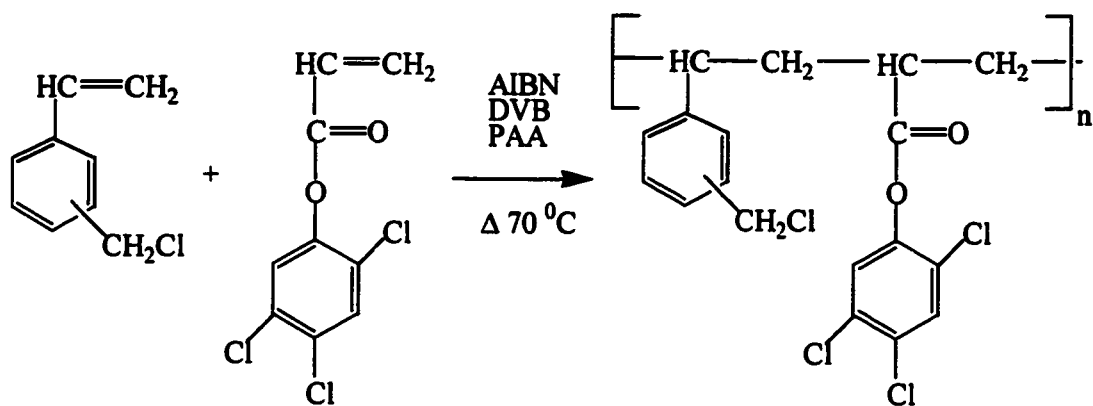


Figure III.2. FTIR showing conversion of 1. TCP(top) into 2. TCPA(bottom).

of the TCP to TCPA. The conversion of TCP into TCPA is seen in the loss of the  $\text{-OH}$  stretch around  $3400\text{ cm}^{-1}$  and the addition of the  $\text{C=O}$  stretch at  $1750\text{ cm}^{-1}$ , as the  $\text{-OH}$  is replaced by the acrylate group. The bands at  $1640\text{ cm}^{-1}$  and  $990\text{ cm}^{-1}$  due to a  $\text{C=C}$  bond appear. The triethylammonium chloride salt was removed by filtering through glass wool. The filtrate was transferred to a 1-liter separatory funnel. The solution was cleaned with 2 washes of 100 ml distilled water, followed by 100 ml saturated sodium bicarbonate, and 100 ml distilled water. The solution was dried over anhydrous sodium sulfate and filtered using a vacuum aspirator. A rotary evaporator was used to remove the dichloromethane solvent, leaving white-yellow TCPA crystals. This was rinsed twice with ethyl acetate, and the solution discarded. The product was then dissolved in hexanes and transferred to a second recrystallization dish. A yellowish sticky material remained in the original container after the hexanes solution was transferred to the dish. The hexanes were allowed to evaporate and the product was dried overnight in a vacuum oven at  $35\text{ }^{\circ}\text{C}$ . The final product was then transferred to plastic bottle and stored refrigerated.

### **III.3.5 Preparation of Microspheres**

The general procedure for the preparation of microspheres was the same regardless of the monomers utilized. Monomers, steric stabilizer(20% wt. based on monomers), and the initiator AIBN(2% wt. based on monomers) were placed in a 500 ml 3 neck flask with a magnetic stirrer and dissolved in ethanol and any cosolvents with stirring. Following the dissolution of the solid components the liquid monomer would be added. The flask was then placed in a water/oil bath at  $70 \pm 2\text{ }^{\circ}\text{C}$  and purged with nitrogen for 20 minutes. All reactions were allowed to proceed for at least 6 hours. While purging, the reaction mixture turns from clear to white. At the end of the polymerization the product was a



**Figure III.3.** Polymerization reaction of VBC and TCPA to form VBC/TCPA microparticles

white opaque latex. Following polymerization, the product is poured into a beaker to which 250 ml of methanol is added. The particles are then cleaned and derivatized or characterized. The polymerization reaction for VBC/TCPA beads is shown in Figure III.3.

### **III.3.6 Cleaning of Microspheres**

Particles were cleaned by centrifuging the reaction mixture, discarding the supernatant, and resuspending the particles in fresh methanol by sonication. This procedure was repeated two additional times. The final step was dictated by the desired use of the product. Products for SEM analysis were poured into a petri dish and allowed to dry. Products to be derivatized were suspended a final time in alcohol and stored in a plastic bottle.

### **III.3.7 Preparation of Porous Microspheres by Seeded Polymerization**

Seed particles were prepared in accordance with the method described in section III.3.5. The procedure for preparation of seeded polymerization was described by Miele.<sup>31</sup> A 1:1:1 volume mixture of seed particles, acetone and 0.25% (wt./vol.) sodium doceyl sulfate, SDS, was combined in a 500 ml 3 neck flask. Water was added so that the volume was doubled. An overhead stirrer was used to stir the particles overnight, which allowed the seed particles to swell with acetone.

A solution consisting of 20.3 %(vol./vol.) VBC, DVB (2 % mole/mole VBC), 25.4 %(vol./vol.) 0.25 % (wt/vol.) SDS, 40.6 %(vol./vol.) water, 13.7 %(vol./vol.) toluene and AIBN (1.5 % wt./vol. VBC) was prepared in a graduated cylinder. This was sonicated for at least 20 minutes to emulsify the mixture. The mixture went from slightly cloudy solution to opaque white. This was added to the flask one third at a time in 10

minute intervals. A solution of 5% (wt./vol.) PVA (MW 85,000 – 146,000) was added to the flask in a volume equal to the monomer mixture added. The monomer mixture was allowed to diffuse into the swollen seeds by stirring the mixture for 24 hours.

The flask was purged with nitrogen for 10 minutes and polymerization proceeded for 12 hours at 70 +/- 2 °C. Following polymerization the reaction product was transferred to a beaker and an equal volume amount of 1:1 water/ethanol was added.

### **III.3.8 Cleaning of Porous Microspheres Prepared by Seeded Polymerization**

The procedure to clean the porous microspheres is similar to that described in section III.3.6 to clean the particles prepared by dispersion polymerization. The polymerization product:water/ethanol mixture was transferred to test tubes and centrifuged for approximately 30 seconds. Particles prepared by this method are easily deformed so care must be taken to limit the centrifuge time. The supernatant was discarded and the particles resuspended in water/ethanol. This procedure was repeated two more times. The procedure was then repeated twice more with methanol as the wash solvent. Cleaned particles were either derivatized for later use or dried for SEM analysis.

### **III.3.9 Derivatization of Microspheres**

Beads were reacted with diethylamine or diethanolamine to introduce pH sensitive functionality. Derivatization was accomplished by displacing the chloromethyl carbon of the chloride and of the chlorophenyl ring of the TCPA. The reaction is shown in Figure III.4. This was carried out by adding acetone to the beads suspended in methanol. After approximately 45 minutes an equal amount of diethylamine was added to the mixture. The total volume was approximately double the initial volume. The beads were stirred at room temperature for 3-4 days. The particles were diluted with 0.1

M HCl until the volume of liquid was doubled. The cleaning method used was analogous to that described in section III.3.6, with deionized water being used instead of methanol. In the final step the beads were suspended in a minimal amount of water. They were then stored in a vial at room temperature.

The derivatization was confirmed by FTIR analysis. The FTIR spectra before and after derivatization with of VBC/TCPA particles and of VBC particles are shown in Figures III.5 and III.6 respectively. Derivatization for VBC/TCPA particles was confirmed by the loss of the  $\text{-Cl}$  stretch at  $1260\text{ cm}^{-1}$ . Also seen is the growth of the band at  $1640\text{ cm}^{-1}$  due to the  $\text{C=O}$  of an amide group. The FTIR for VBC, Figure III.6, confirms derivatization by the loss of the  $\text{-Cl}$  stretch at  $710\text{ cm}^{-1}$  and  $1260\text{ cm}^{-1}$ . The growth of the bond at  $1080\text{ cm}^{-1}$  is due to the  $\text{C-N}$  bond in a tertiary amine.

### **III.4 Characterization**

#### **III.4.1 Swelling Measurements**

Swelling measurement were carried out to measure the size change between swollen and shrunken states of the hydrogel membranes. This was accomplished by punching a 1 cm diameter circle out of a polymer membrane using a hole punch. This was then equilibrated with either pH 4 or pH 10 buffer solution. The diameter was then measured using a translucent ruler and magnifying lamp.

#### **III.4.2 Hydration Measurements**

Percent hydration was determined by soaking the membrane in water or buffer solution for at least 24 hours. The membrane was then patted with a Kim-wipe to remove surface water and weighed on a tared microscope cover slip. Membranes were then dried for 24 hours in an oven at slightly elevated temperature ( $\sim 45\text{ }^{\circ}\text{C}$ ), and reweighed.



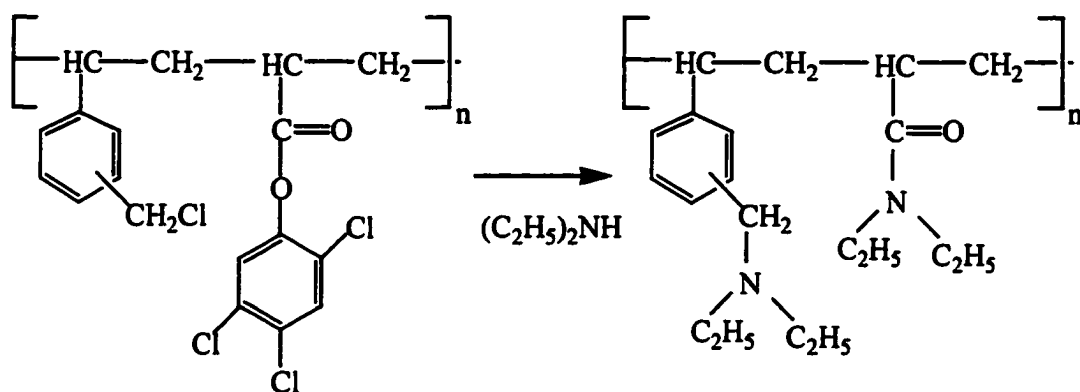


Figure III.4. Derivatization reaction for VBC/TCPA microparticles with diethylamine

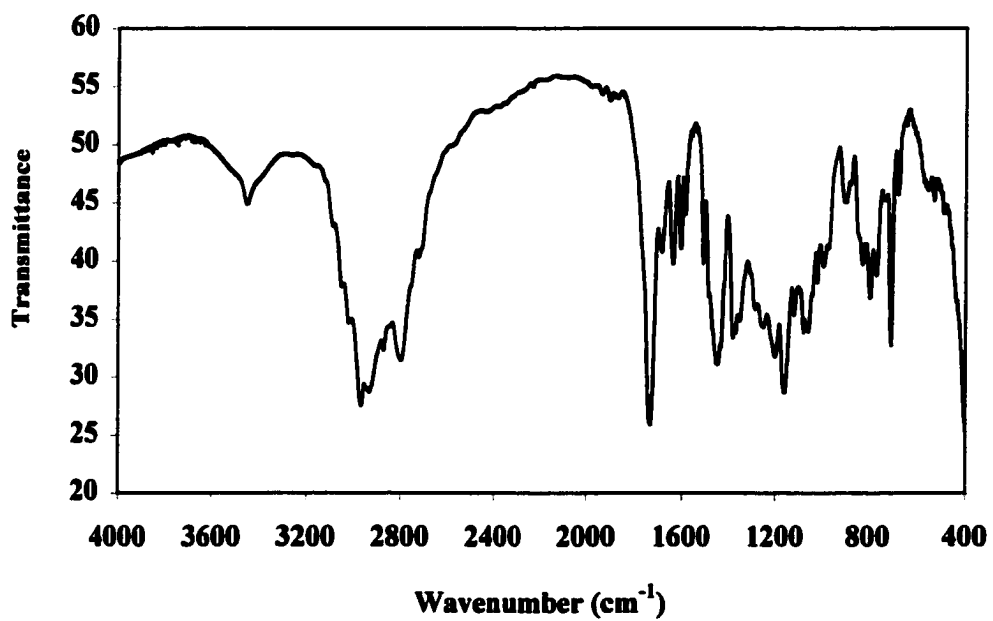
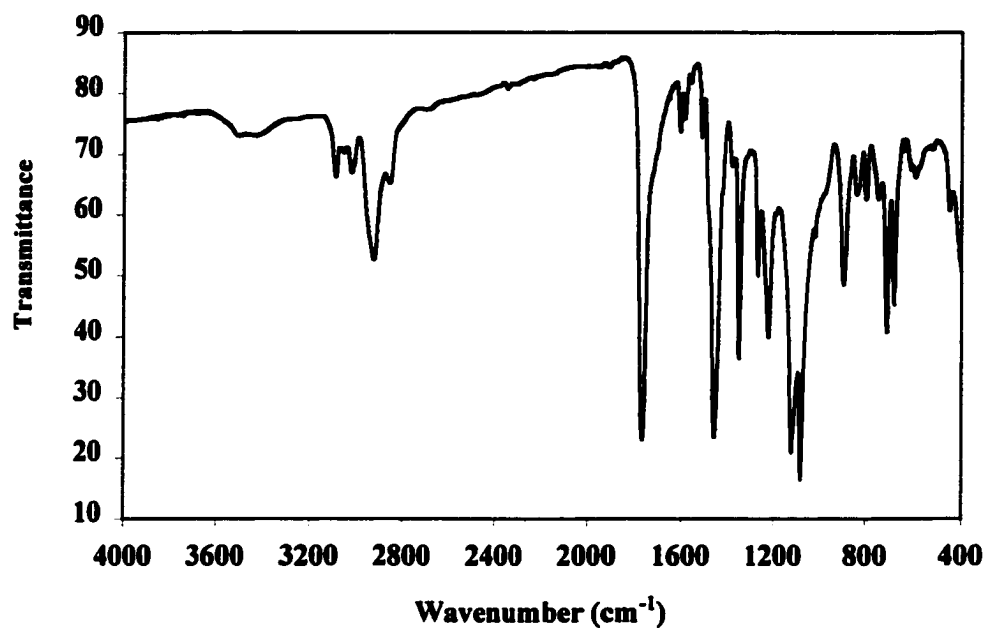


Figure III.5. FTIR of VBC/TCPA microparticles 1. before(top) and 2. after derivatization(bottom).

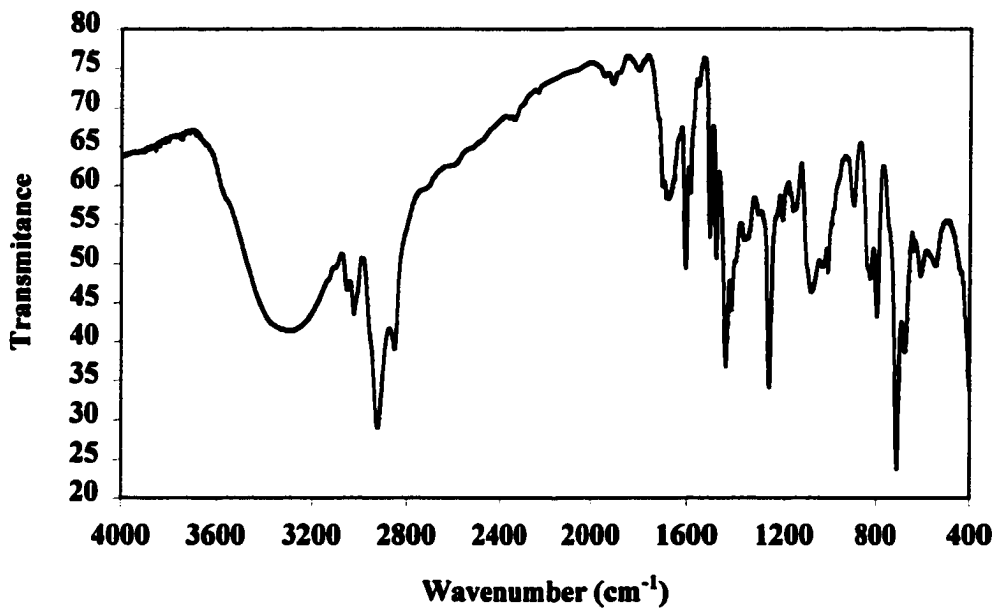
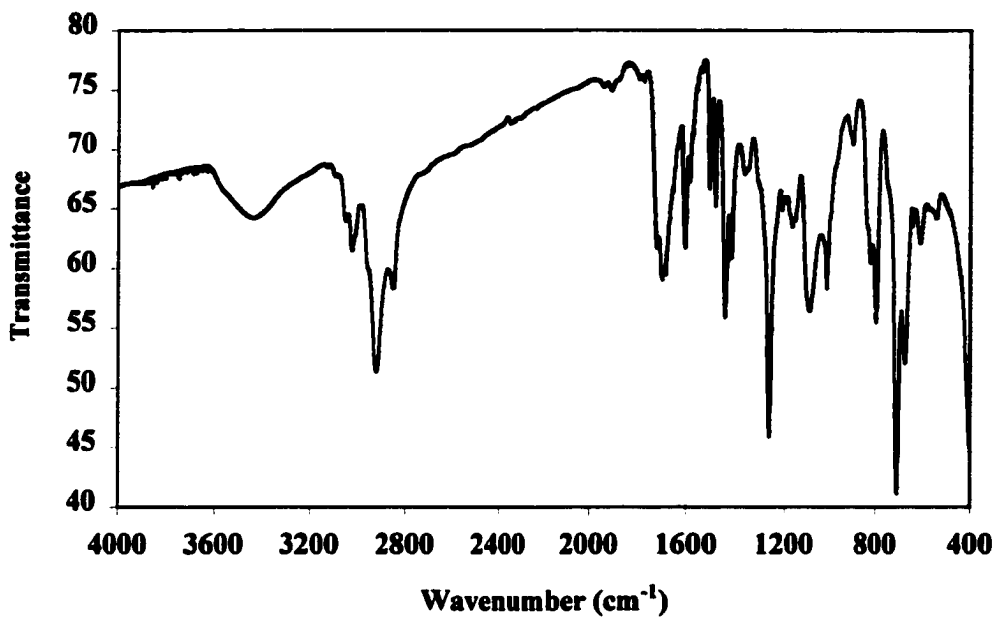


Figure III.6. FTIR of VBC microparticles 1. before(top) and 2. after derivatization(bottom).

### **III.4.3 CHN Analysis**

Functionalized membranes were chilled with dry ice until brittle, then ground to small pieces using a mortar and pestle.

Microspheres were thoroughly cleaned as described in section III.3.6. The particles were then transferred to a petri dish and allowed to dry. Dried sample was collected and analyzed.

### **III.4.4 Scanning Electron Microscopy**

Scanning electron micrographs were obtained using an Amray 3300FE Scanning Electron Microscope. Beads were cleaned as described in section III.3.6. After drying, the beads were scraped into a glass vial using a razor blade. A piece of double-sided carbon tape was placed over the opening of the vial and the vial inverted to cover the tape surface with beads. The tape was then removed and placed on a SEM platform. This was coated with a layer of Au/Pd and placed in the SEM.

### **III.4.5 Size and Distribution of Microspheres**

The size of the microspheres were determined using the scanning electron micrographs. The average diameters of 50-75 particles were measured using a ruler. The mean particle size and standard deviation were then calculated.

### **III.4.6 FTIR Analysis**

Analysis of particles and TCPA was conducted using FTIR to verify derivatization and conversion. Approximately 15 mg of material was added to a small amount of KBr and pressed into a pellet using a pellet press.

### **III.4.7 Magnetic Resonance Measurements**

Measurements of magnetic resonance of metallic glass strips were conducted using a "home-built" resonance meter. Scans were conducted with a resolution of 10 kHz, with a typical scan range of 50-65 kHz. The sample was placed in a plastic holder with any solution and the entire assembly was placed in the detection coils.

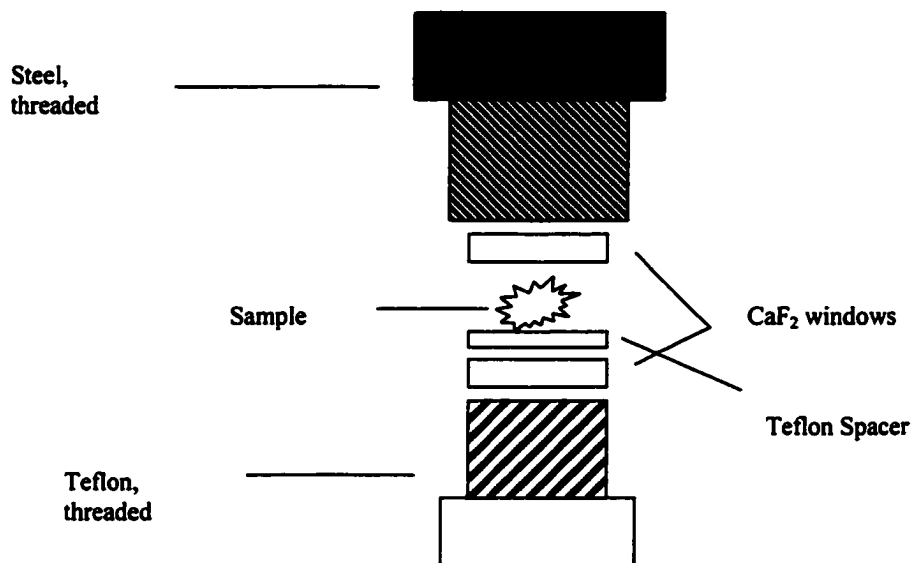
### **III.4.8 Polymerization Monitoring**

#### **III.4.8.1 Monitoring by FTIR**

Monitoring of the polymerization by FTIR was conducted in two different fashions. For thermally initiated reactions, a sample was placed between two windows attached to a heated mount, shown in Figure III.7, and placed into the spectrophotometer.<sup>30</sup> A small aliquot of monomer solution was placed between two CaF<sub>2</sub> windows separated by a Teflon spacer. This was supported in a sample holder consisting of a Teflon threaded male part, on which the windows rested, which was screwed into a steel threaded female part. The entire assembly was placed in a metal block that was heated by a thermostatted bath. An attached thermal couple monitored the temperature of the block. The entire block was then placed in the instrument and the polymerization was monitored.

Polymerizations that were photoinitiated were monitored by a second technique. An aliquot of monomer was placed in a small aluminum dish with an approximate volume of 0.5 ml. The pan was then placed under the mercury lamp. The reaction was quenched by pouring liquid nitrogen over the pan. The sample was then mixed with KBr and pressed into a pellet for examination in the FTIR.<sup>92</sup>

**Sample Cell:**



**Heated Block for Holding Sample Cell in FTIR**

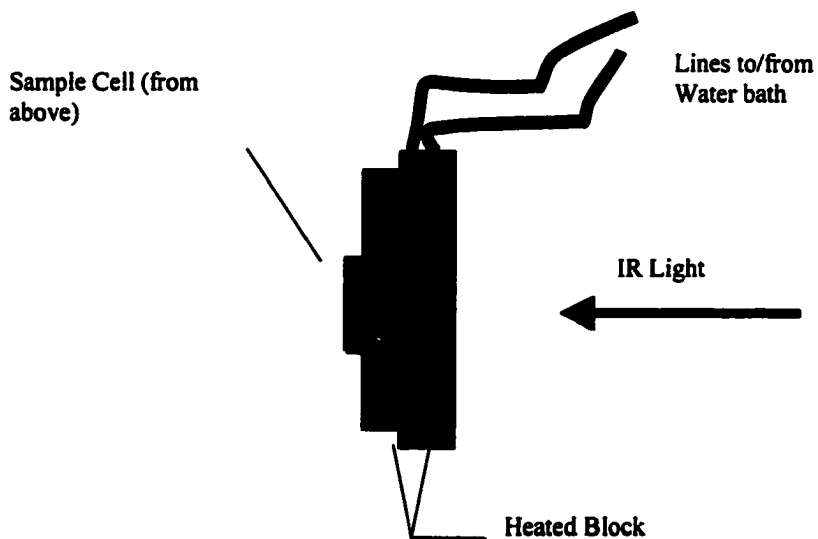


**Figure III.7. Diagram of sample cell and holder for FTIR monitoring of thermal polymerization.**

#### **III.4.8.2 Monitoring by Magnetic Resonance**

An aliquot of the sample was placed on the magnetic strip, which was placed on a glass microscope slide. The slide was then placed under the mercury lamp for photoinitiated reactions or in an oven for thermally initiated reactions. The resonance frequency was periodically measured by placing the sample in the detection coils.

#### **III.4.8.3 Monitoring by Viscosity Measurements**

Thermally initiated samples were monitored by placing an aliquot of sample in the UL adapter, which was connected to a thermostatted bath. The spindle was lowered into the adapter and viscosity measurements were taken at several shear rates and extrapolated back to zero shear unless otherwise noted. Monitoring continued until the solution became too viscous to be safely measured.

Photoinitiated samples were placed in small glass vials into which the spindle was placed. The vials were then irradiated by the mercury lamp and the viscosity monitored as above.

#### **III.4.9 Viscosity Measurements**

Solution viscosities were measured using a Brookfield viscometer with the UL adapter. An aliquot of sample was placed in the sample holder. The spindle was immersed in the solution. Viscosity was measured at several shear rates and extrapolated to a shear rate of zero to obtain the reported viscosity.

#### **III.4.10 Turbidity Measurements**

Unless noted, turbidity was measured on membranes that were 76  $\mu\text{m}$  thick. Thickness of the membrane was controlled by the thickness of the Teflon spacer. The membranes were placed between two plastic holders, which were then placed in a

cuvette. Measurements were referenced against a cuvette consisting of a membrane holder and an appropriate buffer solution. Turbidity scans were conducted from 400 to 1000 nm. All turbidity data refers to 600 nm unless otherwise noted.

#### **III.4.11 Refractive Index Measurements**

Refractive indexes were calculated by group contribution methods.<sup>91</sup> When noted refractive indexes were determined using an Abbe refractometer.

#### **III.4.12 Surface Plasmon Resonance Measurements**

Surface Plasmon Resonance measurements were taken using the disposable gold slides as the substrate with the flow cell adapter. A slide was attached using a small amount of index matching oil and the air reference obtained.<sup>93</sup> Calibration was performed using double distilled water. A PVA hydrogel solution containing microspheres was prepared as described in section III.3.5. The slide was then removed, and the PVA solution was applied and allowed to polymerize. After polymerization had occurred, the slide was hydrated for 15 minutes, and the slide was attached to the SPR using the flow cell as described above. The hydrogel was exposed to buffer by running the buffer through the flow cell using a micropump. Analysis was performed using the operating software provided by Texas Instruments.

#### **III.5 Experimental Design**

Several factorial experiments were carried out. While systematic studies can show general trends of changing one variable, they are limited in the amount of information they can provide. A factorial design allows for many variables to be studied at once, allowing not only the effect of changing a particular variable to be observed, but also the effect that each variable has on the other factors to be obtained. This allows for a



greater understanding of the importance each factor and their interactions have on the observed results.

### III.5.1 Design of Factorial Experiment - Cross-linker Size Ratio – Chapter IV

A factorial design experiment was carried out to study the effect of concentration of pH sensitive copolymer with HEMA, cross-linking level, and cross-linker type on the size ratio of pH sensitive hydrogels. Two levels of each factor were examined, a 2<sup>3</sup> factorial design. All measurements were made in random order and carried out in triplicate. The factorial design and levels of each variable are shown in Table III.1. The concentration of pH sensitive DMAEMA is presented as the percent moles DMAEMA/total moles monomer, concentrations of 25% and 50% were examined. The cross-linking level is presented as the mole percent of the monomer, the levels studied were 1.5% and 3%. Two different cross-linkers were examined, EGDM and TEGDM. DMPAP was employed as the photoinitiator at a level of 1 % wt. of the monomers. Water was also included in the prepolymer solution at a 1:1 mole ratio of water:monomers.

Table III.1 Factorial Experiment Design for Cross-linker Swelling Ratio

Formulation Number	% DMAEMA (mol/mol)	% Cross-linker (mol/mol)	Cross-linker Type
1	50	3	TEGDM
2	50	3	EGDM
3	50	1.5	TEGDM
4	50	1.5	EGDM
5	25	3	TEGDM
6	25	3	EGDM
7	25	1.5	TEGDM
8	25	1.5	EGDM

### III.5.2 Design of Factorial Experiment – Comonomer Size Ratio – Chapter IV

The purpose of this factorial was to investigate the effects that comonomer type and concentration of DMAEMA have on the size ratio of a hydrogel membrane. A  $2^2$  factorial was carried out in random order, and conducted in triplicate. The comonomers were HEMA and HPMA. The DMAEMA monomer was present in concentrations of 50% and 25% (mol. DMAEMA/mol. monomer). Water in a 1:1 molar ratio with the monomers was included in the prepolymer solution. Membranes were crosslinked at 1.5% (mol. EGDM/mol. monomer) with EGDM. Polymerization was initiated with DMPAP at 1% weight of monomers. Table III.2 shows the design of the experiment and levels of each variable.

Table III.2 Factorial Experiment Design for Comonomer Swelling Ratio

Formulation Number	Comonomer Identity	% DMAEMA (mol/mol)
1	HEMA	50
2	HEMA	25
3	HPMA	50
4	HPMA	25

### III.5.3 Design of Factorial Experiment - Surface Adhesion – Chapter IV

This factorial was to study the effect of four factors on the adhesion of a pH sensitive hydrogel membrane to a glass slide through trimethoxysilylpropyl-methacrylate(MPTS). A  $2^4$  factorial design was used, with the four variables being present at high and low levels. The membranes were prepared in random order and replicate experiments were conducted. The levels of each variable, along with the design

of the experiment are shown in Table III.3. The adhesion agent was deposited onto the glass surface from two solvent systems: 2 % MPTS in 95% ethanol adjusted to pH 3 with acetic acid, and 2 % MPTS in water adjusted to pH 3 with acetic acid. The level of pH sensitive copolymer was set at 0 % and 10 % moles of DMAEMA to total moles hydrogel. Membranes were prepared in two different sizes 1 mm x 1 mm and 1.5 mm x 1.5 mm. The adhesion in two different pH solutions was examined, with the pH levels set at pH 7 and pH 10. Water was included in the prepolymer solution at a ratio 1:1 water:monomers. Polymerization was initiated using DMPAP at 1 % wt. of monomers. The analysis of variance was performed on the total time required for the membrane to delaminate from the modified glass substrate.

Table III.3 Factorial Experiment Design for Hydrogel Adhesion

Formulation Number	MPTS Solvent	% DMAEMA (mol./mol. %)	Membrane Size (mm <sup>2</sup> )	pH of Soak Solution
1	EtOH	10	2.25	10
2	EtOH	10	2.25	7
3	EtOH	10	1	10
4	EtOH	10	1	7
5	EtOH	0	2.25	10
6	EtOH	0	2.25	7
7	EtOH	0	1	10
8	EtOH	0	1	7
9	Water	10	2.25	10
10	Water	10	2.25	7
11	Water	10	1	10
12	Water	10	1	7
13	Water	0	2.25	10
14	Water	0	2.25	7
15	Water	0	1	10
16	Water	0	1	7

### III.5.4 Design of Factorial Experiment - Microsphere Particle Size - Chapter V

A factorial design experiment was carried out to examine the effect of three main variables on the production of particles produced by dispersion polymerization. The experiment was carried out as a  $2^3$  design, with each of three factors at two levels. The design of the experiment and the levels of each variable are shown in Table III.4. The concentration of monomers was set at percentages of 4% and 8% wt. monomer/volume. The concentration of water cosolvent was set at volume percentages of 5% and 15%. The stabilizer Poly(Acrylic Acid) ( MW 450,000) was set at 10% or 30% weight of monomer. All reactions were run in ethanol with AIBN initiator at 2% weight of monomers. The reactions were run in a random order in triplicate. Analysis of variance was performed on the size of the beads produced.

Table III.4 Factorial Experiment Design for Microsphere Particle Size

Formulation Number	% Water Cosolvent (vol./vol. %)	% Monomer (wt./vol. %)	% Stabilizer (wt. % of monomer)
1	15	8	30
2	15	8	10
3	15	4	30
4	15	4	10
5	5	8	30
6	5	8	10
7	5	4	30
8	5	4	10

## CHAPTER IV

### Preparation and Characterization of pH Sensitive Hydrogel Membranes and Adhesion of Hydrogel Membranes to a Surface

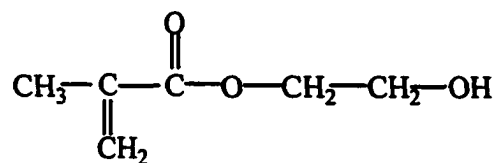
#### IV.1 Introduction

This chapter examines the variables affecting the use of hydrogel membranes as a pH sensitive material for chemical sensing. Hydrogels were chosen as the sensing layer since they have high levels of hydration, which is advantageous in terms of diffusion of aqueous analyte into the interior of the membrane. The goal of this work was to develop a pH sensitive membrane that would have the desired characteristics for use in a magnetochemical sensor. To be useful for this purpose, the membranes needed to exhibit a high degree of reproducible swelling in response to pH and be mechanically stable. Successful adhesion of the polymer to a substrate as it swelled and shrank was also required. The use of hydrogels for chemical sensing has been described in the literature, but not in a manner that involved the polymer swelling as described here. Sheppard *et al.* used a pH sensitive hydrogel in a conductimetric chemical sensor,<sup>57</sup> while Kunz utilized a pH sensitive hydrogel in an optical sensing system.<sup>94</sup>

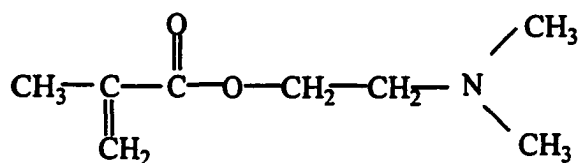
A number of factors are known to affect the swelling ability and the mechanical characteristics of the membrane including: concentration of pH sensitive component, level of cross-linker, cross-linker type, and hydrophilicity of a comonomer. Factorial experiments were conducted in order to examine these factors. Systematic studies were also conducted in order to completely investigate the effect of the main factors.

The structures of the components used in the preparation of pH sensitive membranes are shown in Figure IV.1. Unlike the poly(VBC-co-DVB) pH sensitive membranes used by Rooney, the pH sensitive hydrogel membranes have innate pH sensitivity.<sup>30</sup> The membranes used by Rooney required a derivatization step in order to introduce the pH sensitive amine group.<sup>30</sup> The hydrogel membranes include a pH sensitive component, DMAEMA, which has an amine group as part of its structure. The swelling mechanism for the pH sensitive membrane is shown schematically in Figure IV.2. Another advantage of the hydrogels over the poly(VBC-co-DVB) membranes is the hydrophilicity of the membranes. The hydrogel membranes are much more hydrophilic than the poly(VBC) membranes and do not require the addition of a porogenic solvent to the polymer formulation in order to induce pores. Pore formation is necessary to decrease the response time by allowing the analyte to diffuse into the membrane more rapidly. These two characteristics allow the hydrogel membranes to be prepared more simply, without the need for an additional derivatizing step or cleaning steps.

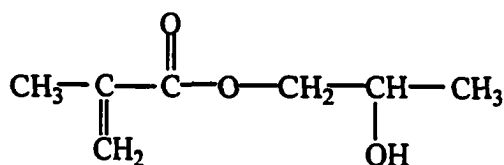
## Hydrogel Monomers



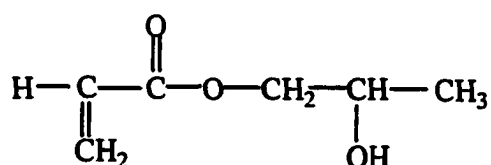
2-Hydroxyethyl methacrylate



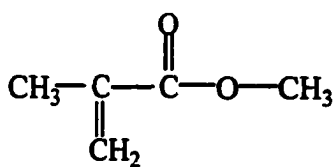
2-(Dimethylamino)ethyl methacrylate



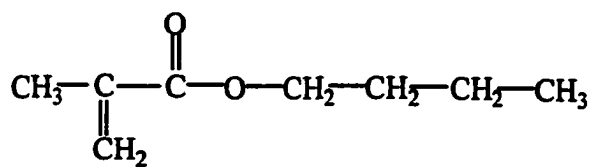
Hydroxypropyl methacrylate



Hydroxypropyl acrylate



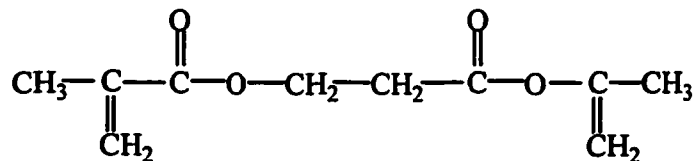
Methyl methacrylate



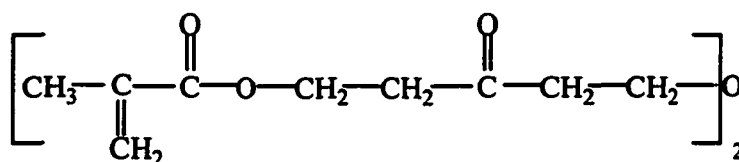
Butyl methacrylate

Figure IV.1. Structure of monomers, cross-linkers and initiators used in pH sensitive membrane preparation.

### Cross-linkers

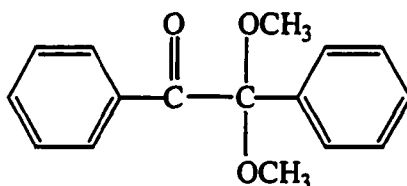


Ethylene glycol dimethacrylate



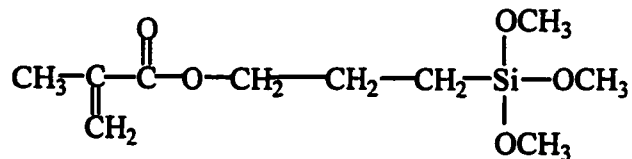
Tetra(ethylene glycol)dimethacrylate

### Photoinitiator



2,2 - Dimethoxy-2-phenylacetophenone

### Adhesion Agent



3-(Trimethoxysilyl)propyl methacrylate

Figure IV.1. Structure of monomers, cross-linkers and initiators used in pH sensitive membrane preparation.(cont.)



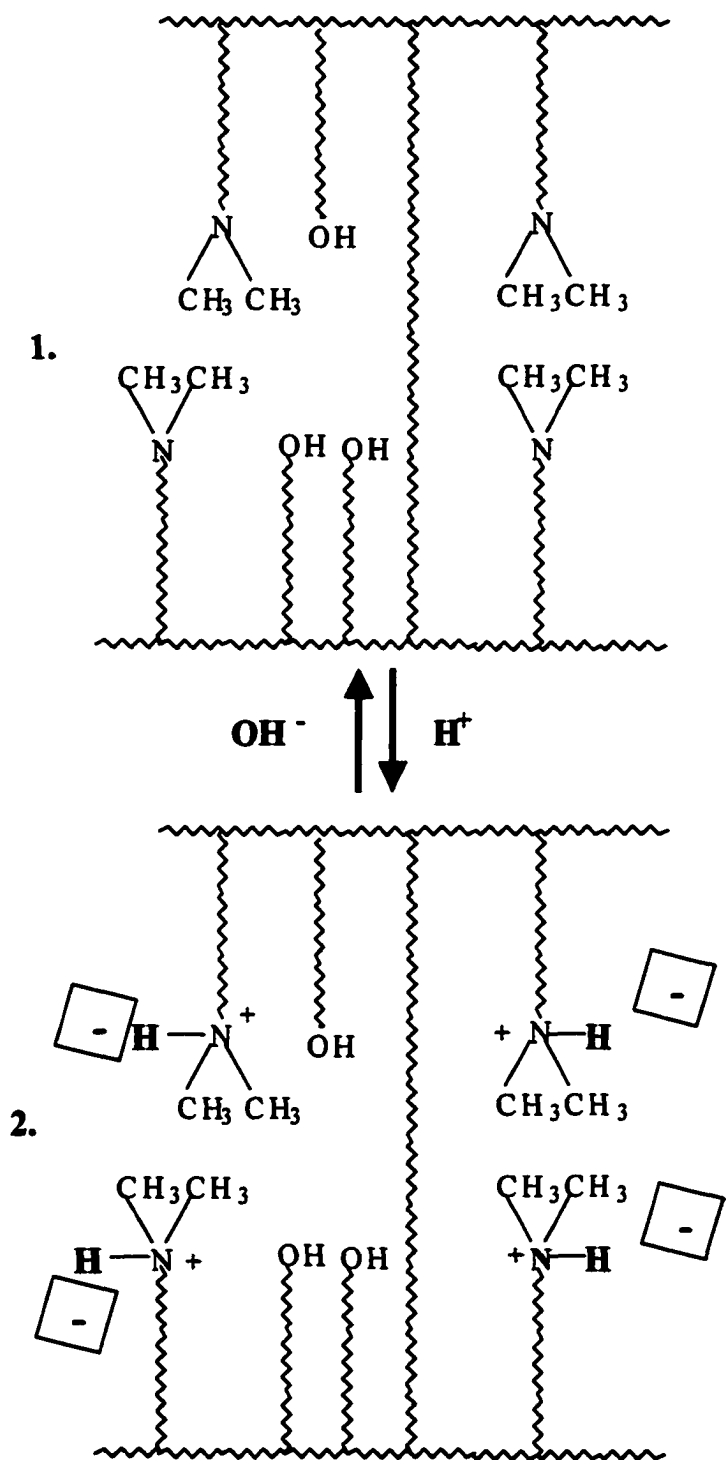


**Figure IV.2. Schematic showing ionic swelling of hydrogel.**  
 (1) Shows unswollen state, (2) shows swollen state with protonated amines and counter ions.

## **IV.2 Results and Discussion of Factorial Experiment Examining Effect of Cross-Linker and DMAEMA Level on Size Ratio**

This factorial dealt with the effect of cross-linking level, cross-linker type and the level of pH sensitive DMAEMA on the degree of swelling of a membrane. The size ratio was determined by dividing the diameter of the membrane in the swollen state, pH 4, by the diameter of the membrane in the unswollen state, pH 10. The greater the size ratio, the greater the size difference between the acid and base states. When in the hydrated state, all membranes were clear to slightly opaque. Visually there was no difference in appearance observed between the different formulations. Membranes with higher cross-linker levels were slightly more brittle than those with lower cross-linking levels. The concentration of each variable for the different formulation was shown in Table III.1.

Figure IV.3 shows the mean size ratios for each formulation used in this study. The error bars represent  $\pm$  one standard deviation for the size ratio and are determined from three replicate measurements. The odd numbered formulations with TEGDM as the cross-linker show higher size ratios than the even numbered formulations with EGDM as the cross-linker. Higher concentrations of DMAEMA, formulations 1-4, showed larger size ratios than those with lower levels.

The analysis of variance(ANOVA) shown in Table IV.1 reveals that a number of main factors, as well as several interactions affect the size ratio. Mean squares(MS) values are estimates of the variation between factors and of the error. The MS error represents the variation of the error, within group variance. The importance of a particular factor is determined by the F ratio. This is determined by the ratio of the MS Factor/MS Error. Comparison of the calculated F ratio with a tabulated F ratio determines whether the null hypothesis is accepted or rejected. If the F ratio is larger

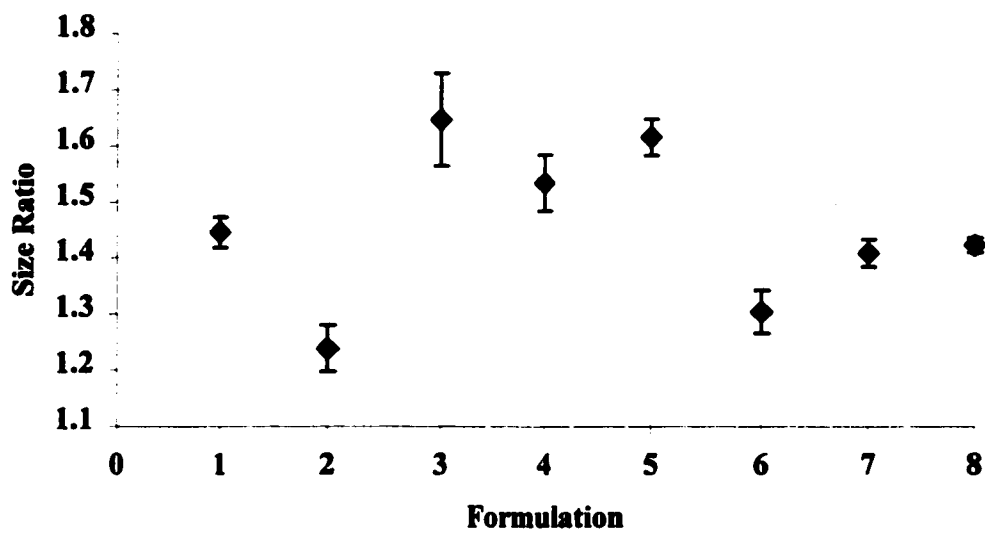


**Figure IV.3** The mean size ratio, membrane diameter in acid (pH 4) divided by membrane diameter in base (pH 10). The error bars represent one standard deviation (n=3).

**Table IV.1 Results of Analysis of Variance for Size ratio Examining Effect of Cross-Linker Level and Concentration of DMAEMA**

Source	DF	SS	MS	F	P
DMAEMA (D)	1	0.004909	0.004909	2.62	0.125
Cross-Linker (XL)	1	0.062501	0.062501	33.38	0.000 **
Cross-Linker Type (XT)	1	0.142494	0.142494	76.11	0.000 **
D*XL	1	0.128079	0.128079	68.41	0.000 **
D*XT	1	0.000211	0.000211	0.11	0.742
XL*XT	1	0.065975	0.065975	35.24	0.000 **
D*XL*XT	1	0.020055	0.020055	10.71	0.005 **
Error	16	0.029957	0.001872		
Total	23	0.454181			

**df** = degrees of freedom

**SS** = sum of squares

**MS** = mean squares

**F** = F statistic, ( $MS_{\text{effect}}/MS_{\text{error}}$ )

**p** = probability of incorrectly rejecting the null hypothesis

**\*\*** = significant at 99% confidence interval,  $F_{\text{critical}}=8.53$  (n=16)

then the tabulated F value, the hypothesis can be rejected. In that case, the particular factor affects the system at the indicated confidence level. The greater the F ratio compared to the tabulated F value, the more significant the effect of the factor. The probability of rejecting the null hypothesis when one should not is represented by the P value. In the case of this factorial, the  $F_{table}$  values are 4.49 and 8.53, for 95% and 99% confidence levels, respectively.

The concentration of DMAEMA is the only main factor that was not shown to have an effect on the size ratio at the 95% or 99% confidence level. However, it is known that the degree of swelling is dependent upon the number of ionizable sites as described by Flory<sup>65</sup>, see section II.7.2. This seeming contradiction can be explained by considering that the difference between the high and low levels of DMAEMA may have been overwhelmed by the other factors.

#### **IV.2.1 Effects of Main Factors**

Figure IV.4 shows the average effect of the main factors on the size ratio. These effects are the average of 4 formulations at the high or low level of each particular variable. Two of the main factors, cross-linker type and cross-linker level, were found to be significant at the 99% confidence level, see Table IV.1. The importance of each factor can be related to the slope of the lines shown in Figure IV.4. The steeper the slope, the more significant the effect the factor has on particle size.

##### **IV.2.1.1 Effect of Cross-linker Type**

Cross-linker type is the factor that has the largest effect on the size ratio of the hydrogel membrane. This factor has the largest F value of the main factors, Table IV.1, and the greatest slope showing the largest and smallest size ratio, Figure IV.4.

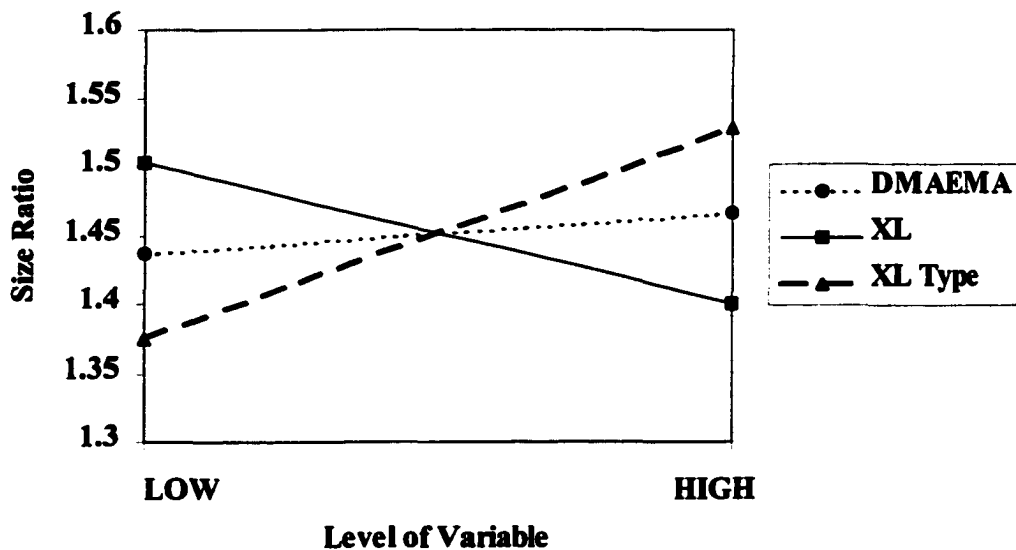


**Figure IV.4** The average effect on the size ratio of changing amounts of the main factors. Points are the average values of all membranes from formulations containing either high or low levels of a particular factor.

Cross-linkers have the effect of counteracting the swelling of the membrane. A certain degree of swelling will occur, before the cross-links are stretched and act to hold the polymer chains together. The two levels of cross-linker reflect the two different types of cross-linker. The high level represents TEGDM and the low level represents EGDM. Structures of these molecules are shown in Figure IV.1. Because TEGDM has a longer carbon chain than EGDM, it can be stretched to a greater amount. The longer chain allows the polymer chains to move further apart before the swelling is curtailed by the cross-links. This allows the membrane to have a larger size difference between the swollen and unswollen states, giving rise to the larger size ratio for the TEGDM cross-linked membrane.

#### **IV.2.1.2 Effect of Cross-linker Level**

Cross-linker level was the other main factor that had an effect on the size ratio of the membrane, Table IV.1. Membranes that used low levels of cross-linker showed the highest level of swelling, Figure IV.4. Formulations with the high cross-linker level had a size ratio of 1.40, while those with the low level had a size ratio of 1.54. There is an inverse relationship between the cross-linker level and the amount of swelling that occurs in the membrane. Because the cross-linker acts to restrain swelling, higher cross-linker levels exhibit smaller degrees of swelling. Flory describes(4.9), the effect of cross-linker in equation II.5. The higher the cross-linking level the lower the average molecular weight of a polymer chain unit( $M_c$ ) and the lower the swelling of the polymer.

## **IV.2.2 Effects of Two-way Interactions**

The interactions can further explain the effect the factors have on the size ratio of the membrane. If one of the factors has a very large effect, it is more likely that the interaction will be seen as significant.

### **IV.2.2.1 Effect of D\*XL Interaction**

At high levels of cross-linker, the size ratio is lower at high DMAEMA levels than when the cross-linker level is low, Figure IV.5. The larger size ratio is seen when cross-linker levels are low and DMAEMA levels are high. In this situation, there is a maximum number of potentially ionizable sites to enhance the swelling and a minimum number of cross-links to curtail swelling, so the situation is optimal for a large increase in size. An inconsistency is seen in the size ratios observed at low DMAEMA levels. It is observed that the membranes show a larger size ratio at high cross-linker levels than at low cross-linker levels. This is the opposite of what would be expected. The most probable explanation for this is the variation between the size ratios of the replicate membranes at high cross-link levels was much larger than that of the membranes at lower levels. The standard deviation for high levels was approximately ten times greater than the low levels, 0.17 and 0.019 respectively. This indicates the effect we see could actually be caused by measurement error.

### **IV.2.2.2 Effect of XL\*XT Interaction**

The interaction between the cross-linker level and cross-linker type shows that the difference between size ratios with TEGDM compared to EGDM is greater at the high level of cross-linker, Figure IV.6. Membranes with TEGDM have a size ratio of 1.53, compared to 1.27 for EGDM. A membrane that has high cross-linking and a smaller



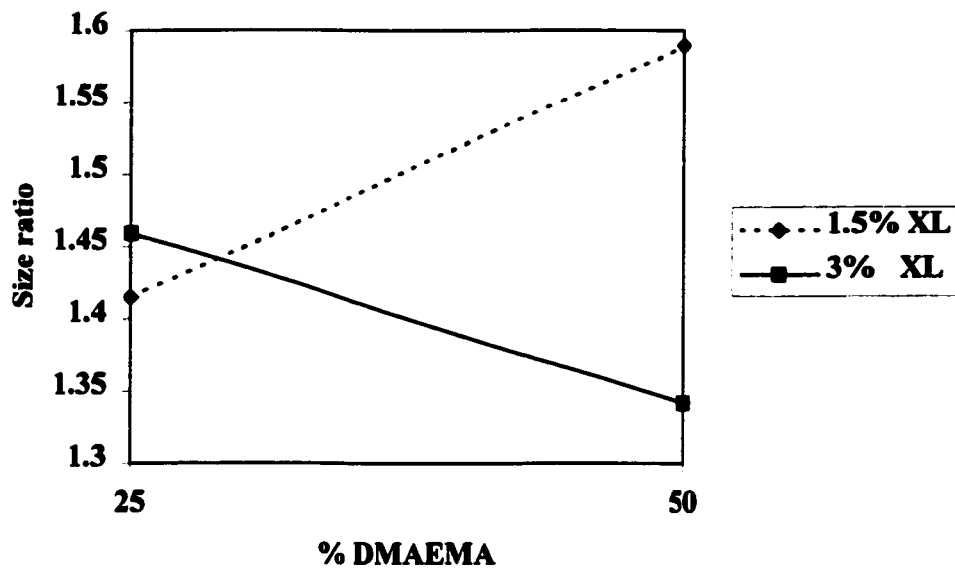


Figure IV.5. The effect of DMAEMA \*% cross-linker interaction on the size ratio.

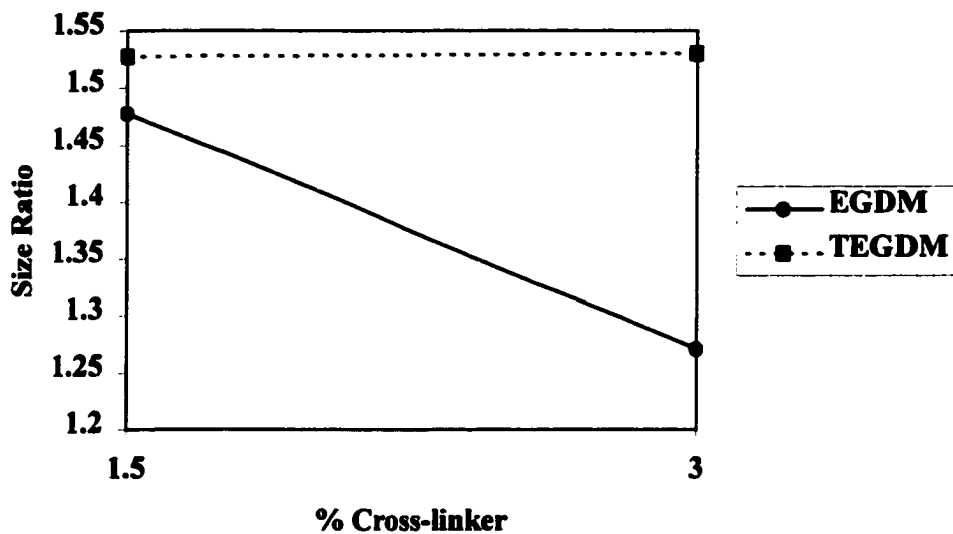


Figure IV.6. The effect of % cross-linker\*cross-linker type on the size ratio.

cross-link chain will result in a membrane with a low amount of swelling. Comparison of the size ratios for each cross-linker type shows that the difference between high and low cross-linking levels is greater for EGDM than for TEGDM. This could be explained if the TEGDM is more hydrated in the unswollen state. If TEGDM was more hydrated in the unswollen state, then the membrane size ratio would not be as large as expected for a low cross-linker level, since the size difference between the swollen and unswollen states would be smaller. The effect of cross-linker level would be masked by the effect of hydration.

### **IV.2.3 Effect of Three-way Interaction**

#### **IV.2.3.1 Effect of D\*XL\*XT Interaction**

The interaction of cross-linker type and cross-linker level at high DMAEMA is as expected. Higher size ratios are seen at low cross-link levels and using the high type cross-linker TEGDM, Figure IV.7.A and IV.7.B. The interaction at low levels of DMAEMA looks very similar to the two-way interaction for the cross-linker type and cross-linker level. The largest difference is seen at high cross-linker levels. Most unexpected is the apparent decrease in size ratio with decreasing cross-linker levels that is seen for TEGDM. Again the explanation may be that the membrane is in a more hydrated state when unswollen so the difference between the swollen and unswollen states is lower.

### 50% DMAEMA

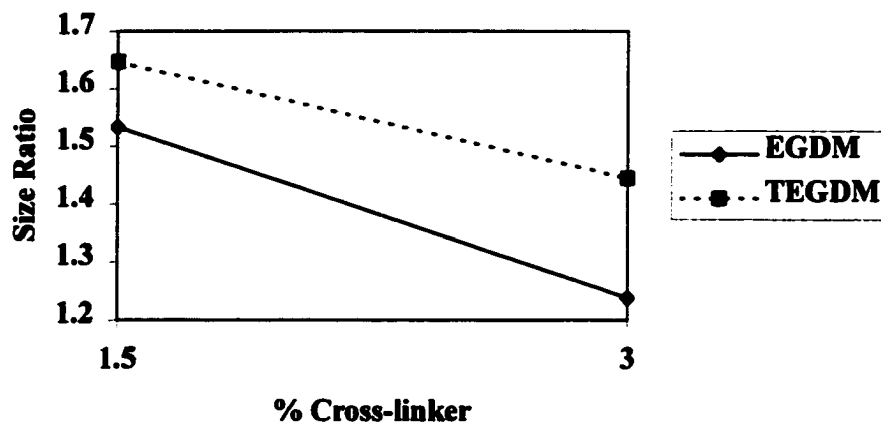


Figure IV.7.A. The effect of DMAEMA\*% cross-linker\*cross-linker type on the size ratio for 50 % DMAEMA membranes.

### 25% DMAEMA

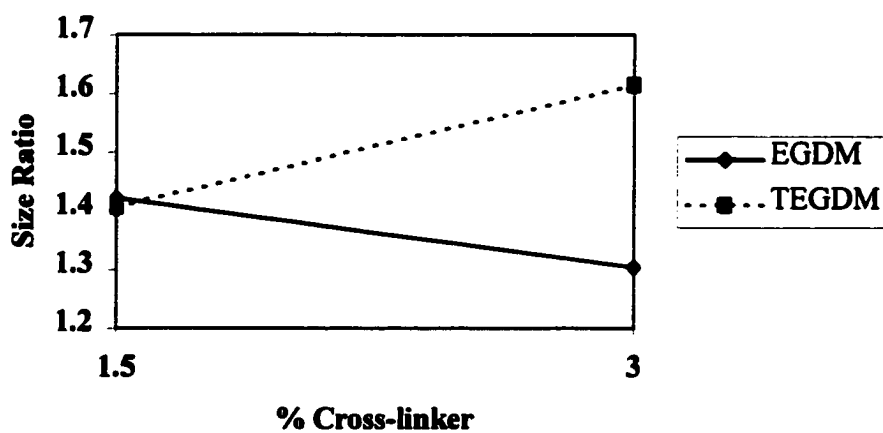


Figure IV.7.B. The effect of DMAEMA\*% cross-linker\*cross-linker type on the size ratio for 25 % DMAEMA membranes.

## **IV.3 Results and Discussion of Systematic Studies of Cross-linker Concentration and DMAEMA Concentration on Size Ratio**

### **IV.3.1 Effect of Cross-linker Concentration on Size Ratio**

As was seen in the cross-linker factorial, section IV.2, the cross-linker level has a large effect on the size ratio of a membrane. To further study the effect of cross-linker and cross-linker type, a systematic study was carried out. Table IV.2 shows that the size ratio decreases with increasing cross-linker level, confirming the factorial experiment. There is a sharp decrease in size ratio as the cross-linker level increases from 0 % to 1.5 %. At 0 % cross-linker the size of the membrane more than doubles going from the unswollen to swollen state. In the case of no cross-linker, the swelling is constrained only by the amount by which the membrane can be stretched. In this case, the number of ionizable sites and the uptake of water into the membrane control the swelling. Size ratios decrease as cross-linking increases. For both cross-linkers there is an almost 30 % decrease in size ratio as cross-linking increases from 0 % to 1.5 %. The size ratio seems to be leveling off as the cross-linker level continues to increase. This appears contradictory, since it would be expected that the size ratio would continue to decrease as the cross-linker level went up. However, it is possible that the membrane reaches a point where further cross-linking will not change the size ratio as much. That is the cross-links constrain the membrane to such a degree that a “saturation point” has been reached. Further cross-links serve to reinforce the swelling constraint, but do not add to it. The level at which this occurs would be dependent upon the number of ionizable sites, since that would affect the force of outward expansion. It is unclear why the size ratio seems to reach a minimum at 1.5 % cross-linking.

**Table IV.2. Effect of cross-linking level and cross-linker type on size ratio.**

% Crosslinker (mol/mol)	EGDM		TEGDM	
	Size Ratio	r.s.d. %	Size Ratio	r.s.d. %
0	2.24	10.2	2.24	10.2
1.5	1.42	1.9	1.41	2.7
3	1.43	5.1	1.62	7.4
4.5	1.33	2.9	1.51	6.0

**All membranes prepared with 25 % DMAEMA (mol/mol) and 15 % (vol/vol) water solvent.**

The effect of cross-linker identity on size ratio was as expected. TEGDM with the longer cross-links had a greater size ratio than the EGDM. The decrease in size ratio with increasing cross-linking is similar for both types of cross-linkers. It was observed that the TEGDM membranes had relative standard deviations slightly higher than for EGDM. Also observed in both types of cross-linker is the leveling off at high cross-linking levels.

The mechanical stability of the membranes was also observed. As the degree of cross-linking increased, the membranes became more brittle. This is the result of the cross-links holding the polymer chains together to a greater extent. The polymer chains are not able to bend as much making the membranes more brittle. These results agree with the Chirila group who also observed that increasing cross-linking levels caused both a decrease in the energy needed to break membranes and a decrease in the amount by which membranes elongated prior to breaking.<sup>95</sup> The brittleness was more pronounced in the EGDM cross-linked membranes compared to the TEGDM membranes. The longer chain length of TEGDM allows the polymer to be more flexible.

#### **IV.3.2 Effect of DMAEMA concentration on size ratio**

It is expected that an increase in the DMAEMA concentration would have the effect of increasing the size ratio. The higher DMAEMA concentration membranes would have more ionizable sites and therefore a greater potential for swelling. The increase in ionizable sites is the result of an increase in amine sites in the membrane. This can be seen as an increase in the nitrogen concentration of the membrane, Table IV.3. The nitrogen increases from 0.80 % to 5.40 % for an EGDM cross-linked membrane and from 1.00 % to 6.03 % for a TEGDM cross-linked membrane. The

experimental nitrogen concentrations correlate well to the theoretical values showing that the membrane composition was as expected. This confirms that one monomer was not dominating more in the membrane than it had in the prepolymer mixture.

Figure IV.8 shows that an increase in DMAEMA causes an increase in size ratio. From 10 % DMAEMA there is an increase in size ratio from 1.17 to 1.55 at 75 % for EGDM and from 1.18 to 1.76 for TEGDM. There is little difference between the size ratios of EGDM and TEGDM observed at the lower DMAEMA levels, but the difference becomes pronounced at the higher DMAEMA levels. At the lower DMAEMA levels, 10 % and 25 %, the membranes may not become protonated to enough to completely swell the membrane. In this instance, the degree of swelling would be controlled by the number of ionized sites and not by the constraining effect of the cross-links.

A decrease in the amount in which the size ratio increases occurs as the DMAEMA concentration increases. This is seen as a leveling of the size ratio when the DMAEMA level of the membrane increases above 50 %, Figure IV.8. This may be attributed to the membrane reaching a maximum swelling level that is limited by the constraint of the cross-links and not the number of ionizable sites. In this condition, the swelling force will be enhanced, but the cross-links will resist it. This will result in the membrane being less mechanically stable. The difference between cross-link type can be seen as in previous experiments. TEGDM shows a higher size ratio compared with EGDM.

As the concentration of DMAEMA in the membranes was increased, the mechanical stability of the membrane decreased. Table IV.4 shows in qualitative terms the effect of increasing DMAEMA levels. Low DMAEMA membranes can be handled



**Table IV.3. CHN analysis results and expected values for HEMA membrane with varying DMAEMA concentrations and cross-linkers**

% DMAEMA	X-Linker Type	% C		% H		% N	
		Theory	Exp.	Theory	Exp.	Theory	Exp.
10	EGDM	56.16	56.21	7.96	7.82	1.03	0.80
10	TEGDM	56.23	55.62	7.95	8.20	1.01	1.00
25	EGDM	57.10	57.41	8.27	8.05	2.50	1.78
25	TEGDM	57.16	57.06	8.25	8.05	2.46	1.73
50	EGDM	58.56	57.84	8.74	8.57	4.77	4.29
50	TEGDM	58.59	57.91	8.72	8.94	4.70	4.64
75	EGDM	59.89	57.10	9.18	8.70	6.84	5.40
75	TEGDM	59.90	58.68	9.15	8.93	6.74	6.03

All membranes prepared with 1.5 % cross-linking(mol/mol) and 15 % (vol/vol) water solvent.

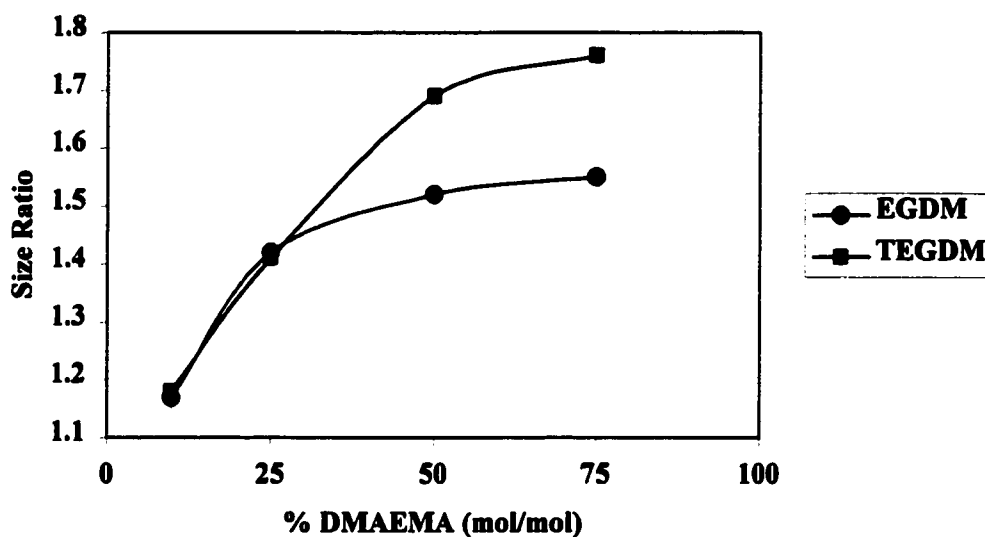


Figure IV.8. Effect of varying DMAEMA concentration and cross-linker type on size ratio.

**Table IV.4. Mechanical properties of membranes with varying DMAEMA concentration**

<b>DMAEMA Concentration</b>	<b>Mechanical Observations</b>	<b>Comments</b>
10 %	Very good membrane stability	Undergoes multiple swell/shrink cycles with no loss of stability, easily handled without breaking
25 %	Very good membrane stability	Undergoes multiple cycles with no loss of stability, easily handled
50 %	Fair membrane stability	Undergoes a number of cycles before cracks develop, holds together well with cracks for several cycles before breaking, may be handled with care without breaking
75 %	Poor-fair membrane stability	Cracks develop early and results in membrane failure within several cycles, membrane may be handled with some difficult
100 %	Very poor membrane stability	Cracks develop in 1 <sup>st</sup> or 2 <sup>nd</sup> cycle and membrane breaks apart very quickly, membrane somewhat difficult to handle due to high hydration

**All membranes prepared with 1.5 % cross-linking(mol/mol) and 15 % (vol/vol) water solvent.**

and undergo numerous shrinking and swelling cycles. As the DMAEMA level goes up the membranes become less able to handle the stresses of shrinking and swelling. The membranes can still be handled in water. It is not until cycling begins that the mechanical problems become evident. Mechanical instability as cycling is carried out is the result of the stresses that arise during the swelling cycle. At higher DMAEMA levels, there is a greater level of stress applied to the membrane as a result of the higher level of ionization on the polymer backbone. For a given level of cross-linking, the amount of stress applied to the membrane will increase as the DMAEMA level is increased. This higher level of swelling will cause the membrane to break apart if the cross-linking level is too great. In this situation, the containing force applied by the cross-links is less than the swelling force applied by the ionized sites. Membranes prepared with 100 % DMAEMA broke apart completely in an acidic environment, because the swelling force was greater than the force of the cross-links constraining it. This makes the process of finding an optimal DMAEMA amount difficult, since the level should maximize swelling but still leave the membrane mechanically stable.

#### **IV.3.2.1 Effect of Solution pH on Size Ratio**

The size ratio depicts the extremes in pH observed, pH 4 and pH 10, however the size will be affected by the pH of solutions at intermediate pH's as well. Size ratios were determined in several buffer solutions of constant ionic strength from pH 4 to pH 10, Figure IV.9. The size ratios were determined by normalizing the membrane size with the membrane size at pH 10. Measurements were made by exposing the membrane to successively higher pH buffer solutions. Membranes were allowed to equilibrate for 30 minutes between measurements. The membrane is fully protonated and largest at low

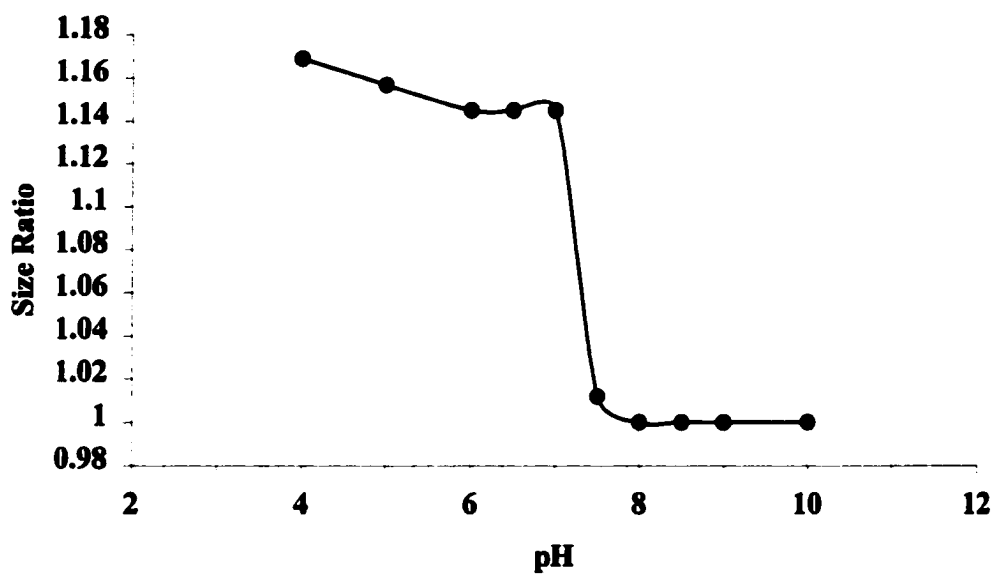


Figure IV.9. The size ratio of 25 % DMAEMA-co-HEMA membrane as a function of buffer pH. All buffers 0.1 M and I.S. 0.1 M.

pH. At intermediate pHs, the membrane is not fully protonated and is smaller in size. When unprotonated at high pH, the membrane is in its' shrunken and smallest form. The figure indicates that the pKa is around 7.25. This is slightly lower than the expected pKa for DMAEMA in solution, which was observed to be approximately 7.9.<sup>96</sup> Sheppard observed a pKa of 7.7 for the HEMA-co-DMAEMA system.<sup>57</sup> A possible reason for the shift to a lower pKa may be that the amine is not completely solvated by water in the polymer. The results are similar to those obtained by Rooney for a diethanolamine derivatized VBC bead.<sup>30</sup>

#### **IV.4 Effect of Changing Comonomer Identity on Size Ratio**

##### **IV.4.1 Introduction**

Both Davies<sup>45</sup> and Kudela<sup>44</sup> mention HEMA as the most widely used hydrogel. However, a number of alternative hydrogels are available for use. This section describes some of the results obtained by investigating other hydrogels to be used as the comonomer with DMAEMA. Two hydrogels, hydroxypropyl methacrylate(HPMA) and hydroxypropyl acrylate(HPA), were chosen because their structures are somewhat similar to HEMA. Also the hydrogels exhibit hydrophilicities slightly higher than HEMA, HPA, and slightly lower than HEMA, HPMA. Two other hydrogels with different structures were also evaluated, methyl methacrylate(MMA) and butyl methacrylate(BMA). The structures of these monomers are shown in Figure IV.1. The structure of these monomers, which lack the hydroxyl group found on the others, makes these monomers much more hydrophobic than the others.

The first experiment undertaken was to ensure that the various comonomers would form usable membranes when reacted with DMAEMA. This evaluation was

carried out using various levels of DMAEMA, 25 %, 50 % and 75 % with 1.5 % cross-linking. The polymerizations were initiated using the photo-initiator DMPAP. Table IV.5 summarizes the results obtained in the preliminary experiment. In the table the observations for all DMAEMA levels are summarized together.

The comonomers with low hydrophilicities, MMA and BMA, did not produce membranes that were usable for sensing. Membranes prepared with MMA monomer had low hydration and were very brittle. Given the hydrophilicity level of the monomer this is not surprising. The rubbery and tacky nature of the BMA membrane is somewhat surprising. The results at first seemed to indicate that the polymerization was not complete. To overcome this, the reaction was allowed to continue for longer periods of time. Photopolymerization was carried out for over 3 hours with no change in results. Polymerization of BMA without DMAEMA showed similar results, indicating that the inability to form a usable polymer was not the result of interaction of the BMA and DMAEMA during polymerization. The results obtained for BMA cannot be completely explained. BMA and MMA were not investigated further.

The more hydrophilic comonomers produced more promising results. Both monomers gave membranes that were quite similar in characteristics to the HEMA membranes. The membranes prepared were brittle at first, but became pliable and usable upon hydration. HPMA gave a slightly more brittle membrane, even when hydrated, than HPA. This correlates with HPMA taking up less water than HPA, as predicted by the hydrophilicities of the monomers. The membranes obtained from both comonomers proved to be usable for sensing.

**Table IV.5. Results of DMAEMA Comonomer Preliminary Study**

<b>Comonomer Identity</b>		<b>Results</b>
<b>Methyl methacrylate</b>	<b>(MMA)</b>	<b>Membranes were extremely brittle, unusable</b>
<b>Butyl methacrylate</b>	<b>(BMA)</b>	<b>Membranes were rubbery, unusable</b>
<b>Hydroxypropyl methacrylate (HPMA)</b>		<b>Membranes were well formed, easily handled when hydrated, clear to slightly opaque, usable</b>
<b>Hydroxypropyl acrylate</b>	<b>(HPA)</b>	<b>Well formed membranes, easily handled when hydrated, clear to slightly opaque, usable</b>

**All membranes prepared with 1.5 % EGDM(mol/mol) and 15 % (vol/vol) water solvent.**



#### **IV.4.2 Results and Discussion of Factorial Experiment Examining Effect of Comonomer Hydrophilicity and DMAEMA Level on Size Ratio**

This factorial was undertaken to study the effect of the comonomer hydrophilicity and DMAEMA concentration on the size ratio. The average size ratios for the formulations used in the factorial study are shown in Figure IV.10. Error bars represent  $\pm$  one standard deviation and are determined from three replicate measurements. The membrane with low hydrophilicity showed a greater size ratio, formulations 3 and 4. It was also observed that membranes with higher levels of DMAEMA had larger size ratios. This is especially noticeable for membranes of low hydrophilicity.

The ANOVA Table IV.6 reveals both main variables and the interactions that significantly affect the size ratio at the 99% confidence level. The  $F_{\text{critical}}$  value for 99% confidence level is 11.26. Membrane hydrophilicity showed the largest effect on size ratio.

##### **IV.4.2.1 Effects of Main Factors**

Figure IV.11 shows the average effect on the size ratio of the main factors. Each point represents the average of 2 formulations for the points at each level.

##### **IV.4.2.1.1 Effect of Comonomer Hydrophilicity**

The HEMA is more hydrophilic than the HPMA. The hydroxyl group of the HEMA is at the end of the carbon chain and can be more readily hydrated. In the HPMA, the hydroxyl group is in the carbon chain and is better shielded. The result is that the HEMA is more easily able to take up water.

The hydrophilicity of the comonomer proved to have the largest effect on the size ratio. The largest size ratio was seen in membranes with low comonomer hydrophilicity. This seemed contradictory at first, since you would expect that a more hydrophilic

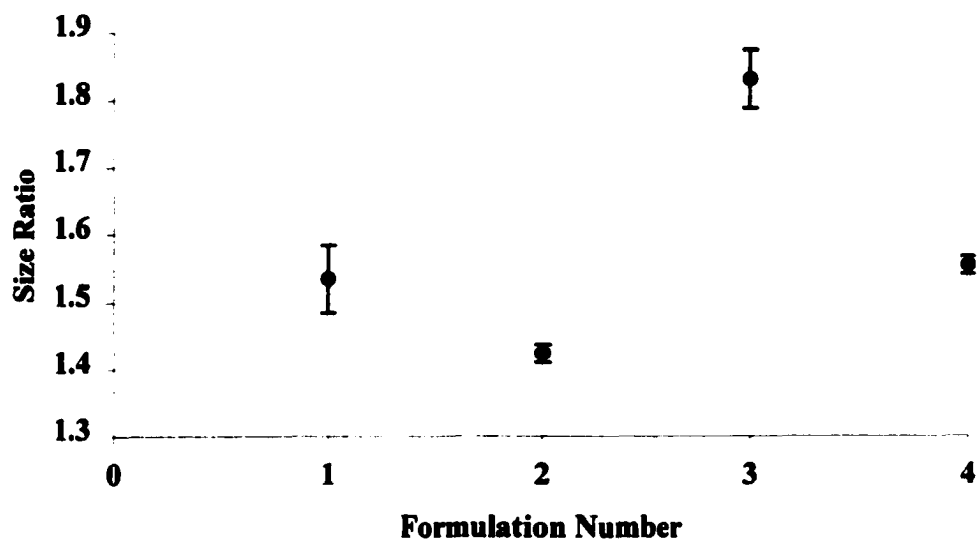


Figure IV.10. The mean size ratio and standard deviations for formulations of comonomer factorial experiment(n=3).

**Table IV.6 Results of Analysis of Variance for Size ratio Examining Effect of Comonomer Hydrophilicity and Concentration of DMAEMA**

Source	DF	SS	MS	F	P
Comonomer (C)	1	0.136939	0.136939	117.22	0.000 **
DMAEMA (D)	1	0.112889	0.112889	96.63	0.000 **
D*C	1	0.020675	0.020675	17.70	0.003 **
Error	8	0.009346	0.001168		
Total	11	0.279849			

df = degrees of freedom

SS = sum of squares

MS = mean squares

F = F statistic, ( $MS_{\text{effect}}/MS_{\text{error}}$ )

p = probability of incorrectly rejecting the null hypothesis

\*\* = significant at 99% confidence interval,  $F_{\text{critical}}=11.26$  (n=8)

membrane would take up more water and therefore swell to a greater extent. However, if it is considered that the more hydrophilic membrane is more swollen in the unswollen state because of its increased hydrophilicity, the results are as expected. Cross-links and the degree of ionization control the size in the swollen state. Since the high hydrophilicity membrane would be more swollen in the unswollen state, the size difference between the swollen and unswollen state is less and therefore the size ratio is lower.

#### **IV.4.2.1.2 Effect of DMAEMA Concentration**

The effect of DMAEMA shows that the higher the DMAEMA level the higher the size ratio. This is as expected, since higher DMAEMA levels will have greater numbers of ionizable sites. More ionizable sites allow for a higher charge build up and therefore more swelling, as shown in Equation II.5. The effect of comonomer hydrophilicity is not as overwhelming as cross-linker, resulting in the effect being significant.

#### **IV.4.2 Two-way Interaction**

##### **IV.4.2.1 Effect of DMAEMA Concentration\*Comonomer Interaction**

The interaction between % DMAEMA and comonomer hydrophilicity shows that larger size ratios are obtained at lower comonomer hydrophilicity than at higher comonomer hydrophilicity, Figure IV.13. The results are as expected from the main factor effects. High % DMAEMA and low comonomer hydrophilicity both act to increase the size ratios. Larger size ratios are produced by less hydrophilic comonomers at all DMAEMA levels.

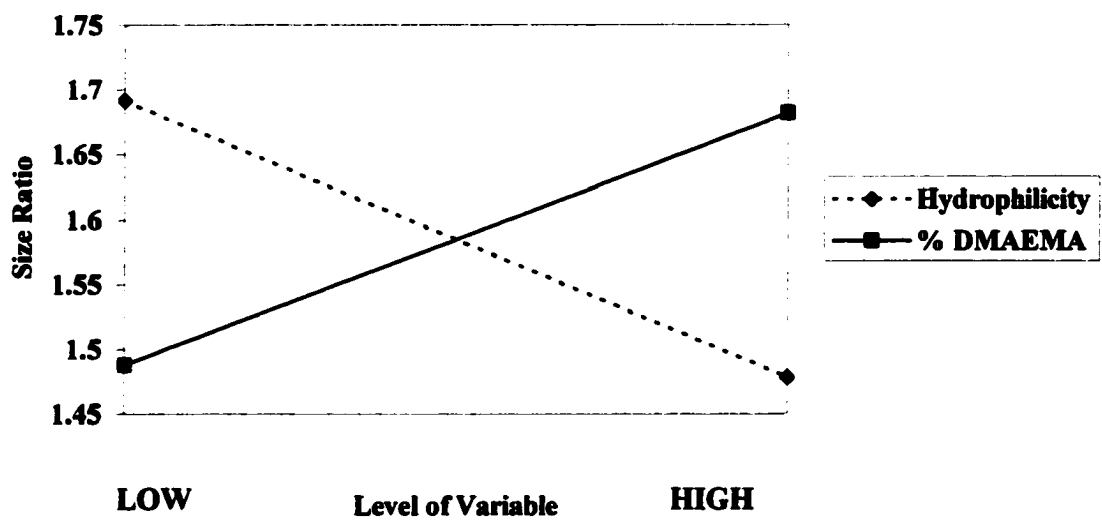


Figure IV.11. The average effect on the size ratio of changing amounts of the main factors.

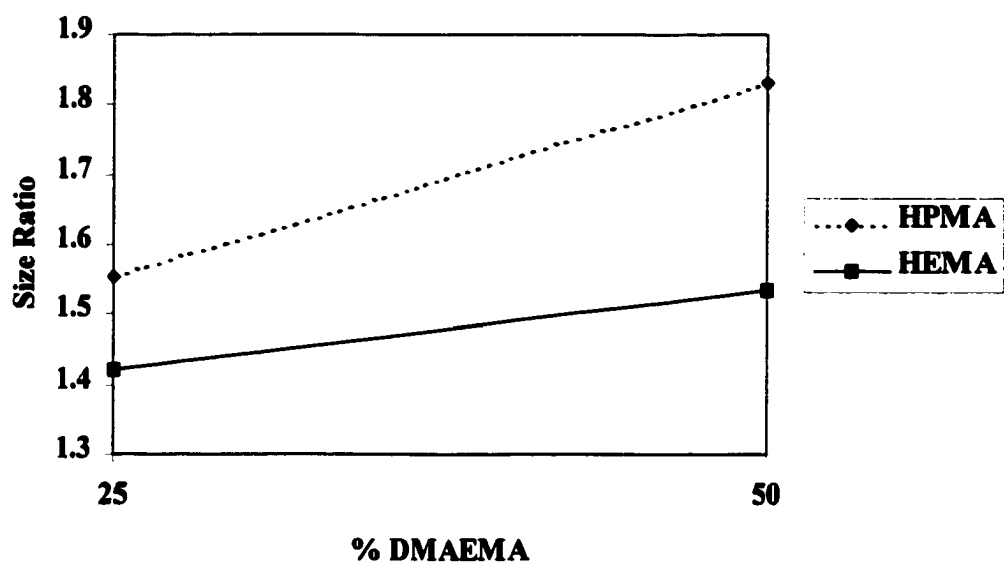


Figure IV.12. The effect of % DMAEMA \*Comonomer Type on the size ratio.

#### **IV.4.3 Comonomer Systematic Study**

The factorial described in section IV.4 showed that the hydrophilicity of the comonomer has a large effect on the size ratio that is observed. To study the effect of comonomer on size ratio, a systematic study was conducted to study the size ratio of three different comonomers at three different DMAEMA concentrations, Figure IV.13. The comonomers evaluated in order of increasing hydrophilicity were hydroxypropyl methacrylate(HPMA), hydroxyethyl methacrylate(HEMA) and hydroxypropyl acrylate(HPA). As observed in sections IV.3.2 and IV.4.2, the size ratio increased with increasing DMAEMA concentration. The comonomer factorial showed an increase in size ratio with decreasing comonomer hydrophilicity. This is believed to be the result of the unswollen membrane being more hydrated in the more hydrophilic membrane. The swollen state size is still controlled by the amount of ionization or cross-linking level. As a result there is a smaller difference between the swollen and unswollen states, resulting in a lower size ratio.

An interesting phenomenon is the apparent increase in slope, as the comonomer becomes more hydrophilic. HPA increases from 1.07 to 1.33 when % DMAEMA is increased from 10 to 50 %. HEMA increases from 1.17 to 1.52 and HPMA from 1.17 to 1.82. The difference is 0.26, 0.35 and 0.65 respectively. The explanation for this may be that the hydrophobic comonomer membrane reaches its equilibrium hydration size more rapidly. The membranes with more hydrophilic comonomers will take up more water at each DMAEMA level. This allows the membrane to increase in size until constrained by the cross-links.

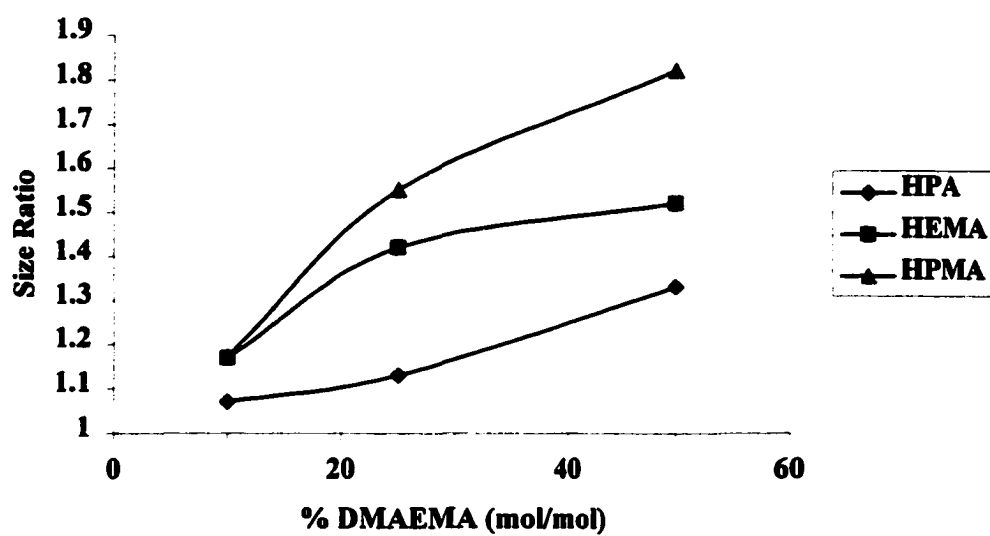


Figure IV.13. Effect of varying DMAEMA concentration and comonomer type on size ratio.



**Table IV.7. CHN analysis results and expected values for various comonomer membrane formulations**

<b>Comonomer Type</b>	<b>% DMAEMA</b>	<b>% C Theory</b>	<b>% C Exp.</b>	<b>% H Theory</b>	<b>% H Exp.</b>	<b>% N Theory</b>	<b>% N Exp.</b>
HPMA	10	58.66	55.46	8.52	8.15	0.94	0.69
HPMA	25	59.10	57.36	8.70	8.25	2.33	2.02
HPMA	50	59.80	57.42	9.01	8.91	4.56	4.27
HPA	10	56.16	55.71	7.97	8.05	1.03	0.73
HPA	25	57.11	55.40	8.27	7.94	2.50	2.18
HPA	50	58.56	56.80	8.75	8.74	4.77	4.76

**All membranes prepared with 1.5 % EGDM cross-linking (mol/mol) and 15 % (vol/vol) water solvent.**

The results of CHN analysis for the copolymer membranes are given in Table IV.7. The values obtained experimentally were in reasonable agreement with those calculated theoretically. This indicated that the reaction between copolymers and HEMA is producing membranes whose composition is the same as that of the prepolymer mixture, as was the case with HEMA copolymer. It confirms that the polymerization is not favoring a particular monomer and excluding the other as the reaction proceeds. The results show the predicted increase in nitrogen content with increasing DMAEMA concentration. The values for nitrogen content seem to be consistently lower by approximately 0.3 %.

#### **IV.5 Hydration of Membranes**

Water is an extremely important component in hydrogels. Hydrogels such as HEMA are often brittle when dry, but upon immersed in water will absorb the water and become much more elastic and pliable. When hydrogels are used as a sensing material water is necessary to keep the membrane pliable, and also to transport the analyte of interest. When a pH sensitive membrane is immersed in a buffer solution, the hydrogen ions diffuse through the water and into the membrane. Any factors that affect the hydration of the membrane have the potential to affect the operation of the sensor. The effect of cross-linker levels, cross-linker type and concentration of DMAEMA were examined to see the effect that these factors would have on the amount of water in the membrane.

The effect of increasing cross-linker would be expected to reduce the water content of a membrane. Cross-linking would hold the polymer backbone chains together more tightly, which would prevent them from swelling as much in water. Figure IV.14

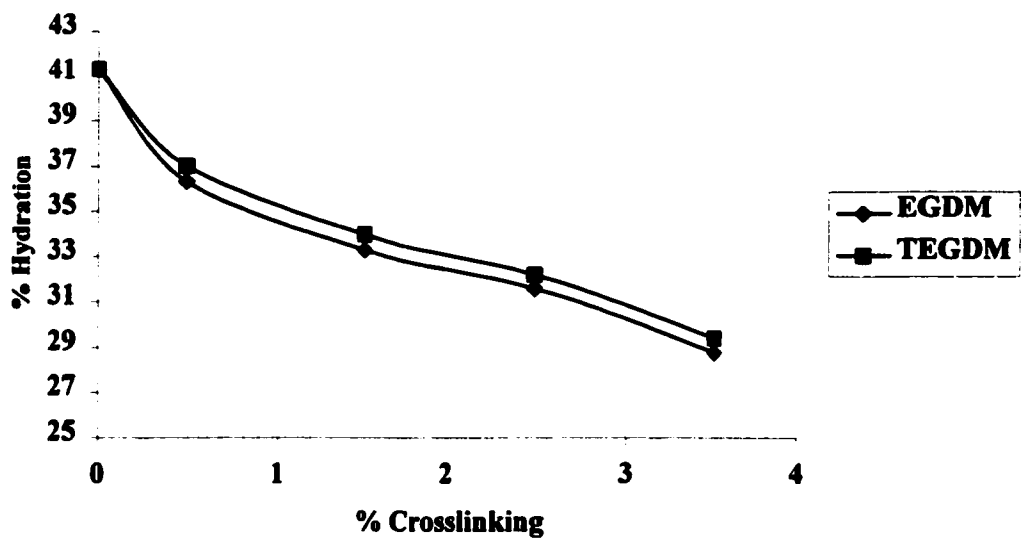


Figure IV.14. The effect of cross-linking level and type on hydration of poly-(HEMA) membrane.

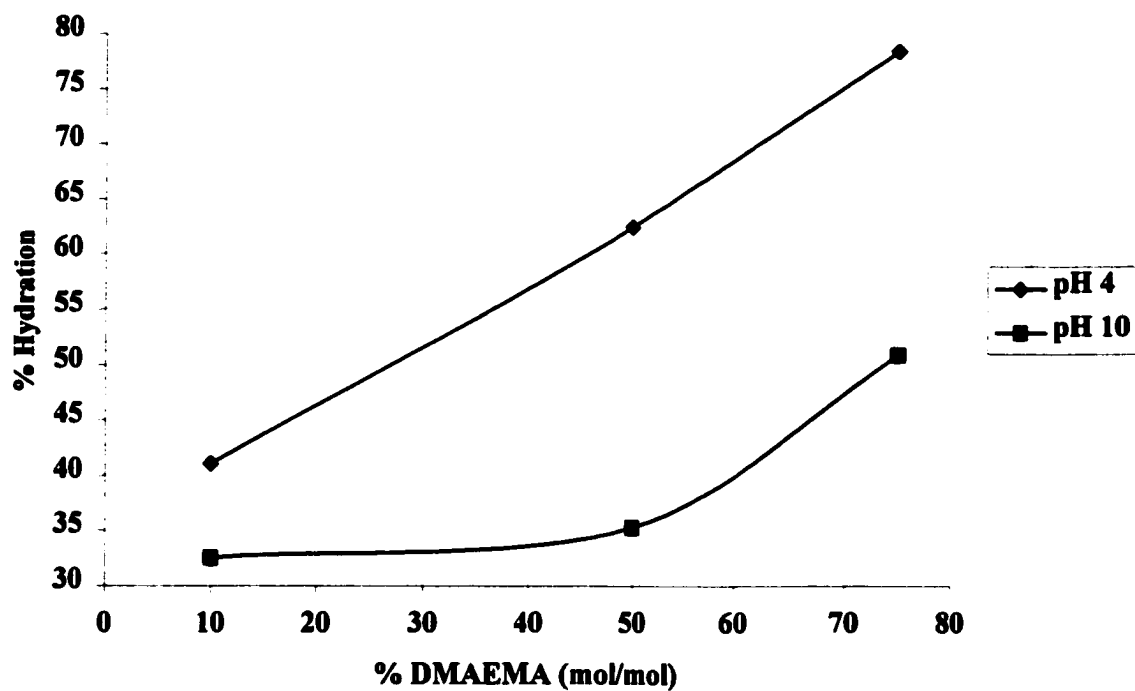
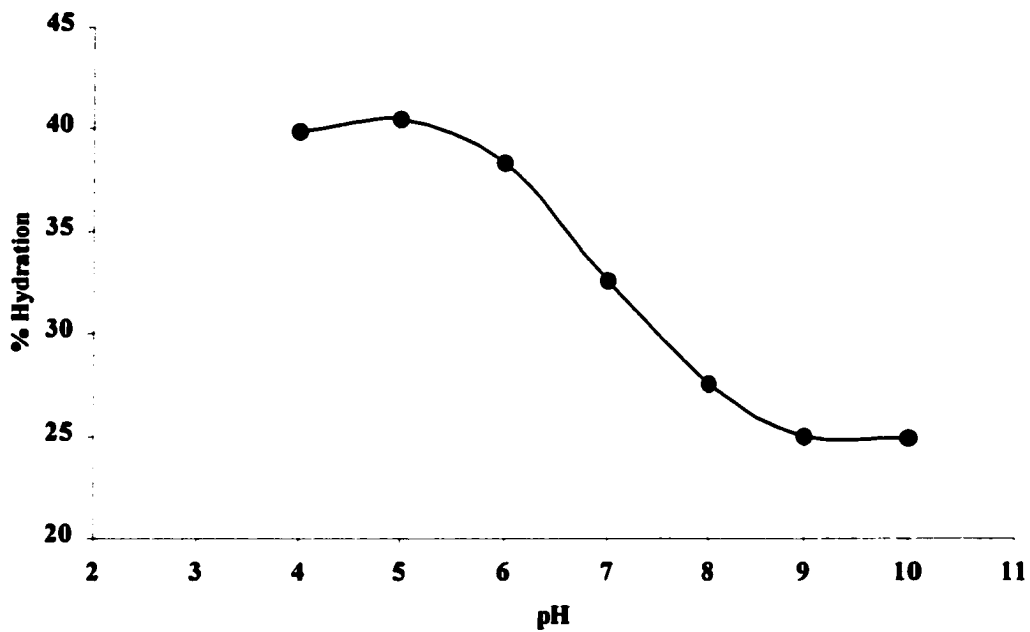


Figure IV.15. The hydration level of HEMA membrane as a function of DMAEMA concentration. Membrane cross-linked with 1.5 % TEGDM. Buffers 0.1 M and I.S. 0.1 M.



**Figure IV.16. The hydration level of 25 % DMAEMA-co-HEMA membrane as a function of buffer pH. All buffers 0.1 M and I.S. 0.1 M. Membrane cross-linked with 1.5 % EGDM.**

shows the effect of cross-linker type and increasing cross-linking level on the percent hydration of the a poly-HEMA membrane. Increasing the cross-linker concentration caused a decrease in the hydration level of the membrane for both types of cross-linker used. The water content of EGDM cross-linked membranes decreased from 41.3 % to 28.8 % when cross-linking levels rose from 0 % to 3.5 %. In TEGDM cross-linked membranes the water content decreased from 41.3 % to 29.4 % over the same interval. The decrease is slightly less in TEGDM cross-linked membranes than EGDM cross-linked membranes and TEGDM membranes show slightly higher hydration levels at all cross-link levels. This is most likely the result of the longer length of the TEGDM cross-link. The effect of cross-linker type on hydration level is much lower than that of cross-linking level.

The concentration of DMAEMA may also have an effect on the hydration of the membrane. DMAEMA concentration was examined for its effect on the hydration of the membrane in either the swollen or unswollen state. The results of DMAEMA concentration on the swollen and unswollen hydration levels of a membrane are shown in Figure IV.15. As expected the hydration levels are larger in the swollen state, pH 4. This represents the polymer chains being far apart due to electrostatic forces and the membrane being filled with water. In the case of the unswollen membrane, the membrane is not stretched and therefore not filled with water and shows a lower overall level of hydration. The increase in hydration as DMAEMA concentration increases is clearly seen in the pH 4 membranes. Increasing the DMAEMA concentration from 10 % to 75 % causes the hydration level to increase from 41.1 % to 78.4 %. The increase is not as apparent in the pH 10 membrane, where the hydration level increases from 32.5 %

to 50.9 % over the same interval. The reason for this difference is not apparent. For a 50 % DMAEMA membrane the ratio of percent hydration in pH 4 to pH 10 is 1.77. The size ratio for the same membrane was 1.69. This shows a strong correlation between the size ratio and the hydration level of membranes, confirming that the observed size change is the result of water uptake.

Figure IV.15 showed that membranes in more acidic solutions have higher hydration levels. This effect was further investigated to determine the effect of solution pH on the hydration level of the membrane, Figure IV.16. The figure resembles the size ratio plot, Figure IV.9, in that it starts high and is level at low pH, then drops before again leveling at high pH. At low pHs the membrane is in its swollen state and fully hydrated. At the intermediate pHs, the membrane is partially protonated, therefore the membrane is not fully swollen with water. At high pHs, the membrane is not protonated and stretched, therefore the membrane is not swollen with water. Although similar to the shape of Figure IV.9. Figure IV.16 lacks the sharp transition and begins to decrease at a lower pH, around 5.5 instead of 7. These differences are likely the result of the larger pH intervals between measurements and the experimental difficulty of determining hydration levels of membranes. The results obtained are similar to those obtained by Sheppard.<sup>57</sup>

#### **IV.6 Results and Discussion of Factorial Experiment Examining Adhesion of Hydrogel Membranes**

In order for the sensor to operate properly, it is essential that the hydrogel membrane remain attached to the surface of the sensor as it shrinks and swells. Adhesion of the membrane to the substrate was accomplished through the use of 3-(trimethoxysilyl) propyl methacrylate as a coupling agent. The reaction is shown in Figure IV.17.

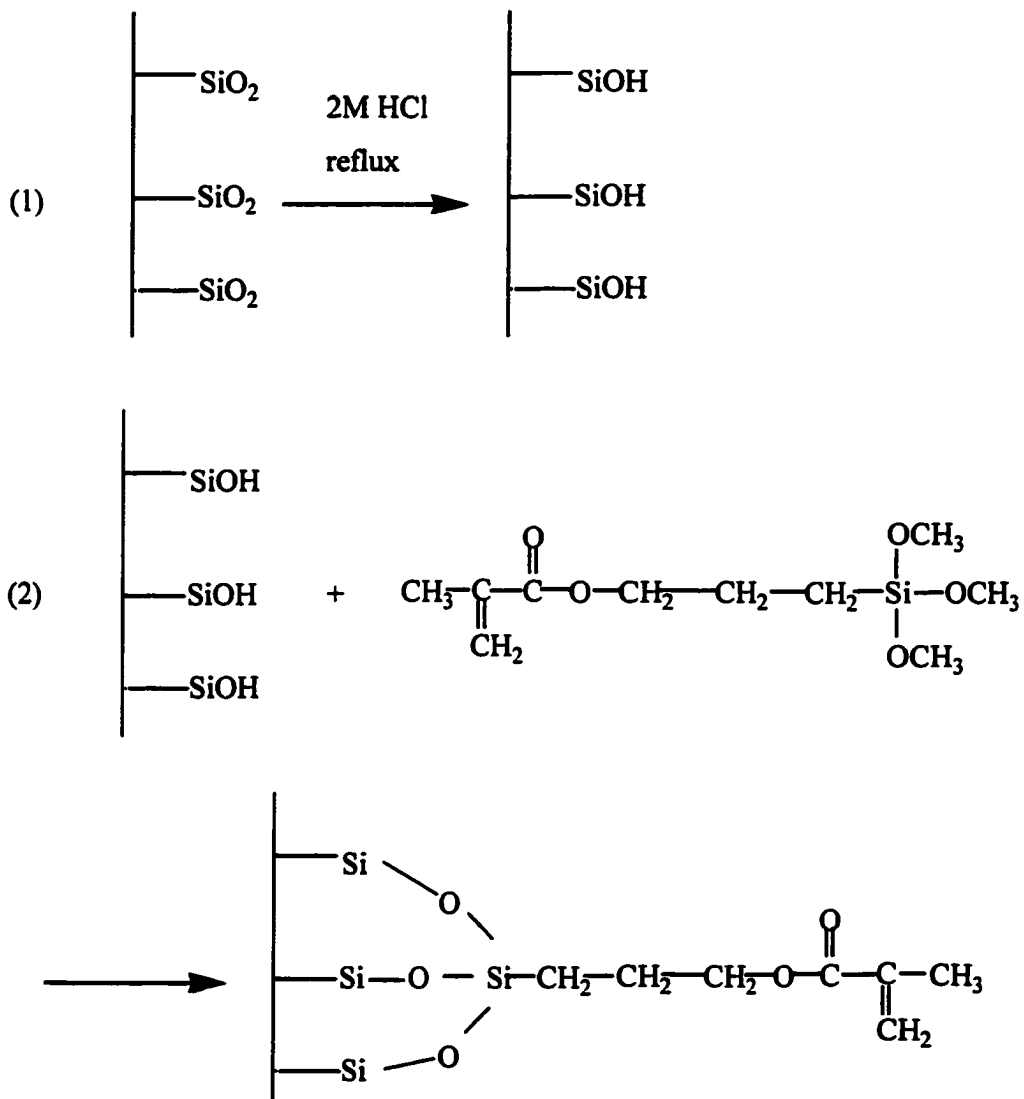


Figure IV.17. Surface derivatization for hydrogel adhesion with Trimethoxysilyl propyl methacrylate



Adhesion to a glass substrate is accomplished through displacement of the methoxy groups as the silane reacts with the glass surface. Polymer membranes can then be attached through the vinyl group at the methacrylate end of the coupling agent.

A factorial was undertaken to examine the factors that may affect adhesion using this adhesion agent. Table III.3 shows the concentration of all formulations used in this experiment. The mean length of time for delamination to occur for each formulation is shown in Figure IV.18. The values are obtained for duplicate measurements and the error bars represent  $\pm$  one standard deviation. The figure clearly shows that the formulations in high pH solutions, odd numbered formulations, delaminate much more quickly than those in low pH, even numbered formulations.

The ANOVA Table IV.8 reveals that several main factors and interactions have significant effects on the performance of the coupling agent. The pH of the buffer solution had the largest effect on performance. DMAEMA concentration was also significant. The  $F_{\text{critical}}$  value for 95 % confidence is 4.49 and the value for 99 % confidence level is 8.53.

#### **IV.6.1 Effect of Main Factors**

The effect of the main factors is shown in Figure IV.19. Solution pH and DMAEMA concentration were seen to be significant at the 99% confidence level in Table IV.8. Each point is the average of 8 formulations at each level.

##### **IV.6.1.1 Effect of Solution pH**

The pH of the soak solution was seen to have the largest effect on the time for the membrane to delaminate. Membranes in a high pH solution will delaminate first. This is the result of the basic solution attacking the silane groups. It is known that highly basic

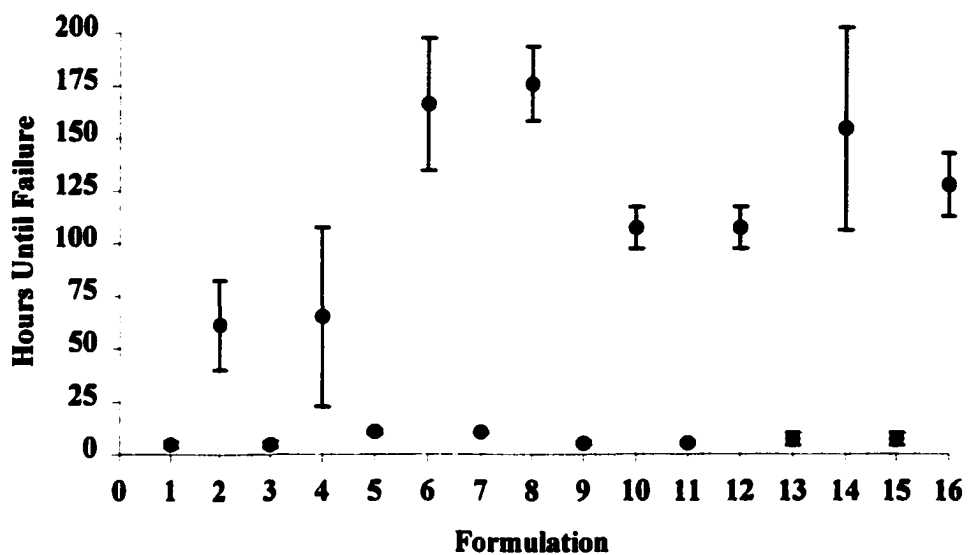


Figure IV.18. The mean time until failure(n=2) and standard deviations for formulations used in hydrogel adhesion experiment.

Table IV.8. Results of Analysis of Variance for Time Until Adhesion Failure of Hydrogel Membranes

Source	DF	SS	MS	F	P
Solution (S)	1	63.3	63.3	0.16	0.694
DMAEMA (D)	1	11137.8	11137.8	28.27	0.000 **
Size (Z)	1	21.1	21.1	0.05	0.820
pH (pH)	1	103285.1	103285.1	262.20	0.000 **
S*D	1	3022.5	3022.5	7.76	0.014 *
S*Z	1	200.0	200.0	0.51	0.486
S*pH	1	144.5	144.5	0.37	0.553
D*Z	1	55.1	55.1	0.14	0.713
D*pH	1	8911.1	8911.1	22.62	0.000 **
Z*pH	1	19.5	19.5	0.05	0.827
S*D*Z	1	128.0	128.0	0.32	0.577
S*D*pH	1	2450.0	2450.0	6.22	0.024 *
S*Z*pH	1	205.0	205.0	0.52	0.481
D*Z*pH	1	52.5	52.5	0.13	0.720
S*D*Z*pH	1	132.0	132.0	0.34	0.571
Error	16	6302.7	393.9		
Total	31	136130.5			

df = degrees of freedom

SS = sum of squares

MS = mean squares

F = F statistic, ( $MS_{\text{effect}}/MS_{\text{error}}$ )

p = probability of incorrectly rejecting the null hypothesis

\* = significant at 95% confidence interval,  $F_{\text{critical}}=5.32$  (n=8)

\*\* = significant at 99% confidence interval,  $F_{\text{critical}}=11.26$  (n=8)

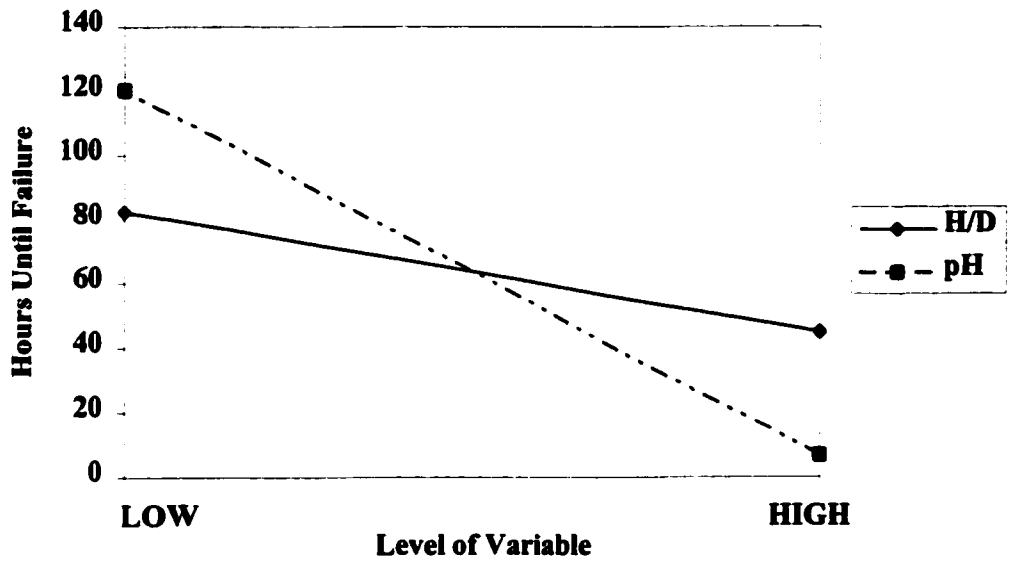
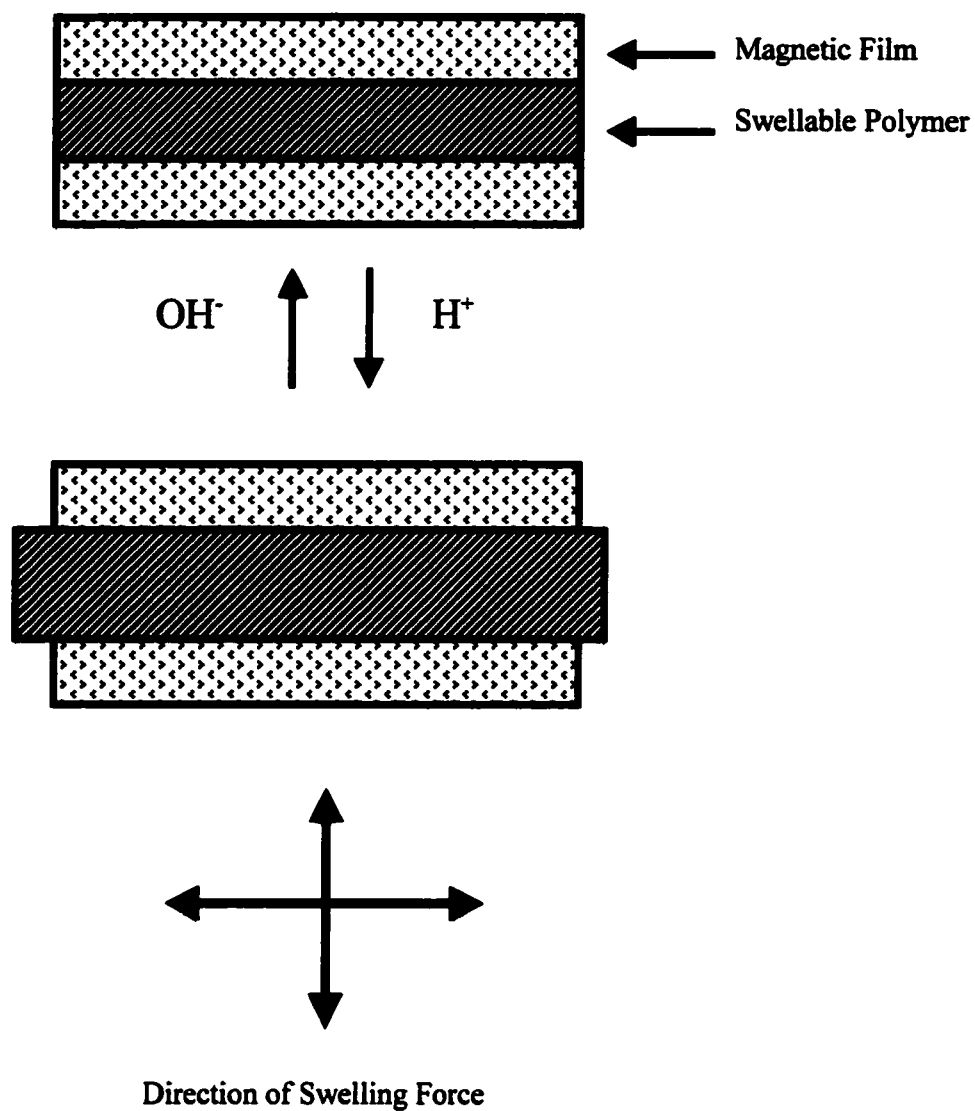


Figure IV.19. The average effect on time until adhesion failure of changing amounts of main factors.

solutions will etch glass, and the same is true of the bonds between the coupling agent and the glass. Both types of bonds are silicon-oxygen bonds, which are readily attacked by the hydroxyls group of basic solutions. Formulations in high pH had the shortest delamination time and those in low pH had the longest times. In the low pH solution the glass-silane bond is not attacked as severely and the delamination time is much longer. The delamination time increases from 6.7 hours at high pH to 120.3 hours at low pH.

#### **IV.6.1.2 Effect of DMAEMA Concentration**

The concentration of DMAEMA within the membrane has the second highest effect on the delamination time of the membrane. Membranes that contained 10 % DMAEMA had a shorter adhesion time than those without DMAEMA. The average adhesion time for a membrane without DMAEMA was 82.2 hours, with 10 % DMAEMA that time decreased to 44.9 hours. This decrease in time until delamination occurs is the result of the stress applied to the membrane/silane interface by the membrane expanding in lower pH solution. When the membrane is partially protonated and swells, this imparts a force parallel to the surface of the interface between the membrane and substrate, Figure IV.20. This is in addition to the desired swelling force that is perpendicular to the interface. The force is also in opposite directions at each end of the membrane; the membrane is pulled away from its center by the swelling. Higher DMAEMA concentrations would increase the swelling and would be expected to intensify this effect.



**Figure IV.20. Schematic diagram showing direction of swelling forces as polymer swells in acidic solution.**

## **IV.6.2 Two-way Interaction**

### **IV.6.2.1 Effect of DMAEMA Concentration\*pH**

The interaction of DMAEMA concentration with pH shows that shorter delamination times occur at high DMAEMA concentrations than at low concentrations regardless of solution pH, Figure IV.21. Higher DMAEMA levels produce lower adhesion times at low pH because of the partial swelling of the membrane. At high pH the delamination is largely attributed to the attack of the silane bonds. The shorter delamination time at pH 10 for high DMAEMA levels than at low DMAEMA levels may be the result of the less electronegative nitrogen replacing the hydroxyl groups less than the hydroxyl group of the HEMA. Also observed is that the delamination time is lower in high pH regardless of DMAEMA level. The difference between delamination in low pH and high pH is greater at low DMAEMA levels than at high DMAEMA levels. This difference could be the result of the increased stress associated with the protonated membrane at low pH and high DMAEMA levels. In the case of high DMAEMA, at both pH levels there is an effect acting to cause delamination. At low DMAEMA level, only in high pH is there a strong force acting to delaminate the membrane.

### **IV.6.2.2 Effect of MPTS Solution\*DMAEMA Concentration**

The interaction between MPTS solution and DMAEMA concentration shows that ethanol deposited MPTS will give a longer adhesion time in low DMAEMA levels than at high levels, Figure IV.22. The highest adhesion times are achieved at low DMAEMA levels regardless of solution used, as explained in main factors. The largest delamination time is obtained from ethanol at low DMAEMA levels and from water at high DMAEMA levels. The reason for this is not clear.

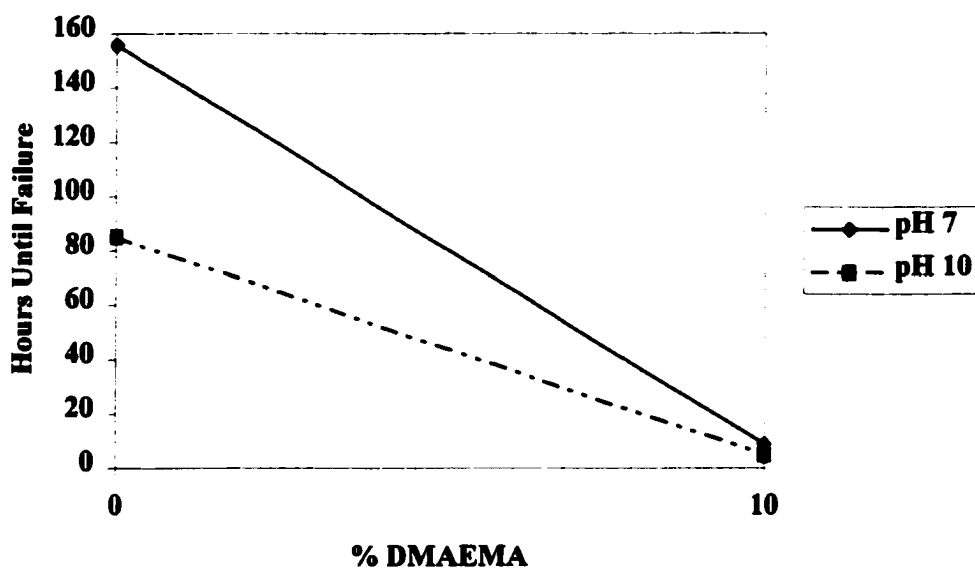


Figure IV.21. The effect of DMAEMA Concentration\*pH interaction on time until adhesion failure.



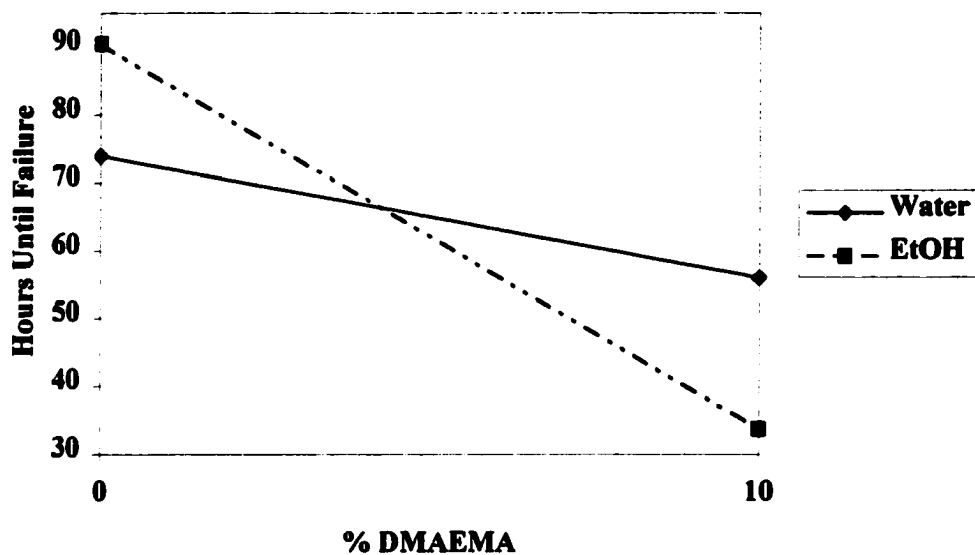


Figure IV.22. The effect of DMAEMA Concentration\*solution interaction on time until adhesion failure.

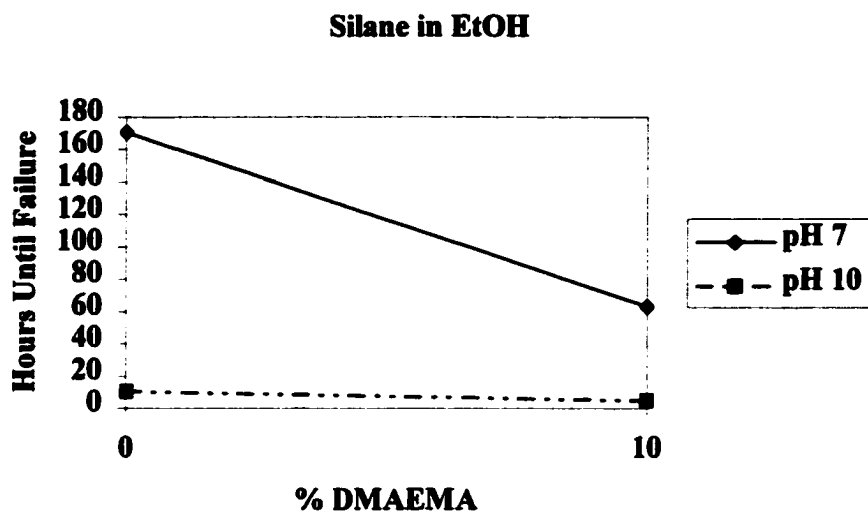


Figure IV.23.A. The effect of Solution\*DMAEMA Concentration\*pH interaction on the time until adhesion failure for ethanol solution.

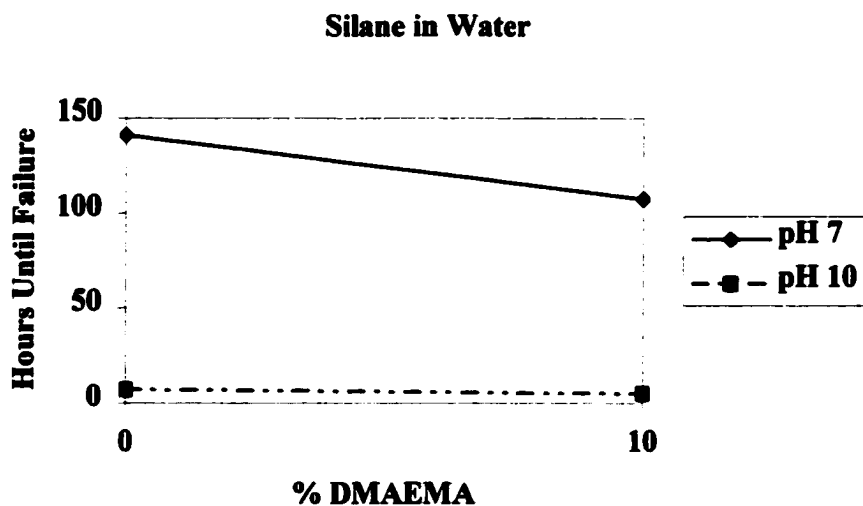


Figure IV.23.B. The effect of Solution\*DMAEMA Concentration\*pH interaction on the time until adhesion failure for ethanol solution.

### **IV.6.3 Three-way Interactions**

#### **IV.6.3.1 Effect of MPTS Solution\*DMAEMA Concentration\*pH**

When ethanol was used as the MPTS solution there was a greater decrease in delamination time from high to low DMAEMA levels at low pH then when water was used, Figure IV.23.A and Figure IV.23.B. In all cases, the shortest delamination time was observed at high pH, as predicted by the main factors. The high pH affected the delamination time less than low pH in both solution types. In both cases the longest delamination time was observed at low DMAEMA and in low pH solutions as predicted by the main factors.

### **IV.7 Conclusions**

The ability to prepare a pH sensitive hydrogel has been demonstrated. The use of a hydrogel monomer component with amine functionality, DMAEMA, imparts pH sensitivity to the membrane. The use of this comonomer eliminates the need for a derivatization step as required with poly(VBC) membranes. For a given membrane formulation, the amount of swelling the membrane undergoes is dependent upon the degree of protonation of the amine group, which is controlled by the pH of the solution. The high water contents of hydrogels allows for aqueous analytes to more easily and rapidly diffuse into the polymer.

The results of the factorial and systematic experiments show that a number of factors are able to affect the size ratio of pH sensitive hydrogel membrane. These factors include DMAEMA concentration, cross-linker concentration, cross-linker type and comonomer hydrophilicity. An increase in cross-linker concentration or the use of a cross-linker with a shorter chain length will cause a decrease in the size ratio of the

membrane. Higher DMAEMA levels will produce membranes with larger size ratios. The hydrophilicity of the comonomer was seen to have a large effect on the size ratio. Larger size ratios were obtained with more hydrophobic comonomers. The observed increase in size at low pH was due to the increase in water content of the hydrogel.

Adhesion of the membrane to a glass surface can easily be accomplished using a 3-(Trimethoxysilyl)propyl methacrylate. The adhesion method provides for strong and stable adhesion at low pH. At high pH, the adhesion was significantly less stable due to the attack of the glass surface by hydroxide ions.

## **CHAPTER V**

### **Preparation and Characterization of Polymer Microspheres by Dispersion Polymerization for Chemical Sensing**

#### **V.1. Introduction**

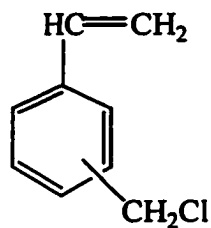
The use of polymer microspheres as the chemical sensing layer was investigated as an alternative to the pH sensitive hydrogel. The rationale for this was that a layer of microspheres would be able to more effectively swell without suffering delamination due to the shear forces involved with swelling. The overall swelling force would be over a smaller area in the microspheres compared to the bulk membrane. In addition, the space between the spheres would act as 'expansion joints', allowing the particles room to expand in the latitudinal direction before it abuts another microsphere. The application of a monolayer of microspheres would allow the thickness of the sensing layer to be controlled by the diameter of the particles.

To enhance the adhesion of the microspheres to a surface, poly-acrylic acid (PAA) was used as the steric stabilizer. The hydroxyl groups of the PAA can be deprotonated, making the microsphere surface poly-anionic. This could be used in conjunction with a poly-lysine coated surface, which is poly-cationic. Electrostatic attraction forces could be used as the adhesion force between the microsphere and the surface. The attachment of poly-lysine to gold surfaces for an adhesion layer has been demonstrated.<sup>97</sup> The expansion of the microsphere due to swelling would allow more PAA groups to come in contact with the surface, enhancing adhesion.

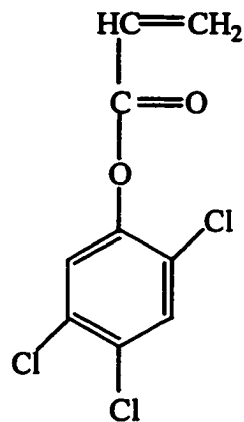
Corner has described the use of PAA as a steric stabilizer.<sup>98,99</sup> Particles with diameters from 0.2-2.2  $\mu\text{m}$  have been obtained using PAA as a stabilizer for styrene polymerized in ethanol.<sup>98</sup> The system studied in the experiments described here was that of VBC copolymerized with TCPA. Kavel and Miele have studied this system using poly-vinyl pyrrolidone as the stabilizer.<sup>31,37</sup> The structures of these monomers and the other components of the polymerization mixture are shown in Figure V.1. VBC-co-TCPA microspheres have been shown to be effective as a pH sensitive material for use in an optical pH sensor.<sup>37</sup> The inclusion of the TCPA makes the particle more hydrophilic and porous following derivatization, which allows for more rapid transport of the aqueous analyte into the particle and a shorter response time. The nature of the swelling process will be the same whether the system is used for optical measurement or as a separation layer between magnetic materials, and is analogous to that shown for the hydrogels in Figure IV.2. The amines are protonated at low pH leading to electrostatic repulsion and an increase in water content.

In order to produce a monolayer of particles to accurately control the thickness of the layer, it is necessary to produce particles with narrow size distributions. This chapter investigates the factors that affect the particle size when PAA is used as the stabilizer. The first experiment carried out was a factorial experiment to look at the effect of several factors and their interaction on the size of the microspheres. In order to obtain a more complete understanding of the variable's effect on particle size, a number of systematic studies were conducted.

### Monomers

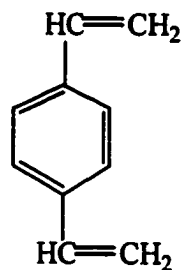


Vinyl benzyl chloride (VBC)



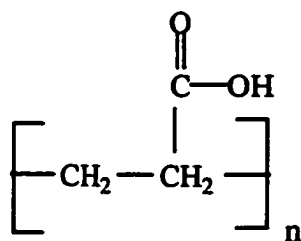
2, 4, 5-Trichlorophenylacrylate (TCPA)

### Cross-linker



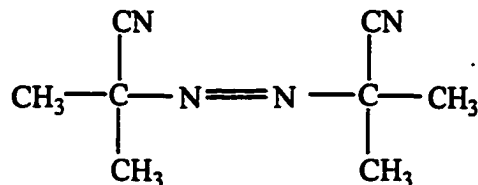
Divinylbenzene (DVB)

### Stabilizer



Poly(acrylic acid)

### Initiator



2,2 - Azobisisobutyronitrile (AIBN)

Figure V.1. Structures of monomers, cross-linker, stabilizer and initiator for preparing microparticles.

## **V.2. Results and Discussion of Factorial Experiment**

This factorial dealt with the effect of three variables on the size of the particles produced. The factors examined were monomer concentration, stabilizer concentration and concentration of water cosolvent. The concentrations of each variable are shown in Table III.4. Figure V.2 shows the mean particle sizes for each formulation used in the factorial. The error bars were determined by conducting the experiment in triplicate and represent  $\pm$  one standard deviation. Formulations with high water concentration produced larger particles, formulations 1-4, than formulations with low water concentrations, formulations 5-8. Formulations with higher stabilizer concentration, odd numbered formulations, seemed to have smaller particles than those with low stabilizer concentrations, even numbered formulations.

Table V.1 shows the ANOVA results of the experiment. The results show that all main factors and some of the interactions are significant at the 99 % confidence level, with a  $F_{\text{critical}}$  value of 8.53. The water concentration was shown to have the largest effect on particle size, followed by the stabilizer concentration and monomer concentration.

### **V.2.1. Effect of Main Factors**

The average effect of the main factors on particle size can be seen in Figure V.3. Each point represents the average of four formulations at each level

#### **V.2.1.1 Effect of Water Concentration**

Water concentration was shown in Table V.1 to have the greatest effect on particle size. Larger particles were produced when the water concentration of the dispersion medium was high, Figure V.3. The average size diameter of particles at low water concentrations was 0.44  $\mu\text{m}$ , while at high concentrations the average size was



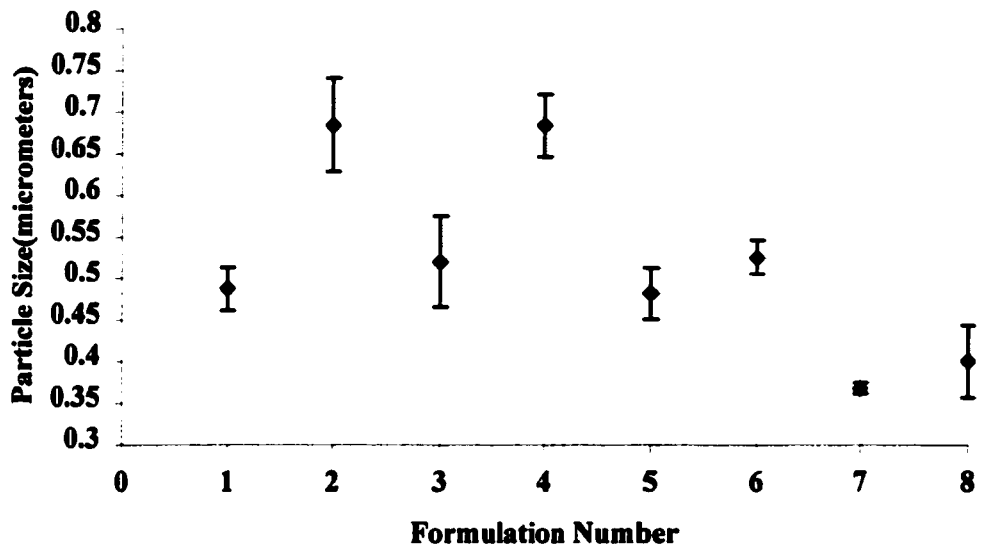


Figure V.2. The mean particle size and standard deviations for formulations used in particle size factorial(n=3).

**Table V.1 Results of Analysis of Variance for Microsphere Particle Size**

Source	DF	SS	MS	F	P
% Water (W)	1	0.134959	0.134959	93.33	0.000 **
% Monomer (M)	1	0.016086	0.016086	11.12	0.004 **
% Stabilizer (S)	1	0.071494	0.071494	49.44	0.000 **
W*M	1	0.027686	0.027686	19.15	0.000 **
W*S	1	0.030404	0.030404	21.03	0.000 **
M*S	1	0.000758	0.000758	0.52	0.480
W*M*S	1	0.000175	0.000175	0.12	0.732
Error	16	0.023137	0.001446		
Total	23	0.304700			

**df** = degrees of freedom

**SS** = sum of squares

**MS** = mean squares

**F** = F statistic, ( $MS_{\text{effect}}/MS_{\text{error}}$ )

**p** = probability of incorrectly rejecting the null hypothesis

**\*\*** = significant at 99% confidence interval,  $F_{\text{critical}}=8.53$  (n=16)

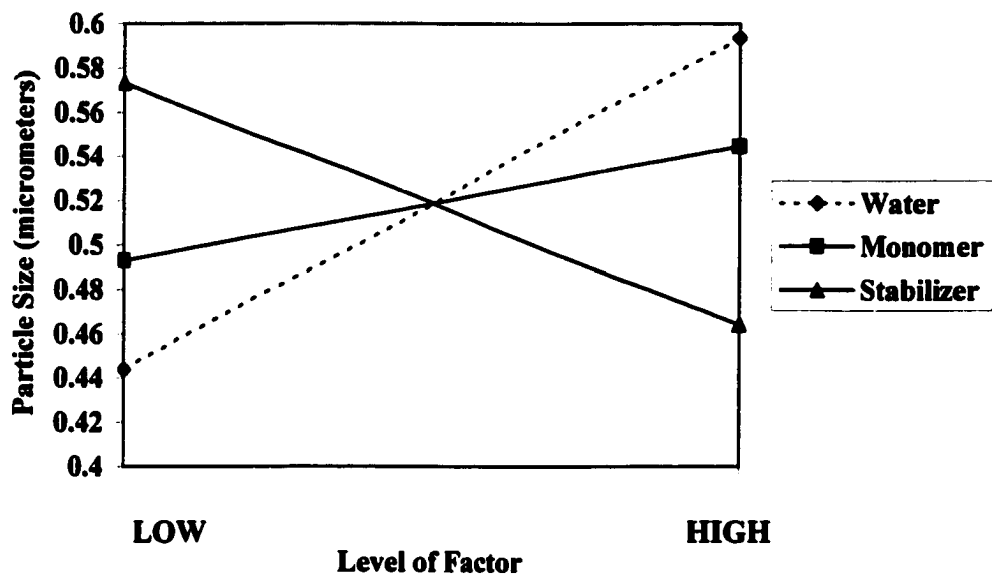


Figure V.3. The average effect on particle size of changing amounts of the main factors.

0.59  $\mu\text{m}$ . The solubility parameter was found by Miele to have the largest effect on the particle size in his factorial on poly-(VBC) microspheres.<sup>31</sup> The concentration of water in the ethanol dispersion medium causes a change in the polarity of the solution. The higher water content causes the dispersion medium to become more polar. Increasing the water concentration has the effect of increasing the initial solubility parameter of the dispersion medium. The efficiency of the steric stabilizer to stabilize a growing particle will be reduced in the more polar medium. The stabilizer is a polar molecule and the hydroxyl group can be deprotonated. This will cause the stabilizer to favor the dispersion medium, particularly at higher water concentrations. The result of decreased stabilization will be an increase in the number of nuclei and oligomers undergoing heterocoagulation. These will continue to grow and will eventually stabilize, but will do so as larger particles. The more polar dispersion medium also causes the particles to grow to shorter lengths before precipitating out. In order for these to grow to a larger size, they must undergo more aggregation and heterocoagulation before they are fully stabilized, resulting in the larger particles observed.

#### **V.2.1.2 Effect of Stabilizer Concentration**

The concentration of stabilizer had the second largest effect on the particle size. As the stabilizer concentration increased, the size of the particles decreased, Figure V.3. Particles produced at high stabilizer concentrations had an average size of 0.46  $\mu\text{m}$ , compared to 0.57  $\mu\text{m}$  at low concentrations. At high stabilizer concentrations, there is more stabilizer present to graft onto the growing polymer, stabilizing it and preventing coagulation with other particles. This produces more stabilized particles of smaller size. The faster the particles are stabilized and the less they coagulate with other particles, the

smaller the final particles produced. At low concentrations of stabilizer, the particles absorb the stabilizer more slowly. They absorb more oligomer or monomer and can undergo more collisions with other particles before they are effectively stabilized. This results in fewer particles of larger size.

### **V.2.1.3 Effect of Monomer Concentration**

The final main factor is the concentration of monomer, which had the smallest effect of the main factors on particle size, Table V.1. Figure V.3 shows that high monomer concentrations produced larger particle sizes. At low monomer concentrations the particle size was 0.49  $\mu\text{m}$ , compared to 0.54  $\mu\text{m}$  at high monomer concentrations. When the monomer concentration is high, there is an increase in the rate at which the oligomer chains will grow. High monomer concentrations will also allow the growing polymer to stay in solution longer prior to precipitating. These two effects allow the polymer to grow larger prior to precipitating out as a particle.

## **V.2.2 Effects of Two-way Interactions**

### **V.2.2.1 Effect of Water Concentration\*Stabilizer Concentration Interaction**

The interaction between water concentration and stabilizer concentration shows that the lower stabilizer concentration increases particle size more at high water concentrations than at low concentrations, Figure V.4. This interaction has the largest effect on particle size compared to other interactions, Table V.1. The difference between particle sizes for high and low stabilizer concentrations is 0.03  $\mu\text{m}$  at 5 % water and 0.18  $\mu\text{m}$  at 15 % water concentration. This follows well with the main factor effects for both components. At high water concentrations, the stabilizer will be more soluble and less accessible to the nuclei, resulting in larger particles from increased heterocoagulation.

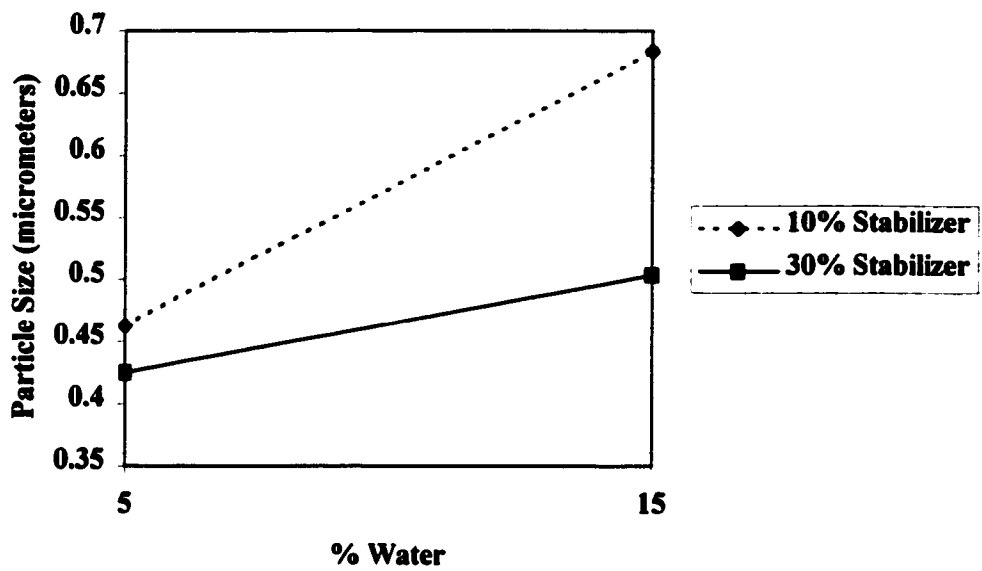


Figure V.4. The effect of % Water\*% Stabilizer on the particle size.

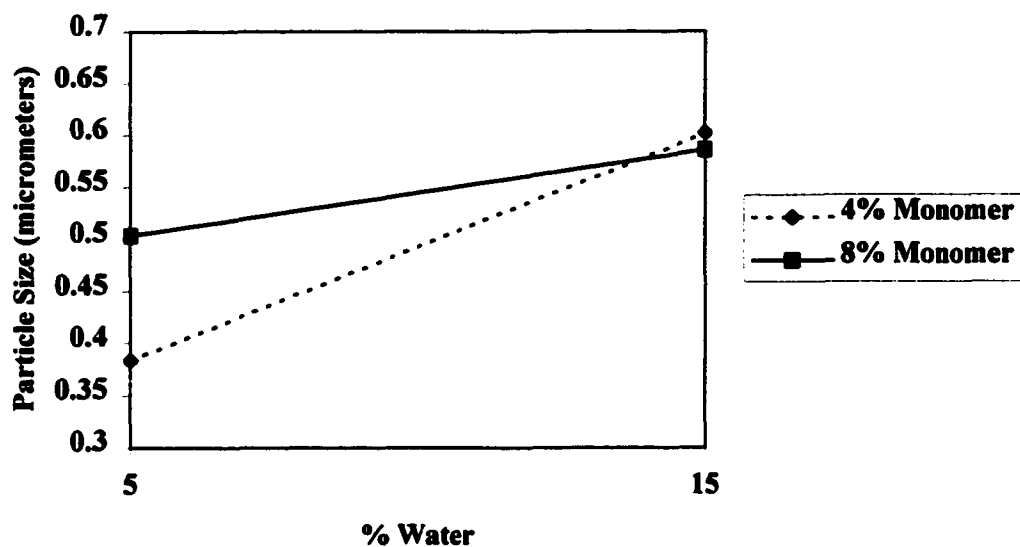


Figure V.5. The effect of % Water\*% Monomer on the particle size.

The effect is enhanced at low stabilizer concentrations. The opposite effect is observed at low water concentrations, when the stabilizer is less soluble in the dispersion medium.

### **V.2.2.2 Effect of Water Concentration\*Monomer Concentration Interaction**

Figure V.5 shows that the interaction between water concentration and monomer concentration produces smaller particles at low water concentrations. The water concentration has a greater effect on the size at low monomer concentration than at high concentration. The change in particle size was larger for the high monomer concentration than the low monomer concentration. The observed results may be attributed to the solubility of the stabilizer. At high water concentrations the stabilizer will be more soluble in the water and its availability to the growing polymer will be limited, regardless of monomer concentration. This will allow the particles to grow to a larger size before being stabilized. At low water concentrations there is more stabilizer in the ethanol. This makes the stabilizer equally available to the growing monomer regardless of monomer connotation. In these conditions the particle size is predominantly affected by the monomer concentration, with higher monomer concentration producing larger particles.

## **V.3 Results and Discussion of Systematic Studies on Particle Size**

### **V.3.1 Effect of Water Concentration on Particle Size**

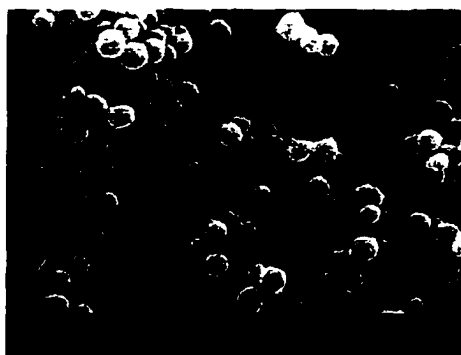
To further examine the effect of water concentration on particle size a systematic experiment was carried out. Table V.2 shows the results of the study. The SEM's for this experiment are shown in Figure V.6. The study confirms the results obtained in the factorial experiment, section V.2, that particle size increases with increasing water concentration. All formulations produced monodispersed particles, with R.S.D.'s less than 10 %. Particle size increased from 0.39  $\mu\text{m}$  at 5 % water to 0.50  $\mu\text{m}$  at 25 % water.



**Table V.2 Average Particle Size and R.S.D. % of Particles with Varying Water Concentrations in Dispersion Media.**

Water Concentration (vol. %)	Solubility Parameter $\delta$ (cal/cm <sup>3</sup> ) <sup>1/2</sup>	Diameter (micrometers)	
		Average	R.S.D. %
5	13.4	0.39	9.5
15	14.7	0.44	6.9
25	16.0	0.50	8.5
35	17.2	Coagulated Product	

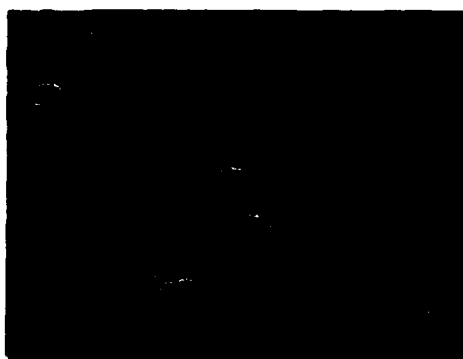
- All reactions prepared with 2.5 % VBC(wt./vol.), 2.5 % TCPA (wt./vol.), PVP:VBC/TCPA 20 % (wt./wt.), AIBN: VBC/TCPA 2 % (wt./wt.), reactions ran for 6 hours at 70 °C.



5 % Water



15 % Water



25 % Water

**Figure V.6. Scanning Electron Micrographs of VBC/TCPA particles in media with various water concentrations.**

This is an increase in size of approximately 25 %. When the water concentration was increased to 35 % a coagulated product was formed. At this level of water concentration, the stabilizer is very soluble in the dispersion media and not effective in stabilizing the particle surface.

These results are consistent with the observations made in the factorial experiment, but are inconsistent with the results observed by Miele for VBC and in other studies on styrene<sup>31,100</sup> The results are also the opposite of the trend observed by Corner.<sup>98</sup> The reason for this is not readily apparent. The most likely explanation is that the PAA is more soluble in water at high water concentrations. The stabilizer is less available to stabilize the growing particles. This allows the particles to reach a larger size before being stabilized.

### **V.3.2 Effect of Monomer Concentration on Particle Size**

The factorial experiment revealed that increasing the monomer concentration of the reaction mixture leads to an increase in particle size. Increased monomer content increases the solvency of the reaction medium, making the polymer more soluble. The polymer remains suspended longer, so it grows to a longer chain length before precipitating out. The effect of the monomer on particle size is complicated because of the dual role it plays as reactant and part of the dispersion medium. As the monomer is used up, the polarity of the dispersion medium shifts. This can then affect the particle size by altering the efficiency of the stabilizer and the solubility of the forming oligomers.<sup>41</sup>

The effect of monomer concentration was examined over the concentration range of 5 % to 15 % by weight. For concentrations above 15 % it was not possible to dissolve all of the solid material, TCPA, PAA and AIBN, in the reaction medium. Table V.3

**Table V.3 Average Particle Size and R.S.D. % of Particles with Varying Monomer Concentrations.**

Monomer Concentration (wt./vol. %)	Diameter (micrometers)	
	Average	R.S.D. %
5	0.54	10.5
7.5	0.57	4.8
10	0.69	7.9
15	0.83	17.3

- All reactions prepared with PVP:VBC/TCPA 20 % (wt./wt.),  
AIBN: VBC/TCPA 2 % (wt./wt.), reactions ran for 6 hours at 70 °C.

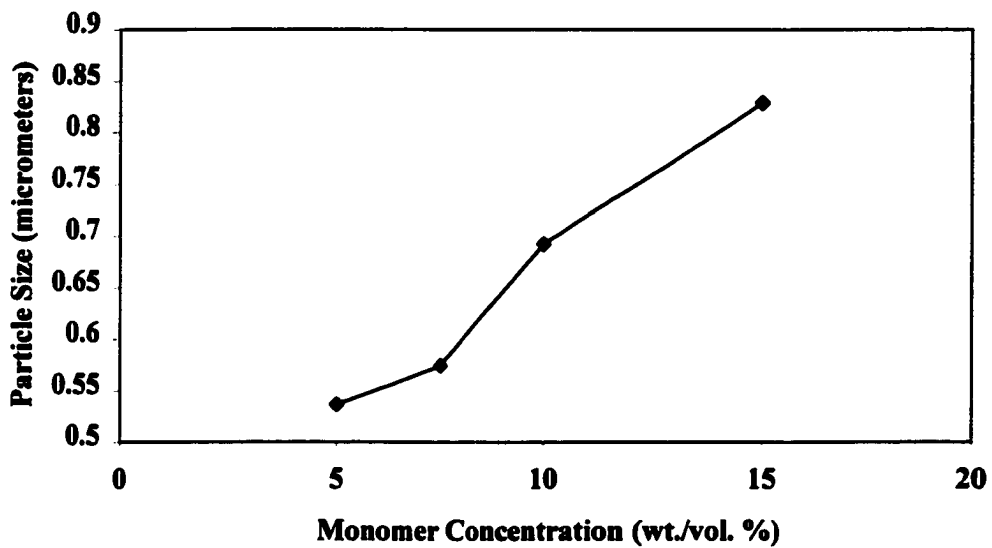
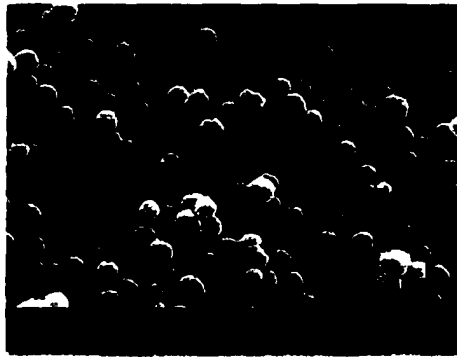


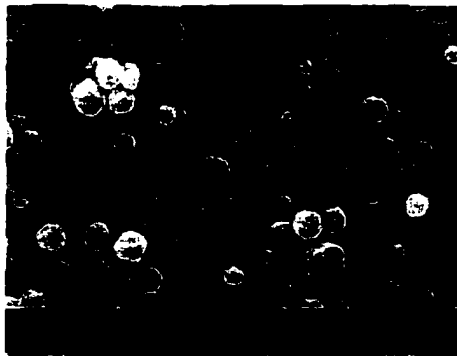
Figure V.7. Effect of monomer concentration on particle size.



**5 % VBC/TCPA Monomer**



**7.5% VBC/TCPA Monomer**



**15 % VBC/TCPA Monomer**

**Figure V.8. Scanning Electron Micrographs of VBC/TCPA particles at various monomer concentrations.**

shows the particle size and distribution for each formulation. The results are presented graphically in Figure V.7. Select SEM's are shown in Figure V.8. The particle size increased from 0.54  $\mu\text{m}$  to 0.83  $\mu\text{m}$ , a 54 % increase, as monomer concentration increased from 5 % to 15 %. The most monodisperse particles were obtained with 7.5 % monomer. The % R.S.D for this formulation was 4.8 %. The most polydisperse preparation had a % R.S.D of 17.3 % at a monomer concentration of 15 %. Particles produced with monomer concentrations in the middle of the range, 7.5 % and 10 %, were the most monodisperse. The extreme monomer concentrations, 5 % and 15 % were less monodisperse.

### **V.3.3 Effect of Stabilizer Concentration and Molecular Weight on Particle Size**

The stabilizer was shown in the factorial to have a significant effect on the particle size produced. The basic role of the stabilizer is to prevent the growing particle from coagulating with other particles by providing a protective layer over the surface of the particle. In section II.2.2.4 the role of the stabilizer and the different types of stabilizers are explained in greater detail. It has been observed in the factorial and in other dispersion studies that an increase in the stabilizer concentration should decrease the particle size<sup>99,101</sup>. The monomer can more easily react with the stabilizer forming a graft copolymer that will stabilize the nuclei. At higher stabilizer concentrations more stabilizer can be absorbed by the nuclei. Both of these effects lead to smaller particle size, due to the increased stabilization of the surface.<sup>41</sup>

The concentration of stabilizer will affect the particle size, as will the molecular weight of the particle. Higher molecular weight stabilizers should enhance the effects listed above and should produce smaller particles for a given stabilizer level.

**Table V.4 Average Particle Size and R.S.D. % of Particles with Varying Stabilizer Concentrations and Molecular Weights.**

Stabilizer Concentration (wt./wt. % of monomers)	Diameter (micrometers)	
	Average	R.S.D. %
<b>PAA Molecular Weight 50,000</b>		
5	1.20	0.4
10	0.93	15.0
15	0.66	3.2
20	0.70	12.6
<b>PAA Molecular Weight 240,000</b>		
5	0.90	5.5
10	0.66	14.4
15	0.47	23.5
20	0.54	9.0
<b>PAA Molecular Weight 750,000</b>		
5	0.55	18.3
10	0.45	1.1
15	0.47	17.8
20	0.42	9.4

- All reactions prepared with 5 % VBC(wt./vol.), 5 % TCPA (wt./vol.), AIBN: VBC/TCPA 2 % (wt./wt.), reactions ran for 6 hours at 70 °C.



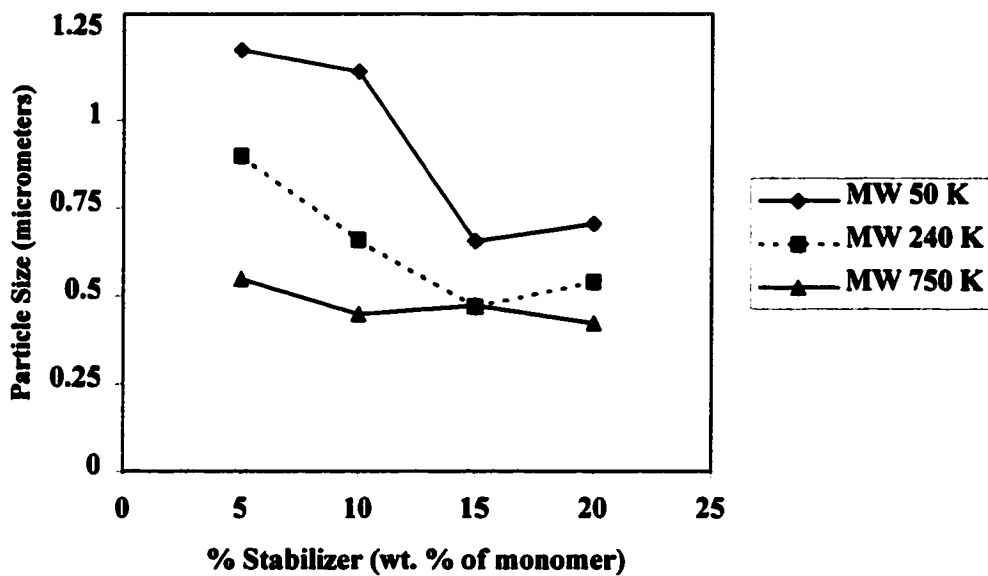


Figure V.9. Effect of stabilizer concentration and molecular weight on particle size.

Miele found that high PVP concentration and a high molecular weight gave the smallest particles for VBC particles.<sup>31</sup> In this study, four PAA concentrations were studied from 5 % to 20 % weight of monomer. The effect of molecular weight was determined by using three different PAAs, with molecular weights of 50 K, 240 K, and 750 K.

The experiment showed that there is a decrease in particle size as the concentration increases. It was also observed that the size decreases as the molecular weight of the stabilizer increases. The results of this study showing the average particle size and distribution are seen in Table V.4. The data is also summarized graphically in Figure V.9. Using PAA with a molecular weight of 50 K, the particle size decreases from 1.20 mm at 5 % to 0.70 mm at 20 %. This is a decrease in particle size of over 40 %. From 5 % to 15 % stabilizer, the particle size decreases by approximately 30 % for each 5 % increase in stabilizer concentration. The % R.S.D. of the particles does not seem to be related to the stabilizer concentration. It starts at 0.4, increases to 15, then decreases to 3.2, before rising to 12.6, as the stabilizer increases from 5 % to 10 % to 15 % to 20 %, respectively. Only two formulations produced monodisperse particles, 5 % and 15 % stabilizer.

Similar results were obtained for the 240 K molecular weight PAA. Particle size decreased from 0.90 mm to 0.54 mm when the stabilizer concentration increased from 5 % to 20 %. The % R.S.D. of each formulation was 5.5 and 9, respectively. In this system, the smallest particle size was actually obtained at 15 % stabilizer, with a particle size of 0.47 mm and a % R.S.D. of 23.5. With a R.S.D. of 23.5 %, this was the most polydisperse formulation of the set. As with the 50 K PAA, only two formulations produced monodispersed particles, 5 % and 20 %.

The same results were seen again when PAA with a molecular weight of 750 K was used. The particle size decreased from 0.55 mm at 5 % to 0.42 mm at 20 %. As in the previous cases only two formulations produced monodispersed particles, 10 % and 20 % stabilizer, with R.S.D. of 1.1 % and 9.4 % respectively. The most polydisperse particles were obtained with 5 % stabilizer, with a R.S.D of 18.3 %.

As seen in Figure V.9, there is a general decrease in particle size as the stabilizer concentration increases. Also observed is that a higher molecular weight stabilizer produces smaller sized particles. The average particle size over all stabilizer concentrations decreased from 0.87 mm to 0.64 mm to 0.47 mm, as the PAA molecular weight increases from 50 K to 240 K to 750 K. Also observed was the effect of stabilizer concentration on particle size decreased as the molecular weight increased. For a molecular weight of 50 K, the difference between the smallest and largest particle size was 0.50 mm. For 240 K PAA the difference was 0.43 mm and for 750 K PAA the difference was 0.13 mm. The size difference decreased by a factor of 4 from the 50 K to 750 K PAA.

#### **V.4 Swellable Membrane**

As described in section V.1, the purpose of preparing microsphere particles was to form a monolayer of particles on the substrate surface and have enhanced adhesion over the bulk hydrogel membrane. The inability to produce a monolayer of particles on the surface necessitated the use of an alternative strategy. This strategy was to try to use the polymer microspheres to force swelling to occur only in the longitudinal direction, as depicted in Figure IV.X. This would produce swelling in the desired direction and limit swelling in the harmful perpendicular direction.

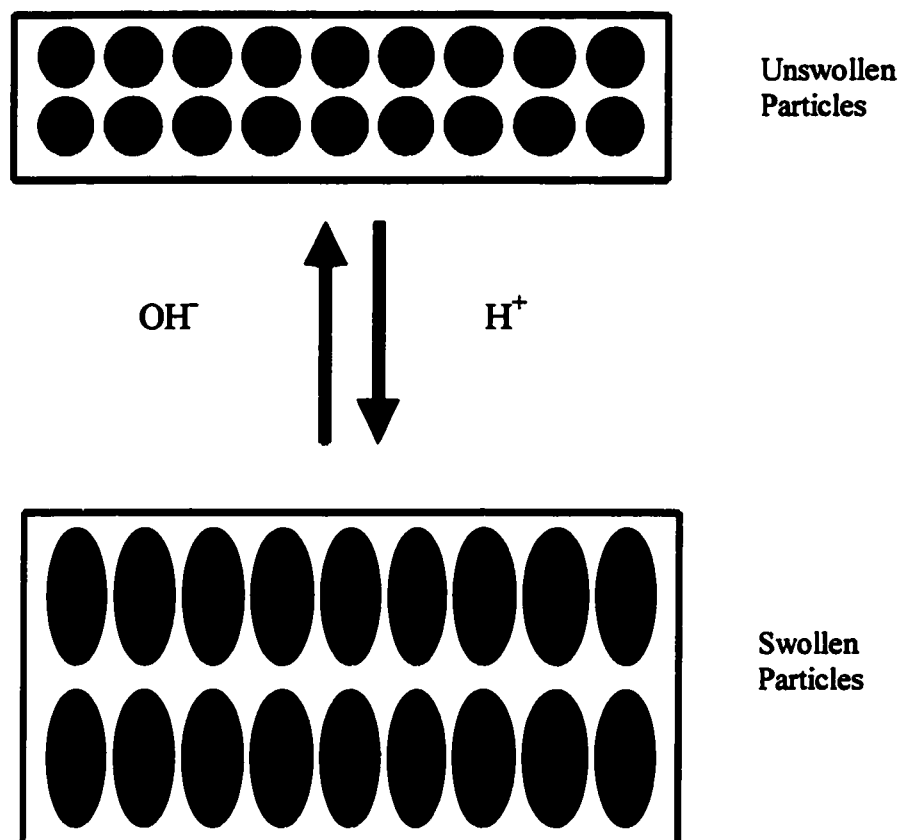


**Figure V.10.** Schematic diagram showing polymer microspheres embedded in hydrogel membrane, causing membrane to swell. The bead is adhered at the top and bottom to a surface. At low pH the beads swell into each other, forcing them to elongate and swell perpendicular to the adhered surface.

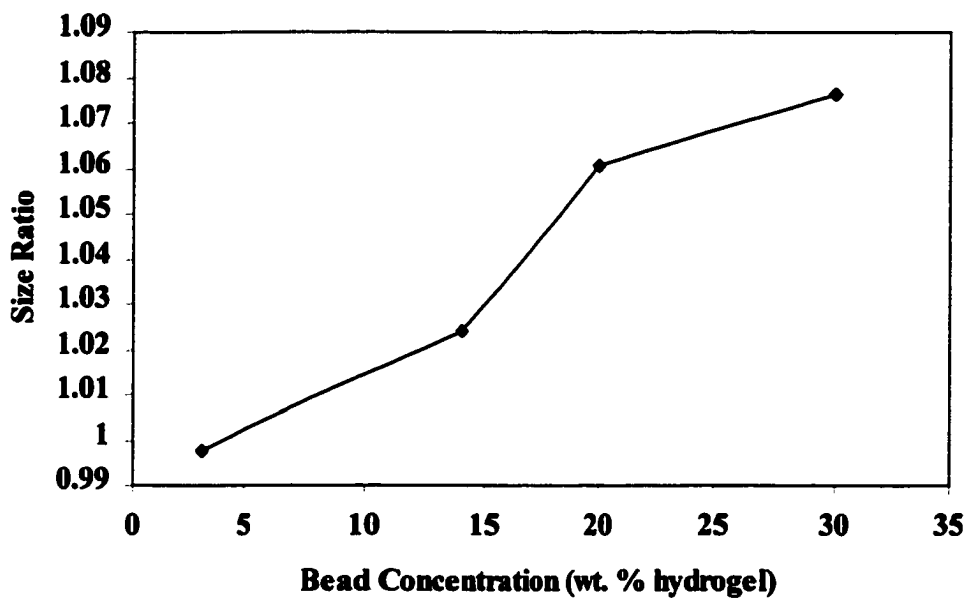


Figure V.11. Effect of VBC/TCPA bead concentration on size ratio of HEMA membrane.

This was accomplished by embedding the microspheres in a hydrogel that was bonded to the substrate surface. As the beads swell in response to changing pH, they will impact each other. As swelling continues, this will force the bead to elongate. By constraining the membrane on the surface, the amount by which it can swell parallel to the surface is limited. The least hindered direction in which swelling can occur is perpendicular to the surface. This arrangement is shown in Figure V.10.

In order to examine if a membrane with beads would swell, a systematic study of size ratio as a function of bead concentration was conducted. In this study poly-(VBC/TCPA) beads were embedded in a poly-(HEMA) membrane and exposed to an acidic and a basic buffer environment. The results are shown in Figure V.11. Typical bead concentrations used in optical measurements were 1 % to 3 % (wt. % to hydrogel).<sup>31</sup> At low levels such as these, it is expected that swelling would not occur. The bead concentrations examined in this study ranged from 1 % to 30 %. At 1 % beads no swelling was observed, with a size ratio of 1.00. When the bead concentration was increased to 14 % the size ratio increase to 1.02. The size ratio continued to increase with increasing bead concentration until 30 %, when the size ratio of 1.08. At this bead concentration it was extremely difficult to get the beads to suspend in the hydrogel mixture. Above a bead concentration of 30 % it was impossible to completely suspend the microparticles.

The experiment showed that it was possible to swell a hydrogel membrane by embedding swellable microparticles in the membrane. The size ratios observed in this technique were significantly smaller than the size ratios obtained using the pH sensitive monomer DMAEMA. The small size ratio and the results of the adhesion factorial

experiment in section IV.6 showing that solution pH, and not swelling dominates delamination, indicated that this method was not as useful as believed.

## **V.5 Conclusion**

This chapter showed that VBC-co-TCPA microspheres could be prepared by dispersion polymerization, using PAA as the steric stabilizer. The experiments also showed it is possible to control the size of these particles by varying the composition of the reaction mixture. The most important factor controlling the size of the particles is the polarity of the solvent, which affects the solubility of the polymer and stabilizer. In contrast to the majority of studies, it was found that increasing the water content of the dispersion medium caused an increase in particle size. Increasing the monomer concentration was also shown to increase particle size. An increase in PAA stabilizer concentration or molecular weight was shown to decrease the size of particles produced. There was no apparent trend in particle size distribution observed for any factor. The data from this chapter indicates that controlling the particle size is readily accomplished. However, the formation of monodisperse particles is more complex. In the experiments conducted for this chapter, monodisperse particles were obtained slightly more than 50 % of the time, indicating the difficulty of accomplishing this goal.

## **CHAPTER VI**

### **Remotely Interrogatable Magnetostatic-coupled and Magnetoelastic Sensors for Environmental Monitoring**

#### **VI.1 Introduction**

This chapter describes the use of magnetostatic-coupled and magnetoelastic sensors for environmental monitoring and chemical sensing. In the first section the use of magnetostatic-coupled sensors will be considered. Three different designs were explored. The first consisted of two magnetic films separated by a swellable polymer layer; the disk design, as shown in Figure II.9. The second design was fabricated by attaching a magnetic film to a polymer membrane, then cutting along the diagonals. The third consisted of small pieces of magnetic material that had been ground into a powder and dispersed throughout the prepolymer mixture prior to polymerization. In this arrangement, the distance separating the magnetic material determined the strength of the induced voltage. The separation was dependent upon the concentration of the analyte solution. The closer the films and powder were to each other, the larger the coupling. A more complete explanation can be found in section II10.1.

The second section describes the evaluation and use of a magnetoelastic sensor. The signal measured by this sensor is the resonant frequency at which the sensor vibrates in a magnetic field. Numerous factors affect the measured resonant frequency, including applied mass, solution viscosity and temperature.<sup>88</sup> This allows the sensor to be used to



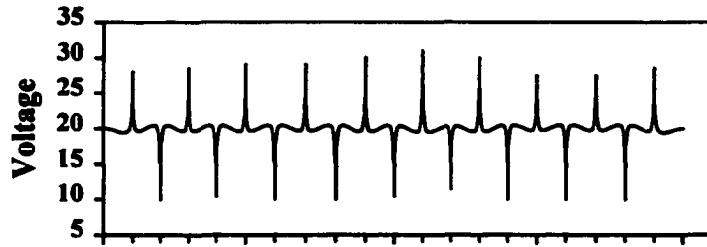
measure a variety of analytes. These characteristics also make the devices susceptible to a variety of interferents, therefore examinations of a number of factors that may affect the measurement were conducted. The use of magnetoelastic materials for measurement is described in section II.10.2.

## **VI.2 Magnetostatic coupled sensors**

This section considers the use of magnetostatic coupled sensors. The theoretical basis for this type of sensing is described in more detail in section II.10.1. Briefly, the closer two magnetic materials are located to each other, the greater the coupling between the magnetic domains in each material. The higher the degree of coupling, the more coherently the domains will change orientation when placed in an alternating magnetic field. As the magnetic domains change orientation, a magnetic flux is produced which can be detected as a voltage spike. The greater the degree of coupling, i.e. the closer the magnetic materials are to each other, the smaller the voltage spike produced. This section describes the use of three magnetostatic coupled sensor designs for pH measurement, the disk design, split-square design and the powder design.

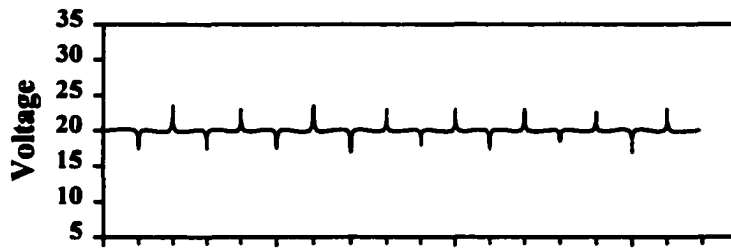
### **VI.2.1 Disk sensor design**

The response of a magnetostatic coupled disk sensor is presented in Figure VI.1. The sensor presented here consisted of a thin layer of DMAEMA thermally polymerized between two magnetic disks. The disks were microscope cover slips, approximately 22 mm x 22 mm in size, on which a 100 nm layer of  $\text{Ni}_{81}\text{Fe}_{19}$  film had been sputter deposited. A 10 nm thick layer of  $\text{SiO}_2$  was deposited on the magnetic layer to enhance polymer adhesion. Analysis of the sensor was carried out by placing the sensor in a 10 Hz sinusoidal magnetic field.



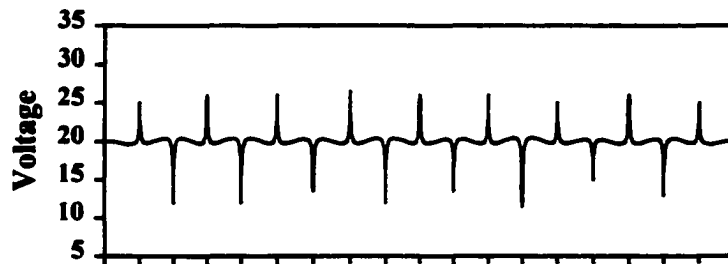
Time

pH 7.5



Time

pH 4



Time

pH 10

Figure VI.1. 10 Hz voltage wavetrain for magnetic sensor. 1) pH 7.5, 2) pH 4, and 3) pH 10. All responses are scaled.

The sensor was first equilibrated in a pH 7.5 buffer. This presented a baseline value at the apparent pKa of the polymer.<sup>89</sup> Figure VI.1(1) shows the sensor response at pH 7.5. The peak to peak height is approximately 8 voltage units. The sensor was then placed in pH 4 buffer for 24 hour. In pH 4 the amine sites are protonated, causing the polymer to swell and move the magnetic films further apart. This results in a decrease in the coupling between the two films, making the flux change direction less coherently, lowering the detected voltage response. As seen in Figure VI.1(2), the signal has been reduced to approximately 3 voltage units.

The sensor was then placed in pH 10 buffer to unprotonate the polymer, which results in the polymer shrinking. As this occurs the magnetic films move closer together, which increases the coupling, causing the flux to change direction more coherently and produce a larger signal. As can be seen in Figure VI.1(3), the signal is much larger than it was for pH 4. The signal has a peak to peak strength of approximately 6 voltage units. This is consistent with the signal growing in intensity, as the magnetic films move further closer together.

The voltage wavetrain shown for pH 10 was taken after 8 hours of immersion in pH 10 buffer solution. We hypothesize that the sensor had not yet reached equilibrium, which is why the sensor response did not exceed that of pH 7.5. Influx of the analyte into the sensor is restricted to the edges only. The sensor response time is, therefore limited by the rate of diffusion of the analyte into the center of the polymer. The estimated time required for the analyte to diffuse into the center of the polymer is approximately 17 hours, based on diffusion through a liquid. The response presented was taken at a time when the analyte was approximately half way to the center of the sensor. The sensor was

interrogated at this time because delamination was becoming evident. As presented in section IV.6 the primary reason for sensor delamination is attack of the silane adhesion agent by hydroxyl groups in a basic solution. As the hydroxide ions were diffusing into the interior of the polymer, they were also attacking the silane bonds causing the membrane to delaminate. In addition, the long diffusion time leads to swelling forces that promote delamination. As the hydroxyl groups diffuse into the polymer the amine sites deprotonate. This happens more rapidly at the edge, where the amines are more accessible. As a result, the edge of the polymer layer shrinks, while the interior is still swollen. This causes a 'bow effect', with the disks further apart at the center and closer at the edge. The swollen center is trying to move the films apart, causing the polymer at the edge to be pulled away from the film, enhancing delamination.

This experiment provided proof of concept that the sensing mechanism was valid. Despite the slow response time, and the delamination before the experiment was complete, it is apparent that the magnetic flux detected as a voltage spike does vary in response to changing pH of the buffer solution in which it is immersed. The challenge was then to improve adhesion and decrease the response time.

### **VI.2.2 Split-Square Design**

The split square design is a variation of the disk design. Rather than arranging the layers in a 'sandwich' arrangement, the different layers are formed by adhering a thin magnetic film on top of the polymer membrane. Attachment of the film was accomplished using "superglue". The magnetic film is then cut to form a series of split squares, as illustrated in Figure VI.2. In this arrangement as the polymer swells it moves the different sections of the squares apart, which decreases the coupling between them.

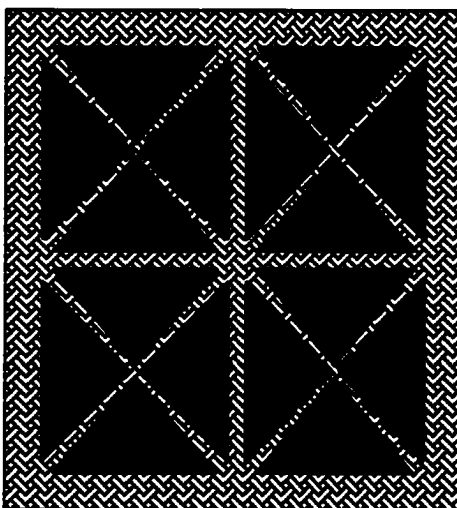


Figure VI.2 Schematic diagram of split square sensor. Gap between squares is 2 mm, within squares gap is 0.05 mm.

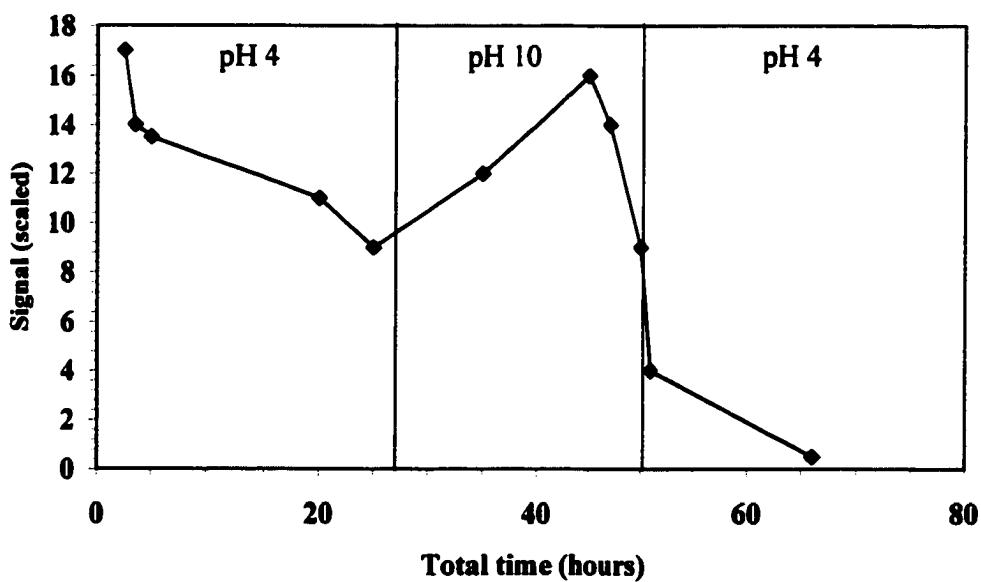


Figure VI.3 Voltage-spike wavetrain of split square design magnetostatic coupled Sensor. Voltage amplitude as a function of time and solution pH.

The advantage of this design is that the accessibility of the analyte is greatly enhanced, since nearly the entire polymer is exposed to the analyte solution.

Results of pH cycling of this type of sensor are shown in Figure VI.3. The polymer layer is 9 % (mol./mol.) DMAEMA in HEMA and was prepared in accordance with the method described in section III.3.2.1. Film thickness is approximately 360  $\mu\text{m}$ . The first data point shown in Figure VI.3 was taken at pH 10, just before placing the sensor in pH 4 buffer. As expected, the signal was high in pH 10 and decreased in pH 4. The results are consistent with the expected results for the most of the first cycle. The signal decreased in pH 4, as the coupling decreased as the distance between the split squares increased. When placed in pH 10 buffer the signal increased as the distance between the squares decreased and the coupling between the magnetic domains increased. This continued until just before the time of 48 hours. At this point the signal begins to decrease. The decreasing signal trend continues when the sensor is placed in pH 4 solution.

The sensor design began by behaving as expected, but then the signal dropped off and did not recover. There are several possible explanations for the observed results. The first is that the magnetic film has a tendency to curl, which exerts a force away from the polymer, enhancing delamination. This result of this would be that the films would appear to be further apart and cause the signal to be lower. There are also sheer forces acting to cause delamination, as described in section IV.6. The swelling of the polymer acts to move the split squares apart as the polymer grows. However, the magnetic film does not change size as the polymer it is attached to does. Although the film is moving with the polymer, the polymer is also swelling underneath the film, putting pressure on

the bonds holding the two layers together. As the bonds break this would cause the magnetic film to delaminate and the signal to decrease as the film moved away. There is also believed to be a degree of irreversibility in the polymer. That is, the polymer does not return to exactly the same size and shape every time. This is especially true when the polymer is not supported on a rigid substrate, but is free floating, as it was in this case. This will affect the reproducibility of the sensor and may allow membrane movements that promote delamination of the film.

### **VI.2.3 Powder sensor**

The powder design consists of iron-nitride particles, with a particle diameter less than 44 microns, suspended in the monomer solution. The mixture was then polymerized to form a membrane, as described in section III.3.2.1. This design has the advantage that the analyte can enter the membrane unimpeded from all directions. It is even superior to the split square design, since none of the membrane surface is blocked. The additional advantage it has over the other magnetostatic coupled sensors is that the response is not dependent on the orientation of the sensor in the pick-up coil. Due to the higher coercive field of the particles, the coercivity of the sensors was obtained as the sensor response. As the magnetic particles move further apart the coercivity increases. Unlike the other sensor designs, a larger signal will be obtained in pH 4 and a smaller signal in pH 10.

Figure VI.4 shows the response of a powder sensor prepared with a solution prepared from 25 % DMAEMA in HEMA, the concentration of magnetic powder was 35 % (wt./wt. monomers). The sensor dimensions were  $10 \times 10 \times 0.724 \text{ mm}^3$ . The signal is initially dropping in pH 7. When placed in pH 4 it begins to rise as expected.

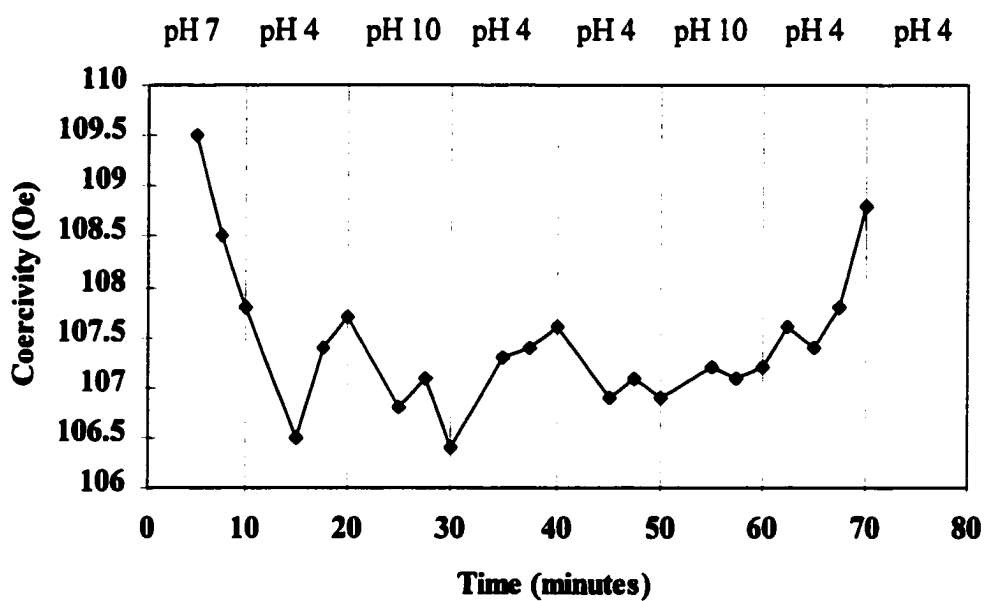


Figure VI.4 Coercivity versus time and pH for powder sensor prepared in 25 % DMAEMA membrane.



The signal then decreases in pH 10. The first two cycles of the membrane have the signal tracking pH as expected, higher in pH 4 and lower in pH 10. Sensor response is not as reproducible as desired, with the difference between pH 4 and pH 10 decreasing with time. The difference in signal between pH 4 at 20 minutes and pH 10 at 30 minutes is 1.3 Oe and a difference of 1.2 Oe is observed between the signal at 30 minutes and 40 minutes. Between pH 4 and pH 10 at 40 and 50 minutes, the signal difference drops to 0.7 Oe. The signal difference decreases even more between pH 10 at 50 minutes and pH 4 at 60 minutes, when the signal difference is only 0.3 Oe. It was also observed that the signal continued to increase, when the sensor was left in pH 4 buffer at the end of the experiment.

The general trend of the signal increasing or decreasing is present. The signal behaves as expected for each case, increasing in pH 4 and decreasing in pH 10. There are several possible reasons for the variations seen in the signals of the powder sensors. As mentioned for the split square design, the polymer membrane does not always return to exactly the same dimensions, which will affect the reproducibility of the response. In addition, the magnetic powder material is highly susceptible to chemical attack and rusts very quickly. The build up of a rust layer on the magnetic powder will alter the magnetic properties of the sensor and the signal measured.

#### **VI.2.4 Conclusions**

The results presented here demonstrate the feasibility of a magnetostatic coupling based chemical sensor. Sensor readings were obtained for various pH solutions, with no physical connection between the sensor and the detection electronics. The response of the sensor to alternating pH solutions was in agreement with that predicted by theory.

Serious limitations in the sensor were observed in terms of response time, mechanical stability of the sensor and reproducibility. The issue of response time is the most easily addressed, with the use of the split square and powder design instead of the sandwich design, making more of the hydrogel surface accessible to the analyte solution. Response time in this sensor is determined by the diffusion of the analyte into the interior of the hydrogel. The use of thinner membranes would improve response time in the split square and powder design, but thinner membranes provide less mechanical stability.

Mechanical stability problems are most evident in the sandwich design, where total sensor failure was observed. In this situation, the swelling force that is required for sensing adds to the problem, by producing a swelling force that contributes to delamination. The attack of the silane bonds is another factor in delamination. To eliminate that problem would require a new attachment mechanism. The problem of mechanical stability also contributes to the problem of reproducibility. The inability of the membrane to perfectly return to its previous shape as it shrinks and swells, results in small changes in the observed signal.

### **VI.3 Magnetoelastic Sensor**

In this section the use of a magnetoelastic strip for environmental monitoring and chemical sensing is examined. When a magnetostrictive material is placed in an alternating magnetic field, a mechanical vibration is initiated in the strip. A magnetoelastic resonance results when the excitation frequency matches the mechanical resonant frequency. The phenomenon is similar to that of acoustic wave devices, except that wave propagation is induced and the measurement is taken using magnetic fields rather than electric currents. The resonant frequency is affected by a number of factors,

including temperature, solution viscosity and density, and mass loads. It is the change in these characteristics that can be exploited for environmental monitoring and chemical sensing. The use of a magnetoelastic strip as a chemical sensor has been reported.<sup>88</sup> In this section the factors effecting the response of a magnetoelastic strip are examined in relation to its use as a chemical sensor.

### **VI.3.1 Solution Viscosity Measurement**

The use of magnetoelastic strips for monitoring solution viscosity has been reported by Grimes.<sup>88,89</sup> In order to gain experience using the strips a series of experiments was conducted to examine the effect of solution viscosity on response and to evaluate the use of the magnetoelastic strips for viscosity monitoring. This was accomplished by preparing solutions of polystyrene in toluene at different concentrations and with different molecular weights. The resonant frequency of the magnetic strips in the solutions and the solution viscosity were measured. The results are presented in Table VI.1.

Figure VI.5 shows the frequency shift as a function of polystyrene concentration and molecular weight. As the viscosity of the solution increases, it is expected that the frequency would decrease, in accordance with equation 10 in chapter II. Higher polystyrene concentrations will have higher viscosities. It is also expected that a solution with higher molecular weight polystyrene will have higher viscosity due to the longer chain length of the higher molecular weight polymer. The longer the polymer, the more easily it will tangle and increase drag. The same holds for higher concentrations, since there is more material to become entangled, both of which will lead to a higher viscosity. The figure shows as expected, the frequency shifts more at higher polystyrene

concentrations and at higher molecular weights. The line for the 280 K polystyrene is steeper than that for the 5 K polymer. The slope for the 5 K line is  $-84.9\%$  PS/Hz and  $-117.2\%$  PS/Hz for the 280 K line. This shows that the viscosity is increasing faster with concentration for the high molecular weight polymer than for the low molecular weight.

Figure VI.6 shows the resonant frequency shift as a function of the square root of the viscosity and density product. The plot shows good linearity, showing the ability to monitor the square root of the solution viscosity and viscosity product by the change in resonant frequency. The slope of the line is a series of constants, the fundamental resonant frequency, the strip thickness and strip density. Given that the solution density change is much lower than that of the viscosity, it may be possible to ignore the solution density and relate the resonant frequency to the solution viscosity.<sup>88</sup> This would allow for the direct measurement of solution viscosity. The plot in Figure VI.7 shows the resonant frequency shift as a function of the square root of the solution viscosity. The plots both suggest that the response is quite linear. For the system shown here, the solution viscosity increases over 18 times from 5 % to 25 % polystyrene, over the same range, the density increases only 1.04 times. The result is the change in viscosity dominates the change in the square root viscosity density product. However, the uncertainty associated with the measurement of the viscosity and the density prevent a more exact analysis.

**Table VI.1 Viscosity effect on resonant frequency of magnetoelastic strip**

<b>Solution #</b>	<b>PS Concentration (%wt./wt.)</b>	<b>Resonant Frequency (Hz)</b>	<b>Frequency Shift (Hz)</b>	<b>Density (g/ml)</b>	<b>Viscosity (cP)</b>
<b>PS MW 5,000</b>					
1-A	5	58372.50	-174.50	1.13	1.81
1-B	10	58075.25	-471.75	1.16	3.94
1-C	20	57561.75	-985.25	1.17	18.25
1-D	25	56507.50	-2039.50	1.17	33.62
<b>PS MW 280,000</b>					
2-A	5	58104.75	-132.75	1.15	5.20
2-B	7.5	57820.25	-417.25	1.14	11.21
2-C	10	57835.00	-402.50	1.15	23.15
2-D	15	56900.00	-1337.50	1.18	179.76

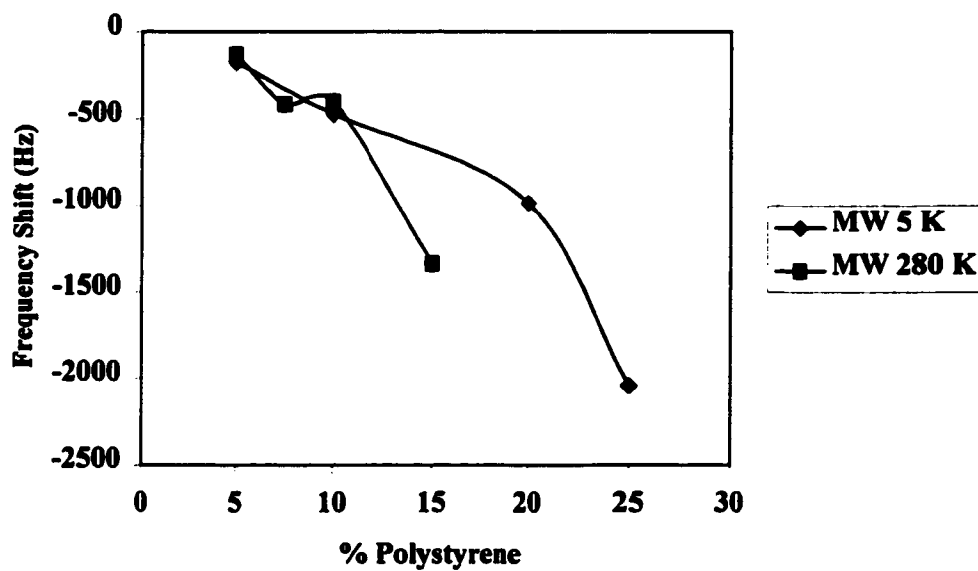


Figure VI.5 Resonant frequency shift as a function of polystyrene concentration and molecular weight.

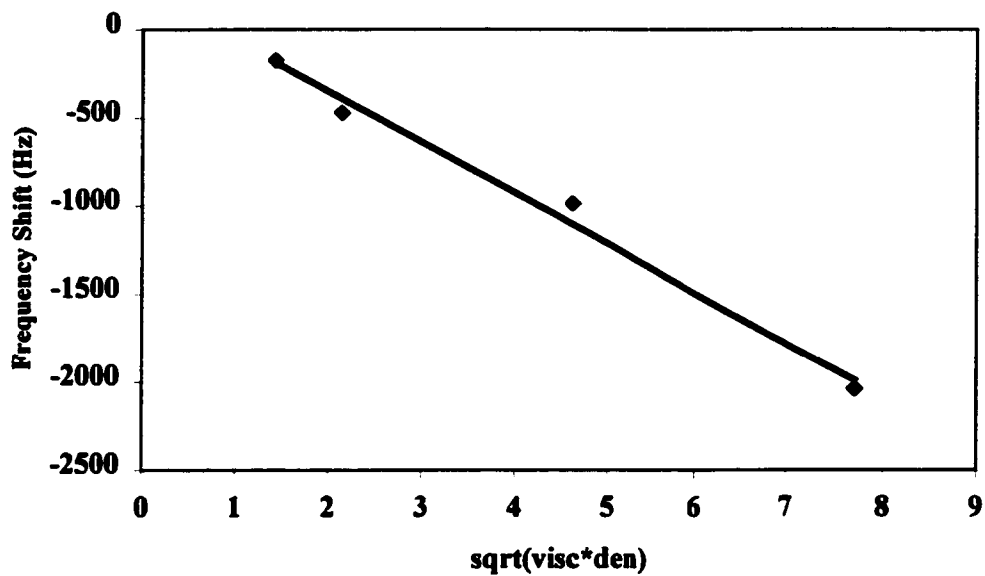


Figure VI.6. Resonant frequency shift as a function of the square root of the viscosity and density product.

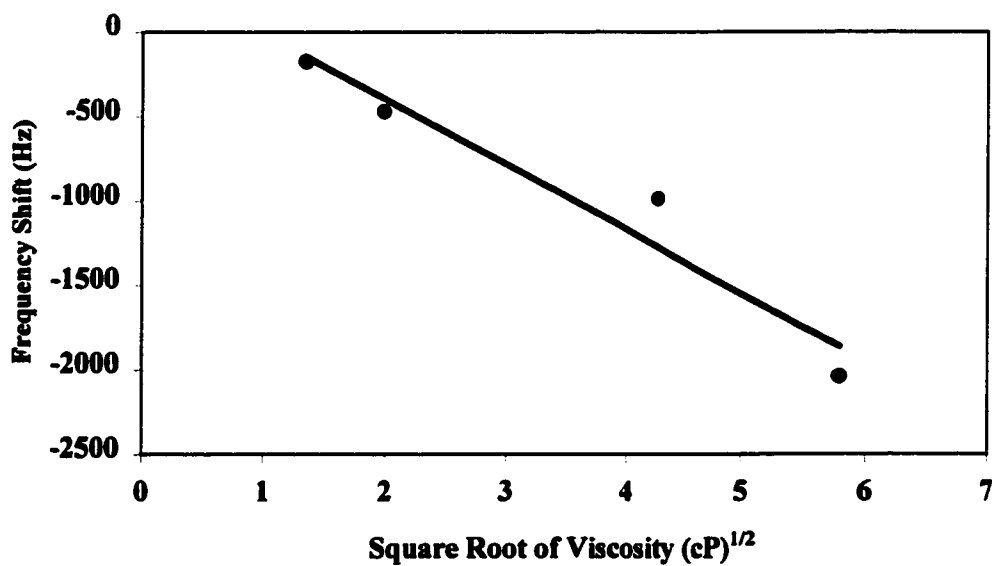


Figure VI.7. Resonant frequency shift as a function of the square root of the solution viscosity.

### **VI.3.2 Effect of Solution Depth**

The first factor examined was the effect of solution depth on the response of the sensor. As the solution depth over a strip increases, the downward pressure exerted by the solution increases. This could be perceived as an increase in mass load by the sensor and cause a decrease in the observed frequency. To investigate this effect a plastic trough was fashioned which would fit into the detection coils of the magnetic resonance meter. The interior dimensions of the trough were 42 x 32 x 9 mm, giving a volume of 12 ml. A sensor strip was then placed in the trough and covered with increasing amounts of water in 0.5 ml increments. This experiment was conducted using the small strip, dimensions of 37 x 6 mm, and the large strip with dimensions of 37 x 13 mm. When the first 0.5 ml of solution was applied it did not cover the entire bottom surface of the trough. The solution was placed on top of the strip at the bottom of the trough. The small strip could be completely covered by the solution, while the large strip could not. The resonant signal as a function of solution volume is shown in Figure VI.8.a and VI.8.b. The results for the small strip, Figure VI.8.a, show that the signal drops when the solution is first added, then levels off and remains constant regardless of the solution volume added. The large strip, Figure VI.8.b, shows the same leveling, but not until the first 1.0 ml of solution was added. The signal decreases when the first 0.5 ml is added, and then decreases slightly more when the second 0.5 ml is added. This is because the sensor is not completely covered when the first 0.5 ml was added. When the second 0.5 ml was added to the trough, the sensor strip was completely covered by solution. As the solution volume increased from 1.0 ml to 7.0 ml, the height of solution over the sensor increased from 0.07 cm to 0.52 cm. This experiment showed that for small amounts of solution



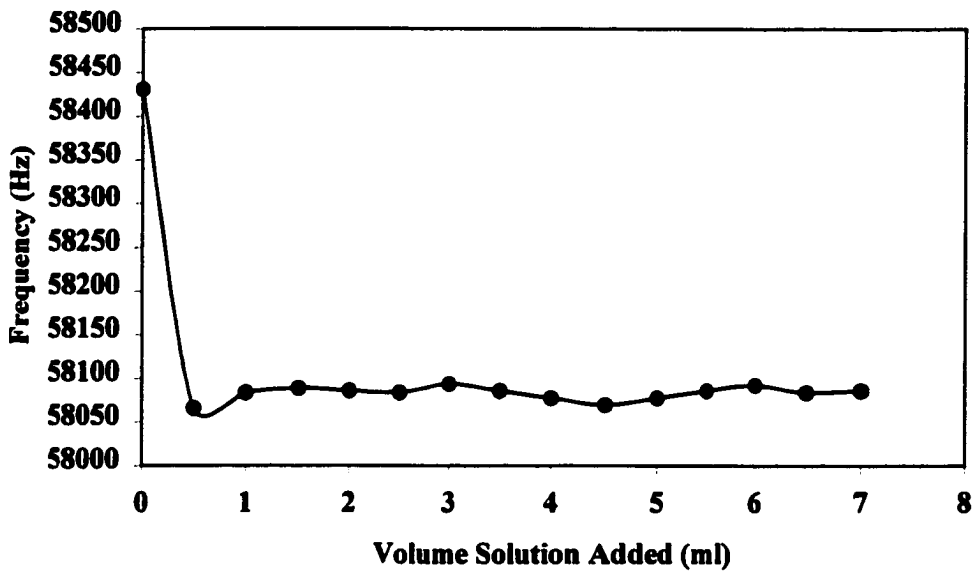


Figure VI.8.a. Resonant frequency as a function of volume ethanol added, small strip.

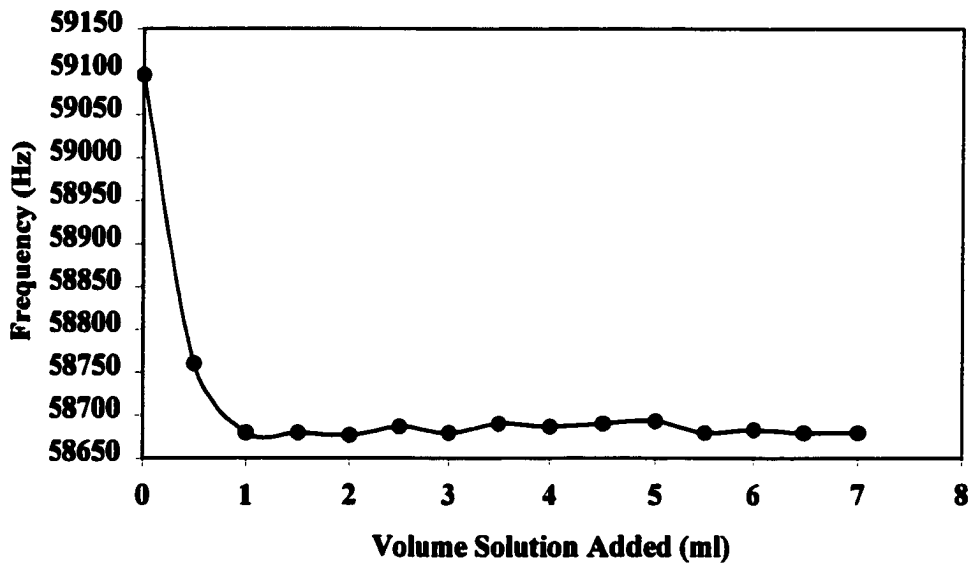


Figure VI.8.b. Resonant frequency as a function of volume ethanol added, large strip.

the solution depth did not affect the resonant signal. It was observed that the amount of the sensor covered by the solution did affect the observed signal. The larger the surface area covered by the solution, the greater the shift.

### **VI.3.3 Effect of Salt Type and Concentration**

Sensor measurements will be taken in buffer solutions prepared with different ionic strengths adjusted using different salts. For this reason the resonant frequency was examined in solutions prepared with different salts at different concentrations. The results of this experiment are shown in Figure VI.9. The plot shows the shift in resonant frequency as a function of salt concentration over four orders of magnitude. The shift was measured from the fundamental resonant frequency in air. As the data shows the frequency shift is fairly constant. This is especially true for the one to one salts, NaCl and KCl. These two salts show a change of only 59.4 Hz for NaCl and 19 Hz for KCl, Table VI.2. The other two salts, Na<sub>2</sub>CO<sub>3</sub> and Na<sub>2</sub>SO<sub>4</sub>, have fairly constant results at the lower concentrations, but show a larger shift at the high salt concentration, 1 M. The frequency shift over the concentration range increases by 171.2 Hz for Na<sub>2</sub>CO<sub>3</sub> and 186 Hz for Na<sub>2</sub>SO<sub>4</sub>. The larger salts show a greater ability to shift the frequency than the smaller salts. This is most likely the result of the higher viscosities associated with the larger salts, particularly at higher concentrations. NaCl and KCl both have viscosities at 1 M of approximately 0.83, while Na<sub>2</sub>CO<sub>3</sub> and Na<sub>2</sub>SO<sub>4</sub> have viscosities of 1.45 and 1.31 respectively. The viscosity change as NaCl and KCl concentration increases from 0.001 M to 1 M is approximately 0.04 cP, while the change is around 0.09 cP for the other salts. The magnitude of the signal change is larger than expected for viscosity effects as seen in

section VI.3.1. This suggests that the salt is causing an effect that results in a frequency shift in addition to that caused by the viscosity change.

The results of this study indicate that the salt concentration will only affect the resonant frequency at high salt concentrations, when the dissolved salt begins to increase the viscosity of the solution. It was also observed that the signal is essentially independent of salt identity at low salt concentrations. The effect of salt identity only becomes apparent at high concentrations, due to the effect of changing solution viscosity. The salt with the higher molecular weight can induce a larger change in solution viscosity, and, therefore, a larger change in response.

#### **VI.3.4 Solution Buffer Capacity**

The effect of the buffer capacity on signal was also investigated since most measurements will be carried out in buffered solutions. Solutions with buffer capacities from 0.0001 M to 0.1 M were examined. The sensor response in pH 4 and 10 at different buffer concentrations is presented in Figure VI.10. As the data shows, in general the signal decreases as the buffer concentration increases. This would be consistent with the viscosity of the solution increasing as concentration increased. However, as in section VI.3.3, the observed frequency shift is larger than that suggested by viscosity effects alone. The data for the salts show that the signal remained constant over most concentrations, decreasing only slightly at high concentrations. Table VI.3 shows the viscosity of the solution at each buffer capacity. The data for pH 10 is consistent with the changes expected for the response following viscosity. However, the data for pH 4 does not. Figure VI.10 shows a steady decrease from 0.0001 M to 0.01M, then staying level to 0.1 M. The viscosity of the solutions stays fairly constant around 1.14 cP. The viscosity

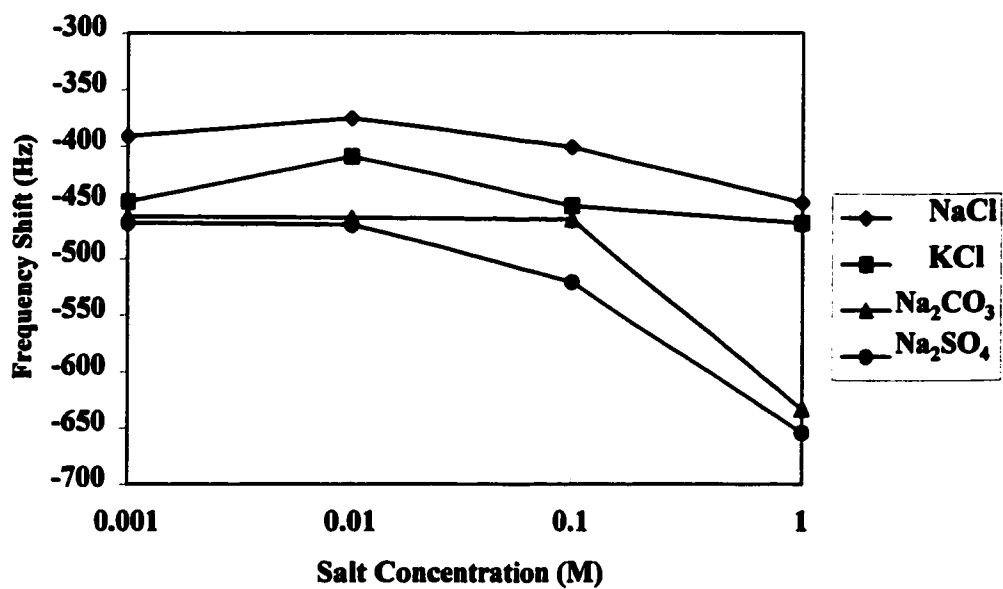


Figure VI.9 Frequency shift as function of salt concentration.

**Table VI.2. Effect of salt concentration on solution viscosity, density and resonant frequency of magnetoelastic strip.**

<b>Salt</b>	<b>Salt Concentration (M)</b>	<b>Viscosity cP</b>	<b>Density (g/ml)</b>	<b>Frequency Shift (Hz)</b>
<b>NaCl</b>	0.001	0.899	0.985	-391.4
	0.01	0.791	0.983	-375.4
	0.1	0.810	0.992	-401.2
	1	0.830	1.025	-450.8
<b>KCl</b>	0.001	0.819	0.975	-449.6
	0.01	0.818	0.979	-409.6
	0.1	0.818	0.985	-453.6
	1	0.825	1.039	-468.6
<b>Na<sub>2</sub>CO<sub>3</sub></b>	0.001	1.295	0.989	-462.6
	0.01	1.305	1.019	-464.0
	0.1	1.310	1.021	-465.6
	1	1.450	1.106	-633.8
<b>Na<sub>2</sub>SO<sub>4</sub></b>	0.001	1.290	0.985	-468.4
	0.01	1.290	1.011	-470.0
	0.1	1.325	1.028	-521.0
	1	1.315	1.025	-654.4

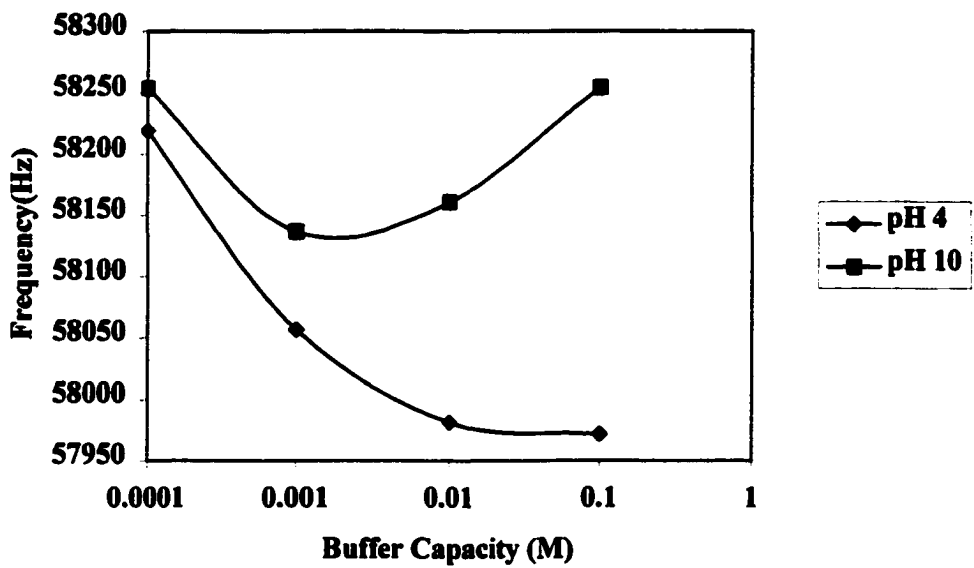


Figure VI.10 Resonant frequency as a function of buffer capacity and pH.

**Table VI.3. Solution viscosity and resonant frequency in pH buffer solutions with different buffer capacities.**

Buffer Capacity (M)	Buffer pH	Viscosity (cP)	Frequency Shift (Hz)	Frequency Shift Difference (pH 4 to pH 10) (Hz)
0.0001	4	1.13	-489.8	- 34.6
	10	1.21	-455.2	
0.001	4	1.13	-652.6	- 80.4
	10	1.66	-572.2	
0.01	4	1.15	-728.0	-179.6
	10	1.58	-584.4	
0.1	4	1.15	-737.6	-282.6
	10	1.36	-455.0	

even increases slightly from 1.13 cP at 0.0001 M to 1.15 at 0.1 M. This indicates that the magnetoelastic strip is interacting with the pH buffer in some chemical fashion. The data trend observed for pH 4 is in agreement with that expected for a mass loading on the strip.

In addition to the solution viscosity, Table VI.3 presents the frequency shift of the sensor at each pH level and buffer capacity. The data shows an increase in the frequency shift as the buffer capacity increases, as well as an increase in the difference between the signal at pH 4 and that at pH 10. This provides further evidence that the strip is chemically interacting with the buffer solution at pH 4. The chemical composition of the magnetoelastic strip is shown in Table VI.4. A possible explanation is that the silicon in the strip is being converted to silicon dioxide and then to silicon hydroxide. At low pH's the silicon hydroxide would be protonated and would be unprotonated at high pH. At higher buffer capacities there would be a greater number of protons present and a greater change expected. This is consistent with the results seen in Figure VI.10. The leveling noticed from buffer capacities of 0.01 to 0.1 M may be due to the saturation of the silicon hydroxide groups with protons.

Table VI.4 Atomic Composition of Magnetoelastic Strip

Element	% Composition (mass)
Carbon	17.0
Silicon	0.51
Iron	28.0
Nickel	26.7
Molybdenum	1.99
Boron	26.0



### **VI.3.5 Effect of Water Immersion on Magnetoelastic Strip**

Most of the factors examined for the effect on response were in aqueous solutions. While investigating these factors, it was observed that over time the magnetoelastic strip would begin to rust. This phenomenon was also observed for the magnetostatic coupled sensors, especially the powder design described in section VI.2.3. As rusting occurs, the composition of the strip is altered, affecting the sensor response. Observation of the strip revealed that the rusting would occur if the strip were left in an aqueous solution overnight. To determine the effect of rusting on the resonant frequency, a strip was placed in water and the resonant frequency observed over a 28 hour period. The results of this are presented in Figure VI.11.

The resonant frequency initially is constant after immersion in water. This is as expected, since solution viscosity is not changing as nothing is being added or removed and the strip is completely covered in solution. After approximately 5 hours, the signal begins to rise. It is at this point that small blemishes on the surface begin appearing that resembles rust. The signal continues to increase until 10 hours after immersion, at which point the signal begins a very slow, steady decline until time 25 hours. At its peak, the signal had increased from the initial resonant frequency by nearly 800 Hz. Over this period the rust spots continue to appear on the surface. After 25 hours, the signal decreases sharply, before beginning a second gradual decline. At this point the resonant frequency signal has decreased by approximately 2500 Hz from the resonant frequency when the strip was initially immersed in water. The first increase, then decrease is not as expected. It was anticipated that the signal would only decrease due to the increase in mass accompanying oxidation. The most probable explanation is that the initial increase

in signal is the result of changes in the chemical composition of the strip. The slow decline is the result of the gradual build up of rust on the surface, which has the effect of increasing the mass on the sensor surface. At 25 hours, the mass loading of the rust on the surface becomes dominant, causing the signal to decrease rapidly. This corresponds to approximately a 6-7 mg increase in mass. However, a mass increase of only 1 mg was observed. The speed at which the signal drop occurs is surprisingly fast for the drop to be only due to mass accumulation. It is possible that there is a change in the magnetic properties as well as a mass build up, which combine to show the change in response observed.

The rusting of the sensor has a dramatic effect on the response of the sensor. In order for the sensor to function as desired it will be necessary to prevent this from occurring. To accomplish this it is necessary to coat the strip with a coating that would be impervious to water. Equally as important as protecting the sensor from water is ensuring that the coating is thin and light enough that it does not interfere with the resonant vibration of the sensor. If the coating is too thick or heavy, the response will be partially or totally dampened.

The first attempts to protect the sensor involved sputter coating the strip with a thin layer of gold/palladium, with a thickness of approximately 100 Å. This proved inadequate to protect the surface from the water. Most likely the surface was not completely covered, but had small holes that allowed water to reach the surface. The problem was especially evident at the edge of the sensor. The procedure was retried with a thickness of 1000 Å, which proved to be adequate for most of the surface. However,

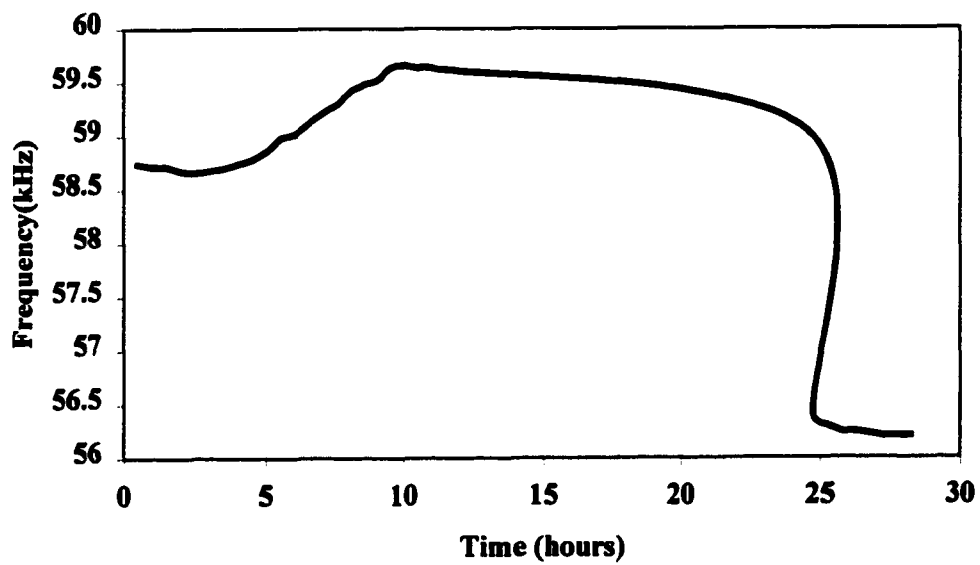


Figure VI.11 Resonant frequency as a function of time immersed in aqueous solution.

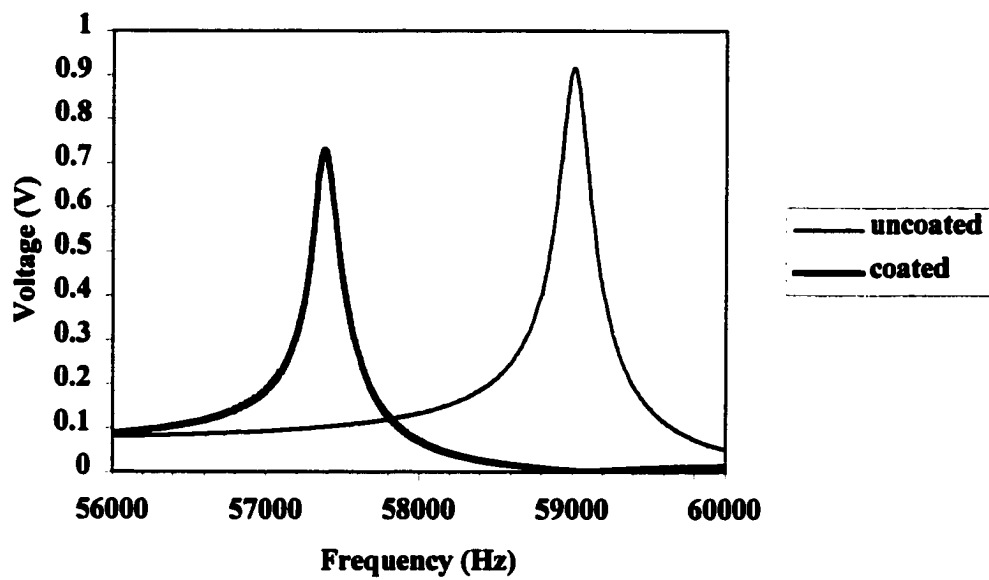


Figure VI.12. Response curve of magnetoelastic strip before and after coating with spin-on-glass protective layer.

the strip would begin to rust at the edge and then the rust would move inward. This indicated that the sides were not adequately protected. Several methods including silver paint and glue were used in an attempt to protect the edges, but these methods damped out the resonant signal.

In an attempt to make the surface more favorable for thiol adhesion, the Au/Pd coating was replaced with only gold. The first attempt used a 1000 Å thick layer of gold. When placed in water, the gold layer was seen to lift off with time and the surface would rust. Chromium, and later titanium, layers were applied to enhance the adhesion. The adhesion layer was 500 Å thick and the gold layer was 1000 Å thick. The sensor surface was protected from rusting, but the edges continued to rust after several hours in water. Analysis of the strips also revealed that the signal had been completely dampened out by the layers of material applied.

The use of a spin-on-glass (SOG) was investigated as a protection material. This is a methylsiloxane in a solvent that cures to form a sol-gel film that protects the surface of the strip. The material was applied by repeatedly spin coating and curing the strip. Analysis by X-ray Photoelectron Spectroscopy confirmed that the strip was completely coated with SOG. In this technique the surface of the strip was irradiated with X rays. This caused electrons to be emitted from the surface. The energy of these electrons was then used to determine the composition of the surface. Figure VI.12 shows the sensor resonant response before and after coating with the SOG. The shift to a lower frequency is consistent with the effect of increasing mass and with increased viscosity, both of which would occur as the strip was coated. The data also shows that the response signal remained sharp, although the signal amplitude was slightly diminished. When placed in

water, the strip was protected from rusting. An additional coating of the SOG on the edges ensured that rust could not start and then move across the surface.

The use of SOG proved to be an effective method of protecting the strip from rusting. Unlike the strips coated by sputter deposition of gold, the layer of SOG was thin enough that the resonant signal was not lost. The coating also proved to enhance the adhesion of the polymer over that of an untreated strip surface. It is believed that the monomer solution can diffuse into the coating layer and as polymerization occurs some of the polymer chains become entangled. Later analysis showed that failure of the coating occurred at high pH, when the silane bonds that make up the coating were attacked by the hydroxyl ions present in basic solutions. This showed that the SOG protection method has a limited range of effectiveness.

### **VI.3.6 Use of Magnetoelastic Strip for pH Sensing**

The use of the magnetoelastic strip for pH measurement was carried out in two systems. The first involved the use of a pH sensitive HEMA-co-DMAEMA hydrogel membrane. The second involved the use of VBC-co-TCPA microspheres derivatized with diethyl amine embedded in a poly-HEMA membrane. Following application of the pH sensitive polymer layer, the strips were alternately placed in pH 4 and pH 10 buffer solutions with a buffer capacity of 0.1 M and an ionic strength of 0.1 M. The resonant frequency was determined after 10 minutes of equilibration time in the appropriate buffer solution.

#### **VI.3.6.1 HEMA/DMAEMA Membrane as pH Sensitive Material**

The use of a HEMA-co-DMAEMA membrane as the pH sensitive material was investigated. The prepolymer solution consisted of 3 % (mol./mol.) of DMAEMA in

HEMA, with 1.5 % (mol./mol.) TEGDM cross-linker and 20 % (vol./vol.) water. An aliquot of the solution was placed on the SOG coated magnetoelastic strip and spun at 1500 rpms for 10 seconds. The strip was then photopolymerized under a mercury lamp for 20 minutes. The procedure was repeated one additional time, with a spin speed of 1000 rpms. Following the second polymerization, the strip was placed in distilled water for 45 minutes to hydrate. Following hydration, the sensor was cycled in the pH buffer solutions.

The data for this experiment, and that described in section VI.3.6.2, is presented in Table VI.5 and is represented graphically in Figure VI.13. The strip was cycled between pH 4 and pH 10 five times. Figure VI.13 shows that the signal is decreasing with each cycle. However, the difference between pH 4 and pH 10 for each cycle remains fairly constant. The difference is approximately 15 Hz for the first two cycles then increases to between 30 and 36 Hz for the next two cycles, before increasing again to 56 Hz for the final cycle. The reason for the decrease in overall response and the increase in the difference is not entirely clear. The increase in the difference between pH 4 and pH 10 may be due to the polymer shrinking and swelling more effectively after a few cycles. Alternatively, the swelling may cause an increase in delamination in pH 4, which then settles back on the surface at pH 10. During the first few cycles, the membrane may develop microcracks and untangle cross-link bonds, which allow it to swell more effectively during later cycles, giving rise to the increased difference. This need to condition the polymer was also observed in derivatized polystyrene beads.<sup>102</sup> Additionally, the SOG coating was worn away with repeated exposure to pH 10 buffer, which would affect the observed response. However, the loss of material would

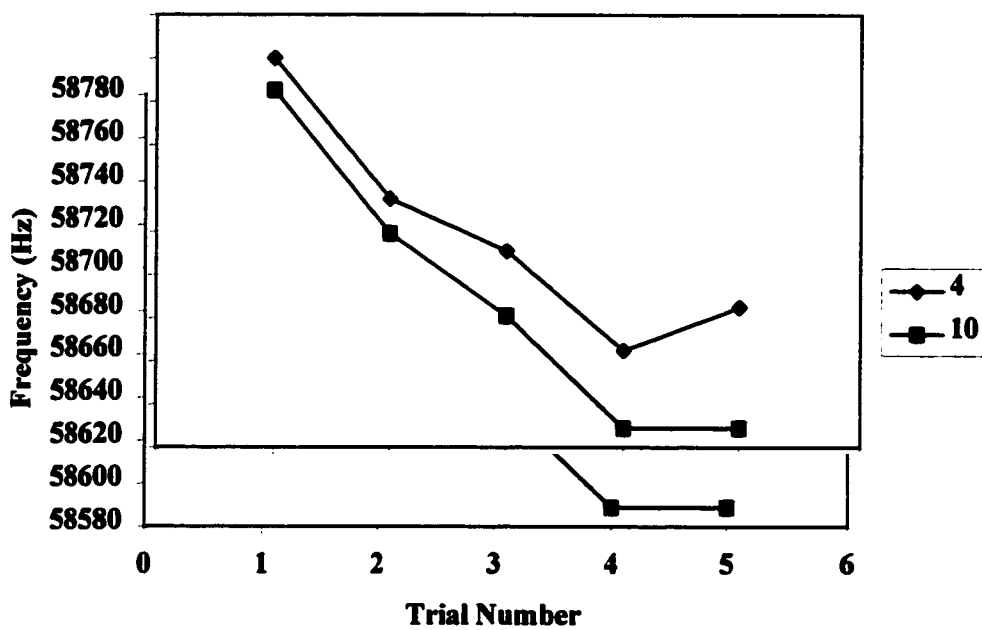


Figure VI.13. Response of magnetoelastic strip coated with 3 % DMAEMA hydrogel in pH 4 and pH 10 buffer solutions.



**Table VI.5. Resonant frequency of polymer coated magnetoelastic strips in pH 4 and pH 10 buffer solutions**

<b>Trial Number</b>	<b>pH 4 Resonant Frequency (Hz)</b>	<b>pH 10 Resonant Frequency (Hz)</b>	<b>Resonant Frequency Difference (Hz) pH 4 to pH 10</b>
<b>3 % DMAEMA membrane</b>			
1	58760	58745	-15
2	58695	58679	-16
3	58671	58641	-30
4	58625	58589	-36
5	58645	58589	-56
<b>1 % VBC/TCPA beads in HEMA membrane</b>			
1	58485	58409	-76
2	58414	58370	-44
3	58370	58325	-45

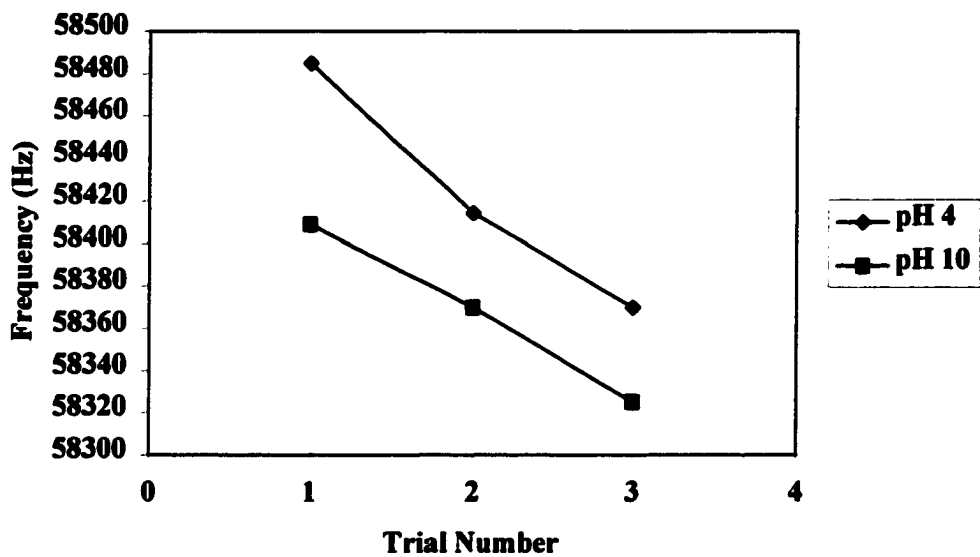


Figure VI.14. Response of magnetoelastic strip coated with 1 % VBC/TCPA microspheres embedded in HEMA membrane in pH 4 and pH 10 buffer solutions.

be expected to increase the frequency signal, so the cause of the decrease in overall signal is unclear.

#### **VI.3.6.2. Microspheres in HEMA Membrane as pH Sensitive Material**

The sensor using a hydrogel embedded with pH sensitive microspheres was prepared in a similar fashion to the hydrogel sensor. A prepolymer mixture was prepared of 1 % (wt./wt.) VBC-co-TCPA microspheres in HEMA, and 1.5 % (mo./mol.) TEGDM cross-linker and 15 % (vol./vol.) water. An aliquot of solution was applied to a SOG coated strip and spun at 1500 rpm for 10 seconds, then photopolymerized for 30 minutes. The strip was then placed in water to hydrate for 45 minutes.

The results of this experiment are presented in Figure VI.14 and in Table VI.5. As with the hydrogel, the overall signal is seen to decrease with each cycle, while the difference between pH 4 and pH 10 for each cycle remains fairly constant. Table VI.5 shows a large initial difference for the first cycle, then the difference is approximately 45 Hz for the second and third cycle. The reason for the overall decrease is again not clear. As mentioned previously, there is some loss of the SOG coating following exposure to pH 10 buffer, but the mass loss would be expected to show an increase in the resonant frequency. Over time the polymer may be adding mass to the strip in some fashion, or may be increasing in brittleness, which would be seen as decrease in signal. However, it would be expected that longer exposure to an aqueous environment would soften the membrane, not harden it.

### **VI.3.6.3. Magnetoelastic Sensor Conclusions**

In both the pH sensitive hydrogel and pH sensitive beads in hydrogel systems, the data obtained would be consistent with a bending of the strip or a decrease in viscosity as the strip is exposed to pH 4 buffer. At low pH the strip is more swollen and has a higher water content. This has the effect of softening the hydrogel and making it appear less viscous, thereby increasing the signal. In high pH the membrane is less hydrophilic and stiffer. An additional effect is that the strip may curl away from the polymer side as the polymer swells. As the polymer swells and increases in size, the metal layer cannot and will tend to curl in on itself. This has the effect of increasing the resonant frequency of the strip.

### **VI.4 Conclusions**

The use of sensors interrogatable using magnetic fields has been demonstrated. These sensors have a significant advantage over other types of sensors, due to the ability to place the sensor completely removed from the detection system, with no wires or other physical connection. The magnetostatic coupled design showed the sensor could be constructed in a variety of arrangements. Designs that exposed more of the polymer membrane to the analyte solution proved to have shorter response times. The response time decreased from approximately 24 hours in the sandwich design, to 10 minutes in the powder design. In addition, the sensor proved to be more robust and could be cycled several times.

The factors affecting the response of magnetoelastic strips were investigated. The depth of the solution over the sensor was seen to have no effect on response, while the amount of surface area covered was found to be significant. The ability to monitor

solution viscosity was demonstrated and shown to be in good agreement with the results predicted by theory. The results also are consistent with the results obtained by monitoring the viscosity with a viscometer.

The effect of ionic strength and buffer capacity on pH was also examined. The ionic strength of the solution was found to have little effect on the resonant frequency. The response stayed constant at most ionic strengths and increased only when the ionic strength approached 1 M. The effect was most prevalent in the higher molecular weight salts. These salts had increased viscosities that were consistent with the observed frequency shift. The buffer capacity was also seen to have an effect on the response signal. For pH 4, the results show a clear downward trend in frequency with increasing buffer capacity, even though the viscosity had remained fairly constant as the buffer capacity increased. The results for pH 10 are not as clear. The response decreases at first, then increases. The viscosity first increases then decreases. This is an indication that there is some chemical interaction between the strip and the buffer solutions. The detrimental effect of water on the strip was investigated, along with methods to protect the strip from contact with water and prevent the strip from rusting.

The response of a strip coated with a pH sensitive polymer was also examined. The overall response frequency was seen to decrease with each cycle, while the response difference within each cycle was observed to stay fairly constant. The ability to conduct pH measurements with the magnetoelastic strip was proven, however the problem of signal reproducibility remains to be addressed.

# CHAPTER VII

## Polymerization Monitoring Techniques

### VII.1 Introduction

Monitoring of the polymerization process is an important aspect of polymer synthesis. It is critical that the polymerization process leads to a consistent product of the desired quality. Most often this can only occur when the polymerization process is held within certain parameters. Currently the dominant method of process control is to examine the end product and then make the determination of product quality.<sup>103</sup> The ability to monitor the polymerization process on-line would greatly simplify the quality control process and allow for more effective control of the polymerization. This would make it possible for changes to be made as the polymerization proceeded, rather than after one batch was complete. Densitometry and viscometry are two common methods of monitoring the polymerization process, or more specifically, the degree of polymerization.<sup>103</sup> Raman<sup>104</sup> and infrared<sup>105</sup> spectrometry, as well as fluorescence<sup>106</sup> have been used to monitor the polymerization process, but in each case samples were removed from the polymerization vessel prior to analysis. The use of sound velocity as a polymerization monitor for on-line monitoring has been described.<sup>107</sup> A review of on-line polymerization monitoring examines the various techniques.<sup>108</sup> In this chapter the use of magnetoelastic strips for polymerization monitoring is examined. Several free radical polymerizations were examined, as was the cross-linking of PVA with glutaraldehyde. The advantage of this method is that the container can remain sealed,

since no sample needs to be removed and no connections to the sensor are needed to allow monitoring to occur.

## **VII.2 Polymerization Monitoring**

### **VII.2.1 Monitoring of Polymerization of PVA**

The polymerization of PVA was the first system monitored to examine the feasibility of using this method. Not a true polymerization, the reaction monitored was the cross-linking of poly-vinyl alcohol with glutaraldehyde. The reaction is initiated by the addition of hydrochloric acid to the solution. The cross-linking reaction is shown in Figure VII.1. The solution will become more viscous as the reaction progresses, the cross-linking level increases and the reaction mixture transforms from a liquid into a gelatinous solid.

The reaction mixture consisted of a 5 % aqueous solution of PVA (molecular weight 14 K), 2.5 % (vol. % PVA solution) of 25 % aqueous solution glutaraldehyde and 5 % (vol. % PVA solution) 4 M HCl. The progress of the reaction was observed by monitoring the solution viscosity using a viscometer. The results for this experiment are shown in Figure VII.2. The data point at time 0 minutes was taken prior to the addition of the HCl. As the reaction proceeds, the viscosity of the solution increases greatly. There is a large increase in solution viscosity over the first minute, when the viscosity increased from 23 cP to nearly 16,000 cP. Solution viscosity continues to increase at a slower rate, reaching nearly 23,000 cP at 6 minutes. The solution viscosity was too high to measure after this point to continue monitoring. When the solution was removed from the viscometer sample holder, approximately 7 minutes after the reaction was initiated, it was a gelatinous solid.





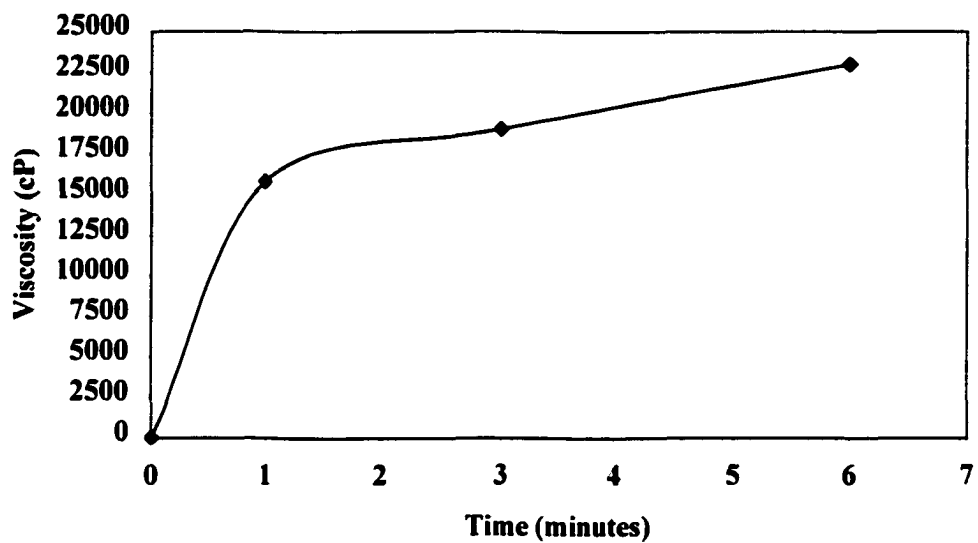


Figure VII.2. Solution viscosity of poly-vinyl alcohol as cross-linking reaction proceeds with time.

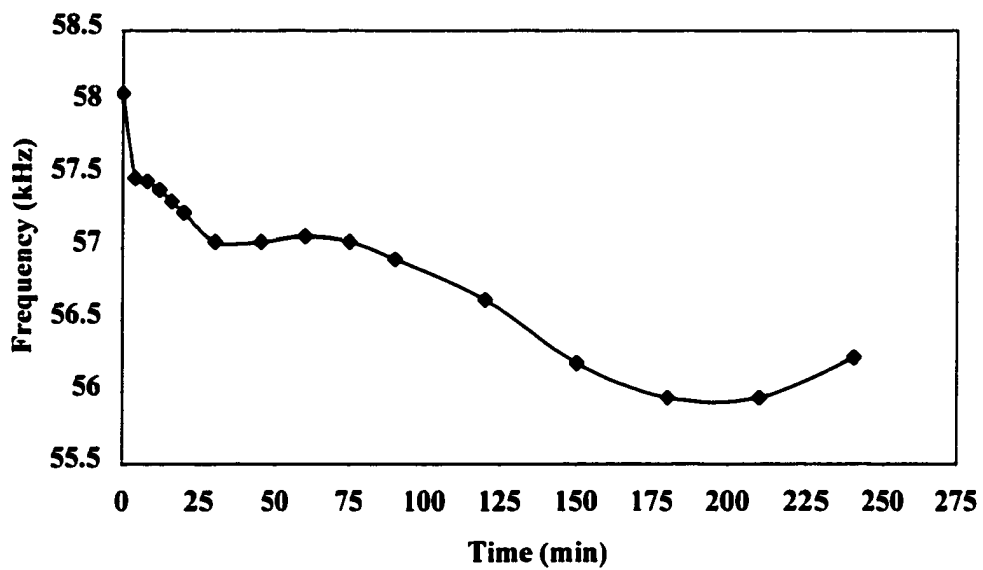


Figure VII.3. Resonant frequency of poly-vinyl alcohol coated magnetoelastic strip as cross-linking reaction proceeds with time.

The same reaction solution was also monitored by magnetic resonant, as shown in Figure VII.3. A longer sample time was required for this measurement, as dictated by the time required for a scan to be completed. As seen in Figure VII.3, there is a large decrease in resonant frequency during the first 4 minutes. During this time the signal decreases by approximately 0.6 kHz, which is approximately a third of the overall decrease in resonant frequency. Russell reported that the reaction was completed within 10 minutes.<sup>109</sup> Similar to that time, the viscosity measurements showed a nearly complete reaction after 6 minutes. It was observed by magnetic resonance that the reaction actually progresses for approximately 3.5 to 4 hours. The major portion of the reaction occurs during the first half-hour, with most occurring during the first 4 minutes. Over time, the reaction then slowly continues to progress and decrease the resonant frequency.

There are several possible explanations for the range of time observed. Practical studies have shown that the gel is usable after 10 minutes of polymerization. This is consistent with the observation of solution viscosity. The magnetic resonant data shows that the reaction is largely completed within a similar time frame. The continued frequency shift is likely due to the continued cross-linking within the membrane. As the solution viscosity increases, it becomes more difficult for the glutaraldehyde to cross-link the polymer chains, since they are no longer as able to twist and bend into position. Also as the cross-linking proceeds, water is expelled from the forming solid. The solid PVA becomes more brittle due to its lower water content, which would be seen as an increase in viscosity and cause the frequency shift. This loss of water could continue to occur even after the reaction is complete, as water is lost to the surroundings by evaporation.

These results are similar to that obtained by Grimes *et. al.* who monitored the curing of refractory cement.<sup>88</sup> The cement was hard to the touch within one hour, but the shift in frequency continues for more than 8 hours. This demonstrates that a reaction can continue long after it appears complete and that magnetic resonant can be used to monitor a reaction after it appears to be complete.

## **VII.2.2 Monitoring of Polymerization of VBC**

The polymerization of VBC was monitored using several different techniques and under different conditions. Polymerization was initiated using both the photo initiator DMPAP and the thermal initiator benzoyl peroxide, BP.

### **VII.2.2.1 Thermally initiated polymerization of VBC**

The thermally initiated polymerization of VBC with benzoyl peroxide was examined by magnetic resonant monitoring. The formulation used consisted of 2 % DVB, 2 % Kraton and 0.5 % BP, and the polymerization was carried out at 80 °C. Figure VII.4 shows the results of this experiment. The reaction shows a large initial decrease in resonant frequency during the first 30 to 45 minutes, then the reaction rate seems to slow before leveling off around 2 to 2.5 hours. A large decrease is seen initially, since the system consists of only monomer, with no polymer present. As the reaction proceeds the monomer is converted into polymer, which increases the solution viscosity. This happens more rapidly at the beginning of the reaction since the monomer is more mobile. Over the course of the reaction, the increase in viscosity caused by the polymer formation and the effect of cross-linking makes it more difficult for the monomer to diffuse through the solution. This slows the rate of the reaction, as seen after approximately 45 minutes. Polymerization is still occurring, which is why the frequency continues to shift, but it is

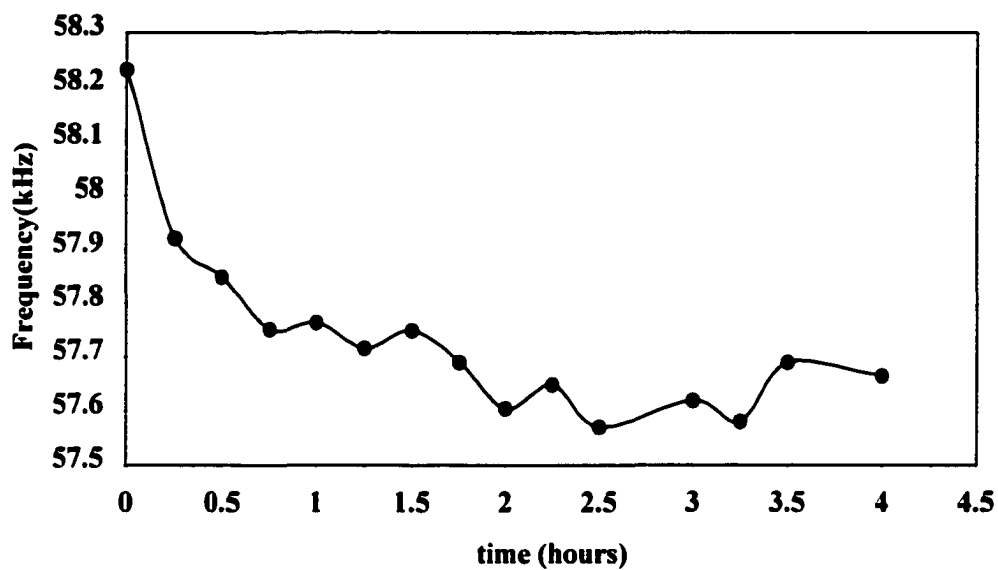


Figure VII.4. Resonant frequency as a function of time for thermally initiated polymerization of VBC

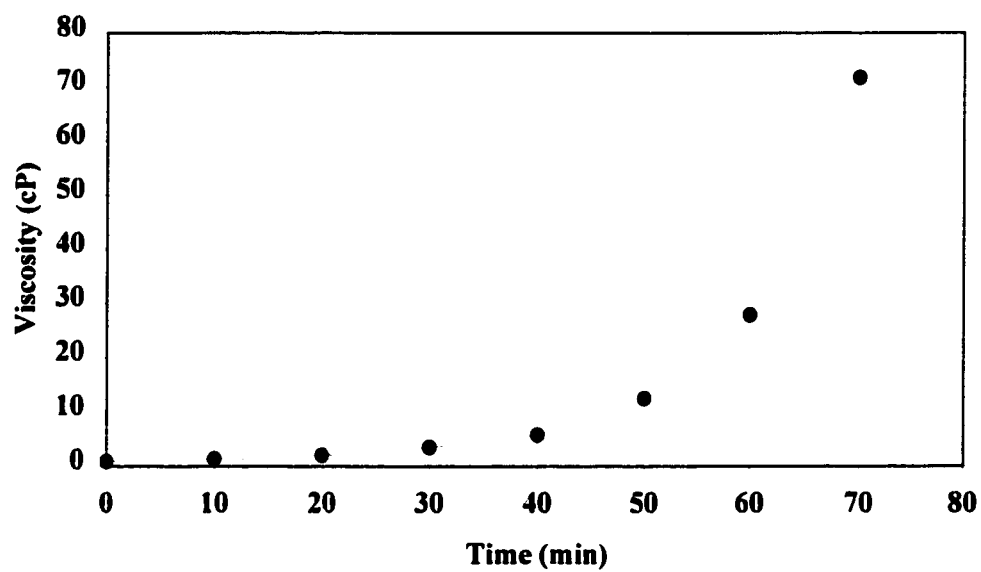


Figure VII.5. Solution viscosity as a function of time for thermally initiated polymerization of VBC

more difficult than initially. When the frequency levels off after 2 hours, the conversion of monomer to polymer is largely complete and there is little or no monomer reacting.

The system was also investigated by measuring the viscosity of the solution as polymerization occurred. The results for this are shown in Figure VII.5. Unlike the results from magnetic resonant monitoring, there is no large initial increase in viscosity. The viscosity increases very slowly over the first 45 minutes. At this point the viscosity increases rapidly, until the experiment was stopped at 70 minutes. It is interesting that the point at which the viscosity is seen to increase in the viscosity measurement, is when the reaction seems to be slowing in the magnetic resonant measurement. The reason for this is not clear. Unfortunately, the viscosity measurements were stopped due to limitations in the experimental set up, so a more complete picture of the viscosity over a longer time could not be obtained.

Rooney had monitored this same system by FTIR spectroscopy by monitoring the bands associated with the vinyl group.<sup>30</sup> In his results, there was no large initial decrease, but a steady decrease in signal as the vinyl groups of the VBC are consumed. The decrease observed is similar to that obtained by the viscosity measurement over the first 45 minutes. The reaction continued steadily for approximately 4 hours. The FTIR technique is very capable of detecting small changes, which may explain the longer reaction time seen in this technique. This would indicate that the reaction is still occurring even after the magnetic resonant method has leveled off and is not measuring a viscosity change. Although this would explain why the FTIR experiment shows the reaction going on longer, it does not explain the lack of a large initial decrease seen in the

magnetic resonant experiment. The steady reaction rate, at least for the first hour, are consistent with the results for the viscosity experiment.

#### **VII.2.2.2 Photo initiated polymerization of VBC**

The polymerization of VBC initiated using the photo initiator DMPAP was also examined. The formulation used was the same as in section VII.2.2.1, with DMPAP replacing the BP. Polymerization was initiated by placing the monomer mixture under a mercury lamp, instead of heating the solution as in section VII.2.2.1. The magnetic resonant frequency experiment shows a steady decline in resonant frequency as the solution polymerizes, Figure VII.6. At approximately 1.5 to 2 hours, the reaction rate appears to be increasing, with the signal decreasing more rapidly, before leveling after 3 hours. According to the data, the rate of reaction appears to be constant at the beginning, but then increases rapidly toward the end of the reaction. It is possible that the reaction starts off slowly, reacting with only a little monomer at a time. The chains of polymer produced are not very long and do not increase the viscosity to a great extent. After a certain length of time, the polymer chains begin to react with each other as the monomer concentration decreases. The reaction of two polymer chains causes the viscosity to increase more rapidly than the reaction between monomer units and polymer chains. Cross-linking also increases. This effect is seen after 1.5 to 2 hours in Figure VII.6. The resonant frequency of the strip shifts by approximately 500 Hz lower over the course of the reaction.

The solution viscosity of a photo polymerized VBC solution was measured, with the results presented in Figure VII.7. As in Figure VII.6 the reaction starts with a gradual increase in the viscosity of the solution. In this case, the viscosity continues to



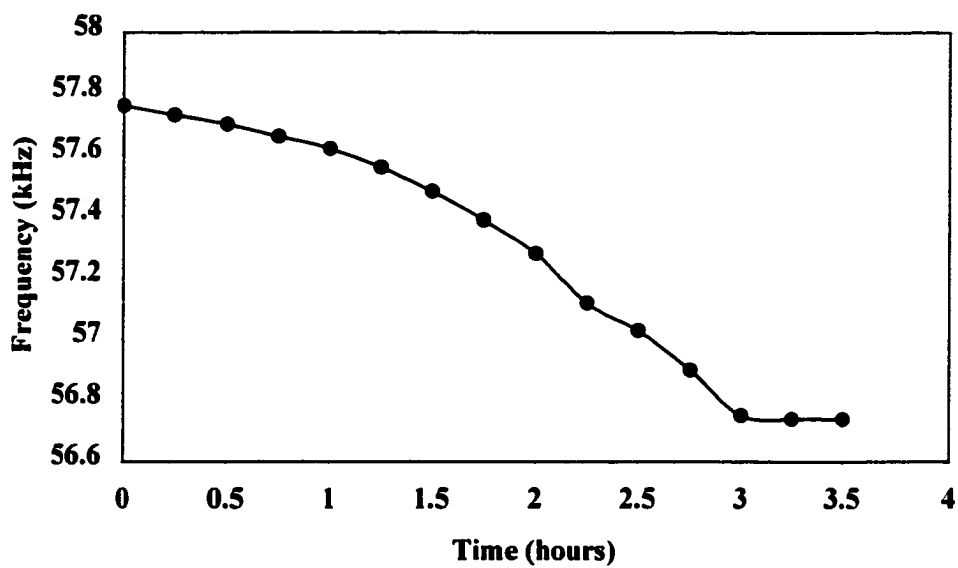


Figure VII.6. Resonant frequency as a function of time for photo initiated polymerization of VBC

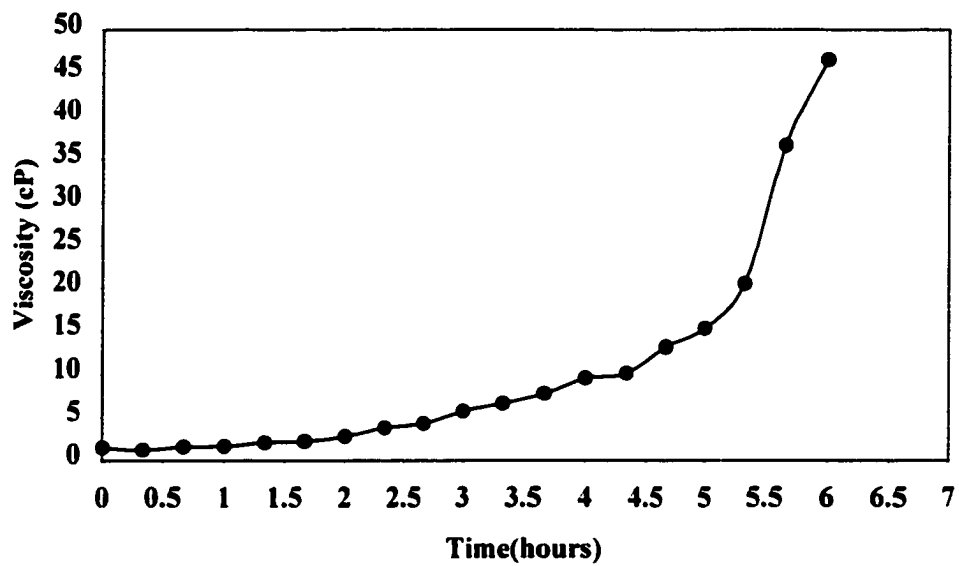


Figure VII.7. Solution viscosity as a function of time for photo initiated polymerization of VBC

slowly increase over 5 hours, before rapidly increasing until the reaction was stopped at 6 hours. This rate of slow increase was approximately 2.5 times longer than that observed in the magnetic resonant response. This difference may be due to the differences in experimental set up. The set up used to measure the solution viscosity had a much lower surface area to volume ratio. When the magnetic resonant measurements were taken there was a large surface area and a small volume. The opposite is true for the solution viscosity. The reaction would have less radical produced per volume and the radicals would have further to travel in the reaction vessel, which would explain the lower reaction rate. The end results are the same, indicating the reaction behaved as expected. The observed difference is most likely the result of experimental conditions.

### **VII.2.3 Monitoring of Polymerization of HEMA/DMAEMA**

This system was initially monitored by FTIR to determine the polymerization times needed to ensure polymerization was complete and the membrane could be used for chemical sensing. Polymerization was initiated using photo and thermal initiators, DMPAP and AIBN respectively. The polymerization was also monitored by two additional techniques, magnetic resonant frequency and solution viscosity, to obtain a more complete picture of the polymerization.

#### **VII.2.3.1 Thermally initiated polymerization of HEMA/DMAEMA**

The thermal polymerization of HEMA/DMAEMA was monitored by the magnetic resonant technique. The formulation used consisted of a 1:1 molar mixture of HEMA and DMAEMA, 1.5 % (mol./mol. monomers) and 1 % (wt./wt. monomers) AIBN. The results of this experiment are shown in Figure VII.8. A steady decrease in the resonant frequency is observed for the first 3 hours of the polymerization, before

leveling off. This indicates that the reaction proceeded at a constant rate until reaching completion, which in this case appears to be after 3 hours. The results are similar to those observed for the thermal polymerization of VBC, Figure VII.4.

The reaction was also monitored by measuring the viscosity of the monomer solution over time as the polymerization was carried out. The results for this are shown in Figure VII.9. The viscosity data shows that the viscosity stays constant for the first 10 minutes of the reaction, before increasing drastically. The viscosity increases from 4.4 cP to 6.4 cP over the first 10 minutes of the reaction, but then increases from 6.4 cP to 116 cP over the following 2 minutes. This indicates that there is little measurable reaction occurring initially, then the reaction proceeds rapidly.

Figure VII.10 shows the polymerization monitored by FTIR spectrophotometer. During the course of the reaction, the carbon-carbon double bond on the vinyl group are consumed and become carbon-carbon single bonds. The carbonyl group remains constant and can be used as an internal standard.<sup>92</sup> The reaction was monitored by plotting the ratio of the carbon-carbon double bond stretch, at  $1635\text{ cm}^{-1}$ , to the carbonyl stretch, at  $1730\text{ cm}^{-1}$ , vs. the time of the reaction. As the carbon-carbon double bonds are consumed, the ratio of C=C/C=O will decrease, since the carbonyl stretch will remain constant, while the absorbance of the carbon-carbon double bond stretch will decrease.

This is confirmed by the results in Figure VII.10. There is a large initial decrease in the C=C/C=O absorbance ratio during the first 25 minutes, then the ratio remained steady until the experiment was halted after 3 hours. This abrupt change is consistent with the results from the viscosity measurement. The change appears to occur more

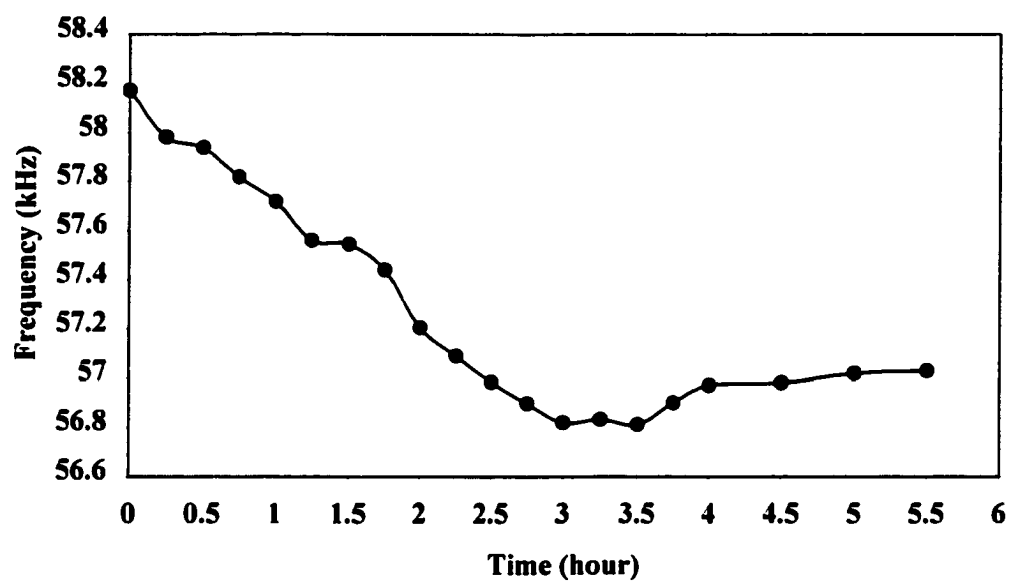


Figure VII.8. Resonant frequency as a function of time for thermal initiated polymerization of HEMA-co-DMAEMA

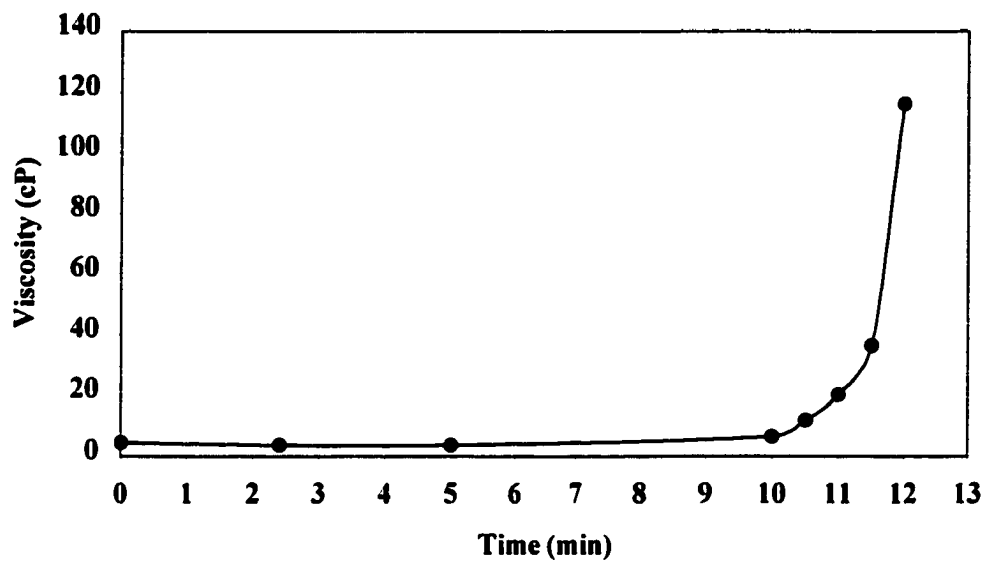


Figure VII.9. Solution viscosity as a function of time for thermal initiated polymerization of HEMA-co-DMAEMA

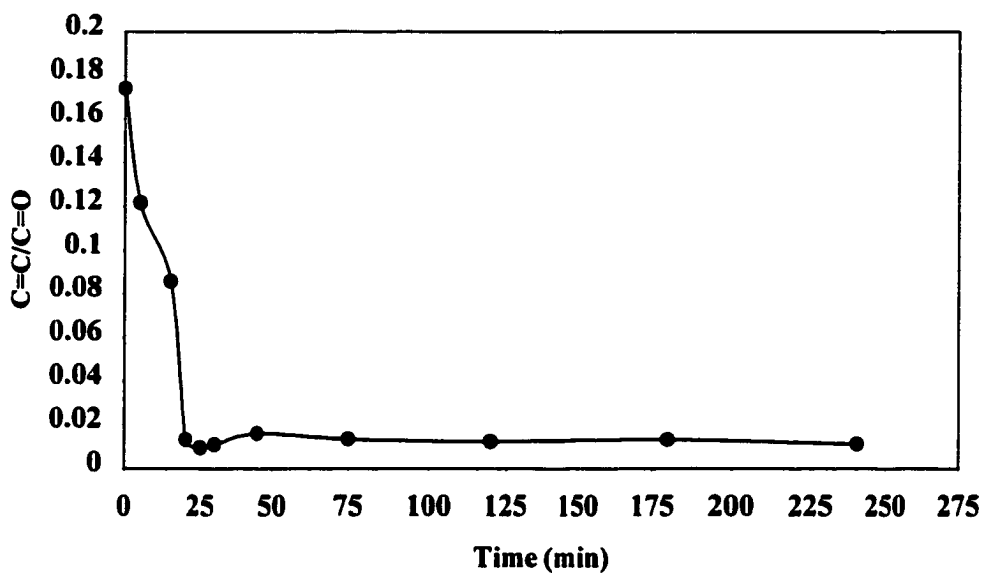


Figure VII.10. Ratio of the intensity of the C=C band to C=O band decreasing as a function of time for thermal initiated polymerization of HEMA-co-DMAEMA

rapidly in the FTIR measurement, since a large change is visible after 5 minutes. However, in the viscosity measurement a change is not observed until after 10 minutes. The probable explanation is that the change is not large enough to measure in the viscosity measurement, while it is visible in the FTIR spectra. Both FTIR and viscosity show a rapid change over the first few minutes of the polymerization. The magnetic resonant data shows a slow steady reaction over several hours. While the FTIR data reaches a constant state after 30 minutes, the magnetic resonant response does not reach a constant state until 3 hours, 2.5 hours later. Data obtained from the viscosity measurement and from FTIR indicates that the reaction would be complete after 15-20 minutes, while the magnetic resonant data indicates that 3 hours are required. A possible explanation is that the magnetic strip is also exhibiting temperature effects, which are the result of the experimental procedure used. The strip is placed in an oven for polymerization, but then is placed in the resonant meter and examined at room temperature. During this time the strip will cool from 80 °C to room temperature. This will cause the resonant frequency to increase due to the temperature sensitivity of the strip.<sup>88</sup>

#### **VII.2.3.2 Photo initiated polymerization of HEMA/DMAEMA**

The photo polymerization of HEMA/DMAEMA was also examined. The formulation was the same as that used in section VII.2.1, except that the AIBN was replaced with DMPAP as the photo initiator. Both the solution viscosity and the FTIR methods were used to examine the system. The solution viscosity monitoring does not have the large increase preceded by a period of constant viscosity, as in the thermally polymerized HEMA/DMAEMA system, Figure VII.11. Instead, there is a continuous



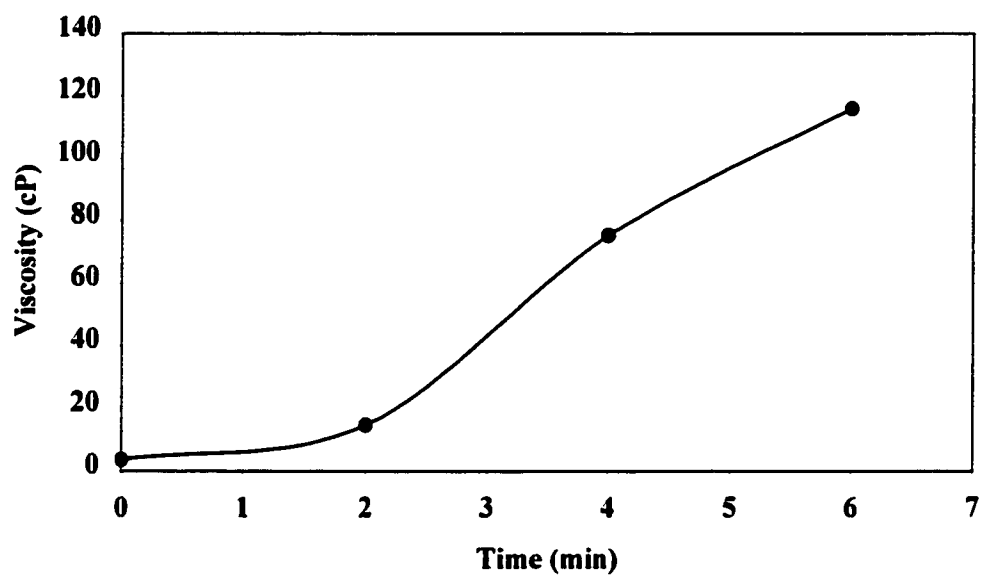


Figure VII.11. Solution viscosity as a function of time for photo initiated polymerization of HEMA-co-DMAEMA

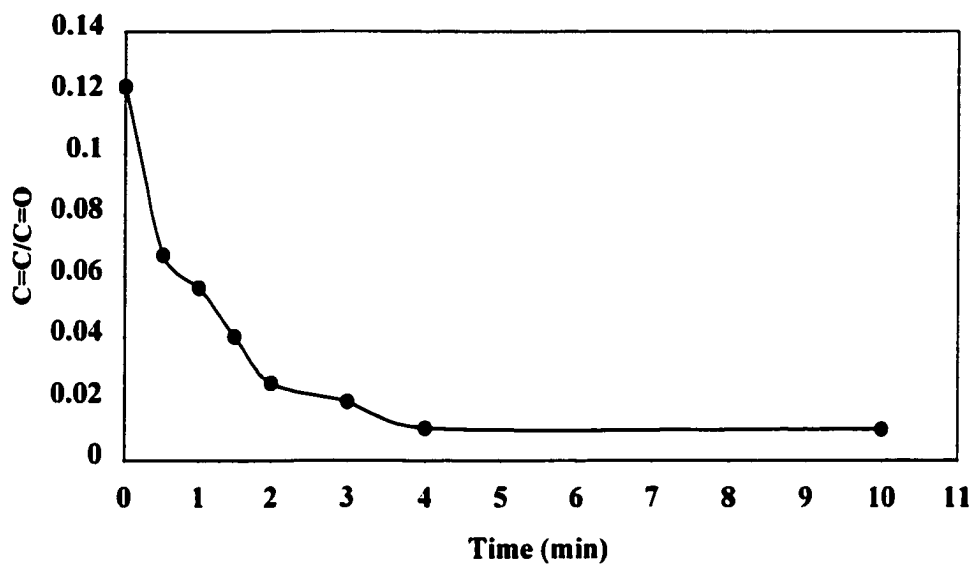


Figure VII.12. Ratio of the intensity of the C=C band to C=O band decreasing as a function of time for photo initiated polymerization of HEMA-co-DMAEMA

increase over the course of the reaction, with the rate continuing to increase, especially after 2 minutes of reaction time. There is an increase in viscosity of 11.1 cP over the first two minutes, 60.5 cP between 2 and 4 minutes and 40.6 cP over the final 2 minutes. Although not as dramatic as the thermal results, the sharp increase in viscosity is seen.

Figure VII.12 presents the results of the FTIR monitoring of the photo initiated reaction. The results here show a large initial decrease in the number of C=C bonds, indicating that the reaction is proceeding rapidly toward completion. The increase in reaction time over the thermally initiated reaction is again evident. In the thermal results, Figure VII.10, the rapid decrease lasted for 25 minutes before leveling off. For the photo reaction the rapid decrease levels off after 4 minutes. It is interesting that the thermal results show the reaction to be complete in a shorter time in the viscosity experiment compared to the FTIR experiment. The photo reaction shows completion first in the FTIR experiment and then in the viscosity experiment. Completion of the reaction is evident by either a constant C=C/C=O ratio or maximum viscosity.

### **VII.3. Conclusion**

This chapter shows the feasibility of monitoring the polymerization process with a magnetoelastic strip. The data show that a reduction in frequency correlates with the progress of the polymerization. As the polymerization proceeds, it is expected that the viscosity will increase as the monomer is transformed into longer polymer chains that are more easily entangled. The viscosity also increases as the polymer chains become cross-linked, the polymer chains are held together and are less able to move about. The actual time of change did not always exactly match the time of reaction seen in the viscosity and FTIR method. However, the correlation does show that the method provides insight into

the polymerization and does indicate when polymerization is complete. Additionally, when the results of several polymerizations were examined, the change in viscosity did not cause a change in frequency of equivalent magnitude. An increase of viscosity of 22.5 kCp in PVA produced a frequency change of -500 Hz. In the thermal VBC system, a viscosity increase of 80 cP produced a frequency decrease of 450 Hz. These differences are probably the result of the different conditions that the strip is exposed to during the polymerization. The advantage of this system is that the system can easily be used in a sealed system, with no physical connection. Also, there is no need to take a sample out of the reaction vessel. This allows for more rapid adjustments in the polymerization process to be made and greater control over the properties of the final product.

The examination of the HEMA-co-DMAEMA polymerization by FTIR had been used to determine the polymerization time of the reactions. This confirmed that the time of photopolymerization was complete in 10 minutes and thermal polymerization was complete in approximately 30 minutes. This confirmed that the polymerization time used of 20 minutes and 2 hours for photo and thermal polymerization respectively, were sufficient to complete polymerization.

## **CHAPTER VIII**

### **Functionalized Microspheres in Hydrogel Membranes for Optical Sensing**

#### **VIII.1 Introduction**

This chapter examines the use of functionalized microspheres embedded in a hydrogel membrane for optical chemical sensing. The monitoring of pH by optical methods has been the focus of research for our group over the past several years.<sup>30,31,34</sup> The phenomenon exploited is the change in reflectance that occurs as the polymer swells and shrinks. As the polymer swells and shrinks, the water content of the polymer changes, which causes the refractive index of the polymer to change, as a result the reflectance changes. When the polymer is swollen it is filled with water, which lowers the refractive index of the polymer. The refractive index of the hydrogel remains constant. It is the difference in refractive indices between the microspheres and the bulk hydrogel that cause the change in reflection that is monitored.

Initially, a bulk derivatized poly(VBC) membrane was used.<sup>30</sup> This membrane has pores that are filled with water. The refractive index difference between the polymer and the water filled pores causes light to scatter. In the present system the bulk polymer does not change its refractive index, but the refractive index of the polymer microspheres changes with water concentration in the microsphere. The system presented here has several advantages over swelling of a bulk membrane. The first advantage is that the entire membrane does not change shape, only the microspheres. This is an advantage when the membrane is attached to a surface, such as a fiber optic. When the entire

membrane swells there are shear forces that can cause the membrane to delaminate from the surface. These forces are minimized in this arrangement, since the bulk hydrogel does not change shape, only the microspheres embedded in it. Additionally, by allowing the microspheres to completely swell in all directions the refractive index change will be maximized. Another advantage is that there is a smaller amount of pH sensitive material, therefore the response time will be minimized. Complementing this is the hydrophilicity of the hydrogel that makes the aqueous analyte more accessible to the pH sensitive polymer. The small size of the microspheres provides a smaller distance that the analyte must diffuse to reach the interior, which also decreases response time.

Hydrogels were chosen as the matrix for the microspheres for a number of reasons. First, as mentioned above, the size of the hydrogel does not change in response to pH. This makes the membrane less likely to detach from the substrate as the result of shear forces. Second, the immobilization of a hydrogel to a glass substrate, such as a fiber optic, can be carried out. Third, is the high water content of hydrogels, which allows for a more rapid response time and lowers the refractive index of the hydrogel. The fourth advantage is that the hydrogel can be biocompatible and isolates the polymer microspheres from direct contact with the sample solution

The degree of light scattering or reflection is dictated by the refractive index difference between the microspheres and the hydrogel. The magnitude of scattering increases as the refractive index difference increases. This is described by the Fresnel equation  $R = (n_2 - n_1)^2 / (n_2 + n_1)^2$ , for normal incidence.

When the microsphere is in an acidic environment the amine sites become protonated and the polymer swells. As it swells, the polymer takes up water, which

lowers the overall refractive index of the microsphere. In a basic environment the microsphere has a lower amount of water and therefore a higher refractive index. The refractive index of the hydrogel remains constant, since there is no pH sensitive material present and the membrane does not shrink or swell. This is an important distinction between the hydrogels described in this chapter and those described in chapter IV. The membranes in chapter IV contained the pH sensitive DMAEMA, while those presented in this chapter do not.

There were several goals for the work in this chapter. The first was to investigate the possibility of using a surface plasmon resonance (SPR) sensor for pH monitoring. This was to be done by monitoring the refractive index change of the membrane in different pH buffer solutions. The second goal was to investigate alternative hydrogels for use with the polymer microspheres. The purpose of this was to see how hydrogel hydrophilicity affected signal magnitude and response time. The third goal was to examine the stability of membranes prepared using animated poly-(VBC) particles prepared by seeded emulsion polymerization. Factors to be examined included reproducibility and the effect of exposure to light and exposure to heat on membrane response over time.

## **VIII.2 pH Monitoring by Surface Plasmon Resonance**

### **VIII.2.1 SPR Sensor Introduction**

This section examines the monitoring of solution pH by monitoring refractive index changes as polymer microspheres swell and shrink in a hydrogel membrane. Surface plasmon resonance (SPR) is used to measure the refractive index of a solution. The technique has been used for the detection of morphine and to monitor

immunoreactions.<sup>37,39</sup> The introduction of an integrated miniature SPR sensor by Texas Instruments has expanded the uses of SPR. Refractive index changes of the polymer as it swells and shrinks provide the basis for the optical sensing conducted by this group. This creates the possibility of monitoring solution pH by SPR using the TI SPR sensor.

The sensor was prepared by suspending microspheres in a poly vinyl alcohol(PVA) hydrogel membrane. The microspheres were prepared by a dispersion polymerization of an equimolar mixture of VBC and TCPA, cross-linked with DVB and stabilized with PVP, as described in section III.3.5, and derivatized with diethyl amine. Figure VIII.1 shows a SEM micrograph of microspheres obtained using this formulation. The percent nitrogen was determined to be 4.6 %, which is slightly less than the expected 8.6 %. The microsphere and hydrogel mixture were polymerized on the surface of a disposable gold coated slide and then placed on the SPR sensor. The slide was held in place by the flow cell attachment of the sensor. After hydrating the hydrogel in water for approximately one hour, the sensor was ready for use.

The water content of the microspheres was determined to be 52 % and 33 % in acid and base, respectively. The method for determining the water content is described in section II.4.2. This is in agreement with the water concentrations determined by Miele to be 54 % and 37 %.<sup>31</sup> The values obtained here are slightly lower, as expected with the slightly lower amine content observed. Based on these observations, the refractive index of the membrane should be higher in pH 10 buffer and lower in pH 4 buffer. Based on group contributions it is possible to calculate the refractive index of a polymer.<sup>91</sup> The refractive index of VBC/TCPA was calculated to be 1.54 when dry. Using the water



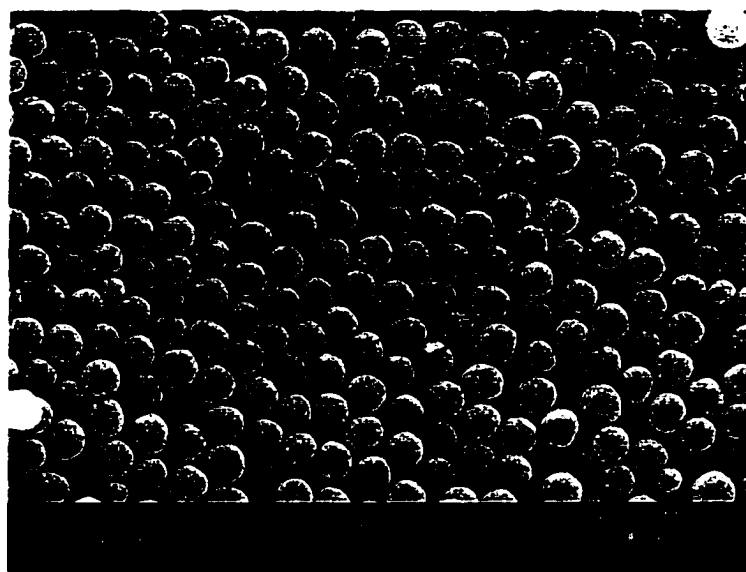


**Figure VIII.1** Scanning electron micrograph of VBC/TCPA microspheres used in SPR and hydrogel studies.

amounts above, the refractive index for VBC/TCPA in the swollen and unswollen states was determined to be 1.43 and 1.47 respectively. The water content of the PVA membrane should remain constant regardless of solution pH and is approximately 90 %. A refractometer was used to measure the refractive index of a PVA membrane, which was determined to be 1.34.

### **VIII.2.1 SPR Sensor Results and Discussion**

A SPR pH sensor was prepared by coating a slide with a solution of 0.2 % (wt./wt.) beads in PVA as described above. The sensor was then cycled between pH 4 and pH 10, allowing a cycling time of approximately 15 minutes. The response curve obtained is presented in Figure VIII.2. The results show good reproducibility between cycles, although there appears to be slight upward trend. Most striking however is the results are the exact opposite of what was expected. The sensor showed a higher refractive index in pH 4 then for pH 10. The reason for this was not immediately apparent. Table VIII.1 presents the expected refractive index of the membrane in pH 4 and in pH 10 buffer. The observed change is in fact larger in magnitude then the expected change, although in the opposite direction. A refractive index change of 0.00008 had been expected, while a change of  $-0.0009$  was observed.

The refractive index changes coincided with the different buffer solutions, but was opposite then that which had been predicted. A blank experiment was conducted to examine if the buffer refractive index changed from pH 4 to pH 10. This was done by measuring the refractive index of each buffer solution. The results of this study are seen in Figure VIII.3. The data shows that there is a change in the refractive index between buffer solutions. It had been assumed that the refractive index would remain 1.33. While

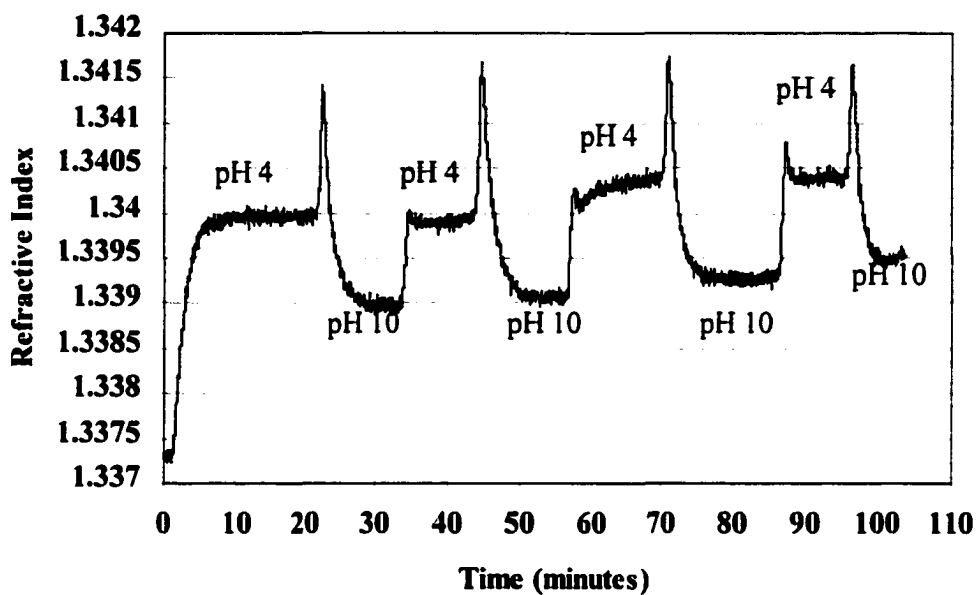


Figure VIII.2 SPR response for 0.2 % VBC/TCPA beads in PVA membrane. Sensor was cycled between pH 4 and pH 10 buffer solutions with buffer capacity of 0.1 M and ionic strength of 0.1 M.

Table VIII.1. Theoretical refractive index of PVA membrane with VBC/TCPA microspheres in pH 4 and pH 10 buffer solutions.

Bead Concentration (% wt./wt.)	Refractive Index pH 4	Refractive Index pH 10	Refractive Index Difference (pH 10- pH 4)
0.2	1.34017	1.34026	0.00008
20	1.357	1.366	0.00882
40	1.374	1.392	0.01764

- microsphere refractive index was 1.43 in pH 4 and 1.47 in pH 10, PVA membrane refractive index was 1.34

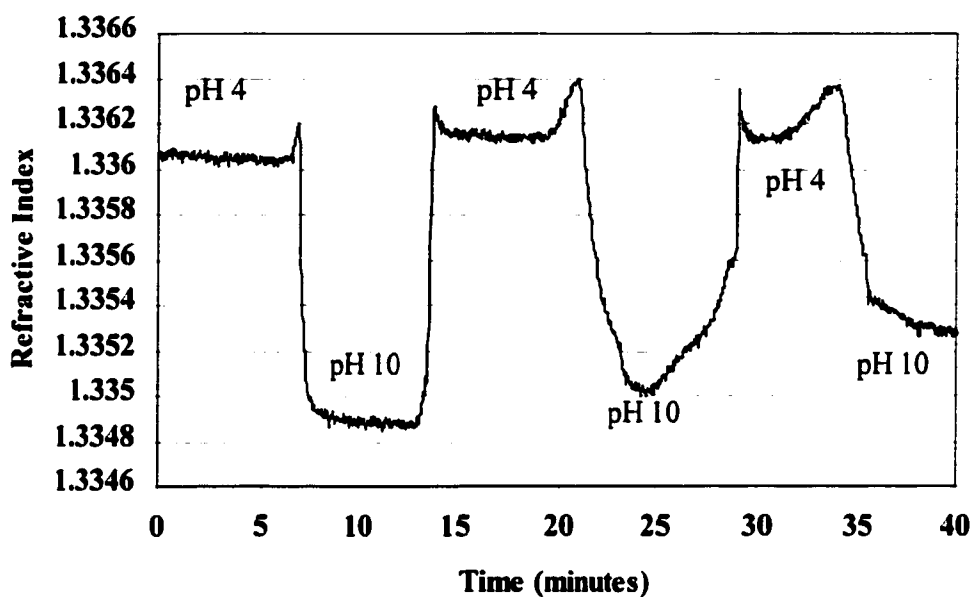


Figure VIII.3 SPR response for pH 4 and pH 10 buffer solutions. Buffer capacity of each solution was 0.1 M and ionic strength was of 0.1 M.

the change is small enough that this assumption is valid for the optical methods discussed later in this chapter, the sensitivity of this device makes the assumption invalid.

Based on the refractive index measurements of the buffer, the expected refractive index change was calculated, substituting the buffer refractive indices for that of water. The revised expected refractive index changes are presented in Table VIII.2. The results show that a refractive index change of  $-0.0094$  is obtained, while a change of  $-0.0093$  is predicted. At low bead concentrations the refractive index change of the buffer in PVA is dominating. In the case of PVA, the different buffers are actually causing a change in refractive index, with the membrane having a higher refractive index in acid, 1.345, then in base, 1.344. In order to better separate the refractive index change of the membrane from that of the buffer, it was necessary to go to higher bead concentrations.

The results of analysis of a 20 % bead suspension are presented in Figure VIII.4. The results for a 40 % bead suspension are shown in Figure VIII.5. Despite the correction for the buffer refractive index, the results are still the opposite of what is expected. There is a greater difference between the expected values and predicted values for these trials than was seen for the 0.2 % bead membrane, Table VIII.2. The reason for this is not entirely clear. A possible explanation is that the beads are not as homogeneous throughout the membrane as expected. The higher the bead concentration in a membrane the greater the difficulty in suspending the beads. Additionally, the membrane may not be attached to the surface as well as desired. This could allow buffer to seep under part of the membrane, which would cause the observed refractive index to follow that of the buffer rather than the refractive index change of the membrane.

Table VIII.2. Theoretical and experimental refractive index of PVA membrane with VBC/TCPA microspheres in pH 4 and pH 10 buffer solutions.

Bead Concentration (% wt./wt.)	Refractive Index pH 4	Refractive Index pH 10	Refractive Index Difference (pH 10- pH 4)	Percent Difference
<b>Theoretical*</b>				
0.2	1.345	1.345	-0.00093	
20	1.363	1.370	0.00687	
40	1.381	1.396	0.01475	
<b>Experimental</b>				
0.2	1.340	1.339	-0.00094	0.99
20	1.337	1.335	-0.0023	134
40	1.336	1.335	-0.0010	107

\* microsphere refractive index was 1.43 in pH 4 and 1.47 in pH 10, PVA membrane refractive index was 1.345 in pH 4 and 1.344 in pH 10 Buffer refractive index was 1.336 for acid and 1.335 for base

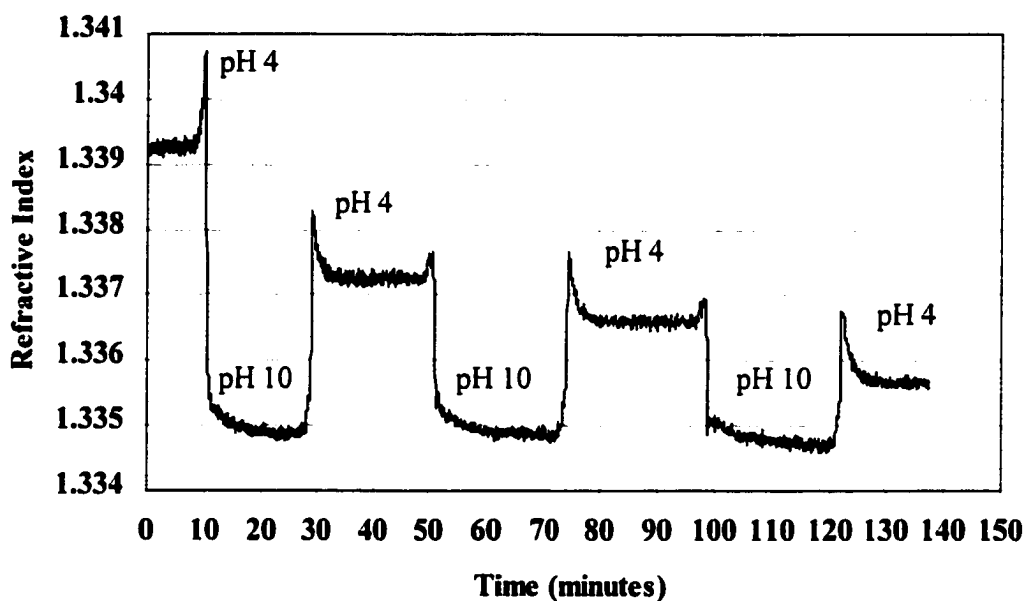


Figure VIII.4 SPR response for 20 % VBC/TCPA beads in PVA membrane. Sensor was cycled between pH 4 and pH 10 buffer solutions with buffer capacity of 0.1 M and ionic strength of 0.1 M.



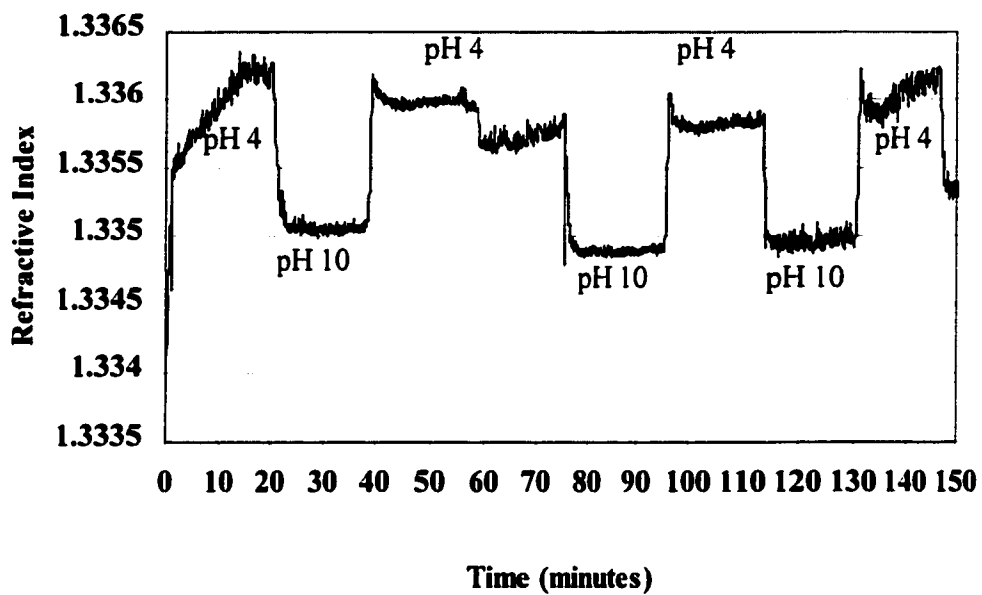


Figure VIII.5 SPR response for 40 % VBC/TCPA beads in PVA membrane. Sensor was cycled between pH 4 and pH 10 buffer solutions with buffer capacity of 0.1 M and ionic strength of 0.1 M.

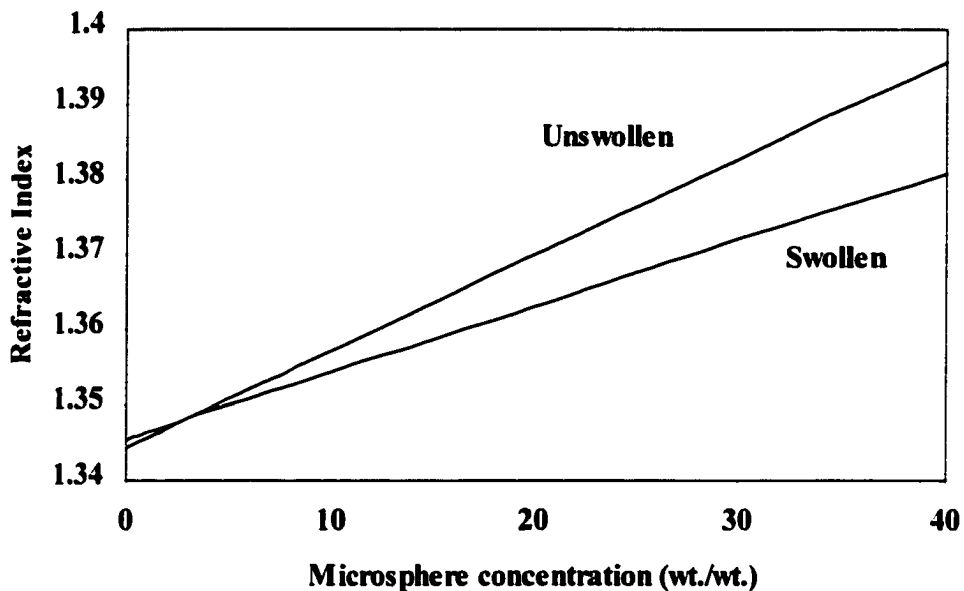
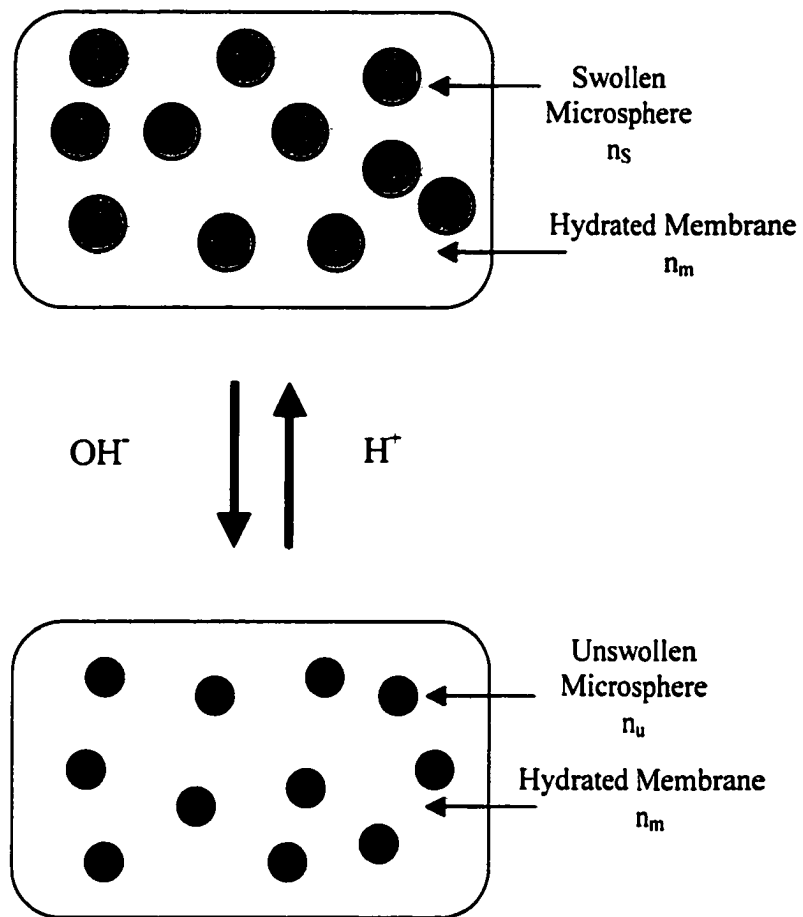


Figure VIII.6 Predicted refractive index for VBC/TCPA microspheres in a PVA membrane as a function of microsphere concentration. Swollen state was in pH 4 buffer and unswollen state was in pH 10 buffer, all with buffer capacity of 0.1 M and ionic strength of 0.1 M. Microsphere refractive indices were 1.43 in pH 4 and 1.47 in pH 10. PVA membrane had refractive index of 1.345 in pH 4 and 1.344 in pH 10.

Also observed, was that the difference in refractive index between pH 4 and pH 10 was decreasing. This was predicted by the calculating the refractive index of the swollen and unswollen membrane as a function of bead concentration, Figure VIII.6. At low bead concentration the refractive index of the membrane will change with the buffer solution. As bead concentration increase, the change will become more connected with the change in bead refractive index. As a result, the refractive index difference will get smaller, until the refractive indices are the same and then the difference will begin to increase. The results obtained for the 20 % and 40 % membrane are becoming less negative, though at a much slower rate, than was predicted.

The results obtained show the feasibility of measuring the refractive index change of swellable polymers as method of monitoring pH. The observed trends fit well with predicted results. A more secure method of membrane attachment to the substrate would be expected to improve the operation of the sensor. The use of a less hydrophilic hydrogel such as poly-HEMA would also be desirable. This would minimize the effect of the buffer refractive index on that of the membrane because the solution content of the hydrogel is lower. Minimizing the buffer effect would make the observed refractive index more closely controlled by the microspheres. Limitations in the refractive index operating range of the SPR sensor available did not allow the use of the poly-HEMA membrane to be evaluated.



**Figure VIII.7** Schematic diagram of hydrogel membrane containing swellable microspheres. The microspheres swell in acidic solution and shrink in basic solution. The refractive index of the membrane( $n_m$ ) remains constant. The refractive index of the microspheres is higher in basic solution( $n_u$ ) and lower in acidic solution( $n_s$ ).

### **VIII.3 Alternative Hydrogel Membranes for Immobilizing Microspheres for Optical Sensing**

#### **VIII.3.1 Introduction of Alternative Hydrogel Membranes**

The use of microspheres embedded in a hydrogel has been examined for use as a chemical sensor. This sensor responds via scattering of light at the interface between the microsphere and the hydrogel. The difference between the refractive indices will affect the degree of reflection in accordance with Fresnel's equation. The refractive index of the membrane will remain constant, while that of the microsphere will change in accordance with the pH of the environment in which it is immersed. This arrangement is shown in Figure VIII.7. As with the SPR sensor, the microspheres were composed of a VBC-TCPA copolymer animated in diethylamine, Figure VIII.1. The hydrogel was the focus of this study.

The primary hydrogels examined for sensing with suspended microspheres have been poly-(HEMA) and PVA.<sup>30,31,37</sup> It has been observed that the response time is faster in the PVA membrane than in the poly-(HEMA) membrane.<sup>37</sup> This is due to the higher water content of the PVA membrane, which allows for the analyte to diffuse more rapidly through the membrane. The response is expected to be larger in the PVA, since the refractive index difference between the microspheres and the membrane is greater. PVA has a refractive index of approximately 1.34, while poly-(HEMA) has a refractive index around 1.44 and VBC/TCPA microspheres have a refractive index around 1.45. The difference between the refractive indices of microspheres and the hydrogel is greater with PVA, which gives a larger reflection and hence a larger signal. The disadvantage of PVA is that it is extremely fragile. The membrane must be kept wet at all times or it will shrivel and crack. It also has poor mechanical stability, making it extremely difficult to

handle without tearing. Although it gives a slower response of less magnitude, poly-(HEMA) is quite robust and does not have to be stored in water.

The major advantage of PVA is its fast response time. The low refractive index results from the high water content of the membrane, approximately 90 %. The goal of the research described in this section was to examine alternative hydrogels to PVA and HEMA. A hydrogel with the response time and signal magnitude of PVA, along with the robustness of HEMA was desired. Several hydrogels similar in structure to HEMA were examined, hydroxyethyl acrylate, hydroxypropyl acrylate and hydroxypropyl methacrylate. The structures of these monomers are shown in Figure IV.1. These hydrogels each have different hydrophilicities, HPMA, HEMA, HPA and HEA, in order of increasing hydrophilicity. As the water concentration of the hydrogel increases, it is expected that the refractive index will decrease, which will increase the magnitude of the response and the response time should decrease. Table VIII.3 presents the hydration levels, calculated by group contributions and adjusted refractive indices of the different membranes.

### **VIII.3.2 Results and Discussion**

#### **VIII.3.2.1 Use of HPMA Hydrogel**

Hydroxypropyl methacrylate is the least hydrophilic of the hydrogels examined. The water content of a membrane equilibrated in water is 23.1 %. Based on group contributions, the refractive index of the polymer was calculated to be 1.49. Taking the hydration level into account, the refractive index is 1.45. The turbidity spectra for VBC/TCPA microspheres embedded in a HPMA membrane are presented in Figure VIII.8. The surprising result is that the signal is larger in pH 4, then it is in pH 10. It was

anticipated that the scattering would be larger in pH 10, since the refractive index of the microsphere would be higher and closer to that of the membrane. When the reflectance was calculated using the Fresnel equation, the reflectance in pH 4 was found to be higher than that of pH 10. This would predict a larger signal in low pH, accounting for the larger signal in pH 4. The turbidity spectra show a sizable difference in the signal between pH 4 and pH 10. The observed reflectance was 4.4. The predicted reflectance is 1.0. This situation is interesting because the refractive index of the membrane is exactly in the middle of the refractive indices of the microspheres. The refractive indices of the microspheres in the swollen and unswollen states were 1.43 and 1.47 respectively, the refractive index of the hydrogel was 1.45. The difference between the expected and obtained results is not entirely clear.

#### **VIII.3.2.2 Use of HEMA Hydrogel**

HEMA is slightly more hydrophilic than HPMA, with an equilibrium water concentration of 35.9 %. The refractive index for HEMA adjusted for hydration is 1.44. Figure VIII.9 shows the turbidity spectra of a HEMA membrane with microspheres. In agreement with theory, the scattering was larger in pH 10 than in pH 4. As with the HPMA, in this situation the refractive index of the membrane, 1.44, is between the swollen and unswollen particles, 1.43 and 1.47 respectively. The refractive index of the hydrogel is much closer to the swollen particles. The difference between the swollen particles and the membrane is 0.01, while the difference between unswollen and membrane is 0.03. This is consistent with scattering being greater in the membrane with unswollen microspheres in pH 10. The observed turbidity ratio for the membrane was

Table VIII.3 Refractive indices and hydration levels of hydrogel membranes

Hydrogel	Water Concentration of Hydrated Membrane (wt./wt. %)	Refractive Index Calculated from Group Contributions	Refractive Index of Hydrated Membrane
HPMA	23.1	1.49	1.45
HEMA	35.9	1.50	1.44
HPA	51.3	1.50	1.41
HEA	65.9	1.51	1.39

-all membranes prepared with 1.5 % cross-linking with EGDM



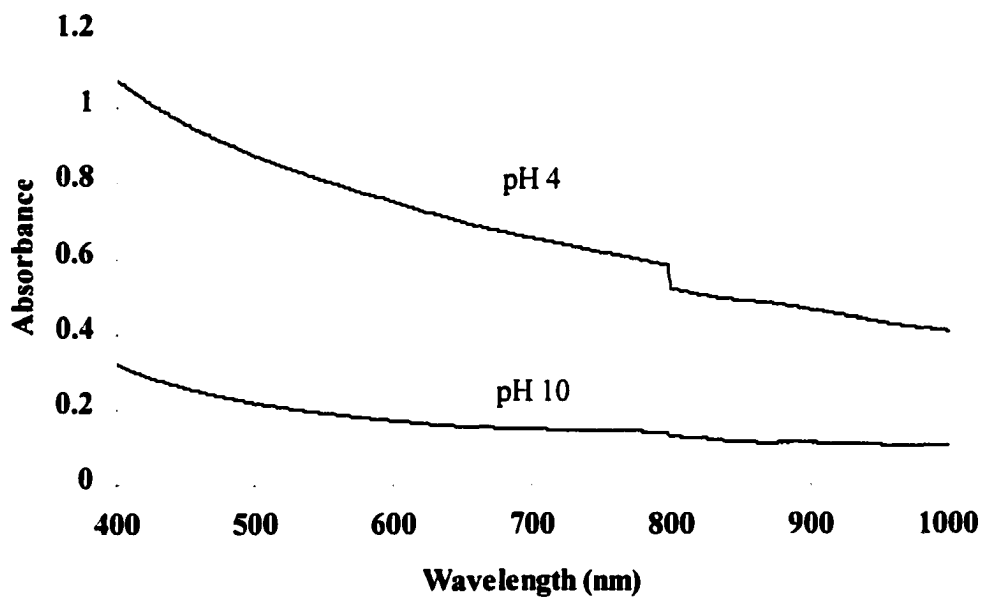


Figure VIII.8 Turbidity spectra of VBC/TCPA microspheres embedded in 76  $\mu\text{m}$  HPMA membrane. Microsphere concentration was 2 % (wt./wt.). Buffers prepared with 0.1 M buffer capacity and 0.1 M ionic strength.

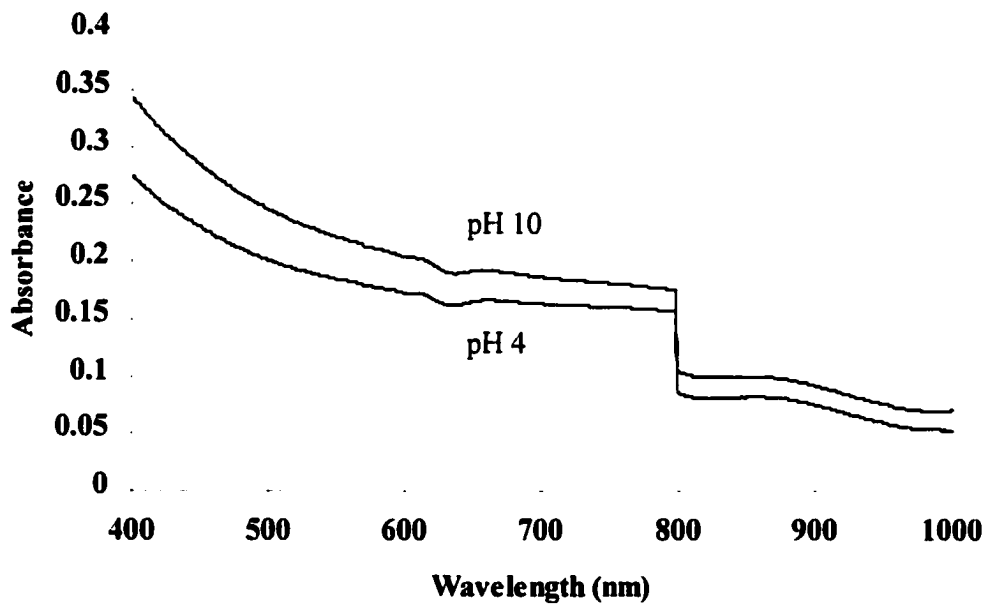


Figure VIII.9 Turbidity spectra of VBC/TCPA microspheres embedded in 76  $\mu\text{m}$  HEMA membrane. Microsphere concentration was 2 % (wt./wt.). Buffers prepared with 0.1 M buffer capacity and 0.1 M ionic strength.

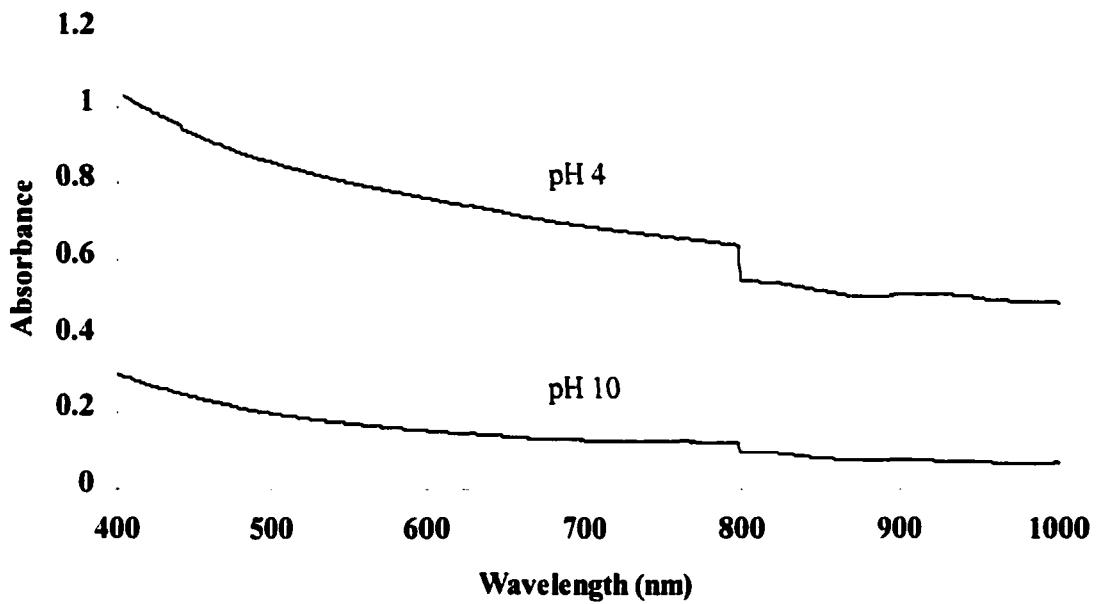


Figure VIII.10 Turbidity spectra of VBC/TCPA microspheres embedded in 76  $\mu\text{m}$  HPA membrane. Microsphere concentration was 2 % (wt./wt.). Buffers prepared with 0.1 M buffer capacity and 0.1 M ionic strength.

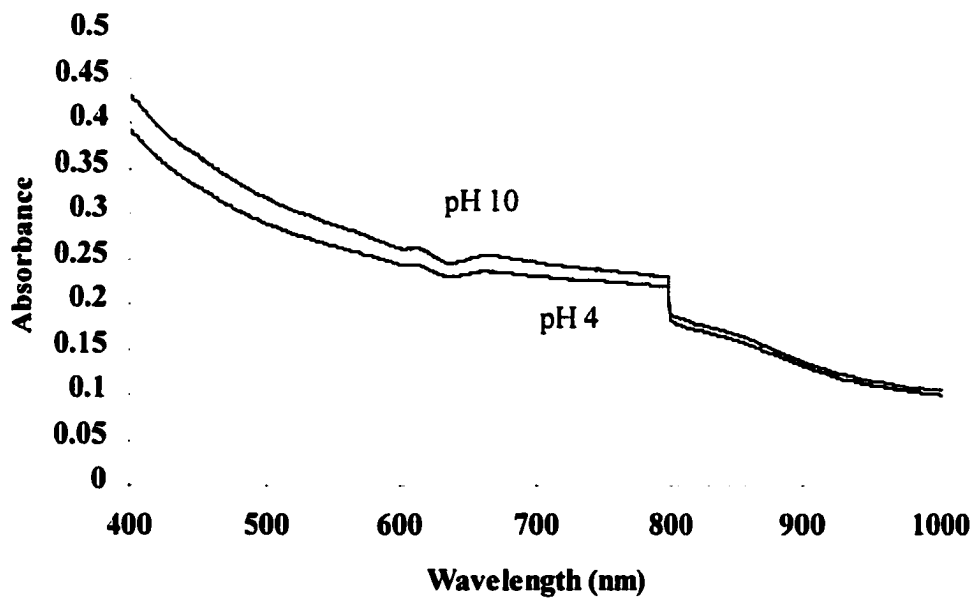


Figure VIII.11 Turbidity spectra of VBC/TCPA microspheres embedded in 76  $\mu\text{m}$  HEA membrane. Microsphere concentration was 2 % (wt./wt.). Buffers prepared with 0.1 M buffer capacity and 0.1 M ionic strength.

1.2. This is much smaller than the expected reflectance of 8.8, based on the refractive indices of the materials.

### **VIII.3.2.3 Use of HPA Hydrogel**

The HPA membrane was slightly more hydrophilic, with a percent hydration of 51.3 %. The refractive index of the membrane based on group contributions is the same as that for HEMA, 1.50. Corrected for hydration, the refractive index is 1.41, compared to 1.44 for the HEMA membrane. This shows the effect that hydration level has on the refractive index. A 15 % increase in hydration decreases the refractive index by 0.03. Unlike the previous systems, the refractive index of the membrane is below that of the microspheres in both pH 4 and pH 10 buffer. This would predict that the scattering would be greater in pH 10, then in pH 4. However, the turbidity spectra in Figure VIII.10 show the opposite results. The scattering is larger in pH 4, then in pH 10. Analysis of the difference between the refractive indices of the microspheres with that of the membrane confirms that the difference is larger in pH 10 than in pH 4, 0.06 and 0.02 respectively. This should provide a larger signal in pH 10 than pH 4. The reason for the discrepancy is not understood. The calculated reflectance based on the refractive indices of the materials was 8.8.

### **VIII.3.2.2 Use of HEA Hydrogel**

HEA was the most hydrophilic of the hydrogels examined for use in optical sensing. The membrane was found to contain 66 % water at equilibrium. Using group contributions the refractive index was calculated to be 1.51. When adjusted for hydration, the refractive index drops to 1.39. Figure VIII.11 shows the turbidity spectra for the HEA membrane with VBC/TCPA microspheres. As with the HPA membrane, in

this system the refractive index of the membrane was below that of the swollen and unswollen microspheres. The small difference is apparent in the figure. The high hydrophilicity of the membrane causes it to swell greatly in water. This may cause the apparent concentration of microspheres to decrease, which would lower the observed signal. In addition, it is hypothesized that the HEA monomer solution enters the microsphere and then polymerizes within the microsphere. This would cause the microsphere to be closer to that of the bulk hydrogel and would result in a smaller refractive index difference between the swollen and unswollen microspheres. It had been expected that this membrane would yield the largest signal, based on hydrophilicity and its effect on the refractive index. The results show this membrane to have the smallest response of the hydrogels. Despite these results being the opposite of what had been expected, the results are consistent with the results observed in the past.<sup>31,37</sup>

#### **VIII.3.2.5 Response Time of Hydrogels**

The response times of the different hydrogels with VBC/TCPA microspheres were also examined. It was anticipated that a more hydrophilic membrane would have a faster response. A more hydrophilic membrane holds more solution, enabling the analyte to diffuse more rapidly throughout the membrane. All membranes used were 76  $\mu\text{m}$  thick, with 1.5 % EGDM cross-linker and 2 % microspheres. Measurements were made in buffer solution prepared with a buffer capacity of 0.1 M and an ionic strength of 0.1 M. The average response times are shown in Table VIII.4. The HEA membrane was not examined, since the observed response was so small, section VIII.3.2.4.

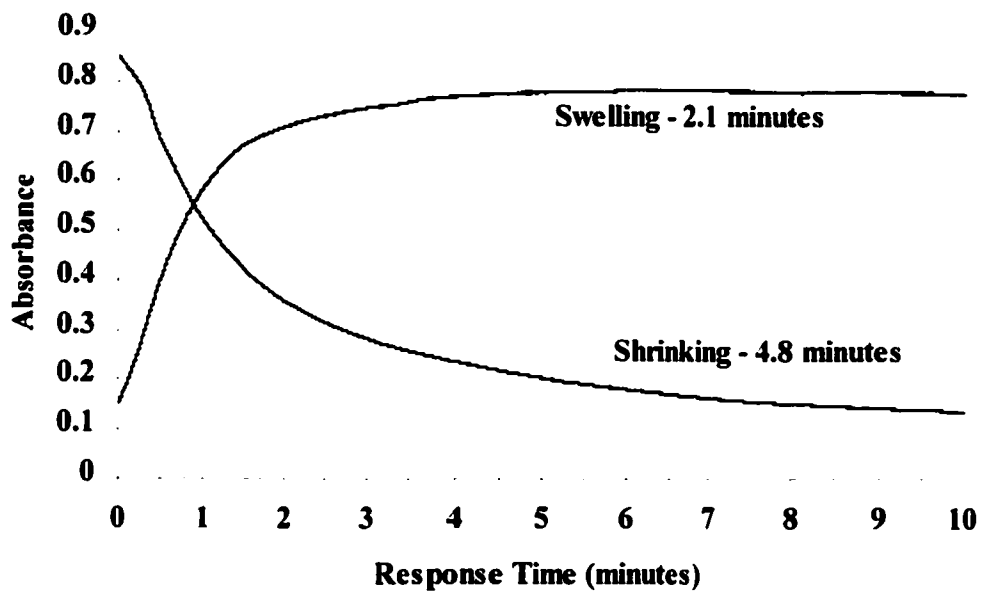


Figure VIII.12 Response time of a 76  $\mu\text{m}$  HPMA membrane embedded with VBC/TCPA microspheres. Microsphere concentration was 2 % (wt./wt.). Buffers prepared with 0.1 M buffer capacity and 0.1 M ionic strength.

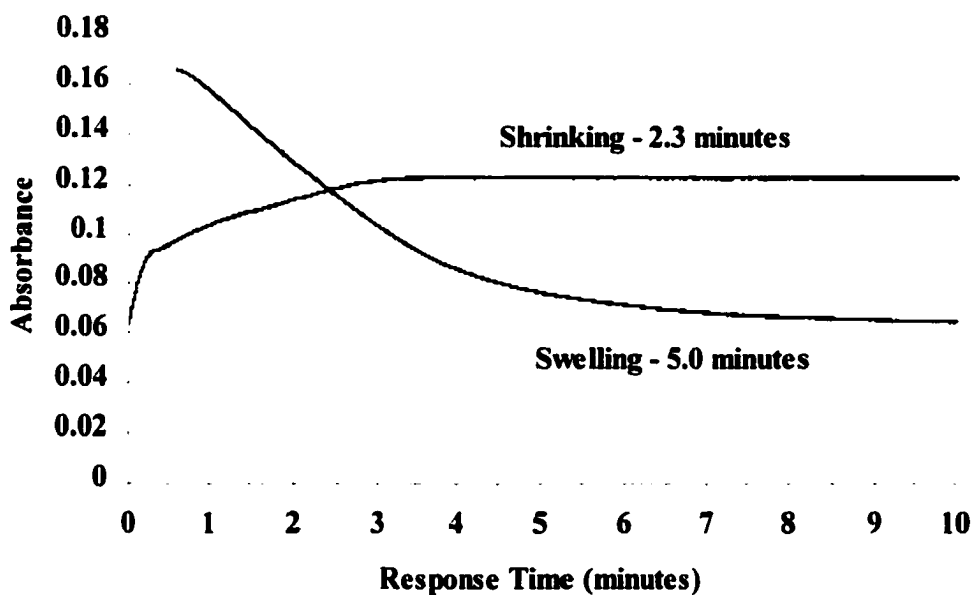


Figure VIII.13 Response time of a 76  $\mu\text{m}$  HEMA membrane embedded with VBC/TCPA microspheres. Microsphere concentration was 2% (wt./wt.). Buffers prepared with 0.1 M buffer capacity and 0.1 M ionic strength.



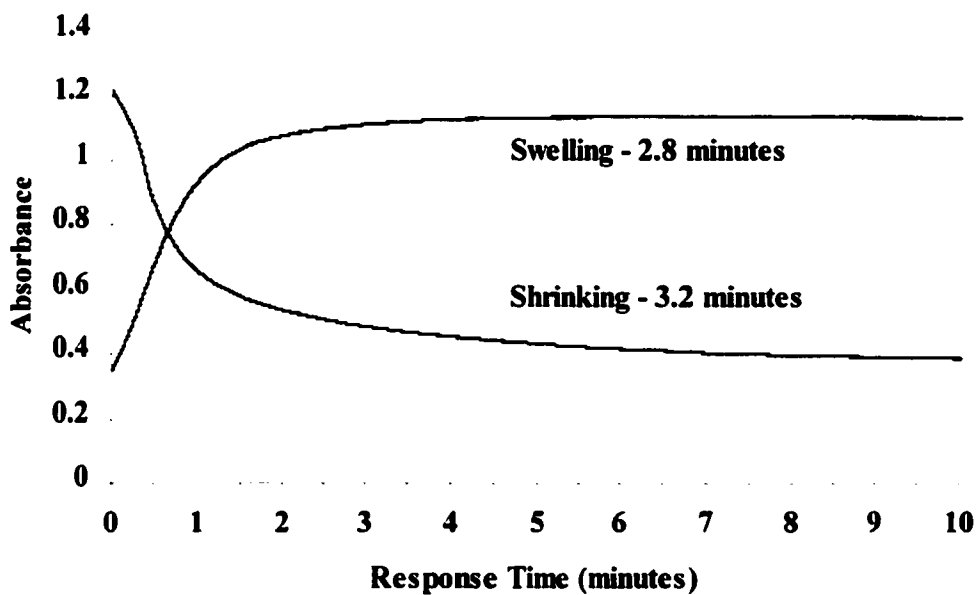


Figure VIII.14 Response time of a 76  $\mu\text{m}$  HPA membrane embedded with VBC/TCPA microspheres. Microsphere concentration was 2 % (wt./wt.). Buffers prepared with 0.1 M buffer capacity and 0.1 M ionic strength.

Table VIII.4. Response times and hydration levels of hydrogel membranes.

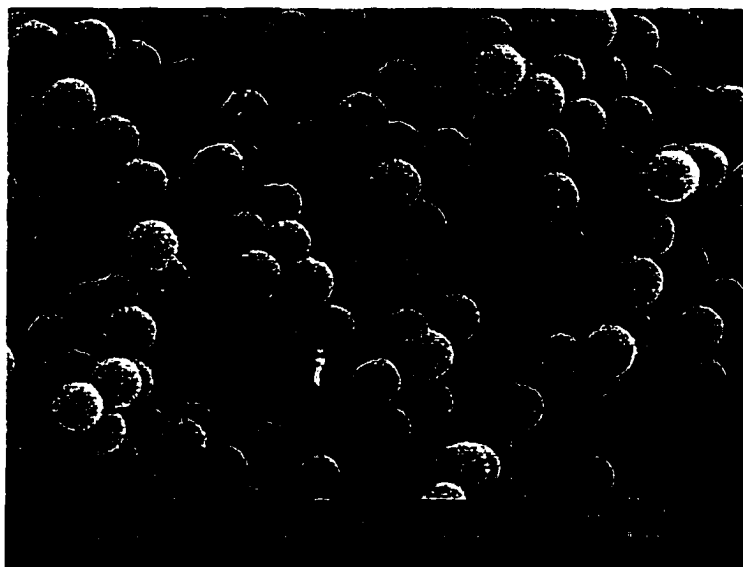
Hydrogel	Water Concentration of Hydrated Membrane (wt./wt. %)	Response Time Swelling (minutes)	Response Time Shrinking (minutes)
HPMA	23.1	2.1	4.8
HEMA	35.9	5.0	2.3
HPA	51.3	2.8	3.2

Response times for the membranes are shown in Figures VIII.12 to VIII.14.

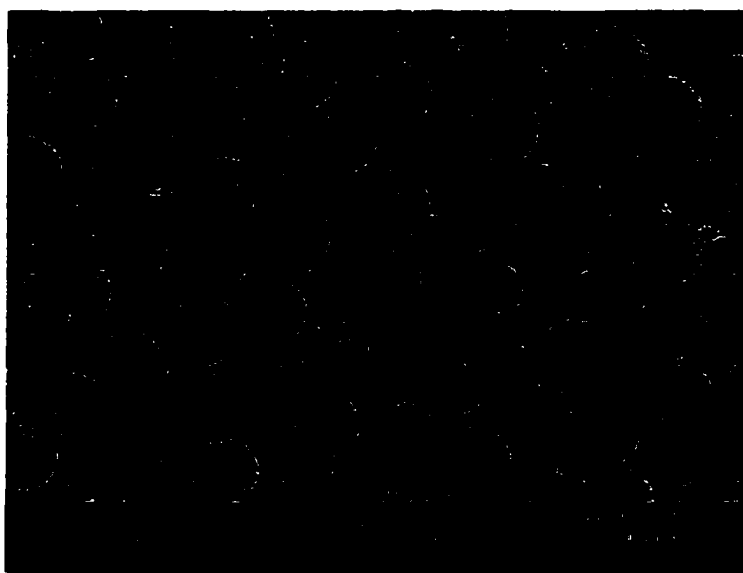
There is not a large correlation between the response time of the membrane and hydrophilicity of the membranes examined. All membranes have response times that average just over 3 minutes. There is a trend of decreasing response time with increasing hydration levels during the shrinking process. The swelling process shows no trend in response time. These results suggest that the response time is dependent upon the ability of the analyte to enter the microsphere and not the permeability of the membrane. The water content of the membrane doubles from 23 % in HPMA to 51 % in HPA. It is possible that this is not enough of a difference in hydrophilicities to be significant.

### **VIII.3.3 Conclusions**

The use of alternative hydrogels has been examined. The hydrogels of HPMA, HEMA, HPA and HEA, were all shown to be useable as the immobilizing matrix for the microspheres. Several surprising results were obtained. The first was that scattering was greater at pH 4 than at pH 10 with the HPA membrane. The similar opposite effect was observed with HPMA but this can be explained based on reflectance calculations. Also surprising was that the magnitude of the signal and the response times did not correlate as closely to hydration level of the hydrogel as had been anticipated. Despite these unexpected results, the study did successfully show that a number of hydrogels could be used to immobilize the microspheres.



a) poly-(VBC) seed particles



b) poly-(VBC) seeded particles

**Figure VIII.15** Scanning electron micrographs of a) poly-(VBC) seed particles, prepared by dispersion polymerization, and b) poly-(VBC) seeded particles prepared by seeded emulsion polymerization

## **VIII.4 Reproducibility and Stability of poly-(VBC) Microspheres Prepared by Seeded Emulsion Polymerization Immobilized in a HEMA Membrane**

### **VIII.4.1 Introduction**

Miele described the first use of seeded microspheres for optical sensing in our research group.<sup>31</sup> The use of particles prepared by this method has two distinct advantages compared to particles prepared by dispersion polymerization. The first is that larger particles can be prepared. This allows the particles to be used at NIR wavelengths with minimal signal loss. The second is that it is possible to incorporate porosity into microspheres prepared by this technique, which allows for more rapid response and a larger signal.

These seeded microspheres were prepared using a two step technique. The first step is the production of uniform seed particles. These particles were prepared by the dispersion polymerization of VBC. The seeds are then placed in an aqueous solution with additional monomer, cross-linker and porogenic solvent that had been prepared as an emulsified suspension. The mixture was then polymerized to produce the seeded particles. The procedure for this is described in section III.3.7. The seed particles were approximately 0.8  $\mu\text{m}$  and the final particles produced were about 1.3  $\mu\text{m}$ . SEM micrographs of the seed microspheres and the final seeded microspheres are shown in Figure VIII.15.

This section examines the characteristics of microspheres prepared by seeded emulsion polymerization for optical chemical sensing. The first factor examined was the reproducibility of response within a membrane and between different membranes of the same formulation. The second factor was the reproducibility of the sensor as it was

cycled between pH 4 and pH 10. The final factor was the stability of the response with time when the membrane was exposed to light or heat.

#### **VIII.4.2 Reproducibility of Membrane Response**

The first factor examined was the reproducibility of the membrane response. This was evaluated by measuring the response of the membrane in pH 4 and pH 10. Three membranes were utilized, so the between membrane reproducibility of the response could be evaluated. Each membrane was divided into three pieces and the response of each piece was monitored to determine the reproducibility within each membrane. The response of each membrane is shown in Figure VIII.16. For each membrane, the responses of each section are grouped with the responses for other sections in the same buffer solution. The responses for each section in pH 4 are grouped together, as are the response for each section when in pH 10. This grouping is especially evident in the response for membrane 1. The standard deviation between different sections of membrane 1 was 0.04 at pH 4 and 0.03 at pH 10. This corresponds to a relative standard deviation of 6.8 % for pH 4 and 3.8 % for pH 10 measurements. In both membrane 2 and membrane 3 there is a single high point at pH 4 and pH 10. In each case this corresponds to the response of a single section. The high signal is possibly the result of a slightly higher bead concentration in that region. Despite the slightly high values the within membrane variation is still very low. In membrane 2 the relative standard deviation was 4.1 % at pH 4 and 5.0 % at pH 10. In membrane 3 the RSD was 9.7 % in pH 4 and 6.9 % in pH 10. This indicates good grouping of the responses of each section within the membranes. The good correlation is the result of the membranes being mostly homogenous in terms of microsphere concentration.

Figure VIII.17 shows the absorbance difference between pH 4 and pH 10 for each membrane. The absorbance difference is quite good. The between membrane RSD was 1.5 %. The within membrane RSDs were 11 %, 7.5 % and 6.7 % for membranes 1 through 3 respectively. The between membrane variation is better than the within membrane. This is in agreement with the results obtained when the absorbance of each membrane in either pH 4 or pH 10 was examined.

The between membrane reproducibility examined the ability to fabricate multiple membranes and obtain consistent results between the different membranes. Three membranes were fabricated using the same hydrogel monomer and microsphere mixture. The between membrane results provided a relative standard deviation of 3.7 % in pH 4 buffer and 2.8 % at pH 10. These results are comparable with the within membrane variations, which averaged around 4 %. The difference between different membranes is mostly likely the result of the microspheres not being completely homogenous in the monomer/microsphere solution. As mentioned for the within membrane variation, this will cause certain membranes to have a slightly higher or lower bead concentration and a slightly higher or lower response.

#### **VIII.4.3 Response Reproducibility with Cycling**

An important consideration in sensor response is the ability of the sensor to respond reproducibly over a period of time with use. To investigate the ability of the sensor to make reproducible measurements, the sensor was cycled between pH 4 and pH 10 to examine the effect on response. In order for consistent readings to be obtained, the microspheres will have to swell and shrink by the same amount in each cycle. The first experiment to examine this involved cycling the sensor between pH 4 and pH 10 and

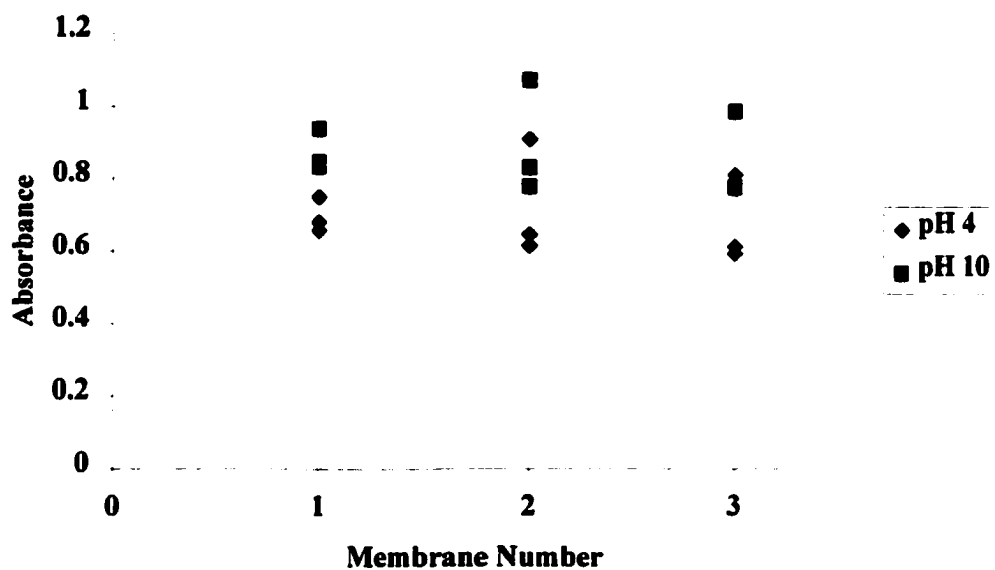


Figure VIII.16. Response reproducibility within and between membranes in pH 4 and pH 10 buffer solutions. The membranes are 1.5 % by weight seeded microspheres in HEMA. Buffer capacity was 0.1 M and buffer ionic strength was 0.1 M.



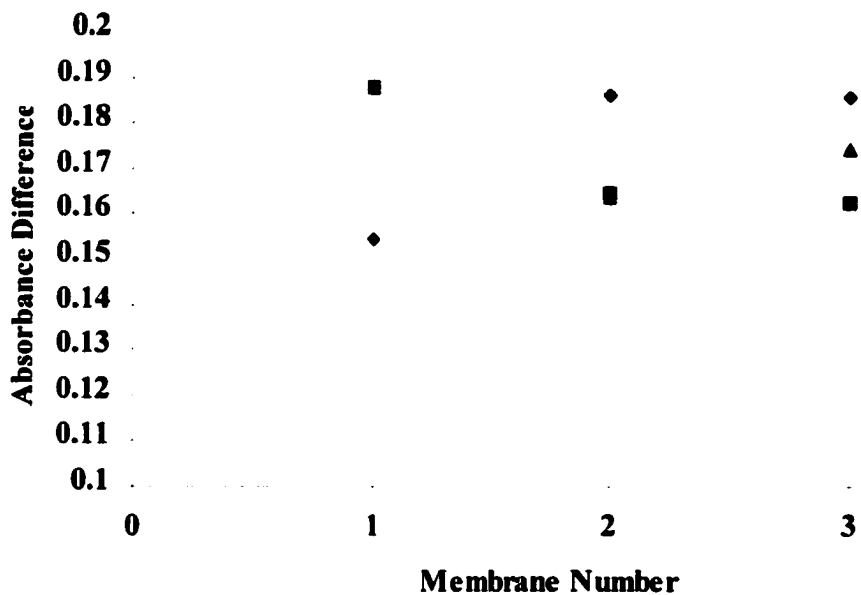


Figure VIII.17 Reproducibility of absorbance difference within and between membranes. Absorbance difference is between membranes in pH 4 and pH 10 buffer solutions. The membranes are 1.5 % by weight seeded microspheres in HEMA. Buffer capacity was 0.1 M and buffer ionic strength was 0.01 M. There are two points at an absorbance difference of 0.19 for membrane 1 and 0.16 for membrane 2.

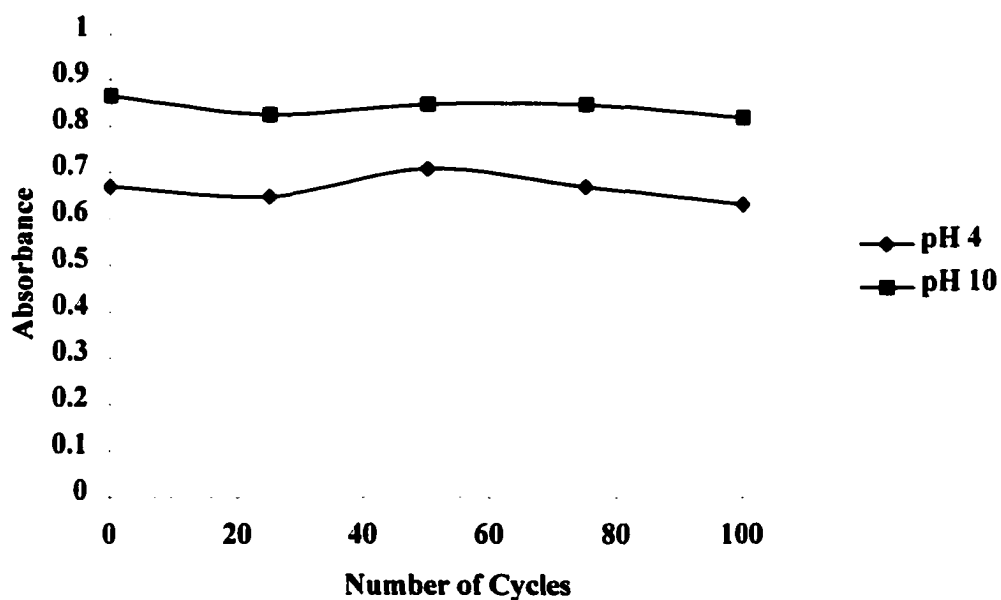


Figure VIII.18 Reproducibility of sensor response as membrane is cycled between pH 4 and pH 10. The concentration of seeded microspheres was 1.5 % in HEMA. Buffer capacity was 0.1 M and ionic strength was 0.1 M.

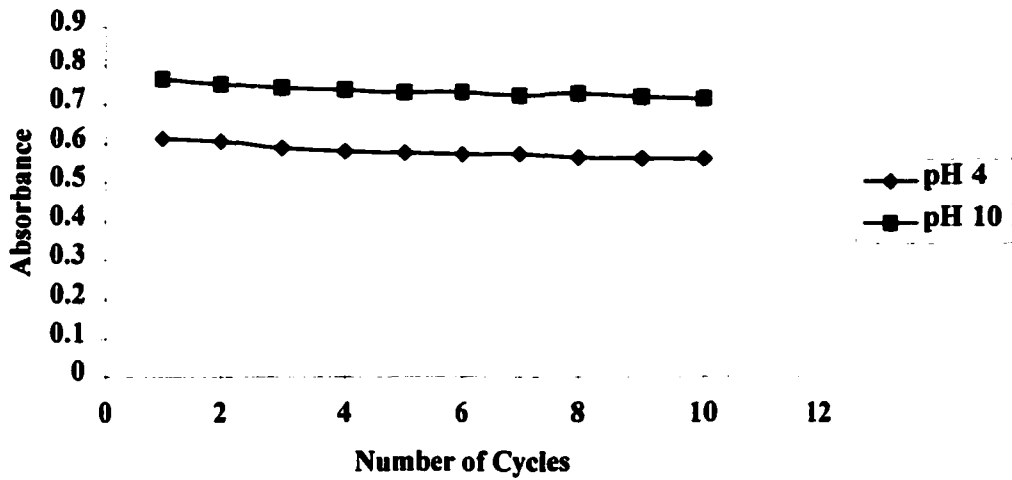


Figure VIII.19 Reproducibility of response as membrane is cycled between pH 4 and pH 10. Membrane remained in sample cuvette during cycling. The concentration of seeded microspheres was 1.5 % by weight in HEMA.

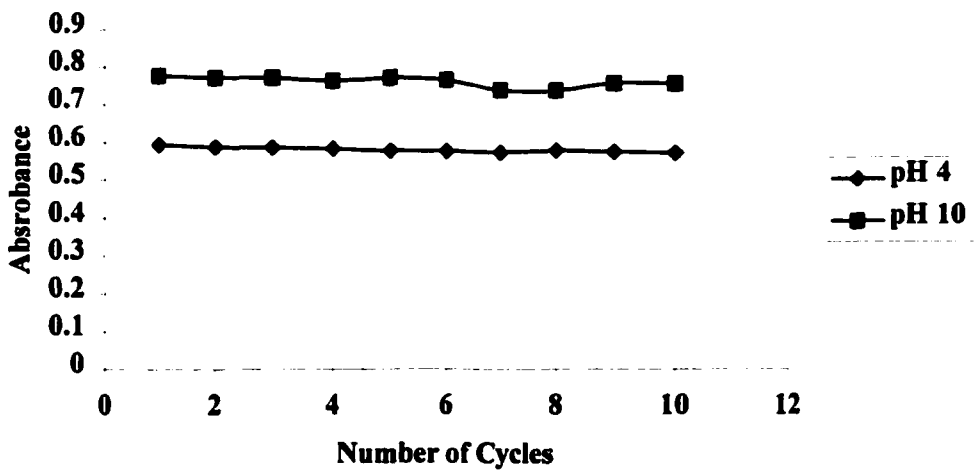


Figure VIII.20 Reproducibility of response as membrane is cycled between pH 4 and pH 10. Membrane was removed from sample cuvette during cycling. The concentration of seeded microspheres was 1.5 % by weight in HEMA

periodically measuring the response.

Figure VIII.18 shows the turbidity of a sensor that was cycled between pH 4 and pH 10 for 100 cycles. The turbidity at high and low pH was measured during the first cycle and during cycles 25, 50, 75 and 100. As the figure shows, there is good reproducibility between the responses in each pH. The only large deviation is at cycle 50, when the pH 4 response is slightly larger than expected. The relative standard deviations for the response were 4.3 % and 2.3 % for pH 4 and pH 10 respectively. This shows that there is good agreement between the responses, and the microspheres can undergo a number of cycles with no degradation in response.

The second experiment to examine the reproducibility of the response was to observe the effect of how the cycling was carried out. The experiments described here were carried out in a Cary 5 UV/Vis spectrophotometer. The cycling of the sensor can be carried out by two methods. The first is to remove the membrane in the membrane holder from the sample cuvette, remove the cuvette and dispose of the buffer solution, fill the cuvette with new buffer solution and replace the cuvette and membrane holder into the spectrophotometer. The second is to use a pipette to remove the buffer solution from the cuvette and replace it with new buffer solution using a second pipette. Using the method of removing the membrane from the cuvette presents the problem of repeatedly replacing the membrane back into the cuvette so that the light path through the membrane is identical each time. The same problem is present when the membrane is not removed from the cell, except in this instance the membrane holder may be moved out of place by the insertion of the pipette. Both methods were observed to determine the effect that the method used for cycling would have on response.

The results of this experiment are presented in Figure VIII.19, membrane remained in cuvette during cycling, and in Figure VIII.20, the membrane was removed during cycling. Both figures show the response to be essentially constant in each pH solution, regardless of the method used. The relative standard deviation for the response when the membrane was removed was 1.2 % in pH 4 and 1.9 % in pH 10. When the sample remained in the cuvette the relative standard deviation was 3.1 % for pH 4 and 2.1 % for pH 10. The low relative standard deviations indicate that each method provided a reproducible response to each pH solution. In addition, the low RSDs in each case shows good agreement between the two methods. The results are also consistent with the RSDs for the sample when cycled for long periods. This shows that the sensor response is constant with use and is not dependent upon the method of cycling used.

#### **VIII.4.4 Stability of Sensor in Response to Heat and Light Exposure**

The final test of stability was to examine the effect of prolonged exposure to heat and light on the sensor response. The stability with heat is important since the polymer could degrade with time due to thermal degradation. The sensor should be able to give a constant signal with time and provide a reproducible response when cycled. To examine this two membranes were used; one was placed in pH 4 and the other in pH 10. The membranes, in membrane holders, were stored in the buffer solutions in a sealed container in an 80 °C oven. The membranes were periodically removed and scanned to determine the response. The results of this are shown in Figure VIII.21.

The data shows good agreement between pH 4 and pH 10, with the difference between them remaining fairly constant. Both response have the same general trend of decreasing early in the experiment from 0 to 10 days, then increasing and leveling off at

15 days. The relative standard deviation of the results is slightly larger when compared to the cycling and reproducibility data. For pH 4 the RSD is 11.1 % and 6.5 % for pH 10. However, if the results only from day 10 through 42 are examined, the RSD's drop to 2.2 % for pH 4 and 2.9 % for pH 10. The variation is larger if the membrane is in the swollen state over the course of the entire experiment. When the results from the last 32 days are examined, the variation is independent of the state of the microspheres. This shows that the initial change in response occurs early in the experiment. During this time it was observed that the membrane developed a slight brown color. It is believed that this is the result of a process in the HEMA membrane, not with the pH sensitive microspheres. When left for several days at elevated temperature, the same effect was noticed in a HEMA membrane without microspheres. The leveling of the response at a constant value after 10 days suggests that the process that causes the color change occurs only during the first several days.

The ability of the membrane to reproducibly cycle between pH 4 and pH 10 was also investigated. Given the change in the membrane that occurred with the discoloration during the first 10 days, it was anticipated that there would be a large degree of discontinuity between the results. This was not the case however, as shown by the results in Figure VIII.22. The agreement between pH 4 initially and after 42 days is excellent, with the spectra being identical. The results at pH 10 are not as consistent, but are still in good agreement. The day 42 results increase more sharply from 600 to 400 nm, but are still in agreement with the results from the initial scan.

The stability of a membrane with microspheres was also examined to determine the effect of light exposure on the response. This was investigated by placing a

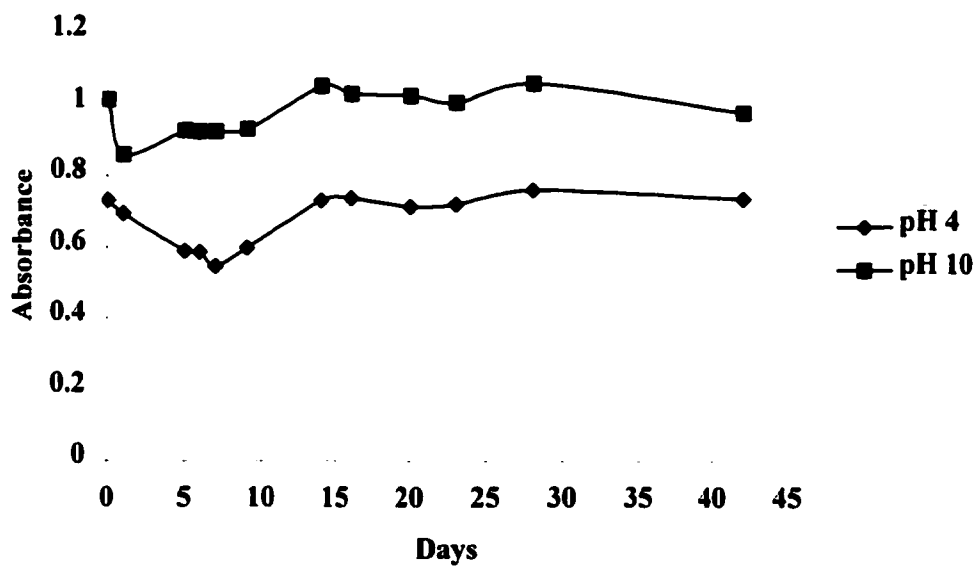


Figure VIII.21 Response of membrane stored in buffer solutions at 80 °C.  
 The concentration of seeded microspheres was 1.5 % in HEMA.  
 Buffer capacity was 0.1 M and ionic strength was 0.1 M.

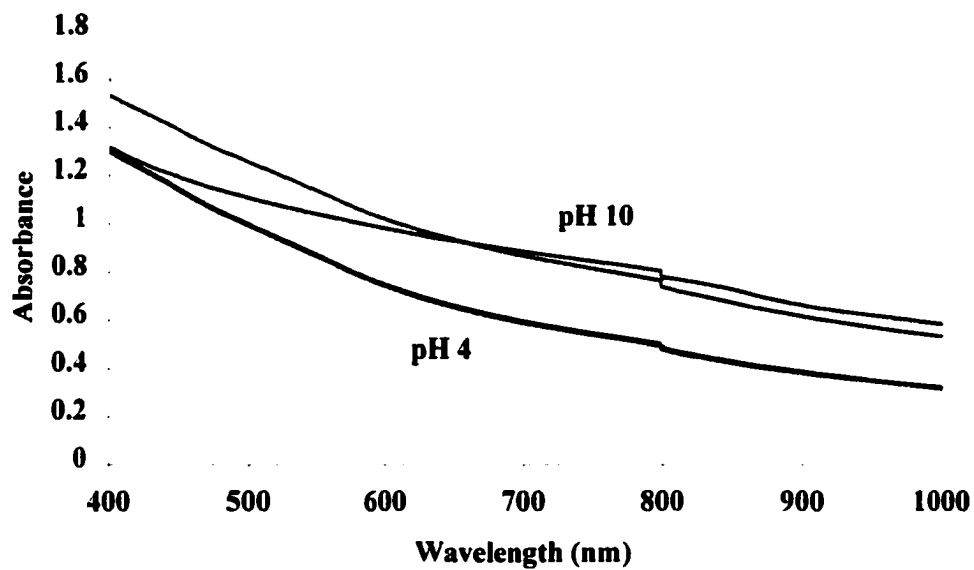


Figure VIII.22 Response of membrane cycled from pH 4 to pH 10 before and after storage for 42 days in 80 °C oven. Microsphere concentration was 1.5 % in HEMA membrane. Buffer capacity was 0.1 M and ionic strength was 0.1 M.



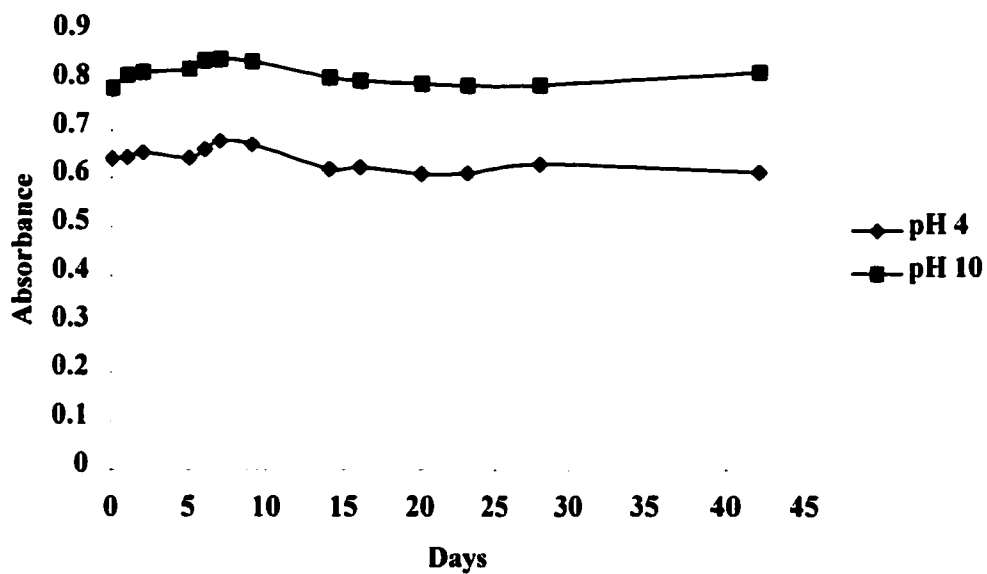


Figure VIII.23 Response of membrane stored in buffer solutions in light.  
 The concentration of seeded microspheres was 1.5 % in HEMA.  
 Buffer capacity was 0.1 M and ionic strength was 0.1 M.

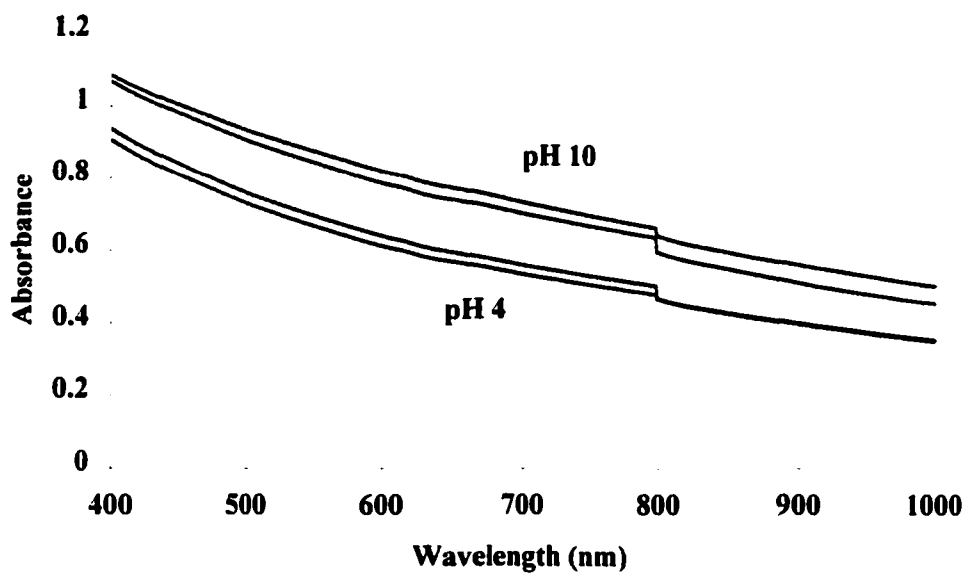


Figure VIII.24 Response of membrane cycled from pH 4 to pH 10 before and after 42 days of storage in light. Microsphere concentration was 1.5 % in HEMA membrane. Buffer capacity was 0.1 M and ionic strength was 0.1 M.

membrane in pH 4 and pH 10 buffer and exposing the membranes to sunlight for a period of time. The membranes were periodically scanned to measure the response in each buffer solution. Photobleaching is a problem with many indicators and occurs as the structure is altered due to exposure to light. The purpose of this experiment was to determine if this would happen with the microspheres. As with the thermal analysis, the ability of the sensor to respond reproducibly when cycled was examined before and after the exposure to light.

Figure VIII.23 presents the results of this experiment. The results show that there is very little variation in the response of each membrane. The relative standard deviations are 3.6 % and 2.5 % for pH 4 and pH 10 respectively. This indicates that the microspheres are not affected by exposure to light for a period of 42 days. The environment of the microspheres in terms of buffer solution does not have an effect on the stability of the response. As in the heat experiment, the largest degree of variation appears to occur during the first week of testing. Then the variation decreases and the response is constant. There was no observed change in the membrane appearance over the course of the experiment.

The response of the membrane as it was cycled between pH 4 and pH 10 was examined before and after light exposure for 42 days. The results of this are shown in Figure VIII.24. The pH 4 response before light exposure is the lower spectrum, while the pH 10 response before light exposure is the upper spectrum. The agreement between the scans before and after light exposure is very good. This indicates that there is little change in the membrane over the course of exposure and that the membrane is stable to light.

## VIII.5 Conclusions

This chapter examined the use of polymer microspheres in a number of optical sensing arrangements. Dispersion polymerization and seeded emulsion polymerization were both demonstrated as methods to produce microspheres suitable for optical sensing. Microspheres of VBC/TCPA were prepared by dispersion polymerization, while seeded emulsion polymerization was used to produce poly-(VBC) microspheres using VBC seed particles that had been prepared by dispersion polymerization. The use of hydrogels for immobilizing microspheres was also investigated.

The use of VBC/TCPA microspheres in PVA for optical sensing by SPR was demonstrated. The method of SPR sensing measures the refractive index of the material that the sensor is exposed to. SPR measurements are usually conducted with a solution, but the application demonstrated here showed the measurement of the refractive index of a hydrogel membrane. Limitations that were observed due to the effect of the buffer refractive index could be addressed by using a less hydrophilic hydrogel to immobilize the microspheres. This would allow the response to be determined only by the change in refractive index due to swelling/shrinking of the microspheres.

Alternative hydrogels were examined for use as the immobilizing matrix and were characterized by UV/Vis spectrophotometry. Hydrogels used for microsphere immobilization should be hydrophilic to allow for a rapid response. The results obtained for this study were somewhat surprising in that the expected signal magnitudes were reversed from what was expected, with the reflectance being higher in pH 4 and pH 10 when the hydroxypropyl membranes were used. The reason for this reversal was not determined for the hydroxypropyl acrylate membrane. The response magnitude did not

correlate with the hydrophilicity of the membrane as expected. Also unexpected was the lack of change in response time with membrane hydrophilicity. Despite these unexpected results, the HPA and HPMA hydrogels were found to be useful materials for immobilizing the microspheres for optical chemical sensing.

The reproducibility and the stability of microspheres prepared by seeded emulsion polymerization were also demonstrated. Microspheres prepared by this technique have several advantages over the VBC/TCPA microspheres. While maintaining the more rapid response time of the VBC/TCPA microspheres, the VBC particles prepared by this method have the potential to produce a larger signal, due to the greater difference in refractive indices between the swollen and unswollen state. The response of the sensor with use as it was cycled between pH 4 and pH 10 was found to be reproducible, as measured by a UV/Vis spectrophotometer. The ability to produce membranes of consistent quality was demonstrated. This indicates that response of one sensor would be comparable with another sensor. The degree of variation between membranes was found to be consistent with the variation between different regions within a single membrane. Response stability when the membrane is exposed to extreme conditions was also examined. The membrane was found to respond reproducibly, even after several weeks of exposure to light or high temperature with little effect on response. The effect of heat was found to be more significant than that of light, although it is believed that the source of variation is the result of changes in the hydrogel membrane, and not in the microspheres. The response of a membrane before and after exposure to heat or light showed that consistent results were obtained.

# CHAPTER IX

## Conclusions

The use of a variety of swellable polymers for chemical sensing and a variety of sensing mechanisms has been described. All of the sensing mechanisms described use a swellable polymer as the sensing layer. The polymer, either a hydrogel membrane or a polymer microsphere of VBC or VBC/TCPA, will swell in an acidic environment following protonation of an amine constituent group. This introduces a charge on the polymer backbone that causes swelling. The swelling of the polymer results in a property change, either magnetic or optical, that can be monitored and related to solution pH.

Swellable hydrogel membranes were prepared by the bulk polymerization of two hydrogels, one being DMAEMA, which contains an amine group which will become protonated at low pH. Hydrogels are well suited for sensing in aqueous solutions due to the high hydrophilicity, which makes the interior of the hydrogel easily accessible to the analyte. Membrane formulations were examined to determine the effect of various components on the size ratio. The hydrophilicity of the comonomer, cross-linker level, cross-linker type and DMAEMA concentration were all found to have a significant effect on the size ratio of the resulting membrane. A number of factorial experiments were conducted to study the various interactions of each factor. Factors that enhance the membranes ability to swell were seen to increase the size ratio. These factors included high DMAEMA concentrations, low cross-linker levels and longer chain length cross-

linkers. The hydrophilicity of the membrane produced an effect opposite of the effect predicted. The more hydrophilic membrane that was expected to swell more showed a smaller size ratio. This is believed to be the result of the membrane being more hydrated, and therefore larger, in the unswollen state, which results in a smaller size difference between the swollen and unswollen states.

A new type of chemical sensor was demonstrated. This new type of sensor is interrogated by the application of magnetic fields. The primary advantage to this type of sensor is that the sensor does not have to be physically connected or in a line of site with the detection system. This allows the sensor to be placed within closed and opaque containers and enables sensing to be carried out in hazardous environments that were previously inaccessible. This new type of chemical sensor demonstrated the ability to use swellable hydrogels for chemical sensing. The pH of solutions was monitored remotely using a variety of sensor designs constructed with a swellable hydrogel and a magnetic material. In addition, the use of a magnetoelastic sensor has been demonstrated as a means to monitor solution viscosity. The ability to monitor polymerizations as they proceed without the need to remove samples for analysis has also been demonstrated.

The use of polymer microspheres for a number of sensing applications was also investigated. The factors affecting the size and distribution of VBC/TCPA microspheres stabilized with PAA was examined for use with the magnetostatic coupled sensor. A factorial experiment determined that stabilizer concentration, monomer concentration and water concentration of the reaction mixture were all significant to the size of the particles produced. The concentration of water, which affects the solubility parameter of the

initial polymerization mixture, was found to have the most significant effect on particle size. Several systematic studies were also conducted to further investigate the effects.

The use of VBC/TCPA microspheres for optical chemical sensing was examined. Using UV/Vis spectrophotometry, the particles were used in the analysis of various hydrogels for microsphere immobilization. The effect of hydrophilicity of the hydrogel on response magnitude and response time was examined. Despite prediction, there was no clear correlation found between membrane response and hydrogel hydrophilicity. The ability to use the microspheres in a surface plasmon resonance sensor by measuring the refractive index change as the microsphere swell and shrink was demonstrated. This proved to be a viable method of monitoring pH, although the system used of VBC/TCPA microspheres in PVA suffered from buffer interference, due to the high hydrophilicity of the PVA. The use of a less hydrophilic membrane should eliminate this interference.

Microspheres prepared by seeded emulsion polymerization were also examined. The microspheres were prepared of VBC and were approximately double in size from the VBC/TCPA particles. The use of seeded emulsion polymerization allowed for the formation of pores in the microspheres, which allows for a more rapid response time. The reproducibility of membranes prepared using these microspheres, as well as the homogeneity of the membrane, was examined. It was found that membranes could be produced that had a high degree of homogeneity both within and between membranes. The stability of the measurements made of HEMA membranes with these particles was also examined. The stability was measured in terms of the number of swelling/shrinking cycles the particles can undergo, as well as the ability of the membranes to be stressed. The membranes were stressed by storing them in acidic or basic buffer for 42 days in



direct sunlight or at high temperature. In all cases the response was found to be reproducible. The largest variation was seen in the membranes that were heated, but it is believed that the variation in the response of membrane is not caused by changes to the microspheres, but by changes in the hydrogel membrane.

## Appendix A

### Calculation of theoretic values of carbon, hydrogen, and nitrogen

#### I. Hydrogels

##### A. Contribution of each component to the mass of C, H, N and O

###### 1. HEMA

1.00 g of HEMA composed of \* 55.38 % C = 0.5538 g C  
1.00 g of HEMA composed of \* 7.75 % H = 0.0775 g H  
1.00 g of HEMA composed of \* 36.88 % O = 0.3688 g O

###### 2. DMAEMA

1.00 g of DMAEMA composed of \* 61.12 %C = 0.6112 g C  
1.00 g of DMAEMA composed of \* 9.62 % H = 0.0962 g H  
1.00 g of DMAEMA composed of \* 20.35 %O = 0.2035 g O  
1.00 g of DMAEMA composed of \* 8.91 % N = 0.2035 g N

###### 3. EGDM

1.00 g of EGDM composed of \* 60.59 % C = 0.6059 g C  
1.00 g of EGDM composed of \* 7.12 % H = 0.0712 g H  
1.00 g of EGDM composed of \* 36.88 % O = 0.3688 g O

###### 4. TEGDM

1.00 g of TEGDM composed of \* 61.00 % C = 0.6059 g C  
1.00 g of TEGDM composed of \* 7.40 % H = 0.0712 g H  
1.00 g of TEGDM composed of \* 13.54 % O = 0.3688 g O

###### 5. HPA

1.00 g of HPA composed of \* 55.38 % C = 0.5538 g C  
1.00 g of HPA composed of \* 7.76 % H = 0.0776 g H  
1.00 g of HPA composed of \* 36.86 % O = 0.3686 g O

###### 6. HPMA

1.00 g of HPMA composed of \* 58.38 % C = 0.5832 g C  
1.00 g of HPMA composed of \* 8.41 % H = 0.0841 g H  
1.00 g of HPMA composed of \* 33.27 % O = 0.3327 g O

## B. Sample Calculation

Formulation contains 1.5 % EGDM and 10 % DMAEMA:

10 g HEMA  
1.34 g DMAEMA  
0.26 g EGDM

### 1. HEMA

10 g HEMA \* 0.5538 g C/g HEMA = 5.538 g C  
10 g HEMA \* 0.0775 g H/g HEMA = 0.775 g H  
10 g HEMA \* 0.3688 g O/g HEMA = 3.688 g O

### 2. DMAEMA

1.34 g DMAEMA \* 0.6112 g C/g HEMA = 0.820 g C  
1.34 g DMAEMA \* 0.0962 g H/g HEMA = 0.129 g H  
1.34 g DMAEMA \* 0.0891 g N/g HEMA = 0.1197 g N  
1.34 g DMAEMA \* 0.2035 g O/g HEMA = 0.273 g O

### 3. EGDM

0.258 g EGDM \* 0.6059 g C/g HEMA = 5.538 g C  
0.258 g EGDM \* 0.0712 g H/g HEMA = 0.775 g H  
0.258 g EGDM \* 0.3688 g O/g HEMA = 3.688 g O

### Totals:

6.516 g C  
0.923 g H  
0.1196 g N  
4.044 g O  
11.603 g Total

56.2 % Carbon  
7.96 % H  
1.03 % N

Note: Calculations based on assumption that components were pure.

## Appendix B

### Calculation of Refractive Index Using Group Contributions

The refractive index of a material can be calculated using group contributions.<sup>91</sup> The following equation is used to calculate the refractive index:

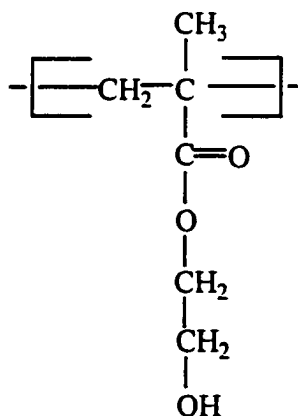
$$n = \sqrt{\frac{1 + 2 \frac{R_{LL}}{V}}{1 - \frac{R_{LL}}{V}}}$$

Where:

$R_{LL}$  = molar refraction  
 $V$  = molar volume at 298 K (cm<sup>3</sup>/mol)

#### I. Sample Calculations for Hydrogels

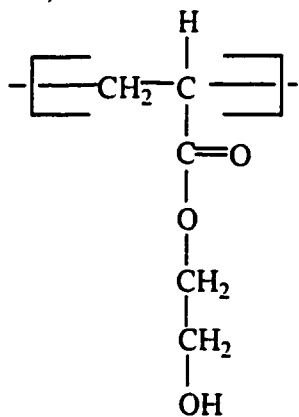
##### A. Poly(HEMA)



	Number	Group	R <sub>LL</sub>	V (298 K)
1.	3	-CH <sub>2</sub> -	4.65	16.37
2.	1	-CH <sub>3</sub> -	5.64	23
3.	1	-COO-	6.71	21
4.	1		2.58	5.32
		$\begin{array}{c}   \\ -C- \\   \end{array}$		
5.	1	-OH	2.45	8.0
Total			31.33	106.43

R<sub>LL</sub> is 31.33 and V is 106.43, therefore the calculated refractive index is 1.50.

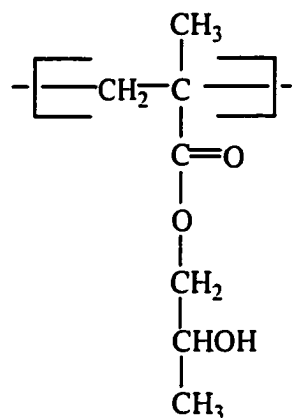
#### B. Poly(HEA)



	Number	Group	R <sub>LL</sub>	V (298 K)
1.	3	-CH <sub>2</sub> -	4.65	16.37
2.	1	-COO-	6.71	21
3.	1		3.62	10.8
		$\begin{array}{c}   \\ -\text{CH} \\   \end{array}$		
4.	1	-OH	2.45	8.0
Total			26.73	88.91

R<sub>LL</sub> is 26.73 and V is 88.91, therefore the calculated refractive index is 1.51.

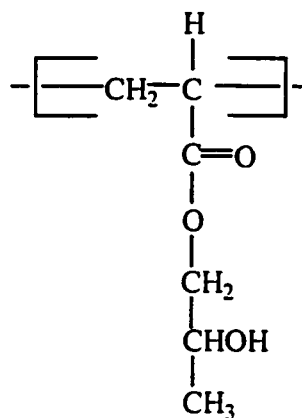
C. Poly(HPMA)



	Number	Group	$R_{LL}$	V (298 K)
1.	2	-CH <sub>2</sub> -	4.65	16.37
2.	2	-CH <sub>3</sub> -	5.64	23
4.	1		2.58	5.32
		$\begin{array}{c}   \\ \text{---C---} \\   \end{array}$		
2.	1	-COO-	6.71	21
3.	1		3.62	10.8
		$\begin{array}{c}   \\ \text{---CH} \\   \end{array}$		
5.	1	-OH	2.45	8.0
<b>Total</b>			<b>35.94</b>	<b>123.86</b>

$R_{LL}$  is 35.94 and V is 123.86, therefor the calculated refractive index is 1.49.

D. Poly(HPA)

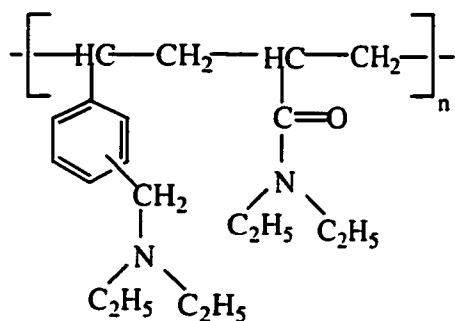


	Number	Group	R <sub>LL</sub>	V (298 K)
1.	2	-CH <sub>2</sub> -	4.65	16.37
2.	1	-CH <sub>3</sub>	5.64	23
3.	1	-COO-	6.71	21
4.	2		3.62	10.8
		$\begin{array}{c}   \\ \text{---} \text{CH} \\   \end{array}$		
5.	1	-OH	2.45	8.0
<b>Total</b>			<b>31.34</b>	<b>106.34</b>

R<sub>LL</sub> is 31.34 and V is 106.43, therefore the calculated refractive index is 1.50.

## II. Sample Calculations for Microspheres

### A. Diethylamine derivatized VBC/TCPA Particles

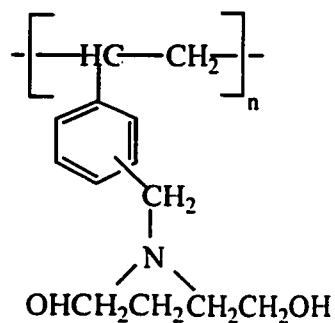


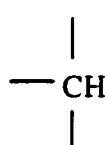
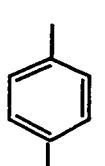
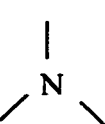
Number	Group	$R_{LL}$	V (298 K)	
1.	3	-CH <sub>2</sub> -	4.65	16.37
2.	2		3.62	10.8
3.	1	-CO-	4.53	11.7
4.	1		25.03	65.5
5.	2		2.8	4.33
7.	4	-CH <sub>2</sub> CH <sub>3</sub> -	4.53	11.7
Total			97.51	310.57

$R_{LL}$  is 97.51 and V is 310.57, therefor the calculated refractive index is 1.54.



B. Diethanolamine derivatized VBC Particles



	Number	Group	$R_{LL}$	V (298 K)
1.	6	-CH <sub>2</sub> -	4.65	16.37
2.	1		3.62	10.8
				
3.	2	-OH	4.9	16.0
				
4.	1		25.03	65.5
				
5.	1		2.8	4.33
<b>Total</b>			<b>64.25</b>	<b>194.85</b>

$R_{LL}$  is 64.25 and V is 194.85, therefore the calculated refractive index is 1.57.

## Appendix C

### Solubility Parameter Calculation

A materials solubility parameter can be calculated based on group contributions, in a fashion similar to the calculation for refractive index determination. The following equations can be used to determine the solubility parameter.<sup>91</sup>

$$\delta_d = \frac{\sum F di}{V} \quad \delta_d \text{ is the dispersion component}$$

$$\delta_p = \frac{\sqrt{\sum F^2 pi}}{V} \quad \delta_p \text{ is the polar component}$$

$$\delta_h = \frac{\sqrt{\sum E hi}}{V} \quad \delta_h \text{ is the hydrogen bonding component}$$

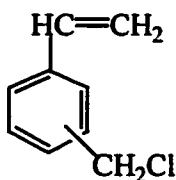
V is the molar volume

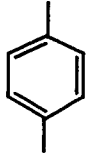
Using the above components the overall solubility parameter can be calculated by the following equation:

$$\delta = \sqrt{\delta_d^2 + \delta_p^2 + \delta_h^2}$$

#### I. Sample Calculations for Dispersion Monomers

##### A. VBC



Number	Group	$F_{di}$ ( $J^{1/2}/cm^{3/2}/mol$ )	$F_{pi}$ ( $J^{1/2}/cm^{3/2}/mol$ )	$E_{hi}$ ( $J/mol$ )	$V$ ( $ml/mol$ )
1) 1	=CH <sub>2</sub>	400	0	0	11.94
2) 1	=CH-	200	0	0	8.47
					
3) 1		1270	110	0	65.5
4) 1	-CH <sub>2</sub> -	270	0	0	16.37
5) 1	-Cl	450	550	400	16.37
Total		2590	660	400	120.7

$$\delta_d = 21.46$$

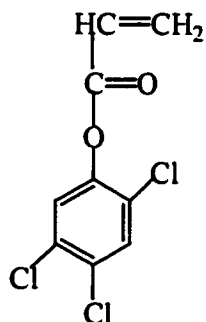
$$\delta_p = 4.65$$

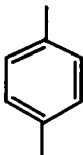
$$\delta_h = 1.82$$

$$\delta = 22.03 (J^{1/2}/cm^{3/2}) \text{ conversion into } (cal/cm^3)^{1/2}$$

$$\delta = 22.03 (J^{1/2}/cm^{3/2}) / 2.046 = 10.8 (cal/cm^3)^{1/2}$$

## B. TCPA



Number	Group	$F_{di}$ ( $J^{1/2}/cm^{3/2}/mol$ )	$F_{pi}$ ( $J^{1/2}/cm^{3/2}/mol$ )	$E_{hi}$ ( $J/mol$ )	$V$ ( $ml/mol$ )
1) 1	=CH <sub>2</sub>	400	0	0	11.94
2) 1	=CH-	200	0	0	8.47
					
3) 1		1270	110	0	65.5
4) 1	-CO <sub>2</sub>	390	490	7000	21
5) 3	-Cl	450	550	400	16.37
Total		3610	2250	8200	162.11

$$\delta_d = 22.27$$

$$\delta_p = 10.64$$

$$\delta_h = 7.11$$

$$\delta = 25.68 (J^{1/2}/cm^{3/2}) \text{ conversion into } (cal/cm^3)^{1/2}$$

$$\delta = 25.68 (J^{1/2}/cm^{3/2}) / 2.046 = 12.6 (cal/cm^3)^{1/2}$$

## II. Calculations of solubility parameter of VBC/TCPA in water ethanol medium

Solution was 2.5 % VBC, 2.5 % TCPA, 5 % water in ethanol

To calculate the solubility parameter of a mixture, the following equation is used:

$$\delta = \sqrt{\sum \phi_i \delta_i^2}$$

solubility parameters for polymerization components:

$$\begin{array}{ll} \text{VBC} & 10.8 (cal/cm^3)^{1/2} \\ \text{EtOH} & 12.7 (cal/cm^3)^{1/2} \end{array}$$

$$\begin{array}{ll} \text{TCPA} & 12.6 (cal/cm^3)^{1/2} \\ \text{Water} & 23.4 (cal/cm^3)^{1/2} \end{array}$$

$$\begin{aligned} \delta &= \sqrt{(0.025) * (10.8)^2 + (0.025) * (12.6)^2 + (.05) * (23.4)^2 + (.9) * (12.7)^2} \\ &= 13.4 (cal/cm^3)^{1/2} \end{aligned}$$

## References

1. Janata, J.; Josowicz, M.; Devany, D. M. *Anal. Chem.* **1998**, *70*, 179R.
2. Kroger, S.; Setford, S. J.; Turner, A. P. *Anal. Chem.* **1998**, *70*, 5047.
3. Cosofret, V.; Erdosy, M.; Johnson, T. A.; Buck, R. P.; Ash, R. B.; Neuman, M. R. *Anal. Chem.* **1995**, *67*, 1647.
4. Murry, R. W.; Dessy, R. E.; Heineman, W. R.; Janata, J.; Seitz, W. R.; Ed., Chemical Sensors and Microinstrumentation; American Chemical Society, Washington, D.C.: **1989**.
5. St. John, P.; Davis, R.; Cady, N.; Czajka, J.; Batt, C.; Craighead, H. *Anal. Chem.* **1998**, *70*, 1108.
6. Nagata, R.; Yokoyama, K.; Clarke, S. A.; Karube, I. *Biosens. Bioelectrons.* **1995**, *10*, 377.
7. Hart, A.L.; Turner, A.; Hopcroft, D. *Biosens. Bioelectrons.* **1996**, *11*, 263.
8. Kriz, D.; Ramstrom, O.; Svensson, A.; Masbach, K. *Anal. Chem.* **1995**, *67*, 2142.
9. Wu, O.; Lee, K.; Liu, C. *Sensors & Actuators B* **1993**, *13-14*, 1.
10. Liu, C.; Zhang, Z. *Selective Elect. Rev.* **1992**, *14*, 147.
11. Cosofret, V.; Linder, E.; Johnson, T. A.; Neuman, M. R.; *Talanta* **1994**, *41*, 931.
12. Janata, J.; Ed., Principles of Chemical Sensors; Plenum Press, New York: **1989**.
13. Grate, J.W.; Martin, S.; White, R. *Anal. Chem.* **1993**, *65*, 940A.
14. Hartevelde, J. L.; Nieuwenhuizen, M. S.; Wils, E. R. *Biosens. Bioelectrons.* **1997**, *12*, 661.
15. Suri, C. R.; Raje, M.; Mishra, G. *Biosens. Bioelectrons.* **1994**, *9*, 325.
16. Barko, G.; Papp, B.; Hlavay, J. *Talanta* **1995**, *42*, 475.
17. Peterson, J. L.; Goldstein, S. R.; Fitzferald, R. V.; Buckhold, D. K.; *Anal. Chem.* **1980**, *52*, 864.

18. Freeman, T. M.; Seitz, W. R.; *Anal. Chem.* **1978**, *50*, 1242.
19. Saari, L. A.; Seitz, W. R.; *Anal. Chem.* **1982**, *54*, 821.
20. Alder, J. F.; Ashworth, D. C.; Marayanaswamy, R.; Moss, R. E.; Sutherland, I. O. *Analyst* **1987**, *112*, 1191.
21. Kulp, T. J.; Camins, I.; Angel, S. M.; Munkholm, C.; Walt, D. R. *Anal. Chem.* **1987**, *59*, 2849.
22. Harris, R. D.; Luff, B. J.; Wilkinson, J. S.; Piehler, J.; Brecht, A.; Gauglitz, G.; Abuknesha, R.A.; *Biosens. Bioelectrons.* **1999**, *13*, 377.
23. Elkind, J. L.; Stimpson, D. I.; Strong, A.; Bartholomew, D.; Melendez, J. L. *Sensors & Actuators B* **1999**, *54*, 182.
24. Lysenko, V.; Delhomme, G.; Soldatkin, A.; Strikha, V.; Dittmar, A.; Jaffrezic-Renault, N.; Martelet, C.; *Talanta* **1996**, *43*, 1163.
25. Bjarnason, B.; Johansson, P.; Johansson, G.; *Anal. Chim. Acta* **1998**, *372*, 341.
26. Yamazoe, N.; Shimizu, Y. *Sensors & Actuators* **1986**, *10*, 379.
27. Grat, J. W.; Klusty, R.A.; McGill, R. A.; Abraham, M. H.; Whiting, G.; Andonian-Haftvan, J. *Anal. Chem.* **1992**, *64*, 610.
28. McCurley, M. F.; Seitz, W. R.; *Anal. Chim. Acta* **1991**, *249*, 373.
29. Conway, V. L.; Dissertation, University of New Hampshire, **1994**.
30. Rooney, M. T.; Dissertation, University of New Hampshire, **1996**.
31. Miele, E. W.; Dissertation, University of New Hampshire, **1999**.
32. Civiello, M. D.; Thesis, University of New Hampshire, **1997**.
33. Dow Chemical Company *Dow Technical Literature: VBC*. **1988**.
34. Pan, S.; Conway, V. L.; Shakhsher, Z.; Emerson, S.; Bia, M. Seitz, W. R.; Legg, K. D.; *Anal. Chim. Acta* **1993**, *279*, 195.
35. Conway, V. L.; Hassen, K. P.; Zhang, L.; Seitz, W. R.; Gross, T. S. *Sensors & Actuators B* **1997**, *45*, 1.
36. Shakhsher, Z.; Seitz, W. R.; Legg, K. D.; *Anal. Chem.* **1994**, *66*, 1731.

37. Kaval, N.; Thesis, University of New Hampshire, 1998.
38. Seymour, R. B.; Carraher, C. E. Polymer Chemistry, 2<sup>nd</sup> ed.; Marcel Dekker, New York: 1988.
39. Billmeyer, F. W. Textbook of Polymer Science, 3<sup>rd</sup> ed.; John Wiley & Sons, New York: 1984.
40. Barrett, K. E. J. Dispersion Polymerization in Organic Media; John Wiley & Sons, London: 1975.
41. Cawse, J. L. in Emulsion Polymerization and Emulsion Polymers; Lovell, P. A.; El-Aasser, M. S. ed. John Wiley & Sons, Chichester, England: 1997.
42. Ojima, M.; Shirasaki, F.; Kitamoto, Y.; Abe, M.; Nagahata, S. *IEEE Trans. Magn.* 1999, 35, 4118.
43. Mathiowitz, E.; Jacob, J.; Jong, Y.; Carino, G.; Chickering, D.; Chaturvedi, P.; Santos, C.; Vijayaraghaven, K.; Montgomery, S.; Bassett, M.; Morrel, C.; *Nature* 1997, 386, 410.
44. Lenzmann, F.; Li, K.; Kitai, A.; Stover, H. *Chem. Mat.* 1994, 6, 156.
45. Bangs, L. B. *Unifrom Latex Particles*, Seragen Diagnostics Inc, Indianapolis, IN, 1984.
46. Ugelstad, J.; Berge, A.; Ellingsen, T.; Schmid, R.; Nilsen, T.; Mork, P.; Stenstad, P.; Hornes, E.; Olsvik, O. *Prog. Poly. Sci.* 1992, 17, 87.
47. Ellingsen, T.; Aune, O.; Ugelstad, J.; Hagen, S. *J. Chrom.* 1990, 535, 147.
48. Wang, Q.; Hosoya, K.; Svec, F.; Frechet, J. *Anal. Chem.* 1992, 64, 1232.
49. Kulin, L.; Flodin, P.; Ellingsen, T.; Ugelstad, J. *J. Chrom.* 1990, 514, 1.
50. Hosoya, K.; Frechet, J. *J. Poly. Sci A: Poly. Chem.* 1993, 31, 2129.
51. Ogino, K.; Sato, H.; Tsuchiya, K.; Suzuki, H.; Moriguchi, S. *J. Chrom. A* 1995, 699, 59.
52. Wichterle, D.; Lim, D. *Nature* 1960, 185, 117.
53. Kudela, V. Hydrogels. Encyclopedia of Polymer Science and Engineering, 2<sup>nd</sup> ed; vol. 7, John Wiley & Sons, New Jersey: 1987, 783.
54. Davies, M. L.; Tighe, B. J. *Selective Electrode Review* 1991, 13, 159.

55. Hui, M.; Nagai, M.; Omi, S. *J. Appl. Poly. Sci.* **1997**, *66*, 1325.
56. Sugiyama, K.; Mitsuno, S.; Shiraishi, K. *J. Poly. Sci A: Poly. Chem.* **1997**, *35*, 3349.
57. Sheppard, N. F.; Lesho, M. J.; McNally, P.; Francomacaro, A. S. *Sensors & Actuators B*, **1995**, *28*, 95.
58. Watanabe, M.; Akahoshi, T.; Tabata, Y.; Nakayama, D. *J. Am. Chem. Soc.* **1998**, *120*, 5577.
59. Grimes, C. A.; Seitz, W. R.; Horn, J. L.; Doherty, S. A.; Rooney, M. T. *IEEE Trans. Magn.* **1997**, *33*, 3412.
60. Grimes, C. A.; Stoyanov, P.; Liu, Y.; Tong, C.; Ong, K.; Loiselle, K.; Seitz, W. R.; Doherty, S. A.; *J. Phys. D: Appl. Phys.* **1999**, *32*, 1329.
61. Wolfbeis, O. S. ed. Fiber Optic Chemical Sensors and Biosensors; Volume I. CRC Press, Boca Raton, FL: 1991.
62. Hecht, J. Understanding Fiber Optics 2<sup>nd</sup> ed.; Prentice Hall, New Jersey: **1993**.
63. Strobel, H.; Heineman, W. R. Chemical Instrumentation: A Systematic Approach; John Wiley & Sons, New York: 1989.
64. Homola, J.; Yee, S.; Gauglitz, G. *Sensors and Actuators B* **1999**, *54*, 3.
65. Flory, P. J. Principles of Polymer Science; Cornell University Press: Ithaca, NY, 1953.
66. Kun, K.; Kunin, R. *J. Poly. Sci. Part A* **1968**, *6*, 2689.
67. Millar, J.; Smith, D.; Kressman, T. R. *J. Chem. Soc.* **1965**, 304.
68. Millar, J.; Smith, D.; Marr, W.; Kressman, T. R. *J. Chem. Soc.* **1963**, 218.
69. Raether, R. Surface Plasmons on Smooth and Rough Surfaces and on Gratings; Springer-Verlag, Berlin, 1988.
70. Earp, R.; Dessy, R. in Commercial Biosensors: Applications to Clinical, Bioprocess, and Environmental Samples; Ramsay, G. ed, John Wiley & Son, New York, 1998.
71. Cepria, G.; Castillo, J. R. *J. Chrom. A*, **1997**, *759*, 27.
72. Liedberg, B.; Nylander, C.; Lundstrom, I. *Biosens. & Bioelect.* **1995**, *10*, i.



73. Miura, N.; Ogata, K.; Sakai, G.; Uda, T.; Yamazoe, N. *Chem. Lett.* **1997**, *8*, 713.
74. Severs, A.; Schasfoort, R.; Salden, M. *Biosens. & Bioelect.* **1993**, *8*, 185.
75. Berger, C.; Beumer, T.; Kooyman, R.; Greve, J. *Anal. Chem.* **1998**, *70*, 703
76. Abdelghani, A.; Chovelon, J.; Jaffrezic-Renault, N.; Veille, C.; Gagnaire, H. *Anal. Chim. Acta* **1997**, *337*, 225.
77. Woodbury, R.; Wendin, C.; Clendenning, J.; Melendex, J.; Elkind, J.; Bartholomew, D.; Brown, S.; Furlong, C. *Biosens. & Bioelect.* **1998**, *13*, 1117.
78. *TISPR-1 Experimenters Kit Operators Manual*. Texas Instruments, Dallas, Texas. 1996.
79. Halliday, D.; Resnick, R.; Walker, H. Fundamentals of Physics, 5<sup>th</sup> ed.; John Wiley & Sons: New York, 1997.
80. Grimes, C. Personal Communication, 1997.
81. Metglass is a trademark of Allied Signal Corporation.
82. Ryan, J. Jr. *Scientific American*, May 1997, 120.
83. Grate, J. W.; Martin, S. J.; White, R. M. *Anal. Chem.* **1993**, *65*, 940A.
84. Grate, J. W.; Martin, S. J.; White, R. M. *Anal. Chem.* **1993**, *65*, 987A.
85. Groves, W.; Zellers, E.; Frye, G. *Anal. Chim. Acta* **1998**, *371*, 131.
86. Suri, C. R.; Raje, M.; Mishra, G. *Biosens. & Bioelect.* **1994**, *9*, 325.
87. Grimes, C.; Ong, K.; Loisell, K.; Stoyanov, P.; Kouzoudis, D.; Liu, Y.; Tong, C.; Tefiku, F. *Smart Mater. Struct.* **1999**, *8*, 639.
88. Stoyanov, P.; Grimes, C.; Ong, K.; Kouzoudis, D. submitted to IEEE Trans. Mag.
89. Grimes, C.; Ong, K.; Stoyanov, P. submitted to Sensors & Actuators
90. Batz, H.G.; Franzman, G.F.; Ringsdorf, H. *Angew. Chem.(Int. Ed.)* **1972**, *11*, 1003.
91. Van Krevelen, D. W. Properties of Polymers; Elsevier Science B. V. Amsterdam, 1990.
92. Huang, C.; Sun, Y.; Huang, W. *J. Polym. Sci. Part A: Polym. Chem.* **1997**, *35*, 1873.

93. Texas Instruments Inc. *Application Brief Number 003, Spreeta: Renewing the Spreeta Surface with Disposable Gold-Coated Glass Slides*. 1998.
94. Dubendorfer, J.; Kunz, R.; Jobst, G.; Moser, I.; Urban, G. *Sensors & Actuators B* **1998**, *50*, 210.
95. Clayton, A.; Chirial, T.; Lou, X. *Polymer International* **1997**, *44*, 201.
96. Tur'yan, Y.; Dokolina, G.; Korshunov, M. *J. Gen. Chem. (USSR)* **1970**, *40*, 1874.
97. Frey, B; Jordan, C.; Kornguth, S.; Corn, R. M. *Anal. Chem.* **1995**, *67*, 4452.
98. Corner, T. *Colloids and Surfaces* **1981**, *3*, 119.
99. Buscall, R.; Corner, T. *Colloids and Surfaces* **1982**, *5*, 333.
100. Tuncel, R.; Kahraman, R.; Piskin, E. *J. Appl. Poly. Sci.* **1993**, *50*, 303.
101. Almog, Y.; Levy, M. *J. Poly. Sci.:Poly. Chem.* **1982**, *20*, 417.
102. Pan, S.; Conway, V.; Shakhsher, Z.; Emerson, S.; Bai, M.; Seitz, W. R.; Legg, K. *Anal. Chim. Acta* **1993**, *279*, 195.
103. Ponnuswamy, S.; Shah, S. L. *J. Appl. Poly. Sci.* **1986**, *32*, 3239.
104. Urlaub, E.; Popp, J.; Roman, V.; Kiefer, W.; Lankers, M.; Rossling, G. *Chem. Phys. Let.* **1998**, *298*, 177.
105. Pasquae, A.; Long, T. *Macromolecules* **1999**, *32*, 7954.
106. Wroblewski, S.; Trzebiatowska, K.; Jedrzejewska, B.; Pietrzak, M.; Gawinecki, R.; Paczkowski, J. *J. Chem. Soc. Perkin Trans.* **1999**, 1909.
107. Siani, A.; Storti, G.; Morbidelli, M. *J. Appl. Poly. Sci.* **1999**, *72*, 1451.
108. Kammone, O.; Chatzi, E.; Kiparissides, C. *J. M. S. – Rev. Macromol. Chem. Phys.* **1999**, *C39*, 57.
109. Russell, Richard, Thesis, University of New Hampshire, 1989.